
**FUNCTIONALLY MODIFIED (DEOXY)RIBONUCLEOTIDES:
SYNTHESIS AND STUDY
OF PHYSICOCHEMICAL AND BIOLOGICAL PROPERTIES**

Dissertation

zur Erlangung des Grades

„Doktor der Naturwissenschaften“

im Promotionsfach Chemie

am Fachbereich Chemie, Pharmazie und Geowissenschaften
der Johannes Gutenberg-Universität, Mainz

vorgelegt von

Isabell Hellmuth

geb. Schütz, in Oberwesel

Mainz, April 2017



JOHANNES GUTENBERG
UNIVERSITÄT MAINZ



Dekan:

1. Berichterstatter:

2. Berichterstatter:

Tag der mündlichen Prüfung: 05.05.2017

D77 (Dissertation Mainz)

Die vorgelegte Dissertation wurde am Institut für Pharmazie und Biochemie der Johannes Gutenberg-Universität in Mainz zur Erlangung des Grades „Doktor der Naturwissenschaften“, unter Betreuung von angefertigt.

Erstgutachter:

Zweitgutachter:

Hiermit versichere ich eidesstattlich:

1. Ich habe die jetzt als Dissertation vorgelegte Arbeit selbst angefertigt und alle benutzten Hilfsmittel (Literatur, Apparaturen, Material) in der Arbeit angegeben.
2. Ich habe oder hatte die jetzt als Dissertation vorgelegte Arbeit nicht als Prüfungsarbeit für eine staatliche oder andere wissenschaftliche Prüfung eingereicht.
3. Ich hatte weder die jetzt als Dissertation vorgelegte Arbeit noch Teile davon bei einer anderen Fakultät bzw. einem anderen Fachbereich als Dissertation eingereicht.

Ort, Datum

Isabell Hellmuth



Abstract

Understanding and controlling the role of RNA in processes of human health and disease, apart from basic cellular mechanisms, is of immense value. Many severe cases are still in need for optimized therapy strategies, a gap, which could be filled in the near future by promising therapeutic RNA applications. Especially the design of tailored siRNA and mRNA strategies towards personal therapy presents an encouraging point of vantage. The development of such techniques requires fundamental knowledge concerning physicochemical properties of RNA, as the implementation of molecular changes could influence the resulting biological activity in manifold directions.

The first project of the current thesis addressed this issue in assessing the influence of a terminal alkyne attached to the exocyclic amine of 2'-O-deoxycytidine phosphoramidites, which were applied in solid phase DNA synthesis of 22mers, exhibiting an analogous sequence to an eGFP-siRNA sense strand. The preferred orientation of this functional group and its influence on duplex stability were investigated *via* 2D-NMR spectroscopy and temperature dependent UV-absorption melting experiments, revealing significant changes of stability in the case of a double modified 5-methyl-2'-O-deoxycytidine. Additionally, the terminal alkyne served as a handle for the copper-I-catalyzed azide-alkyne cycloaddition (CuAAC) with a fluorescent dye.

Driven by the latest insights on the molecular mechanisms of TLR7 and 8 activation, which were suggested to be activated *via* two distinct triggers and pathways, the idea was born to address them simultaneously with one molecule combining both activating patterns, a small molecule TLR agonist and a single-stranded RNA, in one bidentate ligand to manipulate the innate immune system. To this end, the bioorthogonal CuAAC should present again the method of choice to link the desired molecules. Therefore, two small molecules of the imidazoquinoline family were prior equipped synthetically with azide-linkers for immobilization on designed functional alkyne-bearing mRNA molecules. The focus of this study was on the evaluation of cytokine release by human immune cells under the influence of the created new smTLRa-mRNA conjugates and their respective building blocks. Besides the described long and coding mRNAs, investigations involved also the modification and application of siRNA-conjugates, representing short non-coding RNAs. Bearing a potential therapeutic application in mind, which would involve the original function of the applied RNA species, as part of the translational machinery and RNAi mediated expression control, effects by the implemented RNA-modulations on these biological properties were investigated.

Zusammenfassung

Die Rolle von RNA bezüglich physiologischer und pathologischer Prozesse, neben grundlegenden zellulären Mechanismen, zu verstehen und kontrollieren zu können, ist von unschätzbarem Wert. Einer Vielzahl schwerwiegender Krankheiten bedarf es immer noch an optimierten Therapieansätzen, eine Lücke, die in Zukunft durch vielversprechende therapeutische Ansätze mittels RNA gefüllt werden könnte. Besonders das Design maßgeschneiderter siRNA und mRNA Strategien hin zu personeller Therapie stellt einen aussichtsreichen Angriffspunkt dar. Die Entwicklung solcher Techniken bedarf grundlegendem Wissen im Hinblick auf physikochemische Eigenschaften der RNA, da die Durchführung molekularer Veränderungen die resultierende biologische Aktivität in vielerlei Hinsicht beeinflussen kann.

Das erste Projekt der vorliegenden Arbeit adressierte dies durch die Evaluation eines, an das exozyklische Amin von Desoxycytidin-Phosphoramiditen angebrachte, terminalen Alkins. Diese Bausteine wurden in der DNA Festphasensynthese von 22meren, welche die Sequenz eines eGFP-siRNA sense-Stranges aufwiesen, angewendet. Die bevorzugte Orientierung dieser funktionalen Gruppe und deren Einfluss auf die Doppelhelix Stabilität wurden mittels 2D-NMR Spektroskopie und Temperatur abhängigen UV-Absorptions-Schmelzexperimenten untersucht, wobei signifikante Veränderungen in der Stabilität im Fall eines doppelt modifizierten 5-Methyldeoxycytidines beobachtet werden konnten. Zudem, wurde die Funktion des terminalen Alkins in der Kupfer(I)-katalysierten Azid-Alkin Cycloaddition mit einem Fluoreszenzfarbstoff eingesetzt.

Aktuelle Erkenntnisse zu molekularen Mechanismen zur Adressierung von TLR7 und 8, deren Aktivierung über zwei verschiedene Auslösemechanismen vermutet wird, bedingten die Idee diese beiden Pfade durch ein Molekül anzusprechen, welches beide Aktivierungsstrukturen, also einen niedermolekularen TLR Liganden (smTLRa) und eine einzelsträngige RNA, miteinander kovalent verbindet um das angeborene Immunsystem zu manipulieren. Zu diesem Zweck wurde die bioorthogonale CuAAC Reaktion gewählt um die anvisierten Moleküle zu verbinden. Daher wurden zuvor zwei niedermolekulare Immunmodulatoren der Imidazochinolin-Familie synthetisch mit Azid-Linkern für die Anbringung an, ebenfalls designte, funktionelle mRNA versehen. Der Fokus dieser Studie lag auf der Evaluation der, durch humane Immunzellen ausgeschütteten, Zytokine unter dem Einfluss der neu designten smTLR-mRNA Konjugate und deren Bausteine. Neben der beschriebenen langen und kodierenden mRNA, beinhalteten die Untersuchungen ebenfalls die Modifizierung und Anwendung kleiner siRNA Konjugate. Eine potentielle therapeutische Anwendung im Hinterkopf habend, welche die ursprüngliche Funktion der eingesetzten RNA Spezies, als Teil der translationalen Maschinerie und der RNAi bedingten Expressionskontrolle, beinhaltet, wurden die Effekte der durchgeführten RNA-Modulationen bezüglich ihrer biologischen Eigenschaften untersucht.

Contents

LIST OF FIGURES.....	XV
LIST OF SCHEMES	XVII
LIST OF TABLES	XVIII
ABBREVIATIONS.....	XIX
1 INTRODUCTION	1
1.1 Laboratory synthesis & modification of DNA & RNA.....	1
1.1.1 The phosphoramidite method and solid phase oligonucleotide synthesis 1	
1.1.2 Pre- and post-synthetic modification of nucleic acids	5
1.2 Impact of synthetic nucleoside modifications on oligonucleotide characteristics	9
1.3 Toll like receptors (TLRs) and innate immunity.....	12
1.3.1 TLR 7 and 8: ligands and mechanisms.....	14
2 MOTIVATION AND OBJECTIVES.....	19
3 RESULTS AND DISCUSSION.....	21
3.1 Conversion of dU to a “clickable” deoxycytidine for incorporation into oligonucleotides: juxtaposition to its opponent, a 5mdC derivative.	21
3.1.1 Nucleoside modification and phosphoramidite synthesis.....	23
3.1.2 Orientation of the propargyl group on the nucleoside level.....	25
3.1.3 Double helices confronted with the N ⁴ -propargyl moiety	28
3.2 Steric shielding of RNA from recognition by endosomal toll-like receptors (TLR7 & 8)	37
3.2.1 Azide-functionalized small molecule TLR-agonists.....	39
3.2.2 From plasmid to mRNA.....	44

3.2.3	mRNA, small molecules and endosomal TLRs in human immune cells: collaboration & opposition	49
3.2.4	Transfer to siRNA.....	54
3.2.5	The effect of bioconjugates on TLR7-mediated immunostimulation is distinct from inhibition by ribose methylation	56
3.2.6	Influence of RNA-modification on biologic activity	57
4	CONCLUSION AND OUTLOOK.....	61
5	EXPERIMENTAL SECTION	64
5.1	Materials	64
5.1.1	Instruments	64
5.1.2	Chemicals & Consumables.....	66
5.1.3	Buffers & Media.....	67
5.1.4	Enzymes & Oligonucleotides	69
5.1.5	Software	70
5.2	Organic syntheses	71
5.2.1	Synthesis of 3'-O-CEP-5'-O-DMT-N ⁴ -propargyl-2'-deoxycytidine 25b ..	72
5.2.2	Synthesis procedures azide-modified TLR ligands.....	81
5.3	Molecular biology techniques.....	84
5.3.1	Solid phase oligonucleotide synthesis & work up	84
5.3.2	pDNA amplification, preparation and linearization.....	86
5.3.3	mRNA synthesis & purification.....	86
5.3.4	Click functionalization of RNA through CuAAC	87
5.3.5	Hybridization of siRNA double strands	87
5.3.6	Temperature-dependent UV melting curves.....	87
5.3.7	Electrophoretic mobility shift assays (EMSA) by means of agarose- & polyacrylamide gel electrophoresis.....	88
5.3.8	Purification & concentration methods for oligonucleotides	89
5.3.9	Liquid chromatography (LC) methods	91
5.3.10	Stimulation of PBMCs	92
5.3.11	Generation and transfection of human dendritic cells [xx].....	93
5.3.12	Knock down in HeLa MAZ	93
5.3.13	Tritium incorporation assay of 5'-mRNA capping reaction	94
6	APPENDIX.....	95
6.1	Ad 3.1	95
6.2	Ad 3.2.....	96

6.3	Spectra	100
6.3.1	Spectra of 3'-O-CEP-5'-O-DMT-N ⁴ -propargyl-2'-deoxycytidine (25b) .	100
6.3.2	Spectra of N ⁴ -propargyl-2'-deoxycytidine (27b).....	103
6.3.3	Spectra of 5-methyl-N ⁴ -propargyl-2'-deoxycytidine (27a).....	106
6.3.4	ROESY kinetic studies	109
6.3.5	Spectra of Resiquimod-PEG ₄ -N ₃ / RPA 29	110
6.3.6	Spectra of 2-(2-(2-azidoethoxy)ethoxy)ethyl methanesulfonate (N ₃ -EEEt-OMs) 31	113
6.3.7	Spectra of Gardiquimod-DEG-N ₃ / GDA 33.....	115
BIBLIOGRAPHY.....		118
PUBLICATIONS AND COLLABORATIONS		140

List of Figures

Figure 1.1: The three edges of hydrogen bonding of a base-pairing between guanosine and cytidine.....	10
Figure 1.2: Compilation of extracellular and endosomal Toll-like receptors	13
Figure 1.3: Schematic overview of activation mechanisms for endosomal TLR8 and 7.....	15
Figure 1.4: Selection of small molecule TLR7/8 agonists of imidazoquinoline- and guanosine based structures	16
Figure 3.1: Hypothetical consideration of the orientation of N ⁴ -substituents on cytidines.	22
Figure 3.2: ROESY NMR measurements of the two respective deprotected cytidine derivatives.....	27
Figure 3.3: Proposed arrangement of Watson-Crick base pairing between guanosine and the N ⁴ -substituted cytidine derivatives	28
Figure 3.4: MALDI-TOF spectra of six selected in-house synthesized oligodeoxynucleotides.	30
Figure 3.5: Comparison of melting temperatures obtained between duplexes.....	34
Figure 3.6: Comparison of the click functionalization of the alkyne-modified DNA.....	36
Figure 3.7: Concept of the present study.	37
Figure 3.8: Imidazoquinoline based scaffold of the respective small molecules for the nomenclature.....	39
Figure 3.9: Titration of PBMCs with the small molecules (R848, GQI) and their respective azide-derivative	41
Figure 3.10: Zoom into the 1 st site of MmTLR7-dimer crystal structure.....	43
Figure 3.11: Schematic workflow of mRNA synthesis starting from plasmid DNA	45
Figure 3.12: Investigation of capping reaction through tritium incorporation assay.....	46
Figure 3.13: Evaluation of IVT-eGFP-mRNA purification via the MEGAclear™ transcription clean-up kit.	47
Figure 3.14: Synthesis of small molecule-TLRa bearing eGFP-mRNA by click-chemistry.....	49
Figure 3.15: Zoom into the A-chain (purple) of the MmTLR7-dimer crystal structure.....	50
Figure 3.16: Comparative study of the effect of smTLRa, mRNA, and covalent conjugates of both on IFN-α secretion in human PBMCs.	52
Figure 3.17: Selected azide-bearing molecules for study extension	53
Figure 3.18: Effects of selected azide-bearing molecules of different molecular weight	54
Figure 3.19: Application on mono-alkyne-functionalized sense eGFP-siRNA.....	55
Figure 3.20: A new distinct type of inhibition of TLR7 mediated immunostimulation.....	57
Figure 3.21: Modification does not interfere with, even enhance knock-down capacity.	58
Figure 3.22: Protein expression in DC is inhibited by large mRNA modifications.	59
Figure 5.1: Numbering of small molecule scaffolds for nomenclature.....	81
Figure 6.1: Temperature dependent UV-absorption melting curves.....	95
Figure 6.3: Titration of HEK-blue-hTLR7 with the commercial small molecules (R848, GQI) and their respective azide-derivatives.....	96
Figure 6.4: Cytotoxicity assay of commercial small molecules and azide-derivatives in PBMC.....	96
Figure 6.5: Size exclusion chromatography (Superdex 200 10/300 GL) of mRNA in 1x PBS.....	97

Figure 6.6: PBMC stimulation (A) with eGFP-mRNA, commercial small molecules and their respective azide-derivatives (B).....	98
Figure 6.7: Protein expression in DC is inhibited by high amounts of alkyne modifications.	99
Figure 6.8: ¹ H-NMR (400 MHz, DMSO-d ₆) of 3'-O-CEP-5'-O-DMT-N ⁴ -propargyl-2'-deoxycytidine (25b) ..	100
Figure 6.9: ¹³ C-NMR (100 MHz, DMSO-d ₆) of 3'-O-CEP-5'-O-DMT-N ⁴ -propargyl-2'-deoxycytidine (25b)..	101
Figure 6.10: ³¹ P-NMR (162 MHz, DMSO-d ₆) of 3'-O-CEP-5'-O-DMT-N ⁴ -propargyl-2'-deoxycytidine (25b).	101
Figure 6.11: HR-MS (ESI) of 3'-O-CEP-5'-O-DMT-N ⁴ -propargyl-2'-deoxycytidine (25b).	102
Figure 6.12: ¹ H-NMR (300 MHz, DMSO-d ₆) of N ⁴ -propargyl-2'-deoxycytidine (27b).	103
Figure 6.13: FT-IR of N ⁴ -propargyl-2'-deoxycytidine (27b).	104
Figure 6.14: HR-MS (ESI) of N ⁴ -propargyl-2'-deoxycytidine (27b).....	104
Figure 6.15: ROESY NMR experiments of N ⁴ -propargyl-2'-deoxycytidine (27b)	105
Figure 6.16: ¹ H-NMR (300 MHz, DMSO-d ₆) of 5-methyl-N ⁴ -propargyl-2'-deoxycytidine (27a).	106
Figure 6.17: FT-IR of 5-methyl-N ⁴ -propargyl-2'-deoxycytidine (27a).	107
Figure 6.18: HR-MS (ESI) of 5-methyl-N ⁴ -propargyl-2'-deoxycytidine (27a).....	107
Figure 6.19: ROESY NMR experiments of 5-methyl-N ⁴ -propargyl-2'-deoxycytidine (27b).	108
Figure 6.20: Temperature dependent ¹ H NMR experiments	109
Figure 6.21: Temperature dependent ROESY NMR experiments and Arrhenius analysis	109
Figure 6.22: ¹ H-NMR (300 MHz, CDCl ₃) of RPA (29).....	110
Figure 6.23: ¹³ C-NMR (75 MHz, CDCl ₃) of RPA (29).	111
Figure 6.24: FT-IR of RPA (29).	111
Figure 6.25: Full range MS (FD) of RPA (29).....	112
Figure 6.26: HR-MS (ESI) of RPA (29).	112
Figure 6.27: ¹ H-NMR (300 MHz, CDCl ₃) of N ₃ -EEEt-OMs (31).....	113
Figure 6.28: ¹³ C-NMR (75 MHz, CDCl ₃) of N ₃ -EEEt-OMs (31).....	114
Figure 6.29: ¹ H-NMR (300 MHz, MeOD), GDA (33).....	115
Figure 6.30: ¹³ C-NMR (75 MHz, MeOD), GDA (33).	116
Figure 6.31: Full range MS (ESI) GDA (33).	116
Figure 6.32: HR-MS (ESI) GDA (33).	117

List of Schemes

Scheme 1.1: The phosphoramidite method and solid phase oligonucleotide synthesis.....	2
Scheme 1.2: Mechanism involved in the activation step of the PA 3 with and 1H-tetrazole	3
Scheme 1.3: Overview of different reactions, which fit into the click chemistry concept.	6
Scheme 1.4: Proposed mechanism of the Cu(I)-catalyzed-[3+2]-azide-alkyne-cycloaddition.....	7
Scheme 3.1: Synthesis of the CpDCII phosphoramidite building block 25b.....	23
Scheme 3.2: Synthesis of the CpDCI phosphoramidite building block 25a.....	24
Scheme 3.3: Acid induced detritylation	25
Scheme 3.4: Possible isomers of compound 27a/b	26
Scheme 3.5: Synthesis of azide-functionalized small molecule TLR-agonists.....	40

List of Tables

Table 3.1: Sequences of the synthesized unmodified and the seven modified DNA oligonucleotides	29
Table 3.2: Listing of melting temperatures obtained for duplexes formed between the fifteen synthesized DNA sense strands and complementary DNA or RNA	32
Table 3.3: Significance evaluation for statistical differences in IFN- α and TNF- α secretion).....	42
Table 5.1: Denaturing TBE-PAGE gels for separation of single stranded nucleic acids in 100 mL.....	67
Table 5.2: Native TBE-PAGE gels for separation of double stranded nucleic acids in 100 mL.....	68
Table 5.3: Sequence information for applied commercial RNA oligonucleotides.	69
Table 5.4: Plasmid DNA applied for transformations.....	70
Table 5.5: Program settings for DNA (RNA) SPOS on Expedite 8909 DNA/RNA synthesizer.....	84
Table 5.6: Sequences of the synthesized unmodified and the seven modified DNA oligonucleotides.....	85
Table 5.7: Settings for gel scans based on spectroscopic properties of staining dyes and dye-labels.....	89

Abbreviations

5-EU	5-ethynyluridine
5-EdU	5-ethynyl-2'-deoxyuridine
5mdC	5-methyl-2'-deoxycytidine
A	Adenosine
Ac ₂ O	Acetic anhydride
APC	Antigen presenting cell
APS	Ammonium persulfate
BMDC	Bone-marrow derived DCs
br s	broad singulett
BSA	Bovine serum albumin
Bu ₄ NF	<i>t</i> -butyl ammonium fluoride
C	Cytidine
CDCI ₃	Deuterated chloroform
CEP-Cl	2-cyanoethyl- <i>N,N</i> -diisopropylchlorophosphoramidite
CHCl ₃	Chloroform
CH ₃ CN	Acetonitrile
cHex	Cyclohexane
CPDC	3'-O-CEP-5'-O-DMT-5-methyl- <i>N</i> ⁴ -propargyl-2'-deoxycytidine
CPDCII	3'-O-CEP-5'-O-DMT- <i>N</i> ⁴ -propargyl-2'-deoxycytidine
CPG	Controlled pore glass
CRC	Collaborative research centre
CuAAC	Copper(I)-catalyzed azide-alkyne Huisgen cycloaddition
d	Doublet
dd	Doublet of a doublet
DAD	Diode array detector
DC	Dendritic cell
DCA	Dichloroacetic acid
DCM	Dichloromethane
DCVC	Dry column vacuum chromatography
DMAP	4- <i>N,N</i> -dimethylaminopyridine
DMF	<i>N,N</i> -dimethylformamide
DMSO	Dimethyl sulfoxide
DMSO- <i>d</i> ₆	Deuterated DMSO
DMT-Cl	4,4'-dimethoxytrityl chloride
DNA	Deoxyribonucleic acid
DOTAP	<i>N</i> -[1-(2,3-Dioleoyloxy)propyl]- <i>N,N,N</i> -trimethylammonium methylsulfate
dr	Diastereomer ratio
dT (T)	Deoxythymidine (thymidine)
DTT	Dithiothreitol
dU (U)	Deoxyuridine (uridine)

<i>E. coli</i>	<i>Escherichia coli</i>
EDTA	Ethylenediaminetetraacetic acid
eGFP	Enhanced green fluorescent protein
ELISA	Enzyme-linked immunosorbent assay
EMSA	Electrophoretic mobility shift assay
ESI	Electron spray ionization
EtN ₃	Triethylamine
EtOAc	Ethyl acetate
EtOH	Ethanol
EUTP	5-ethynyl-uridine triphosphate
eq	Equivalent
EXSY	EXchange SpectroscopY
FD	Field desorption
FLD	Fluorescence detector
FT-IR	Fourier transform infrared spectroscopy
G	Guanosine
GDA	Gardiquimod-diethylene-glycol-azide
Gm	2'-O-methylguanosine
GQI	Gardiquimod
HEK cells	Human embryonic kidney cells
HeLa	Henrietta Lacks cells
HPLC	High-performance liquid chromatography
HPV	<i>Human papillomavirus</i>
IC ₅₀	Half maximal inhibitory concentration
iEDDA	Inverse electron demand Diels-Alder cycloaddition
IFN	Interferon
IRES	Internal ribosomal entry site
IVT	<i>In vitro</i> transcription
<i>J</i>	Coupling constant
LB	Lysogeny broth (Luria-Bertani broth)
LNA	Locked nucleic acid
LP	Long pass filter
LPS	Lipopolysaccharides
LRR	Leucine rich repeat
m	Multiplet
MALDI-TOF	Matrix assisted laser desorption/ionization time-of-flight
MCK	MEGAclean™ (transcription clean-up) kit
MeOH	Methanol
MgSO ₄	Magnesium sulfate
<i>Mm</i>	<i>Macaca mulatta</i>
MMA	Monomannose azide
Mp	Melting point
mRNA	messenger RNA
MS	Mass spectroscopy
MTT	3-(4,5-dimethylthiazol-2-yl)-2,5-diphenyltetrazolium bromide
MYD88	Myeloid differentiation primary-response protein 88
NHS	<i>N</i> -hydroxysuccinimide
NLR	NOD-like receptor
NMR	Nuclear magnetic resonance
NOD	Nucleotide-binding oligomerization domain
NOESY	Nuclear Overhauser Effect <i>SpectroscopY</i>
ns	not significant

nt	not treated
NTP	Nucleoside triphosphate
ODN	Oligodeoxyribonucleotide
ORN	Oligoribonucleotide
ψ	Pseudouridine, Psi
PAGE	Polyacrylamide gel electrophoresis
PAMP	Pathogen associated molecular pattern
PBMC	Peripheral blood mononuclear cells
PBS	Phosphate-buffered saline
PDB	Protein data bank
pDC	plasmacytoid dendritic cells
pDNA	plasmid-DNA
PDI	Perylene dye
PEG	Polyethylene glycol
POI	Point/Position of interest
PRR	Pattern recognition receptor
R848	Resiquimod
RIG-I	Retinoic acid inducible gene I
RNAi	RNA interference
ROESY	Rotating-frame nuclear Overhauser Effect <i>Spectroscopy</i>
RP	Reversed phase
RPA	Resiquimod-polyethylene-glycol-azide
rpm	Rotation per minute
SAM	³ H-S-adenosyl-L-methionine
SD	Standard deviation
SEAP	Secreted embryonic alkaline phosphatase
SEC	Size exclusion chromatography
SEM	Standard error of the mean
siRNA	small interfering RNA
SM	Small molecule
smTLRa	small molecule TLR agonist
ssRNA	single-stranded RNA
T2A	<i>Thoseaasigna</i> virus 2A
TBAF	Tetrabutylammonium fluoride
TBDMS-Cl	<i>Tert</i> -butyldimethylsilyl chloride
TBE	Tris-boronic acid-ethylenediaminetetraacetic acid
TCA	Trichloroacetic acid
TEA	Triethyl amine
TEAA	Triethylammonium acetate
TFA	Trifluoroacetic acid
THF	Tetrahydrofuran
TIR	Toll-IL-1-resistance
TLC	Thin layer chromatography
TLR	Toll-like receptor
T _m	Melting temperature
TMA	Trimannose azide
TNF	Tumor necrosis factor
TPS-Cl	2,4,6-triisopropylbenzenesulfonyl chloride
TPTA	Tris-((1-hydroxypropyl-1H-1,2,3-triazol-4-yl)-methyl)-amine
TRIF	TIR domain-containing adaptor protein inducing IFNβ
VCE	<i>Vaccinia</i> virus capping enzyme
W-C	Watson-Crick



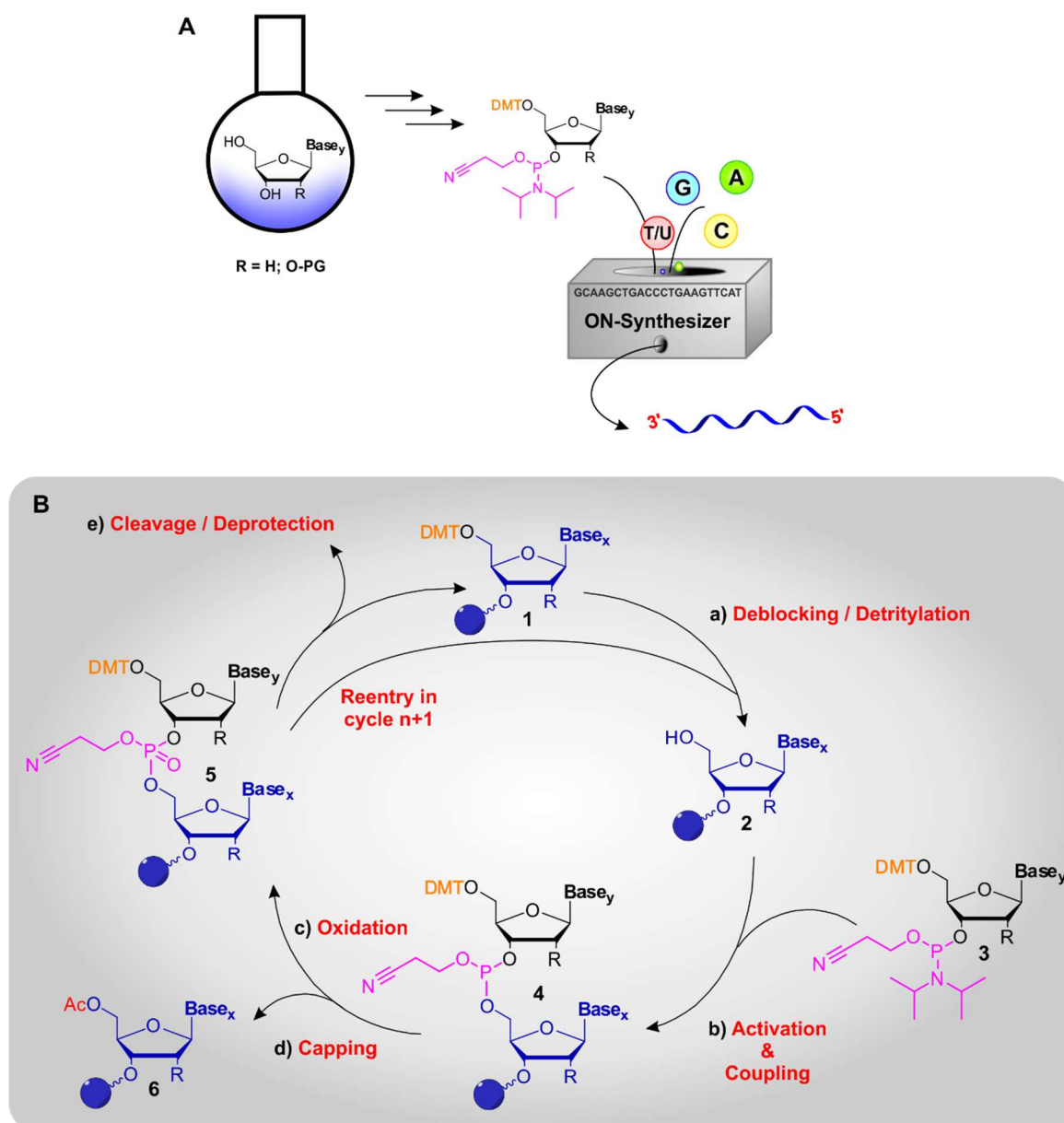
1 Introduction

1.1 Laboratory synthesis & modification of DNA & RNA

1.1.1 The phosphoramidite method and solid phase oligonucleotide synthesis

Similar as in peptide synthesis, one differentiates between liquid phase and solid phase oligonucleotide synthesis (SPOS) [1], both based on the conjugation of the same synthons, the nucleoside-phosphoramidites (PAs). Before these building blocks, for DNA and RNA, can undergo the essential 3'-phosphorylation of the ribose sugar, all other free nucleophilic groups as the exocyclic amino groups of the bases adenine, guanine and cytosine and the 5'-sugar-hydroxyl group (plus 2' in RNA) need to be protected in an orthogonal manner. Favorable base labile nucleobase protection groups, which remain stable through the processes of SPOS, are e.g. benzoyl (Bz), isobutyryl, phenoxyacetyl (pac) and 4-*t*-butylphenoxyacetyl (tac) groups [2]. Likewise required, is the protection of the 5'-hydroxyl group, commonly with the aromatic ring system of an acid labile 4,4'-dimethoxytrityl (DMT) moiety [3], [4]. Due to the lower nucleophilicity of the 3'-OH and steric effects, the DMT group is introduced very selectively at the 5'-OH. Further on, this moiety adds excellent detectability on thin-layer chromatography by Seebach's reagent staining (see Section 5.2) and facilitates, due to its lipophilicity, column purification of the desired nucleoside derivative. The synthesis of RNA requires the additional protection of the 2'-hydroxyl group, which is explained in more detail below. Thus, the fully protected deoxynucleoside can now be phosphorylated at the 3'-position *via* the introduction of 2-cyanoethyl-*N,N*-diisopropylchlorophosphoramidite (CEP) and subjected to SPOS.

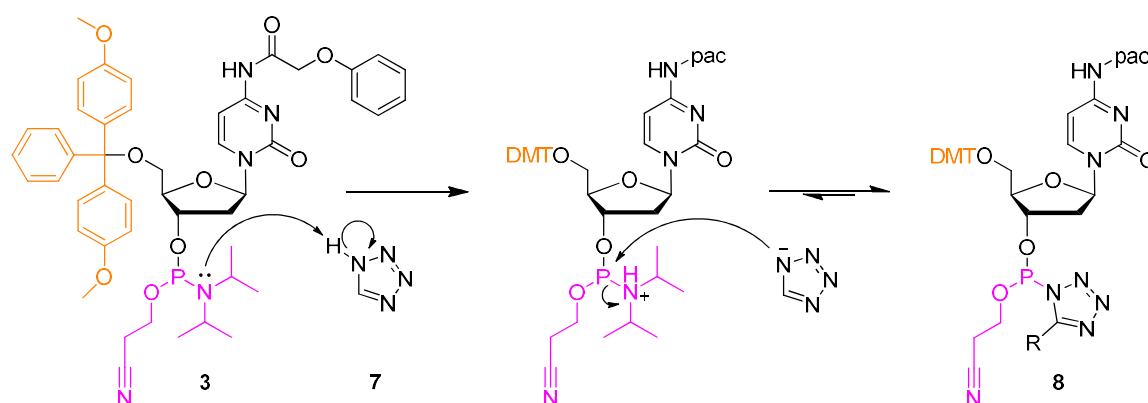
After the application of the phosphite triester method by Letsinger *et al.* [5], the Caruthers group developed its further installation on polymer supports [6], which consist often, among other materials as e.g. polystyrene, of controlled pore glass (CPG) packed into small columns. This development allowed the evolution towards automated procedures [7]. In contrast to biological DNA and RNA synthesis, the SPOS is directed from the 3'- to the 5'-end. The first nucleoside **1** is attached covalently with its 3'-hydroxyl group *via* a succinyl-linker to the solid phase and is in the following series of synthesis cycles, as illustrated in Scheme 1.1, sequentially elongated with nucleoside PAs **3** of the desired sequence. Each cycle is in general, alternating with an acetonitrile wash, composed of four steps (a-c), which are detailed below.



Scheme 1.1: The phosphoramidite method and solid phase oligonucleotide synthesis. **(A)** Protected PA (PG = protection group) building block for application in SPOS on a DNA/RNA synthesizer (grey illustration). **(B)** Synthesis cycle of the solid phase DNA(RNA)-oligonucleotide synthesis, starting with the first nucleoside **1** attached to the solid support (blue sphere): **(a)** Release of the 5'-OH **2** through acidic removal of the DMT-group. **(b)** Activation and coupling of the next incoming PA **3**. **(c-d)** Oxidation of the phosphite- **4** to the phosphate triester **5** with subsequent capping of unreacted 5'-hydroxyl groups **6** before reentry into the cycle ($n+1$). **(e)** Final column cleavage and deprotection of the obtained oligonucleotide.

The procedure is initiated by the 5'-deprotection, also known as deblocking or detritylation (a), of the solid support bound nucleoside **1** by means of acids, e.g. di- (DCA) or trichloroacetic acid (TCA), diluted in organic solvents like dichloromethane to prevent depurination [8], [9]. Here, a further advantage of the DMT group comes into play, as its cleaved cation evolves an orange color and thus, an absorption maximum at 498 nm [10], which can be utilized to evaluate the efficiency of

each previous coupling step. Next, the activation of the incoming PA **3** to form a reactive intermediate for the coupling step is required (b). Acidic tetrazole derivatives as 1*H*-tetrazole **7**, 5-(ethylthio)-1*H*-tetrazole or 5-(benzylthio)-1*H*-tetrazole (BTT) are employed as proton donating activators [11], leading in a rate-determining step to *P*-tetrazole intermediates **8**, which allow a nucleophilic attack by the free 5'-hydroxyl group of the bound nucleoside (Scheme 1.2). Another potential and less acidic activator for this condensation is 4,5-dicyanoimidazole (DCI), which affords shorter coupling times with higher yields due to its stronger nucleophilicity and diminishes undesired early cleavage of the 5'-*O*-DMT group of the incoming PA [12].



Scheme 1.2: Mechanism involved in the activation step of the PA **3** with and 1*H*-tetrazole **7** as activator to provide the reactive *P*-tetrazole intermediate **8** for the following coupling step during SPOS.

Thus, the two nucleosides can now be coupled *via* the β-cyanoethyl protected and activated 3'-phosphate of the PA to build the phosphite triester **4** [13]. This is followed by an oxidation step with an aqueous solution of iodine in THF to form the phosphate triester linkage **5** (c), which allows already at that point to introduce modifications at the phosphate backbone (see Section 1.1.2). Released hydrogen iodide is neutralized through the conditions of the next step. In order to avoid side products of shorter length to occur in the subsequent cycles, unreacted free 5'-hydroxyl groups, which cannot completely be excluded, are blocked in a so-called capping step (d) through esterification with acetic anhydride **6** in a mixture with 2,6-lutidine and *N*-methylimidazole in THF [14]. From here, this synthesis cycle is repeated until the desired sequence is completed, which can be finished with an additional detritylation of the last nucleoside, leaving a free 5'-OH also known as "DMT-OFF". Otherwise, the last DMT group can be kept, as so-called "DMT-ON" mode, for the purpose of purification of shorter nucleotides, since it facilitates the strand separation during reversed phase HPLC due to its lipophilicity [15], a feature that becomes negligible for strands longer than 20 bases. A cleavage of this remaining moiety can be carried out afterwards through acidification. Subsequent to the final cycle, the achieved oligonucleotide can be cleaved from the solid support (e), which involves the treatment with an ethanolic ammonia solution or equivalent bases under thermolytic conditions. Both, the nucleobase protection groups and the β-cyanoethyl

protection of the phosphate backbone are removed in parallel through diacylation and β -elimination with this treatment [16], [17].

Variations for RNA-SPOS

As a consequence of the additional 2'-hydroxyl group in RNA, a few considerations need to be taken into account for the oligonucleotide synthesis. The RNA polymer would be prone to degradation under basic conditions, such as from the β -cyanoethyl cleavage, thus, the 2'-OH needs an orthogonal protection group. These are attached *via* esterification and contain commonly a silyl-group in the center [18], which can be cleaved/deprotected due to its affinity for fluorine ions with fluorinated acids as tetrabutylammonium fluoride (TBAF). Among these protective groups, *t*-butyldimethylsilyl (TBDMS) and the further branched variant triisopropylsilyloxymethyl (TOM) are widely applied [19], [20]. Thereby, the more stable TOM group has the advantage over the TBDMS group, that it bears a lower risk of a 2' to 3'-isomerization, which would lead to 2'-5'-linked RNA. Even higher coupling efficiencies let TOM become more and more favorable in RNA-SPOS [21]. Another alternative is represented by the bis(2-acetoxyethoxy)methyl group (ACE), which can be cleaved by mild acidic conditions and therefore, incompatible with the DMT-5'-protection. In these cases, the latter is subjected instead *vice versa* by a silyl ether [22]. Due to the additional bulky 2'-protection group, the accessibility of the phosphoramidite is reduced and coupling times need to be prolonged, which are generally twice as long as in DNA synthesis. Furthermore, as the base protection of RNA building blocks usually involves the so-called UltraMild protection groups (Glenresearch, Virginia/USA) like *pac* and *tac*, these can be removed in aqueous solutions of ethanolic ammonia or in methanolic potassium carbonate, both at ambient temperature.

Typically for both, DNA- and RNA-SPOS, coupling efficiencies vary for each base depending on type and sequence position, which could entail due to cumulative effects error rates for longer nucleotides up to 10^{-2} [23], [24]. Over the course of time, method variations, like the synthesis on super-paramagnetic beads [25], optimizations concerning protection and deprotection [16], [26], [27], phosphitylating agents and coupling reagents [28]–[31] for ODN synthesis were developed till today.

Purification

It must be assumed, that the resulting mixture after cleavage and deprotection contains, besides the deprotected full-length product, contaminations of shorter protected and unprotected ODN-fragments, plus a series of residual reagents, *i.e.* organic salts from protection group removal. To obtain the desired oligonucleotide in sufficient purity and quality for downstream experiments, methods like desalting by size exclusion gel-filtration, polyacrylamide gel electrophoresis (PAGE) or chromatographic procedures, as (ion-pair) reversed phase- [32], [33], anion exchange HPLC or in special cases an affinity tag supported chromatography, are involved. Typically, the desalting is applied in combination with one of the other (size-) separation techniques and a final concentration method, such as precipitation or lyophilization (Section 5.3.8.5). Separation by PAGE, based on

electrophoretic mobility, is particularly beneficial to receive long and otherwise unmodified oligonucleotides of high purity (> 95 %), however, with the consequence to lose a certain amount of product, which cannot be completely eluted from the gel matrix. For modification carrying oligonucleotides it is recommended to purify by one of the chromatographic methods [34], depending *i.e.* on the respective affinity of the modification, with regard to lipophilicity and charge distributions, which influence as well the selection of stationary and mobile phase. The latter techniques are also able to separate oligonucleotides smaller than 20 bases, where PAGE is already limited to be just an analytical method, not for workup.

1.1.2 Pre- and post-synthetic modification of nucleic acids

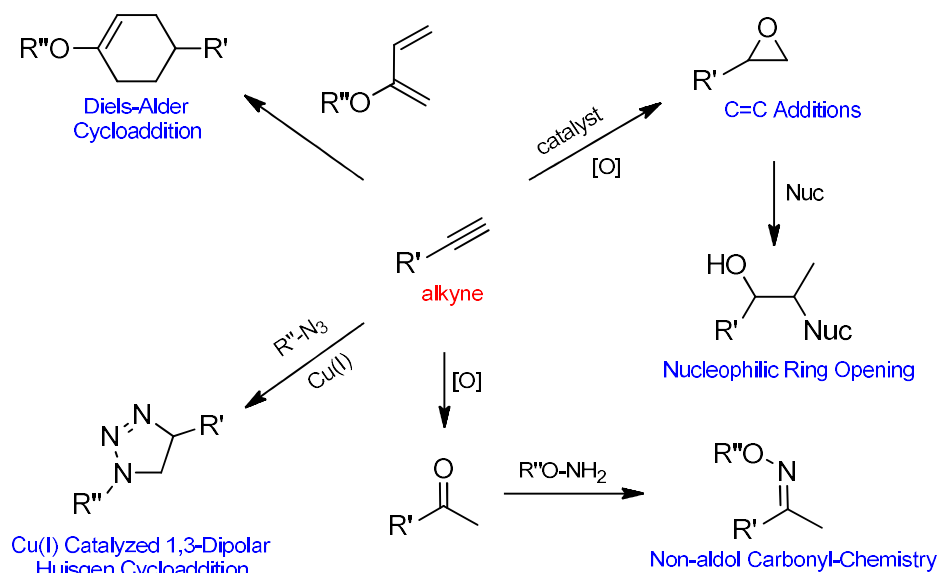
As outlined above, many techniques in nucleic acid research require the introduction of modifications to nucleosides or nucleotides, may it be in terms of functional studies, analytical method development or to strive for therapeutic applications. There are nearly no technical restrictions to attachment sites for labels like fluorescent dyes, tags, linkers like biotin and other functionalities. Modifications have been made to the nucleobases at endo- and exocyclic positions [35], [36] or even with an entirely different “base” right up to abasic structures [37], [38], as well as to the sugar-, typically at the 2'-hydroxyl group, and with several achievements at the phosphate-backbone. Furthermore, the site-specific position throughout a certain sequence may be of interest. Restrictions have only to be considered concerning the purpose of the particular DNA- or RNA application and the effect such alterations could bring about. These aspects will be discussed in detail in Section 1.2.

There are two classical policies for this purpose: the pre- and the post-synthetic strategy and combinations thereof. In the pre-synthetic approach, the label is introduced into the building block, which may either be an activated monomer as a phosphoramidite for solid phase synthesis, or a ribo-/deoxynucleotide triphosphate ((d)XTP), the natural substrates for polymerases. Besides that, the post-synthetic method introduces the modification into the already existing nucleic acid polymer, which would happen in a random distribution if the nucleic acid strand contains only its four major nucleotides, unless a specific target strategy for either of the two ends is applied by specific synthetic or enzymatic strategies (see below). A hybrid approach consists of the combination of both methods, which includes incorporation of non-standard building blocks at the pre-synthetic level, followed by its specific modification post-synthetically on the full-length oligonucleotide. This concerns than in general the chemical synthesis of a nucleotide monomer bearing either a specific reactive site, *e.g.* an azide moiety [39], or a suitable leaving group. As such, the so-called “convertible nucleoside approach” [40], [41] introduces replaceable functionalized tethers for further selective derivatization. Prior to be processed in enzymatic or chemical DNA/RNA synthesis, these modules must be converted into (d)XTPs or PAs as described before. These chemical handles are usually smaller than the final modifications and easier to shield *via* protection groups, which causes higher stability and less steric limitations. Yet, the capacity of polymerase enzymes to tolerate modified (d)XTPs might be limited and delivers additionally an unspecific and statistically distributed

introduction of the modification, as witnessed in Section 3.2 of this work by mRNA synthesis. Random incorporation can be avoided then by the automated oligonucleotide synthesis, allowing to program a site-specific introduction, as applied in the first project in Section 3.1.

1.1.2.1 Click chemistry, a versatile approach

With the intention to describe a reliable set of conjugation reactions, which facilitate the introduction of certain molecular properties, Kolb, Finn and Sharpless created in 2001 a new chemical term, the “click chemistry” [42]. A member of this reaction library combines several advantageous features, which are labeled as *modular, wide in scope, high yielding, stereospecific, requiring mild and nonhazardous reaction conditions and easy to purify* [42]. Further on, such reactions have usually in common, that they are energetically benefitted through high thermodynamic driving forces, leading to short reaction times with complete and highly selective conversion.

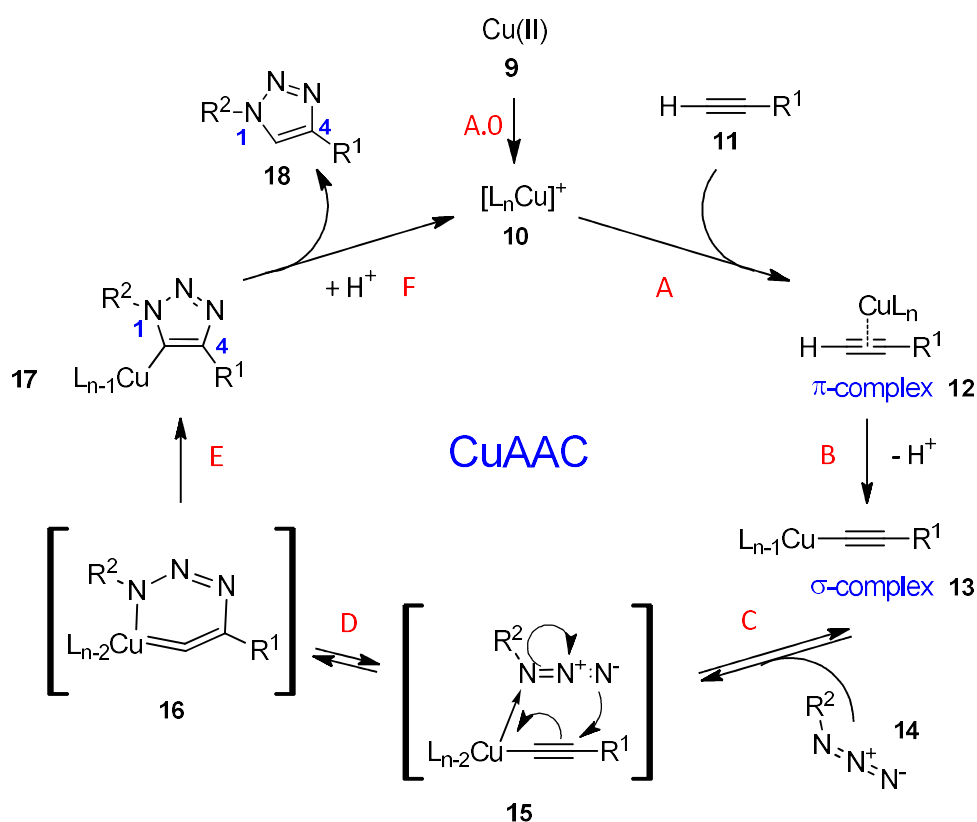


Scheme 1.3: Overview of different reactions, which fit into the click chemistry concept. (Figure adapted from Moses and Moorhouse 2007).

Reactions that fulfill these attributes of the click chemistry concept are summarized in Scheme 1.3. These include additions to carbon-carbon multiple bonds, which proceed often oxidative like dihydroxylation, nucleophilic *Michael* addition, epoxidation and aziridination, whereas the latter can be followed by another click variety: the nucleophilic substitution, such as ring-opening reactions. Continuing with non-aldol carbonyl chemistry like the formation of ureas, aromatic heterocycles, oximes and hydrazones. Furthermore, there are the cycloadditions of unsaturated carbonyl compounds as 1,3-dipolar cycloadditions, including the $Cu(I)$ -catalyzed-[3+2]-azide-alkyne- ($CuAAC$), the copper-free strain promoted azide-alkyne cycloaddition ($SPAAC$) [43], and finally the *Diels-Alder* reaction with its inverse electron demanding variant (*iEDDA*) [42], [44], [45], reactions,

that are all feasible and favored *in vitro* and *in vivo* [46]. Another Cu-free reaction, which can be associated with click-chemistry is the *Staudinger* ligation, a variation of the *Staudinger* reaction by Bertozzi [47], to form stable amide linkages.

Still, the most common representative of the click reactions is the copper(I)-catalyzed variety of the 1,3-dipolar *Huisgen* cycloaddition between a terminal alkyne and an azide, also known as Cu(I)-catalyzed-[3+2]-azide-alkyne-cycloaddition (CuAAC). It features to proceed 10^7 -times faster, in aqueous solution without heating and generates selectively the 1,4-triazole stereoisomer [48]. As revealed by computational and kinetic studies, the reaction follows a stepwise mechanism, in contrast of being concerted like the original *Huisgen* cycloaddition [49], [50].



Scheme 1.4: Proposed mechanism of the Cu(I)-catalyzed-[3+2]-azide-alkyne-cycloaddition. **(A.0)** Generation of the active monovalent copper catalyst **10**. **(A)** Coordination of the terminal alkyne **11** and π -complex formation **12**. **(B)** Deprotonation and formation of the acetylide σ -complex **13**. **(C)** Approximation of the azide **14** and coordination to the copper catalyst **15**. **(D)** Cyclization of the acetylide and the catalyst by formation of six-membered Cu(III)-cycle **16**. **(E)** Ring contraction to the five-membered triazole ring **17**. **(F)** Release of the triazole **18** and recovery of the catalyst by protonation. (Figure adapted from [49]).

Initially, a Cu(II)-species **9**, e.g. a sulfate salt, is reduced *in situ* with ascorbic acid or sodium ascorbate as common reductants to generate the active Cu(I)-catalyst **10**. As displayed in Scheme 1.4, a terminal alkyne **11** coordinates to the Cu(I)-catalyst yielding in a π -complex **12** (A), which

results in a decreased pK_a for the terminal alkyne [51]. Thus, a deprotonation in water is feasible without an additional base (B), yielding the active acetylide σ -complex **13**. In a further step (C), the azide **14** approximates the Cu(I)-complex, whereby the nitrogen adjacent to the carbon coordinates to the copper atom **15**. This is followed by the cyclization through the nucleophilic attack of the terminal nitrogen at the C-2 carbon of the acetylide, which builds an unusual six-membered Cu(III)-cycle **16** (D). After that, ring contraction forms the triazole ring, which is still bound to the copper atom **17** (E). Finally, the 1,4-disubstituted 1,2,3-triazole **18** and the recovery of the catalyst are achieved through a further protonation (F).

The CuAAC presents a powerful, bioorthogonal strategy for the derivatization (e.g. labeling) of biomolecules, since alkyne- and azide functionalities, which do not occur in biological systems as such, are substantially inert towards water, oxygen and a further wide range of common reaction conditions [48]. The application in labeling and ligation of nucleic acids, is popular among pre- and post-synthetic strategies and widely established for both, DNA [52]–[54] and RNA [55], [56].

Accordingly, click chemistry, particularly the CuAAC reaction, presents another important modification strategy applied throughout the entire project.

1.1.2.2 Enzymatic strategies for DNA/RNA synthesis and modification

Further strategies, not only for introducing modifications, but also for complete DNA/RNA-strand synthesis, are represented by enzymatically supported methods. Enzymes as ligases, kinases, restriction endonucleases for further processing and typically polymerases could be involved for such purposes [57]. The standard building blocks for polymerase-mediated applications are, *in vitro* and *in vivo*, the nucleoside triphosphate (d)NTPs. These represent a molecule class, which is still not straight forward to synthesize, as the success of each method is highly dependent on the substrate itself and a suitable purification method, in other words, they could work extremely well for one (d)NTP, but not for another [58]. Therefore, a series of different approaches have been developed to facilitate this process, to name but a few, the *Yoshikawa* protocol *via* a reactive phosphorodichlorate, the *Ludwig-Eckstein* method *via* an activated phosphite and the *Borch* approach by means of a reactive pyrrolidinium phosphoramidite [59]. Recently, the application of 5'-*H*-phosphonates has also gained interest as starting material for the triphosphate formation [60]. As already indicated, these building blocks deliver, analogously to the former described phosphoramidites, the possibility to introduce modifications pre-synthetically in a similar manner, starting with the conversion of the nucleoside, followed by the triphosphate formation and introduction during enzymatic synthesis [61]. Again, this could also be used to incorporate a convertible tether, which can be post-synthetically (-transcriptionally) functionalized, e.g. through click-chemistry reactions [62], a concept, which was applied in the current work as well.

Although to limited application sites, it is possible to label DNA/RNA ends site-specifically by enzymatic strategies, e.g. by the 5'-end labeling with radioactive phosphorus (^{32}P) of 5'-capped mRNA (see also Section 3.2.2.1) conducted by the combination of three enzymatic reactions [63]. This series of three includes the removal of the 5'-cap by tobacco acid pyrophosphatase,

dephosphorylation by alkaline phosphatase and finally the labeling with γ - ^{32}P -ATP by T4 polynucleotide kinase. The 5'-cap further allows chemo-enzymatic modification of mRNA by means of methyltransferases utilizing the methylated substrate *S*-adenosyl-L-methionine (SAM) and derivatives for labeling- or analytical purposes [64], [65], which offers once more the application for post-synthesis click chemistry. Very simple than, is the transcription priming method through the provision of modified nucleotides or cap-analogs in excess [66], which provides by the combination with ligases the possibility for site-specific internal labeling. Finally, the opposing site, the 3'-end, can be labeled as well, here by using a poly(A) polymerase to introduce the desired modification [67].

1.2 Impact of synthetic nucleoside modifications on oligonucleotide characteristics

By now there are already more than 160 known natural nucleoside modifications [68], involved in aspects of the “central dogma of molecular biology” like translation regulation [69], [70], and discovery still goes on [71]. As outlined above, there exist many fields of application and strategies, where artificial nucleic acid modifications are desired and come into play, still, their effect on physicochemical and biological properties must be considered carefully.

Approaches for synthetic modifications have been made to all parts of a nucleoside/nucleotide, the nucleobase, the sugar and the phosphates (see also Section 1.1.2). In addition, it must be taken into account at which sequence position these might end up during the respective oligonucleotide synthesis strategy. A smart method to study these key residues of nucleosides and consequent biological effects, is the so-called caging strategy [72], which makes use of photosensitive moieties on nucleosides, introduced by methods described above, in order to block their biologic activity transiently. Upon light activation, the region of interest is exposed through cleavage of the caging group. This method will be addressed among other aspects in the following paragraphs concerning the single nucleoside/nucleotide features.

Base modifications

Desired features through base modifications in nucleotides, can be nuclease resistance, double strand stability and thereby affected, an enhanced performance *e.g.* during RNA interference (RNAi) [73] or mRNA translation [70], [74], [75]. These attributes are offered *e.g.* for siRNA by the introduction of small modifications as pyrimidine 5-methyl- or 5-propynyl groups [76]. A more straightforward method to gain duplex stability is through covalent cross-linking, *i.e.* by means of click chemistry [77]. Instead, nucleobase-caged oligonucleotides make use of bulkier moieties, usually attached to one of the exocyclic base heteroatoms, in order to prevent Watson-Crick base-pairing (Figure 1.1) and to induce an intended functionality at a certain point by light triggered cleavage [78]. In the case of highly structured RNA species, as tRNAs, base modifications on the Watson-Crick edge could also affect an alternative folding of the tertiary structure [79]. Another

variety to alter base-pairing is possible by means of unnatural base pairs, which could even expand the genetic code by combination with the site-specific incorporation of amino acid analogs [80]. In general base-pairing capacities or impairments can be studied and predicted through accessing duplex melting temperatures and theoretical thermodynamics [81], [82].

Furthermore, the modulation of immune reactions, either in the direction of a boost or a suppression, is another favorable feature to address through base modifications and will be discussed in Section 1.3.1.2.

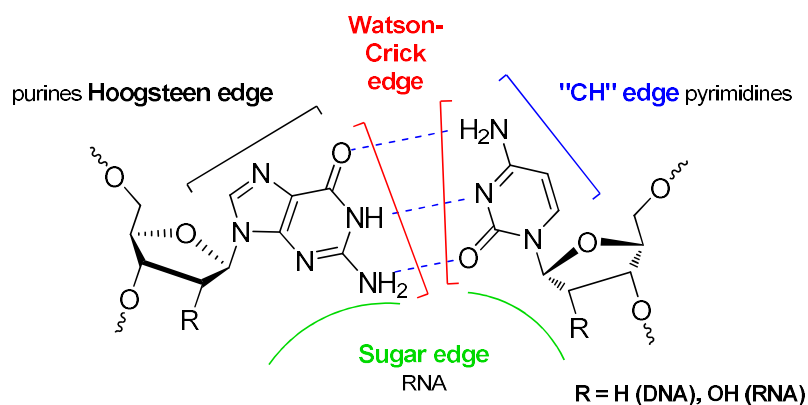


Figure 1.1: *The three edges of hydrogen bonding of a base-pairing between guanosine and cytidine.* (Figure adapted from Leontis and Westhof 1998 [83])

Sugar modifications

More relevant for RNA, favored sugar modifications for the ribose 2'-OH, which was found not to be a required feature for siRNA to enter the RNAi pathway [73], are 2'-O-methyl, 2'-fluoro and locked nucleic acid (LNA) modifications [84]. The 2'-O-methylation increases RNA stability by retaining the canonical right-handed A-form of helix conformation [84], [85] and increases the affinity for complementary RNAs, which leads to improved hybridization behavior [86], and consequently, to increased nuclease resistance. Nevertheless, these benefits are accompanied by the undesirable effect of reduced silencing efficiency, which can be observed in impaired cleavage from the passenger strand as well as for the target mRNA, and can be even completely abolished, when both strands are methylated [73]. Despite the reduced RNAi activity, the ribose methylation acts beneficially immunosuppressive, therefore avoiding Toll-like receptor (TLR) activation [87]–[89], which appears strikingly already in presence of a single modification of a guanosine (Gm18) in a bacterial tRNA [90], [91], further described in Section 1.3.1.2. 2'-fluoro-modifications, which do not naturally exist, exhibited to be particular suitable for the design of effective siRNAs, as they not only stabilized RNA but also could maintain gene silencing activity and abrogate TLR stimulation [73], [92], [93]. Besides the two mentioned sugar modifications, the LNAs contain commonly a 2'-O-methylene-4'-bridge and lock the sugar in its 3'-endo conformation [94], which leads to improved siRNA activity and contributes also to increased cellular stability and translational efficacy when applied for 5'-cap mRNA modifications [95]. Temporary blocking of RNA-3'-ends can be achieved

by the mentioned caging methods, which could reversibly stop polymerase reactions or can be applied with cleavable end-labeling e.g. with a biotinylated photolabile moiety at the 2'-hydroxyl-group facilitating strand collection by avidin magnetic beads [96].

Phosphate modifications

The final modification site is represented by the 5'-3'-phosphate linkages, the simplest variation at this side is the introduction of *P*-chiral phosphorothioates *via* an sulfurization step in SPOS instead of oxidation [97], ending up with a mixture of 2ⁿ stereoisomers of nucleotides [98] of enhanced stability. Phosphorothioates cap analogs have shown an increased stability and long-lasting translational efficiency for mRNA vaccines, including an improved immunogenicity of the RNA for T cell priming [99]. The same position at the phosphate backbone can be modified by the introduction of other functional tethers in PA synthesis, e.g. a cationic "spermine-conjugated phosphotriester" was applied within this respect to enhance membrane permeability [100]. A complete different approach was represented by the work of Sanzone *et al.* [101], who introduced, instead of a phosphate-, a triazole-backbone through linking the nucleoside derivatives *via* the CuAAC reaction and could achieve protein transcription [102].

Sequence positions

Several studies revealed, that the 5'-hydroxyl terminus of an siRNA is a prerequisite for RNAi activity, whereas the 3'-end, which contributes to the overhang region of the double strand, tolerates labeling or blocking [36], [103]. Internal sequence positions of modifications in an siRNA duplex were examined by Prakash *et al.* [104] and revealed no significant influence on the antisense strand, regardless at which position, in contrast to the sense strand. Ingale *et al.* [105] considered the changes in duplex stability upon 2'-fluoro modifications in a double strand with base-pairing partners bearing the same sugar modification, a deoxy- or a ribose-sugar. These sugar-, but also sequence position dependent modifications revealed, *via* melting temperature experiments, increased helix stability in the case of fluorine-fluorine combination and the lowest stability for a 2'-fluoro modification combined with an opposing deoxyribose sugar.

Thus, the cited physicochemical and biological effects of synthetic nucleoside modifications must be kept in mind for the design and synthesis of RNA and DNA constructs, depending on each individual application purpose.

1.3 Toll like receptors (TLRs) and innate immunity

Innate immunity is associated with the sensing of pathogen associated molecular patterns (PAMPs) by germline-encoded pattern recognition receptors (PRRs), which results in the activation of certain signaling cascades and subsequent immune response. These receptors are recruited to discriminate *i.e.* non-infectious self from possible infectious non-self nucleic acids, through scanning of differences in localization, structure and modifications [106], [107]. Consequently, adaptive immunity is also influenced to build an immunological memory. To understand the origin of immune response eliciting nucleic acid structural details, which are recognized as PAMPs, has a major role in deciphering mechanisms of bacterial and viral infections, autoimmune diseases, and cancer biology [107]. By implication, gained insights can be translated into the development and evaluation of therapeutic nucleic acids [108], [109].

Among the germline-encoded PRRs of the innate immune system, Toll-like receptors (TLRs), a class of membrane associated extracellular and endosomal receptors (Figure 1.2), that are involved in the process of uptake and endocytosis, play an essential role in pathogen survival through the inspection and discrimination of exogenous material [110]. First discovered in *Drosophila melanogaster* as mediators of a conserved signaling pathway [111] and assembled by Roach *et al.* [112] in a molecular tree of all known vertebrate TLRs, one can distinguish between six major sequence-related families, each recognizing a certain class of PAMPs. Although, this phylogenetic tree comprises several subfamilies from different species, one consider TLR1-10 as key mediators in human and mice, plus TLR11-13, which are restricted to the mice genome [113]. Their respective signal transduction pathways are summarized in Figure 1.2.

The extracellular receptors TLR1 and TLR6 form heterodimers with TLR2 upon activation with bacterial triacyl- and diacyl lipopeptides, respectively [114]. Further on, TLR2 itself senses *e.g.* lipoteichoic acid from bacteria and mycobacteria, as well as lipoproteins from mycoplasma or Gram-negative bacteria [110]. TLR4, which was the first identified, presents a special case, as it is internalized to endosomes in some cases, and signals therefore *via* two different pathways, mediated by the myeloid differentiation primary-response protein 88 (MYD88) or endosomal *via* the Toll-IL-1 (TIR)-resistance domain-containing adaptor protein inducing IFN β (TRIF) [115]. Thereby, TLR4 can be activated by lipopolysaccharides (LPS) with the help of the myeloid differentiation factor 2 (MD-2). The activation of homodimer TLR5 is triggered then by flagellin, a protein contained in bacterial flagella [116]. The ligand for human TLR10 remains still unknown, but the receptor dimerizes similar to TLR1 and 6 with TLR2. Finally, mouse TLR11, was shown to respond to uropathogenic bacteria and a profilin-like protein from *Toxoplasma gondii* together with TLR12 [117].

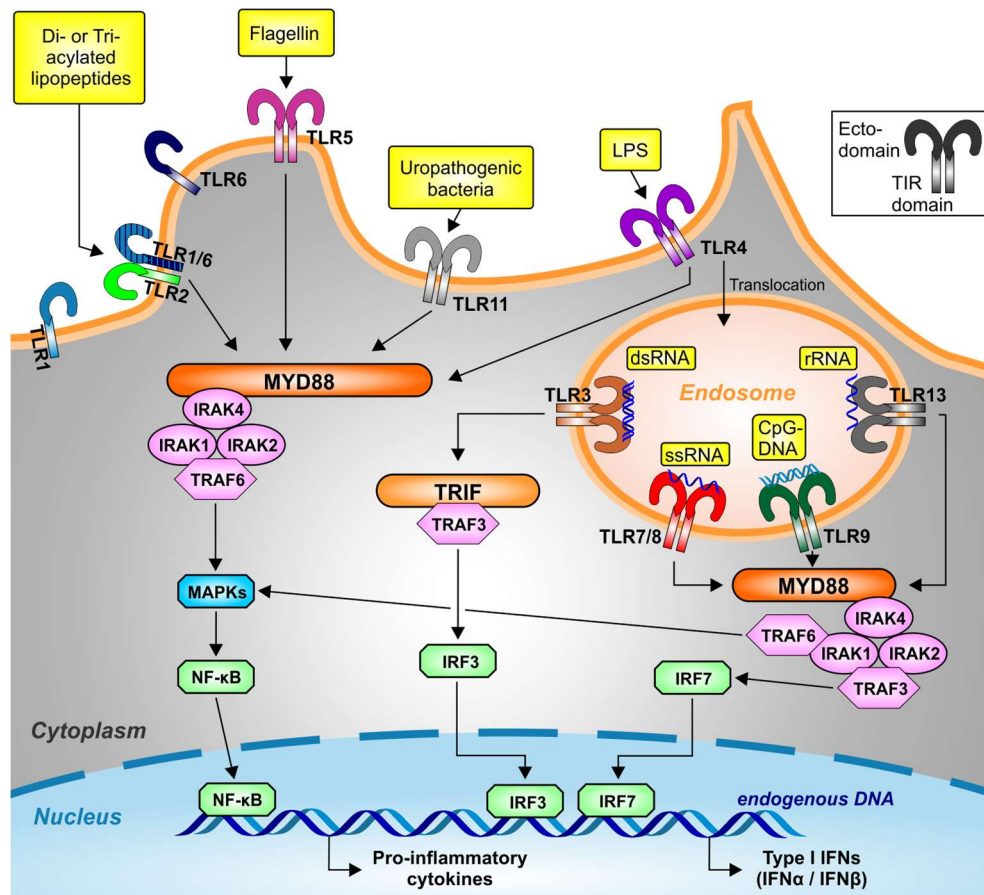


Figure 1.2: Compilation of extracellular and endosomal Toll-like receptors, their pathogenic ligands, signaling pathways and induced expression of cytokines. The set of extracellular receptors induces, via the MYD88 mediated pathway and adaptor proteins, the translation of pro-inflammatory cytokines, such as TNF. Associated TLR-activation mechanisms are triggered: by acylated lipopeptides for heterodimers of TLR1 or 6 (light and dark blue) with TLR2 (light green); for the following homodimers, through flagellin for TLR5 (purple); by fragments of uropathogenic bacteria for TLR11 (light grey) and in the case of TLR4 (dark purple) by lipopolysaccharides (LPS). Endosomal presented, are the nucleic acid sensing TLRs 3 (brown), 7 and 8 (red), 9 (dark green) and 13 (dark grey), which signal via MYD88, except TLR3 and internalized TLR4 via TRIF. (Figure adapted from O'Neill *et al.* [118])

The group of endosomal TLRs consist of the nucleic acid sensing TLR3, 7, 8, and murine TLR13, which recognize microbial RNA, and TLR9, which is involved in sensing of CpG-DNA [119]. Double stranded RNA above a required length of ~40 nucleotides, together with synthetic double strands of a polyribinosinic-polyribocytidinic (poly(I:C)) as well as a poly(A:U) sequence [120], is the trigger of TLR3 activation [121], [122], whose crystal structure was one of the first published TLR structures [123]. However, short siRNA is suspected to induce TLR3 signaling as well, albeit in different binding manner [124]. TLR13 responds specifically to a 13-base sequence from bacterial 23S rRNA, which can be abolished by N6-methylated adenosine [125]–[128]. The key players of the current work, TLR7/8, recognize in particular single stranded RNA and PAMP structure featuring small molecules [129]–[134]. Their individual associated activation modes are discussed in detail in

Section 1.3.1. Briefly, signaling modes, as illustrated in Figure 1.2, initiated through the PAMP recognition *i.e.* by TLR7/8 leads after homodimerization of the receptor to the recruitment of the adapter molecule MYD88 and the TIR domain of the respective TLR. Further recruiting of a kinase (IRAK-4) leads to phosphorylation and activation of a second kinase (IRAK-1), that it is in the following associated by TRAF6 (tumor-necrosis-factor-receptor-associated factor 6). The latter assembles again a protein kinase complex, which mediates the activation of two branched pathways. One of them leads *via* the mitogen-activated protein kinase (MAPK) pathway and the other *via* another kinase complex (IKK), both inducing NF κ B (nuclear factor kappa-light-chain-enhancer of activated B cells) to enter the nucleus and the expression of pro-inflammatory cytokines [118], [135]. A few differences exhibits the pathway towards the expression of type I interferons (IFN- α and - β), also MYD88 dependent, this leads *via* the recruitment of IRAK-4 and -2 over TRAF3 to the IRF7 dependent interferon translation after its entry into the nucleus.

In addition to the above mentioned mechanisms, nucleic acid recognition is not only reserved to TLRs, but is also essentially occupied by cytosolic factors like RIG-I (retinoic acid inducible gene I) [136]–[138], MDA-5 (melanoma differentiation-associated protein 5) [139], AIM2 (absent in melanoma 2) [140]–[143] and cGAS (cGAMP synthase) [144], [145], which are currently in the focus of further understanding molecular processes of nucleic acid driven immunity [146].

1.3.1 TLR 7 and 8: ligands and mechanisms

Among human peripheral blood mononuclear cells (PBMCs), which comprise professional APCs like plasmacytoid dendritic cells (pDCs), B cells and monocytes, together with natural killer cells (NK cells) and T cells, TLR7 and 8 (TLR7/8) differ in their expression pattern [147]. Where TLR7 appears to be highly expressed in pDCs and at minor levels in B cells inducing the secretion of type I IFN, TLR8 is mainly present in monocytes and NK cells with the secretion of TNF [134], [148]. TLR7/8 are, as the whole TLR family, type I integral membrane glycoproteins, with extracellular N-terminal leucine-rich repeats (LRRs). These contain 19-25 tandem LRR motifs, each comprising a length of 24-29 amino acids with conserved motifs [110].

The signaling pathways to the expression of cytokines for TLR7/8 were already outlined above (Section 1.3). Here, the focus lies on the actual activation mechanisms, which initiate receptor dimerization and signal transduction, the basis of the studies in Section 3.2. Although, expression patterns of TLR7/8 differ, both exhibit very similar ligand recognition, which is very likely due to their high sequence homology [131], [149]. They play one of the major roles in the discrimination of self and non-self RNA and related structural elements. However, before this was revealed by researchers around Akira in 2004 [131], [132], TLR7 action was prior assigned to the recognition of small molecule (SM) antiviral agents from the imidazoquinoline family (see Section 1.3.1.1), namely imiquimod and resiquimod (R848) by Hemmi- and Jurk *et al.* in 2002 [129], [130]. Since then, an increasing number of facts about the ligand binding preferences and activation mechanisms could be brought to light, although, first insights were examined *via* homology modeling [150], [151] and

final information on crystallographic structures of TLR8 were available just since 2013 and of TLR7 even since 2016 (last year), both revealed by the Shimizu group [152], [153].

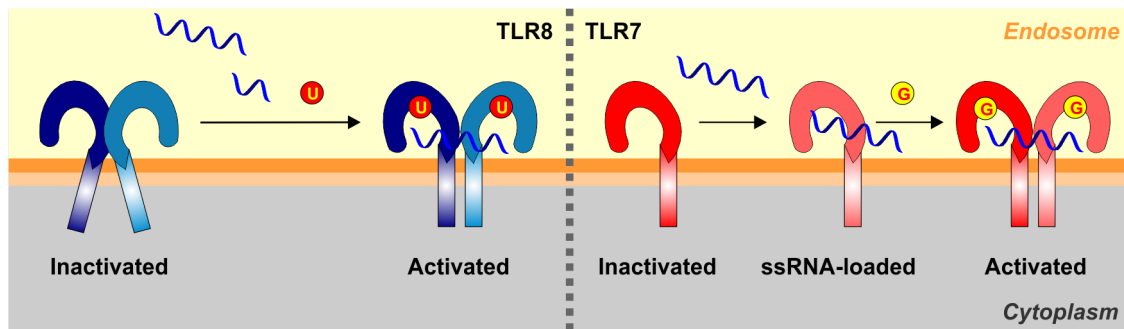


Figure 1.3: Schematic overview of activation mechanisms for endosomal TLR8 and 7 with their specific ligands and binding sites. From inactive receptors to activated homodimers: **(A)** inactive TLR8 dimer, is activated by U in the first site and reacts to ssRNA (GU-containing) in the second site, **(B)** inactive TLR7 monomer, dimerizes to the active form by ligand binding in the first site by G and reacts to ssRNA (U-containing) in the second site. (Figures adapted from Tanji *et al.* and Zhang *et al.* [153], [154])

As illustrated in Figure 1.3 and concluded by Maeda and Akira [155], the similarities in PAMP recognition by TLR7/8 lie in that they possess two distinct different binding sites, one, the so-called 1st site, for small molecules and RNA degradation products, respectively, and another, the 2nd site, for the polymeric ssRNA molecule. A further structural common feature is the Z-loop, which connects the N- and C-termini of the horseshoe monomer in the LRR and is cleaved upon receptor activation (dimerization), a conserved characteristic they share with TLR9. Refined distinctions between the two receptors were published in the time frame of the last four years, regarding both, human and mouse TLRs. Starting chronologically, the investigations on TLR8 activation by means of its crystal structure by Tanji *et al.* [152], [154] showed, that the inactivated receptor exists as preformed dimer including a cleaved Z-loop, but still associated ectodomains. Complete dimerization happens upon ligand binding (Figure 1.3), which is distinguished between the ssRNA binding in the second site and uridines from degradation, or respectively SM-TLR8 ligands, in the first site. Colak *et al.* [151] observed also two different “modes” of signaling and transcriptional events depending on the class of ligand. In contrast to TLR8, which was characterized as uridine-sensor, TLR7 recognizes guanosine and SM derivatives in the 1st site [156]. Zhang *et al.* [153] finally published the monkey TLR7 crystal structure (96.8 % sequence identity with human TLR7) and studied the activation mechanism by means of several combinations of SMs (guanosine, loxoribine and R848) and a poly-U RNA, revealing a similar behavior as described above for TLR8. However, TLR7 exists in the inactivated and RNA-only bound state as a monomer and dimerizes upon occupation of the 1st binding site. Thus, essential for both receptors, a ligand bound in the first site seems to be obligatory for the activation by ssRNA *via* the second site, but the occupation of

the 2nd site is *vice versa* not necessary for the recognition of nucleosides or small molecules *via* the 1st site. The following two sections depict the types and characteristics of TLR7/8 ligand variants.

1.3.1.1 Occupier of the 1st site: RNA fragments & small molecule agonists

As elucidated above, the TLR7/8 crystal structures proved the binding of nucleosides G and U, presumably from RNA degradation, in the first site of the receptor ectodomain, which is analogous to that for small molecule TLR agonists (smTLRa), a compendium of guanosine analogs *i.e.* of imidazoquinoline based molecules (Figure 1.4). These synthetic immune modifiers are applied or at least studied as potential vaccine adjuvants in viral diseases as well as in cancer therapy. To date, imiquimod is still the single representative as therapeutic agent itself, formulated as Aldara™, which was found as potential topical treatment for skin cancer, after it was applied actually against *human papillomavirus* (HPV) derived genital warts [157]. Its activation properties are restricted to TLR7 and primarily to the induction of IFN- α secretion, the same counts for the further developed derivative gardiquimod [158] and the guanosine analog loxoribine [159], [160]. Resiquimod, again a strong imiquimod derivative known as R848, is a potential ligand for both receptors, but reached so far only clinical phase II [109]. The respective binding mode was, as well as for loxoribine, analyzed on the recently published crystal structure of TLR7 by Zhang *et al.* [153] and is considered in more detail in Section 3.2.3.

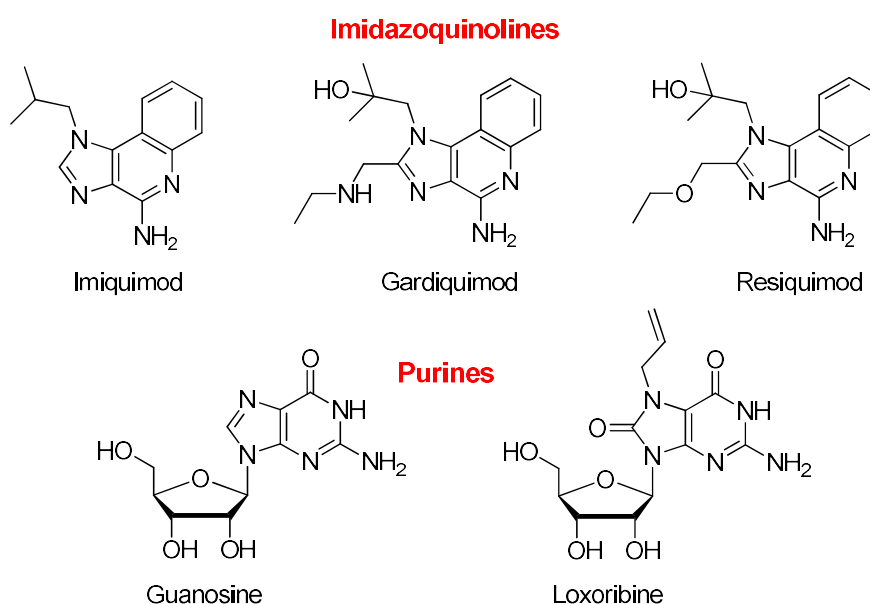


Figure 1.4: Selection of small molecule TLR7/8 agonists of imidazoquinoline- and guanosine based structures.

Small structural variations on these molecules can provoke huge differences in activity, for instance, Shukla *et al.* [161] created with an 3H-regioisomer of gardiquimod complete inactivity of the molecule and an antagonist through further deamination. However, promising studies could show

that antigen-TLR7/8 conjugations for vaccination induced improved quality of immune response [162], but more insights into structure-activity relationship still remain to be revealed.

1.3.1.2 Occupier of the 2nd site: Nucleic acid agonists

The recognition of RNA could be attributed for both receptors to the second binding site [153], [154] and has been described as unique for single stranded RNA [107], [131], [132], which is true for single-stranded regions of mRNA [163] and was monitored even for double-stranded siRNA with two nucleotide 3'-overhangs in PBMCs [164], which lack the actual dsRNA receptor TLR3. siRNA single strands, depending on their sequence/U-content, equal if sense or antisense strand, exhibited stronger immune answer than their respective double strands [165], [166], which has to be considered in therapeutic applications [167]. However, recently published results about bacterial tRNAs, which have a highly structured architecture, and their recognition referred to three structural domains, with only one truly single-stranded [90], [91], might be discussed. A phenomenon, unveiled among others by these studies, was the important strategy to discriminate self from foreign RNA through the recognition of (post-transcriptional) modified nucleotides. Originating from evolutionary developments of RNA [168], a complex variety of nucleotide modifications exists in eukaryotic RNA and, although to a less extend, in bacterial or viral species. Even small modifications as ribose 2'-O-methylations were shown, in a specific sequence context [90], [169], [170], to function as TLR7 antagonist, and could also be observed *in vivo* [89], [171]. Besides inhibiting the recognition by TLR7 of such modified RNA, it even impeded the sensing of co-incubated unmodified, usually stimulatory RNA by just a single 2'-O-methylation at position 18 in the whole sequence of the applied tRNA [90], [91]. It has to be discussed in the future, if the underlying mechanism of this inhibiting effect takes place at a distinguishable site from the activation side. As the latter needs only a trinucleotide to be induced, the impediment by a single 2'-O-methylation throughout a sequence of around 80 nucleotides appears not that insurmountable and provides the structural requirement to activate this mechanism. Karikó and Weissman addressed the immunosuppressive influence of a series of nucleoside modifications [168], [172], such as m⁵C, m⁶A, m⁵U, s²U and Ψ, which are *i.e.* highly abundant in different RNA species and led, especially in the case of Ψ [173], to the suppression of TLR signaling of *in vitro* transcribed RNA.

The presented aspects on the modulation of endosomal TLR7/8 immune response are of high relevance in the design of therapeutic RNA, e.g. in the development of mRNAs for tumor vaccination [174] or in diverse approaches of RNAi [92], [175]. Inhibition of TLR7 stimulation could be on the one hand desirable, as e.g. to limit immunostimulatory side effects by siRNA [87], [88], [176]. Or on the other hand, an intended boost in innate immune response is favorable for nucleic acid derived adjuvants to augment the efficiency of certain vaccines [109], [177], [178]. Very recently, this strategy found a highly relevant application in search of potential vaccines for the explosive pandemic of *Zika virus* [179], through the cooperation of known researchers and companies in this field.



2 Motivation and Objectives

Conversion of deoxyuridine to a “clickable” deoxycytidine

The development of bioconjugation techniques, to label or install certain functionalities on DNA and RNA molecules, as handles to study and manipulate key features of nucleic acids chemistry for further diagnostic and therapeutic approaches, are of great interest. One convincing strategy within this context of molecular biology is presented by the application of bioorthogonal “click chemistry”, e.g. in its version of the Cu(I)-catalyzed azide-alkyne cycloaddition (CuAAC). On the nucleoside level, this can be enabled *via* the introduction of azide- or terminal alkyne-functionalities, e.g. at exocyclic amines of the nucleobases. As such, the current study envisaged to generate an alkyne-functionalized deoxycytidine for incorporation as phosphoramidite into nucleic acids.

Due to the important role of secondary and tertiary structure in the biological performance of nucleic acids, possible influences on these nucleic acid characteristics upon chemical alterations, even if these are as small as the above-mentioned functionalities, have to be taken into consideration and require investigations on physicochemical and biological behavior. These involve in particular variations in base pairing properties, which are again influenced through changes in stacking interactions, hydrophobicity or van der Waals interactions.

Therefore, it was of interest in the current study to determine the effect of the alkyne functionalized deoxycytidine on the nucleoside and nucleotide level concerning its impact on thermodynamic stability of the resulting DNA and RNA duplexes, with regard to varying sequence positions.

Steric shielding of RNA from recognition by TLR7 & 8

A series of severe human diseases, such as autoimmune diseases like *systemic lupus*, cancer development and infections from bacterial or viral pathogens, underlie the mechanisms of the immune system. Further on, geno- and phenotype of these diseases very likely vary from patient to patient, which is the reason, why the development of personal treatments could deliver promising prospects. Here, genetically based immunotherapy comes into play, which can be more conveniently addressed on the RNA-level, than on the DNA-level hidden in the nucleus, and would as transient gene therapy accommodate patient compliance.

The initial motivation, which finally led to the notion to develop suitable (m)RNA constructs, to manipulate the innate immune response by human immune cells, in that they gain the potential to possess a boosted immunostimulatory effect upon activation of endosomal Toll-like receptors (TLR) 7 and 8, was influenced by the work of Colak *et al.* [151]. Via the comparison of a homology model of the already existing crystal structure of TLR8 [152], they revealed distinct recognition sites and activation models of TLR7 for small molecule imidazoquinoline compounds and single-stranded RNA. This drove the idea to combine both activation patterns in one bidentate agonistic ligand to stimulate both pathways at a time, which was supposed to elicit an increased immune response. An appropriate method, offered by the bioorthogonal CuAAC click reaction, had to be chosen to generate a covalent linkage between a small molecule - and a ribonucleic acid TLR agonist, which required to provide both actors prior with suitable functional groups. In order to discuss this concept in a sufficiently wide context, a series of, both, small (siRNA) and large (mRNA), constructs varying in type and frequency of attached molecules had to be considered. Taking into account, that these nucleic acids may serve as well for possible therapeutic purposes, due to their original function in RNA interference and protein expression, attention had to be drawn also to their remaining biological activity.

3 Results and Discussion

3.1 Conversion of dU to a “clickable” deoxycytidine for incorporation into oligonucleotides: juxtaposition to its opponent, a 5mdC derivative.

Bioconjugation techniques to label or install certain functionalities on DNA and RNA for diverse applications are of great interest, not for some time only in the field of basic research [180], but more and more in diagnostic [181], [182] and therapeutic applications [175], [183]. The feature of biorthogonality is highly favored within this respect and presents one convincing advantage of the Cu-catalyzed azide-alkyne cycloaddition (CuAAC), a member of the so called “click-reactions”. This involves usually the introduction of azide- or terminal alkyne-functionalities, *e.g.* at the nucleobase *via* its exocyclic amine. Despite the small size of these functional tags, the possibility still exists that the intrinsic characteristics of the nucleic acid may be compromised upon such chemical alteration. Particularly, the effect of artificial modifications directly on the H-bond interacting edges and its impact on the thermodynamic stability of the resulting duplexes was of interest in the current study. Among natural modified nucleosides, there are several that feature a further moiety on their exocyclic amines *e.g.* *N*⁴-methylcytidine (*m*⁴C) and *N*⁶-methyladenosine (*m*⁶A) [184]–[186], whose free hydrogen was able to point to the Watson-Crick edge in a double helix, *i.e.* shown by Cervi *et al.* on [187] *m*⁴C. Yet, bulkier examples are not tolerated in standard base pairing and are therefore restricted to single stranded regions [68], [188]. Along with earlier reports, that applied alkylation of exocyclic amines [189]–[191], the Helm group published the introduction of a sugar edge *N*²-propargylated guanosine into the 5'-end of an siRNA antisense strand [36], exhibiting only minor effects on RNAi activity and structure. This functionality per se was so far not investigated in that manner. Therefore, the actual study was driven by the idea, that amongst natural occurring modified cytidines no representative of a double modification was known to that point, which occupied both, the “CH”-edge and possibly the W-C side *via* the exocyclic *N*⁴ at the same time. A synthetic 5-methyl-2'-deoxycytidine-*O*-allylhydroxylamine adduct of the Carell group [192], was at that time the only one investigated. This species featured a steric repulsion of the 5-methyl group and the flexible ligand at position 4, which led to a restricted rotation around the C⁴-*N*⁴ bond and the propensity for a W-C interfering *s-cis* conformation. Thus, as already indicated, this work strived to synthesize and bring out the different effects of *N*⁴-propargylated cytidines, with and without a C⁵-methylgroup, on the physicochemical properties of the nucleosides and respectively modified oligonucleotides.

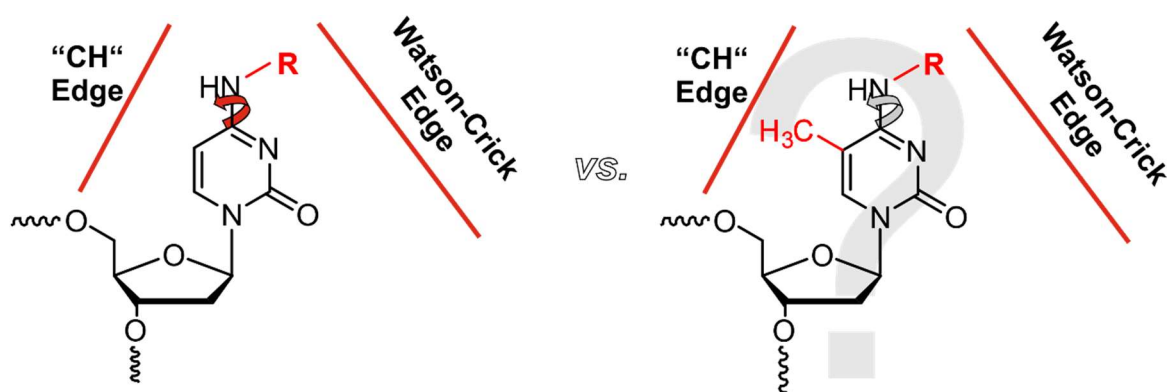


Figure 3.1: Hypothetical consideration of the orientation of N^4 -substituents on cytidines. (a) A single modification (**R**) on the exocyclic amine of cytosine has likely the chance to orient toward the Watson-Crick edge, or be twisted toward the "CH"-edge, thus enabling normal Watson-Crick base pairing within a double helix. (b) An additional methyl group on position 5 of the pyrimidine ring, might impede this free rotation through a steric clash. (Figure designed and published together with Dr. Domingo [193])

An unconventional approach was conducted to synthesize the modified cytidine-derivative, by using 2'-deoxyuridine (dU) as starting material. An early introduction of the 5'-O-DMT group [194] was followed by incorporating an easier leaving-group, the aryl sulfonate ester, onto O⁴ of dU. A reaction with propargylamine made possible the conversion of dU to the cytidine derivative [195], which contains a „clickable“ moiety on its exocyclic amine. A conventional step was followed for the introduction of the phosphite triester onto the 3'-O-position. Further on, the resulting phosphoramidite (PA) was introduced into a DNA sequence by means of solid phase oligonucleotide synthesis (SPOS), which resulted in seven strands, each containing the modification at a varying position. For the comparative investigations of the recent study, this procedure was in parallel conducted for the 5mdC-derivative [redacted].

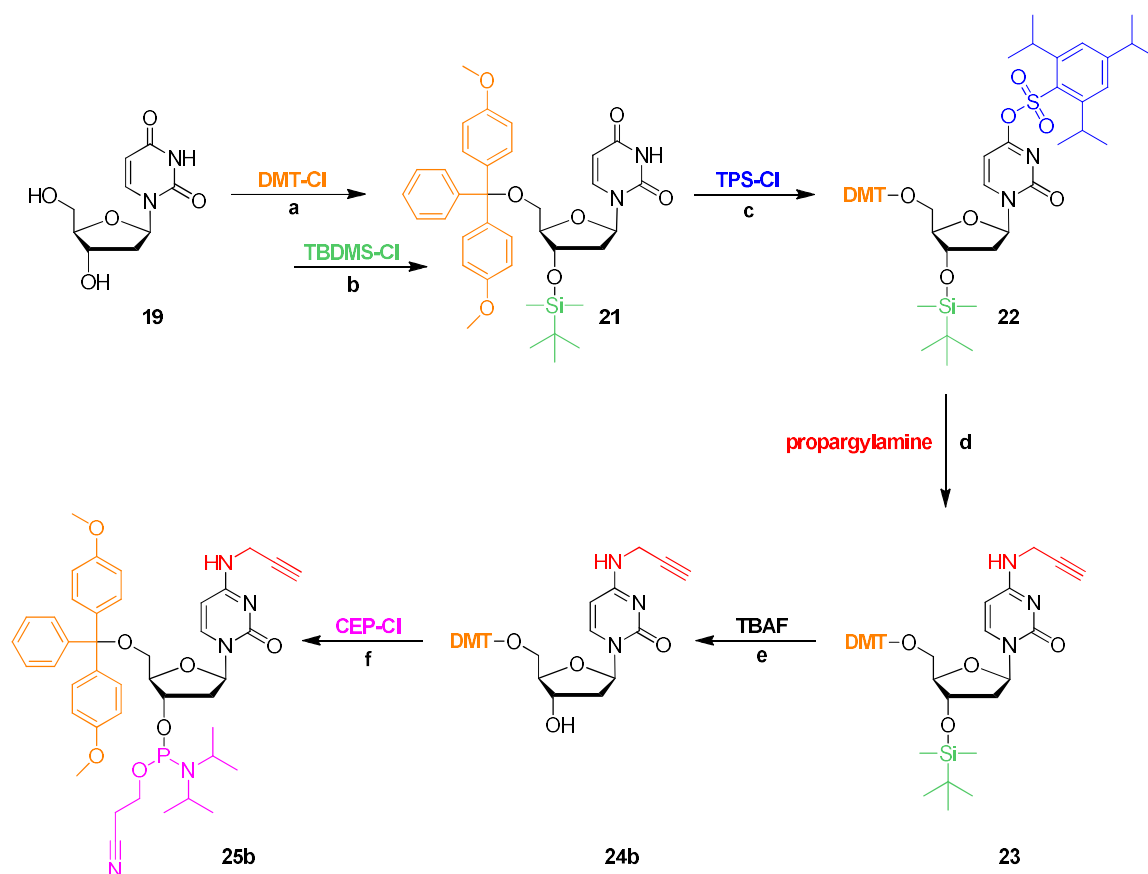
To study the orientation of the propargyl group on the exocyclic N^4 of the cytidines on both, the nucleoside level and in an ODN context, the free nucleosides were obtained from the same phosphoramidite precursor and were subjected to 2D NMR experiments concerning rotating-frame nuclear Overhauser effect spectroscopy (ROESY-NMR) investigations, which were kindly conducted [redacted].

After hybridizing the differently modified sense strands to the same-length (22mer) complementary unmodified DNA antisense strand, measurements of the thermodynamic stability of the different duplexes were pursued by accessing UV-melting profiles. An extension of this topic was made toward DNA strands featuring abasic sites opposite selected modified positions, helping to get a deeper insight into the hypothesized orientation behavior of the respective cytidine derivatives. Finally, it was of interest to assess the "click"-ability of the synthesized alkynylated oligonucleotides as single and double strands, to see whether the structural differences exhibit an influence in fluorescent labeling.

This chapter contains research, which was published by Domingo and Hellmuth *et al.* [193].

3.1.1 Nucleoside modification and phosphoramidite synthesis

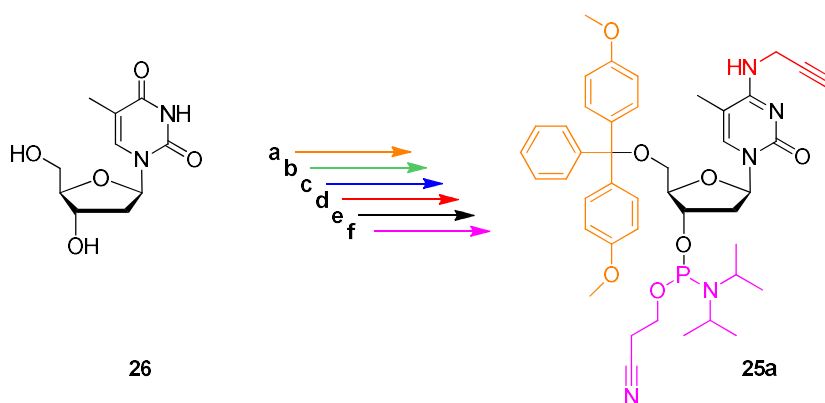
The crucial part for the synthesis of the modified cytidines to be studied in this work, was the interconversion of 2'-deoxyuridine at the C⁴-carbonyl to the desired amine functionality. Already half a century ago, this was also the topic of the first chemical synthesis of 5-methyl-2'-deoxycytidine by means of thiation (known as well as thionation) [196], which involved the amination of a 4-thio intermediate. Another approach for the U to C conversion, which mainly influenced the current work, was in 2011 essential for the studies of Hansen *et al.* [194] concerning the synthesis of 5-hydroxymethyl-2'-deoxycytidine and at the same time for the group around A. Heckel [197], who focused on the labeling of dC and dA at their exocyclic amines with photolabile "caging" groups. Both involved the temporal incorporation of an activating trisopropylbenzenesulfonyl group, which was later substituted with the favored amine.



Scheme 3.1: Synthesis of the CpDCII phosphoramidite building block **25b**. Reaction conditions and respective yields for (a) the 5'-O-tritylation: DMT-Cl (4,4'-dimethoxytrityl chloride), pyridine, RT (83 %), (b) the 2'-O-protection: TBDMS-Cl (*tert*-butyldimethylsilyl chloride), DCM, RT (98 %), (c) the incorporation of the better leaving-group: TPS-Cl (2,4,6-trisopropylbenzenesulfonyl chloride), DCM, RT (53 %), (d) the aminolysis: propargylamine, dioxane, RT (33 %), (e) the desilylation: TBAF (tetrabutylammonium fluoride), THF, RT (91 %) and (f) the PA formation: CEP-Cl (2-cyanoethyl-*N,N*-diisopropylaminechlorophosphoramidite), DCM, RT (60 %). (Procedure as published in Domingo *et al.* [193])

The synthesis route towards the phosphoramidite building block of the *N*⁴-propargylated 2'-deoxycytidine derivative *CpDCII* **25b** comprised six reaction steps as depicted in Scheme 3.1. Starting from 2'-deoxyuridine **19**, the DMT-group was installed early at the 5'-end in a so called tritylation reaction of the alcohol and followed by an additional, temporary protection of the 3'-hydroxyl group of the ribose with a *tert*-butyldimethylsilyl (TBDMS) residue, allowing the orthogonal incorporation of the activating sulfonyl ester at the carbonyl-O at position four of the pyrimidine by 2,4,6-triisopropylbenzenesulfonyl (TPS) chloride and a catalytic portion of 4-*N,N*-dimethylaminopyridine. Alike the convertible nucleoside approach [40], [41], the key step of the uridine to cytidine conversion involved the substitution of this good leaving group through aminolysis with propargylamine [194], which turned out to be preferably applied in an excess of 20 molar equivalents amine reactant. After removal of the silyl ether protecting group by the quaternary ammonium fluorine salt TBAF, the otherwise protected nucleoside was equipped at the 3'-position with the essential 2-cyanoethyl-*N,N*-diisopropylaminechlorophosphoramidite by standard phosphitylation. Purification by column chromatography, as it was applied for the preceding steps as well, afforded the desired building block **25b** with a yield of 60 % and an overall yield for the six synthesis steps of 8 %.

As part of the collaboration with Dr. Olwen Domingo on that topic [193], the described procedure was applied analogously by her to synthesize the respective phosphoramidite of the methylated counter-part in this study, 5-methyl-2'-deoxycytidine, starting from thymidine **26**, ending with an overall yield of 1 % for *CpDCI* **25a** (Scheme 3.2).



Scheme 3.2: Synthesis of the *CpDCI* phosphoramidite building block **25a**. Reaction conditions are equal to those described in Scheme 3.1, with corresponding yields for (a) the 5'-O-tritylation: 94 %, (b) the 2'-O-protection: 87 %, (c) the sulfonylation: 50 %, (d) the aminolysis: 10 %, (e) the desilylation: 42 % and (f) the PA formation: 52 %. (Procedure as published in Domingo *et al.* [193])

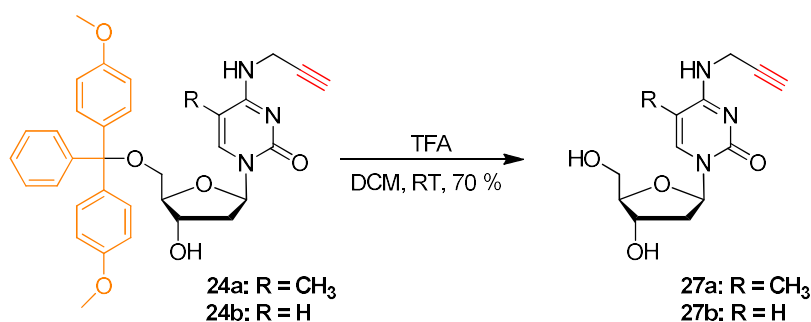
For the subsequent automated oligonucleotide syntheses in Section 3.1.3.1, further protection of the nucleobases, as is in general necessary for cytidinic amines during SPOS, was redundant through the already existing *N*⁴-functionality.

3.1.2 Orientation of the propargyl group on the nucleoside level

An N^4 -substituent attached to a cytosine has in general the possibility to turn into a *cis*- or a *trans*-conformation regarding the position towards the carbonyl-oxygen. As this can be substantially influenced by surrounding conditions, there will be usually a preference for one of the conformations, as investigated by the groups of Hippel and Becker [198], [199], which was the case in presence of a further modification as a methyl group at the pyrimidine ring. Therefore, to transfer and investigate this for the current modified cytidines, which let assume a *cis*-direction to the Watson-Crick (W-C) edge for the N^4 -functionality of the nucleoside, a comparative study by NMR measurements, involving ROESY experiments, were conducted on the nucleoside level.

3.1.2.1 Preparation for ROESY-NMR experiments

For the 2D-NMR evaluation of the orientation of the N^4 -propargyl moiety of both cytidine-derivatives, they had to be prepared as free, unprotected nucleosides. Therefore, the two pre-phosphoramidites **24a** and **24b** were detritylated at the 5'-position through treatment with trifluoroacetic acid (Scheme 3.3), which yielded after column purification *via* silica gel chromatography 70 % of each nucleoside **27a** and **27b**. The reaction monitoring *via* thin layer chromatography indicated the formation of side products for both, which were identified as thymidine and 2'-deoxyuridine, respectively, and occurred most likely through an additional acid induced deamination, probably leading to the reduced yield for **27a** and **27b**.

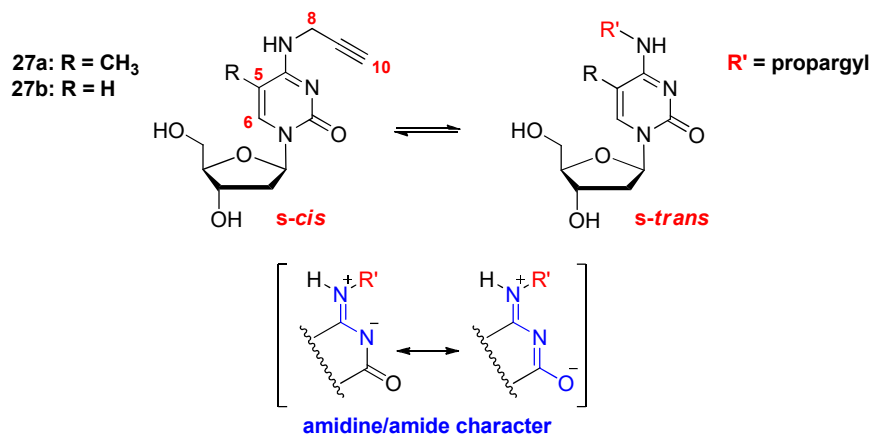


Scheme 3.3: Acid induced detritylation of 5'-O-DMT-5-methyl- N^4 -propargylaminyl-2'-deoxycytidine (**24a**) and 5'-O-DMT- N^4 -propargylaminyl-2'-deoxycytidine (**24b**) yielding the free nucleosides pCl (**27a**) and pClII (**27b**). (Procedure as published in Domingo *et al.* [193])

The investigation of the free nucleosides, for their preferred orientation of the exocyclic amine group, as part of a collaboration with [REDACTED], was now of interest and discussed in the next section.

3.1.2.2 ROESY-NMR spectroscopy

NMR techniques were employed to evaluate the orientation of the N^4 -propargyl in both nucleoside variants regarding a preferred direction toward the W-C face. As in Domingo *et al.* [193], ^1H -NMR spectra were obtained *via* measurements in a mixture of $\text{H}_2\text{O}/\text{D}_2\text{O}$ (9:1) at 278 K and the application of a double-pulsed field gradient spin-echo pulse sequence [200]. By means of ROESY-NMR and the Nuclear Overhauser Effect (NOE), it is possible to ascertain spatial proximities between interrelated atoms and thus, to determine the degree of rotation round a distinct bond axis [198], [201]. In the current case, two conformational isomers are conceivable for both derivatives, namely an *s-cis* or an *s-trans* as illustrated in Scheme 3.4. One could expect NOEs between $N^4\text{H}$ or H8 and either H5/ CH_3 or H6. Although, a certain energy barrier for the isomerization must be expected, resulting *i.a.* from a, *via* an amidine resonance hybrid conjugated, amide system, briefly a temporary C4- N^4 double bond character [199].



Scheme 3.4: Possible isomers of compound 27a/b, including resonance hybrid structures (blue).

Figure 3.2 A/B demonstrates for both compounds **27a/b** the preference for the *s-cis* conformer, which was reasoned from (missing) NOEs/ROEs. In detail spoken, no detectable ROEs for CH_3 -H8 of compound **27a** and accordingly, no H5-H8 signal for **27b**, plus no ROEs for H6 from both. However, evidences occurred for a CH_3 - $N^4\text{H}$ NOE in compound **27a** and analogously, an H5- $N^4\text{H}$ signal for **27b**. Still, cross peaks for H5 and H6 occurred in the acquired ROESY spectrum for Yb, caused by an exchange process between the *cis* and *trans* conformation. A ratio of 90:10 was observed for the two species A (*s-cis*) and B (*s-trans*), based on the evaluation of the two populations found. According to earlier published protocols [202], [203], specific exchange kinetics was acquired by EXSY spectra at varying temperatures (273-288 K) and mixing times (10 to 1000 ms) (Figure 3.2 C and annexed in **Figure B.X**). Data concerning H5 could not be adduced for kinetics acquisition through impairing resonance overlap, nevertheless H6 delivered exchange data for the evaluation. Figure 3.2 D (details in **Figure B.X**) illustrates the activation barriers for the isomerization ($E_a(\text{AB}) = 27 \text{ kcal mol}^{-1}$; $E_a(\text{BA}) = 19 \text{ kcal mol}^{-1}$), which were calculated using the temperature dependence of the rate constants and implying a ΔH of $7.81 \text{ kcal mol}^{-1}$ between both

conformations of **27b**. A difference in Gibbs free energy (ΔG) around 1.1-1.4 kcal mol⁻¹ could be determined through the comparison of the ratio of the two populations at the applied temperatures.

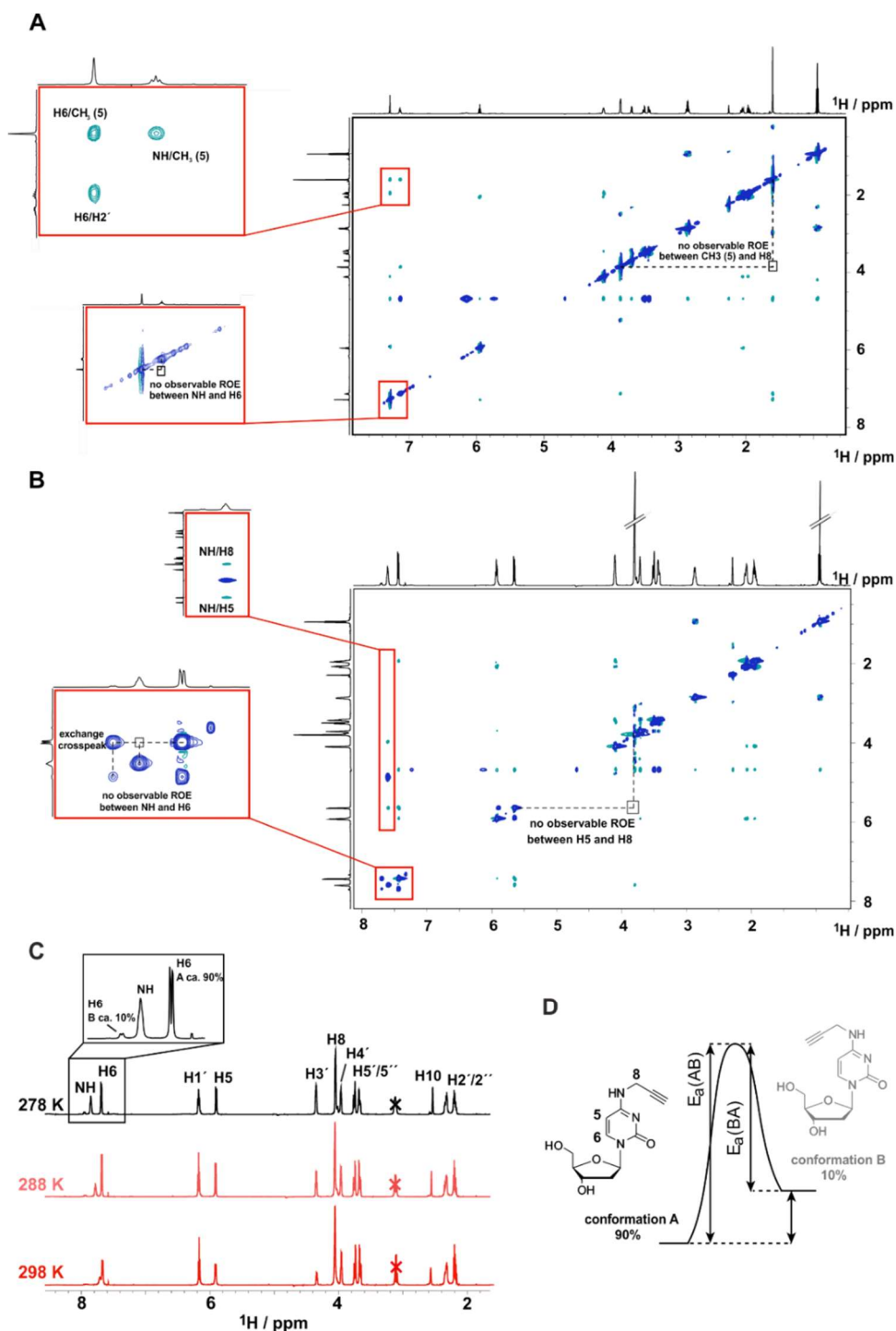


Figure 3.2: ROESY NMR measurements of the two respective deprotected cytidine derivatives (**27a** and **27b** in Scheme 3.3), either (**A**) with or (**B**) without a methyl group on position 5 of the pyrimidine. In both cases, the propargyl preferentially adapts an *s-cis*-conformation, but a minor population of *s-trans*-conformation was also found in **27b** by inspection of chemical exchange in the H6 signal (red and black boxes) (**C**), which was identified in depth at various temperatures to derive activation energy and thermodynamic parameters for the equilibrium between both conformations, as shown in (**D**). NMR experiments and calculations were kindly performed by [REDACTED]. (Fig. published in [193]).

3.1.3 Double helices confronted with the N^4 -propargyl moiety

The findings in Section 3.1.2, together with specified investigations on N^4 -substituted cytidines regarding the rotation about the exocyclic carbon-nitrogen bond and the stability of nucleic acids [198], [199], endorse a preference for the *s-cis*-conformation of the modified cytidine derivatives. Several publications dealt with resembling studies on N^4 -methylated cytidines, not showing any destabilizing effects in helical structures of oligonucleotides [41], [187], [204]–[208], which led to the assumption, that the present N^4 -propargylcytidine might show up in a similar manner. This included the hypothesis, that the propargyl group might in a double helix direct away from the Watson-Crick site for a sufficient base-pairing, which would demand a certain energy for the rotation from the preferred *cis*- to *trans*-conformation. Presumably, such could be delivered from the free energy of DNA duplex formation by hybridization [209]. The following section deals with this investigation on the basis of temperature dependent differential UV-absorption measurements, a method, which has been applied already in the past together with NMR studies in order to probe DNA structure [210], [211], and click chemistry with prior synthesized ODNs.

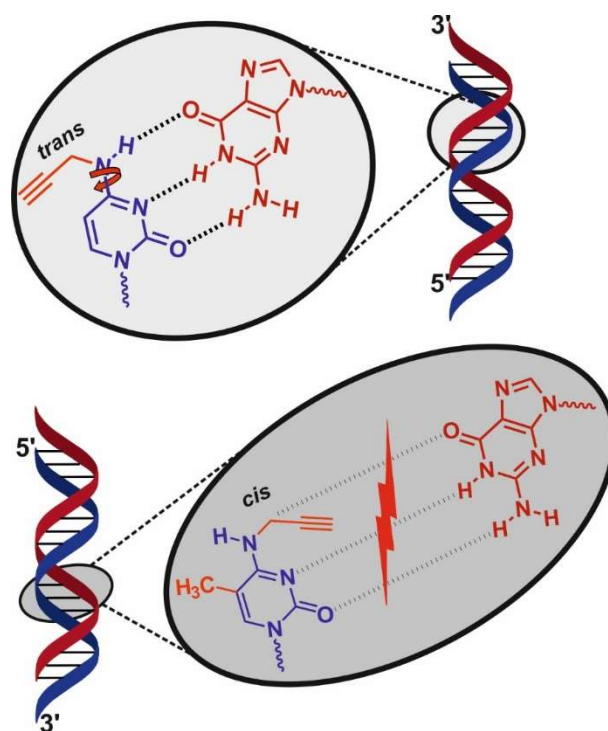
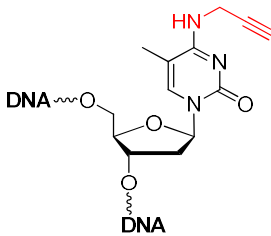
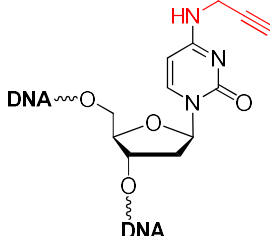


Figure 3.3: Proposed arrangement of Watson-Crick base pairing between guanosine and the N^4 -substituted cytidine derivatives, without and with a methyl group on position 5 of the pyrimidine. A free rotation of the propargyl group, away from the Watson-Crick edge during base pairing, is likely prevented, thus abolishing corresponding H-bonding completely. (Figure designed and published together with Dr. Domingo [193])

3.1.3.1 Incorporation of PAs into DNA strands: SPOS, purification & analysis

To look at the above-mentioned hypothesis from the angle of an oligonucleotide context, the methylated (*CpDCI*) and unmethylated (*CpDCII*) propargyl-cytidine derivatives were incorporated *via* SPOS into DNA strands of 22 nucleotides, bearing the model sequence of an anti eGFP-sense siRNA strand [36], which was synthesized as unmodified reference ODN0 as well (Table 3.1). The applied nomenclature for the corresponding modified oligonucleotides in Table 3.1, each bearing a single cytidine replaced by a propargylated one within its sequence, uses the position of substitution counted from the 5'-end and the type of modification, which uses 1 for the 5-methyl-*N*⁴-propargylaminyl-2'-deoxycytidine and 2 for the *N*⁴-propargylaminyl-2'-deoxycytidine replacements. Besides the substitution of the mentioned C-residues, one construct, ODN21, included the exchange of the penultimate nucleoside of the 3'-end, an adenosine contained in the siRNA 3'-overhang-region. This particular one, as well as ODN2, was intended to serve as object of comparison towards end- and internal labeling regarded in Section 3.1.3.2 and 3.1.3.3. In fact, this position was expected have the least influence on duplex stability, as a similar study on the alkylation of exocyclic amine of guanosine has shown [36].

Table 3.1: Sequences of the synthesized unmodified (ODN0) and the seven modified DNA oligonucleotides: Asterisks (*) indicate the positions of incorporated cytidine derivatives *CpDCI* (grey), synthesized by Dr. Domingo, and *CpDCII* (black) as part of this work. (Table as published in Domingo *et al.* [193])

	ODN0	
	5' -GCAAGCTGACCCTGAAGTTCAT-3'	
ODN2.1	5' -G*AAGCTGACCCTGAAGTTCAT-3'	ODN2.2
ODN6.1	5' -GCAAG*TGACCCTGAAGTTCAT-3'	ODN6.2
ODN10.1	5' -GCAAGCTGA*CCTGAAGTTCAT-3'	ODN10.2
ODN11.1	5' -GCAAGCTGAC*CTGAAGTTCAT-3'	ODN11.2
ODN12.1	5' -GCAAGCTGACC*TGAAGTTCAT-3'	ODN12.2
ODN20.1	5' -GCAAGCTGACCCTGAAGTT*AT-3'	ODN20.2
ODN21.1	5' -GCAAGCTGACCCTGAAGTTC*T-3'	ODN21.2

In customized syntheses on an Expedite 8909 DNA/RNA synthesizer (ABI/PerSeptiveBiosystems), all seven ODNs of 22mer length, each including the respective modification at the indicated position

in Table 3.1, were produced on a 1 μ mol-scale in “DMT-off mode” from thymidine-preloaded controlled pore glass, so was the reference ODN0. After deprotection and cleavage from the CPG, all strands were purified by PAGE separation and gel-extraction to isolate the full-length products, which were more error-prone, the nearer the modified PA was introduced to the 3'-end, as it was e.g. for ODN21.

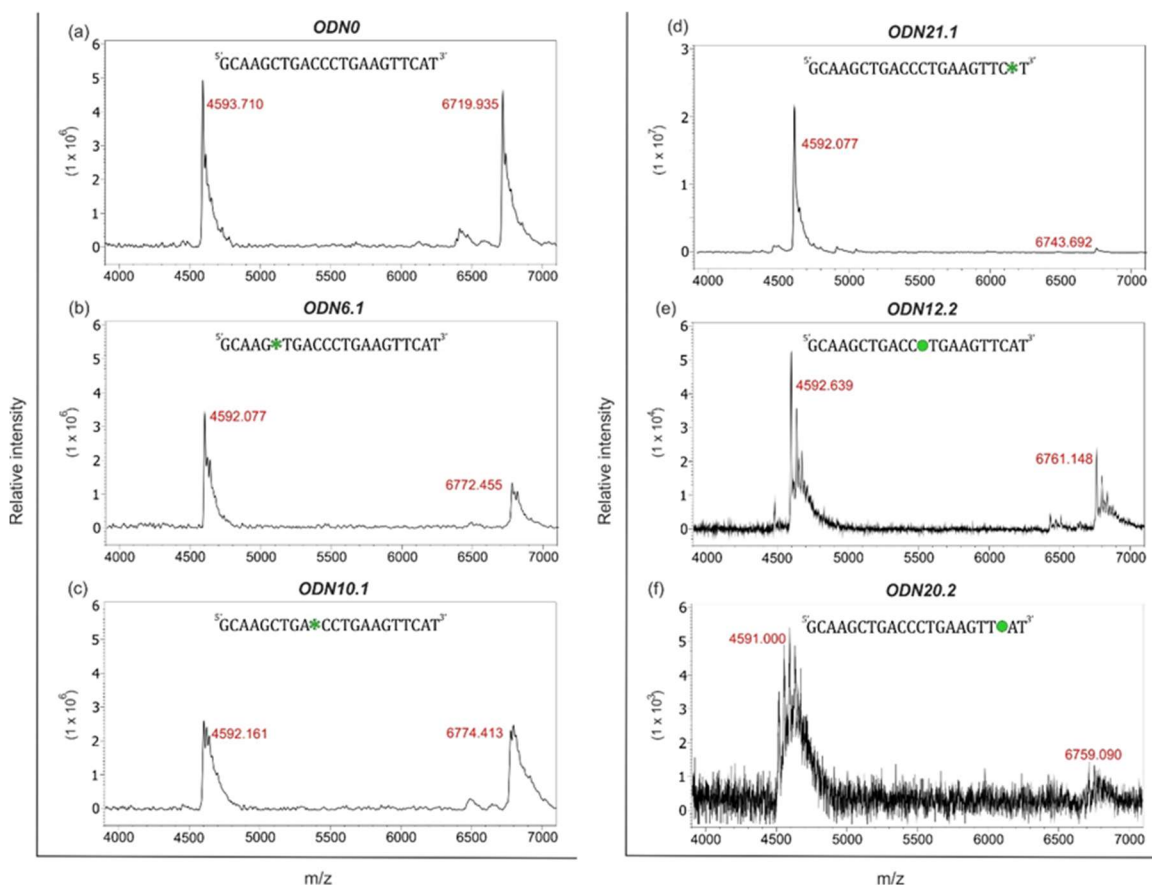


Figure 3.4: MALDI-TOF spectra of six selected in-house synthesized oligodeoxynucleotides. Besides the internal standard DNA strand (calculated m/z: 4592), displayed are the results for the following samples: **(a)** the unmodified strand ODN0 (calculated m/z: 6719); **(b)** the 5-methyl-*N*⁴-propargyl-2'-deoxycytidine (*) bearing ODN6.1 and **(c)** ODN10.1 (calculated m/z for both: 6771), **(d)** ODN21.1 (calculated m/z: 6747) and **(e)** the *N*⁴-propargyl-2'-deoxy-cytidine (●) carrying ODN12.2 and **(f)** ODN20.2 (calculated m/z for both: 6757). (Data as published in Domingo *et al.* [193])

Molecular masses of prior desalted DNA strands were determined through MALDI-TOF mass spectrometry [212], [213], kindly conducted by Heiko Rudy (Jäschke lab/Heidelberg). Figure 3.4 confirms the molecular masses by six exemplary MALDI-TOF spectra of the final fifteen ODNs considered in this study, each including a DNA oligonucleotide of 4592 g/mol and random sequence as internal standard. As calculated for the unmodified DNA strand ODN0, the MS measurement was expected to result around 6719 g/mol. C substitutions by the methylated derivative *CpDCI*

result in a calculated molecular weight of 6771 g/mol for these 22mers, and the respective one for an A exchange in 6747 g/mol. For the unmethylated CpDCII carrying strands it is calculated for 6757 g/mol and 6733 g/mol, respectively.

3.1.3.2 Hybridization and temperature dependent UV-absorption studies

The differentially modified sense strands, as well as the appropriate control ODN0, were hybridized to the same-length (22mer), complementary DNA and RNA antisense strands, respectively, in a 1:1 ratio to result in the final duplexes of siRNA character with 3'-overhangs of two nucleotides. An example of successful hybridization is depicted *via* gel analysis in Figure 3.6, exhibiting in an unlabeled and fluorophore-labeled fashion only a minimal residue of excess antisense-strand.

Regarding helix conformation, the DNA/DNA constructs usually form less stable B-type helices than the DNA/RNA hybrids, which were expected to assume the shape of an A-type helix structure with a likely increased duplex stability [214]. However, prediction of helix stability is not trivial and often dependent on neighboring nucleotides and the sequence itself [81], [215]. Moreover, the influence on helix geometry and stability is also affected by environmental salt-ion-conditions, since these interact with the polyanionic oligomers and shield the electrostatic repulsions emanating from their charged phosphate backbones [216], [217]. Measurements *via* temperature dependent differential UV-absorption of the thermodynamic stability of the different duplexes and helix conformations were therefore conducted in a phosphate and sodium chloride buffered solution, creating a general stabilizing environment, in contrast to low-salt conditions. Furthermore, determination of melting temperatures give indication on the influence of the sequence position of the current nucleobase modifications, which let assume a mitigated to even abolished effect from locations at either end, especially for the 3'-overhang. The modification type and position on the nucleotide itself, may it be in the sugar-, the phosphate backbone or, as in the actual case, on the base, can play various roles in the context of duplex stability. It was reported previously, that modifications on the major groove of an siRNA by introducing 5-methyl and/or 5-propynyl pyrimidine nucleotides added further stability and improved biological activity to the oligomer [76]. Another research group applied fluorine substitutions at the 2'-position of the ribose [105] in duplexes of DNA and DNA/RNA hybrids, which substantially enhanced the corresponding melting temperatures. The same results for introduced locked nucleic acids (LNA), which influence the sugar pucker and induced A-type duplex geometry [218].

Table 3.2: Listing of melting temperatures obtained for duplexes formed between the fifteen synthesized DNA sense strands and complementary DNA (MH663) or RNA (MH533) antisense strands, respectively, where * indicates again the position of modification. The melting temperatures are shown as: $T_m \pm$ Standard error of the mean (SEM), as was calculated from the mean of three measurements for the range 20 – 85 °C for each duplex. (Data as published in Domingo *et al.* [193])

DNA/DNA			DNA/RNA	
60 °C \pm 0.5 °C		5'GCAAGCTGACCCTGAAGTTCAT ^{3'}	62 °C \pm 0.3 °C	
* 5-methyl- <i>N</i> ⁴ -propargyl-aminyl-2'-deoxycytidine (ODNx.1 series)			* <i>N</i> ⁴ -propargylaminyl-2'-deoxycytidine (ODNx.2 series)	
DNA/DNA	DNA/RNA		DNA/DNA	DNA/RNA
56 °C \pm 0.3 °C	59 °C \pm 0.6 °C	5'G*AAGCTGACCCTGAAGTTCAT ^{3'}	58 °C \pm 0.6 °C	59 °C \pm 0.3 °C
51 °C \pm 0.5 °C	52 °C \pm 0.3 °C	5'GCAAG*TGACCCTGAAGTTCAT ^{3'}	59 °C \pm 0.3 °C	61 °C \pm 0.0 °C
51 °C \pm 0.3 °C	54 °C \pm 0.3 °C	5'GCAAGCTGA*CCTGAAGTTCAT ^{3'}	58 °C \pm 0.3 °C	59 °C \pm 0.3 °C
54 °C \pm 0.3 °C	55 °C \pm 0.3 °C	5'GCAAGCTGAC*CTGAAGTTCAT ^{3'}	57 °C \pm 0.3 °C	59 °C \pm 0.0 °C
53 °C \pm 0.2 °C	51 °C \pm 0.3 °C	5'GCAAGCTGACC*TGAAGTTCAT ^{3'}	59 °C \pm 0.3 °C	59 °C \pm 0.3 °C
60 °C \pm 0.5 °C	57 °C \pm 0.5 °C	5'GCAAGCTGACCCTGAAGTT*AT ^{3'}	58 °C \pm 0.5 °C	60 °C \pm 0.6 °C
60 °C \pm 0.5 °C	62 °C \pm 0.6 °C	5'GCAAGCTGACCCTGAAGTTC*T ^{3'}	60 °C \pm 0.6 °C	62 °C \pm 0.3 °C

The summarized results in Table 3.2 let observe a clear decrease in stability, *i.e.* melting temperature T_m , for internally incorporated modifications (*), resulting for the 5mdC-derivatized duplexes even in distinct differences. Nevertheless, the cytidine modification was in both cases much better tolerated in the DNA/RNA hybrid compared to the DNA-only constructs. Those, that contained the modified nucleotide at either of the two sequence ends, which in the case of the 3'-end do not participate in the involved base-pairing, are finally the least affected in comparison to the unmodified controls. In detail, the ODNs of the *CpDCII* (ODNx.2) set, without the 5-methylgroup, exhibited in comparison to the ODN0 control temperature declines down to a difference of 3 °C and in case of ODN21.2 an increase of 2 degrees Celsius, apposite to the above statements on the overhang-region. For the methylated ODNx.1 series, more pronounced differences in melting temperatures, subjected to the particular sequence positioning of the 5mdC -derivative, occurred. Precisely spoken, contrasting to the control, inner introductions like at position 10 exhibited an about 11 °C reduced T_m , whereas those for position 21 remained nearly untouched. Earlier reports [219] and research from Xuan *et al.* [220], which was published almost at the same time as the current work, presented stabilized or at least unaltered melting temperatures from a single introduction of cytidine derivatives, such as 5-formylcytidine (fC) or 5-hydroxymethylcytidine (hmC). However, in the present case, the sterically demanding, twofold base modification evokes a distinct impediment at the Watson-Crick interface as a result of the predicted rotation of the amine away from the Hoogsteen-/“CH”-edge. Here, the hypothesis of Figure 3.3 comes into play, along with the results

obtained from the NMR experiments above (section 3.1.2.2), which indicate the impeded rotation around the bond-axis between the methylated pyrimidine and the exocyclic amine of the 5mdC product and at the other hand the ability for the *CpDCII* constructs to tilt towards the opposite direction enabling a free W-C face.

To further investigate this, two antisense strands COMP10 and 11 were designed, each presenting an abasic site at the complementary position to the modifications in ODN10.1/.2 or 11.1/.2, respectively (Figure 3.5 A). Despite changed roles, this type of apurinic modification, which was expected to be unable to base pair, was expected to evoke more or less a similar outcome in melting behavior, when hybridized to ODN0, alike the base pair hindered double strands of ODN10.1/11.1 and the unmodified COMP0. Additionally, the COMP10 and 11 would leave more space, in combination with their counterparts ODN10.1 or 11.1, for the aminyl-groups to rotate and enter the W-C region. The corresponding first derivations of T_m -curves (original melting curves in Figure 6.1) and illustrations in Figure 3.5 B and C, deliver the made assumptions in black and white, where section B-(a) shows, that a single missing base in the middle of the double helix lowers the melting temperature about 10 °C. Comparable to that, as in parts investigated [REDACTED], was the melting behavior of the ODNs of the *CpDCII* series (ODNx.2), when the single-modified cytidines were in combination with an opposing abasic site, as depicted in section B-(c) of Figure 3.5, and unaltered with COMP0. Against this, the 5mdC -derivative series ODNx.1 came up, even when not combined with an abasic partner, with declines of 6 to 10 °C, underlining the occurrence of a sterical clash, as illustrated in the left middle part of Figure 3.5 C.

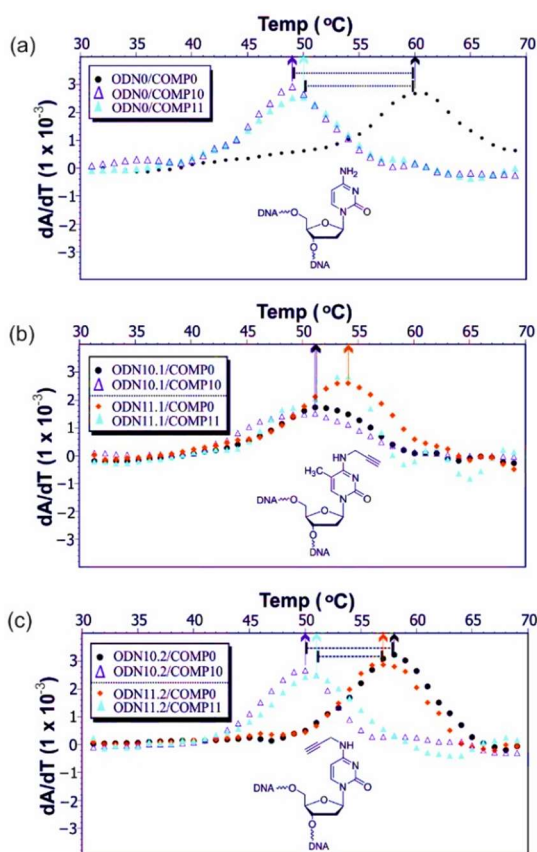
Noteworthy, several studies on alternative or unnatural base pairs have described the formation of A- or B-helices, which benefit from characteristic local non-Watson-Crick base pairs that employed the Hoogsteen edge [221], alternative hydrogen bonds [80], or instead, made use of base stacking and other electrostatic effects [222], [223]. To classify the current data within such a context, one can only suggest, that the impact depends so far on the position the modified cytidines throughout the sequence. A more detailed investigation to expound more about base-pairing/stacking and sequence effects, would preferably involve *e.g.* NMR studies considering the incorporated modification in an ODN single and double strand.

In conclusion, the present results let state, that incorporation of the monosubstituted *N*⁴-propargyl cytidine was indeed well accepted in helices of DNA and DNA/RNA, exhibiting a similar melting profile as unmodified duplexes. Thus, consistent with the afore made speculations, the evolving free energy from hybridization processes seems to be sufficient to rotate the exocyclic amine towards the “CH”-edge, although this would require further physicochemical investigations for an entire evaluation. However, this modification, in combination with an additional CH₃-group at position 5 of the pyrimidine, led to interruptions in the W-C face and interrupts base pairing similar to helices that included an abasic site, which was for both reflected in a distinct decrease of duplex stability.

A

SEQUENCE NAME	SEQUENCE
ODN0	5'GCAAGCTGACCCTGAAGTTCAT3'
ODN10.1	5'GCAAGCTGA*CCTGAAGTTCAT3'
ODN10.2	5'GCAAGCTGA•CCTGAAGTTCAT3'
ODN11.1	5'GCAAGCTGAC*CTGAAGTTCAT3'
ODN11.2	5'GCAAGCTGAC•CTGAAGTTCAT3'
<i>Complementary strands</i>	
COMP0	3'GCCGTTGACTGGGACTTCAAG5'
COMP10	3'GCCGTTGACTΔGGACTTCAAG5'
COMP11	3'GCCGTTGACTG▲GACTTCAAG5'
* 5-Methyl- <i>N</i> ⁴ -propargylaminy-2'-deoxycytidine • <i>N</i> ⁴ -propargylaminy-2'-deoxycytidine	Δ Abasic sites ▲ Abasic sites

B



C

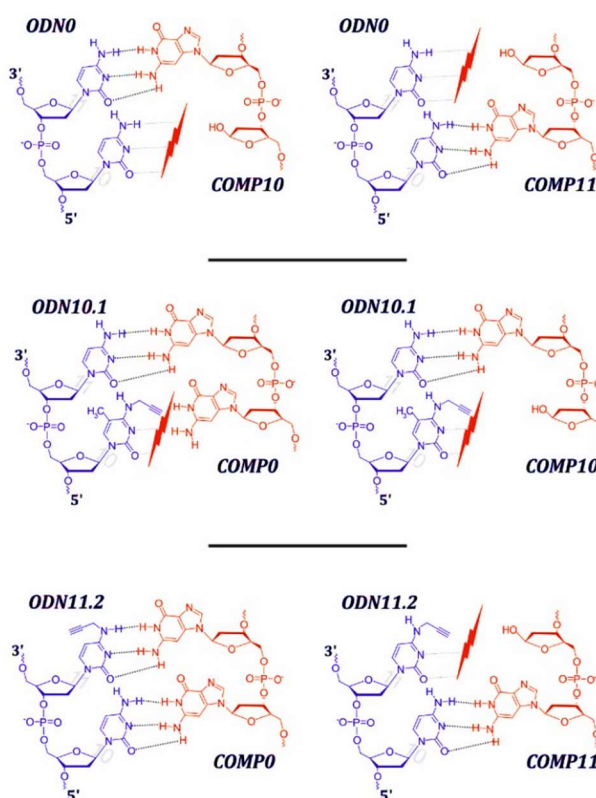


Figure 3.5: Comparison of melting temperatures obtained between duplexes, both with and without abasic sites: **(A)** Overview of the applied sequences. **(B)** First derivatives of temperature dependent UV-absorption melting curves for duplexes formed between **(a)** the unmodified strand ODN0 and the two complementary abasic-site carrying strands COMP10 (dark blue) and COMP11 (light blue), as well as the unmodified complementary strand COMP0 (black). Accordingly, duplexes were formed with the modified strands: **(b)** 5mdC-derivativized strands ODN10.1 (dark blue) and 11.1 (red and light blue), as well as **(c)** those with the single modified cytidine derivative ODN10.2 and 11.2 (color code as before), lacking the methyl group on position 5. **(C)** Illustration of the present base-pairing variations. (Modified figure as published in Domingo *et al.* [193])

3.1.3.3 Click functionalization and electrophoretic mobility shift assay

Chemical modification of nucleic acid molecules is of immense importance in modern life sciences, not only to reach enhanced physical, and therefore biological properties, of DNA and RNA, but also in the field of detection and fluorescence based analytics [181], [182], [224]. To date, powerful strategies for such bioconjugation purposes, combined under the synonym of “click reactions”, have been developed [42]. In particular, the copper(I)-catalyzed variety of the 1,3-dipolar Huisgen cycloaddition between a terminal alkyne and an azide, also known as CuAAC reaction (see Section 1.1.2.1), is among others a favored method to introduce extended functionalities to nucleic acids [45], [53], [54], [225]–[227].

In reference to the work of Hong *et al.* [228] and previous lessons learned, the current applied conditions of CuAAC reaction were adapted and optimized concerning reagent concentrations, especially regarding the application of azides in at least an excess of 10 molar equivalents. Furthermore, reaction times were varied from half an hour to 24 h, revealing a duration of two hours as optimal for complete, respectively no further, conversion. The observance of an argon atmosphere, to exclude oxidation of the starting materials as *i.e.* to maintain the copper catalyst in its active state [228], [229], additionally improved the reaction outcomes.

Figure 3.6 B summarizes, on a 15 % non-denaturing polyacrylamide gel, the proof of the ability of the synthesized propargyl-bearing DNA strands to participate successfully in CuAAC-reactions with the azide-providing fluorescent dye Atto647N [230]. Representative for all alkyne-containing strands listed in Table 3.1, ODN10.1 and ODN10.2 and their respective double strands with the complementary antisense siRNA strand (MH533) were chosen, which were in principle expected, through the strand-internal placement of modification, to display one of the catchier accessible strands concerning the applied click-reaction. The conducted PAGE, which was run at 8 W and under temperature control to avoid double strand separation, clearly separated the prior purified single from double strands in the unlabeled and clicked fashion. Double strand hybridization was in general also successful, leaving just a minor amount of excess antisense strand.

Via the imaging and overlay of the gel, pre- and post-staining as loading control with Stains-All, only a slight discrimination of click-efficiencies between the in-house synthesized strands and the RNA-control (MH662), which carries its alkynylated nucleotide right at the easier accessible 3'-end, could be made. Along with the above established differences in duplex stability (Table 3.2) for the DNA/RNA constructs of the modified cytidines (**25a** and **b**) at position 10, only a minor, but not significant, effect in labeling efficiency could be noticed. An interpretation based on an underlying possible impeded accessibility of the propargyl group on the 5mdC -derivative, could, also by further experiments under milder conditions (not shown) and lower reaction yields, not be clearly stated.

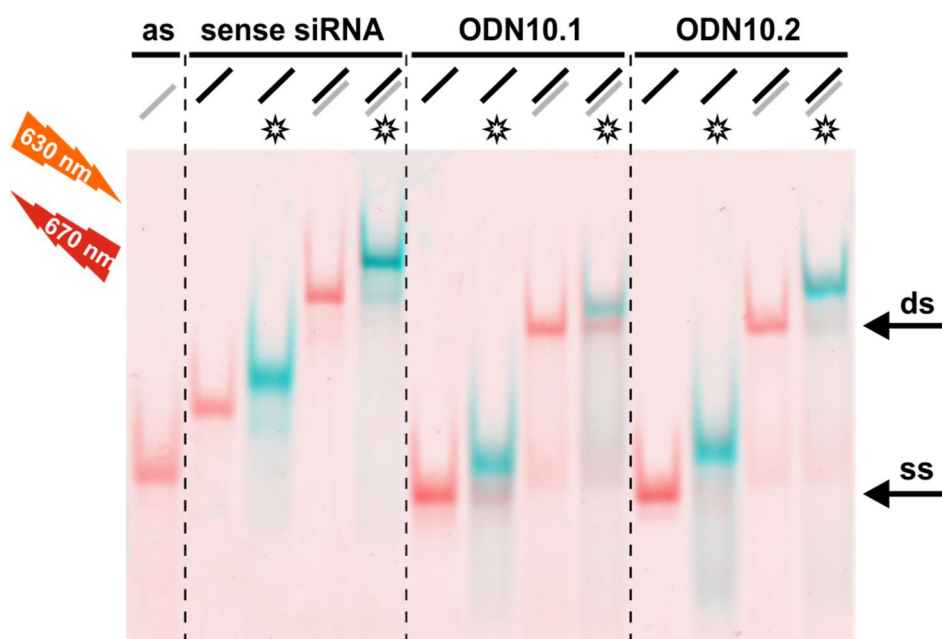


Figure 3.6: Comparison of the click functionalization of the alkyne-modified DNA as single strands (ss; 50 pmol) and hybridized double strands (ds; 25 pmol) with the respective antisense (as) siRNA strand (MH533) by an electrophoretic mobility shift assay (EMSA): As a control, the 3'-end-alkyne-modified sense siRNA (MH662) is presented alone, clicked, as a double strand and as the clicked ds. The same series was applied for ODN10.1 and ODN10.2. Atto647N azide was used as azido functionalized dye in all cases. For efficiency analysis of the CuAAC reactions, native polyacrylamide gel electrophoresis was followed by fluorescence scanning at different wavelengths to distinguish unclicked (red bands) and clicked (*) oligonucleotides (see blue bands). Excitation, before (blue) and after staining (red) with Stains-All, was done at 633 nm. Emission signals were recorded at 670 nm and presented as overlay. (Figure as published in Domingo *et al.* [193])

3.2 Steric shielding of RNA from recognition by endosomal toll-like receptors (TLR7 & 8)

This part of the work deals with the design of suitable (m)RNA constructs to manipulate the innate immune response by human immune cells *via* interaction with intracellular pattern recognition receptors (PRR), in particular the endosomal located toll-like receptors 7 and 8. As described before (Section 1.3.1), these receptors are known to be activated either by small molecules, which could serve as vaccination adjuvants, or by ssRNA, representing as pathogen associated molecular pattern (PAMP) a possible vaccine by itself. Within this context, Colak and co-workers [151] described two distinct mechanisms for the sensing of ssRNA and small molecule agonists of the imidazoquinoline family by TLR7 and 8, which was even supported by recent reports from Zhang *et al.* based on the crystal structure of monkey TLR7 (96.8 % sequence identity with human TLR7) [153].

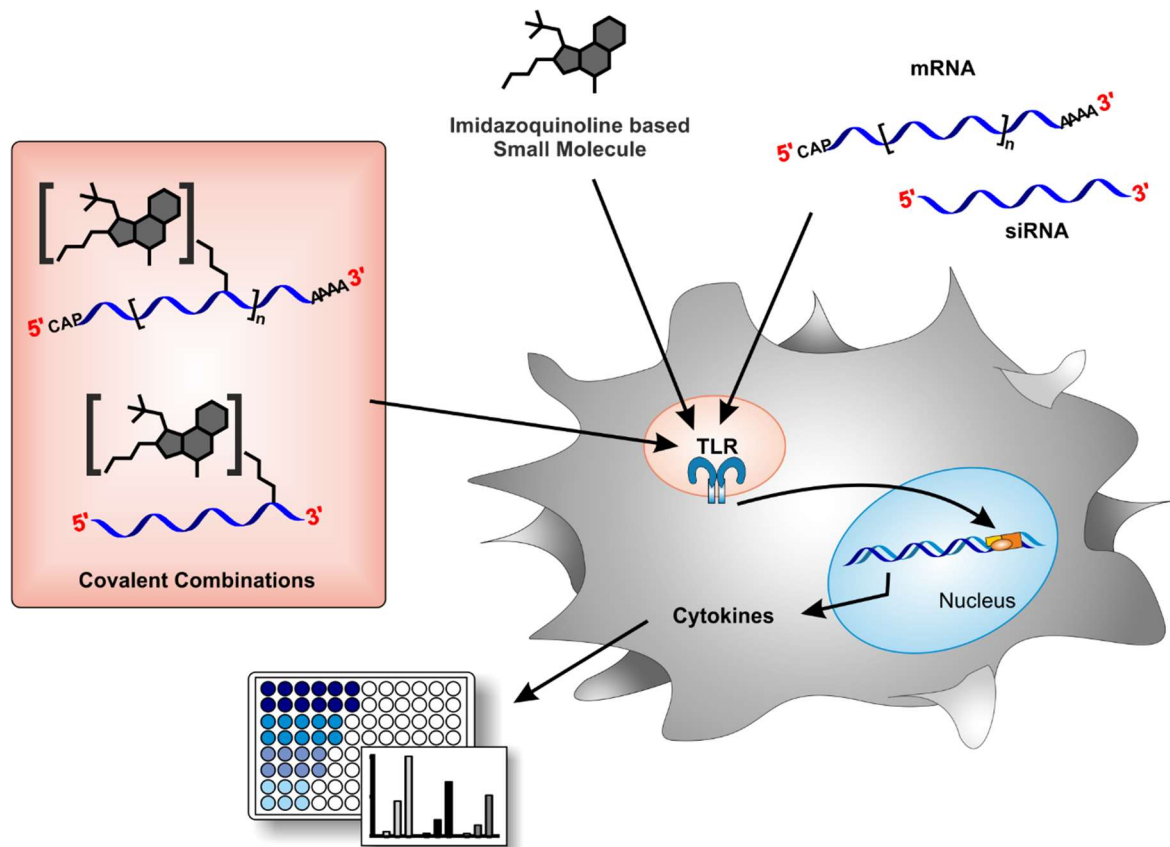


Figure 3.7: Concept of the present study. Evaluation, through ELISA based measurements, of the influence on cytokine secretion by cell-subsets of human peripheral blood mononuclear cells (PBMCs; symbolized by grey cell) through interaction with either small molecules of the imidazoquinoline-family, RNA-oligonucleotides or synthesized covalent conjugates of both (orange box) with endosomal toll like receptors. (Modified figure as published in Hellmuth *et al.* [231])

Encouraged by these findings, the targeted strategy was to trigger both signaling pathways at once by chemically combining the two patterns in one bidentate molecule (Figure 3.7), to address the question, if it could be possible to customize the stimulatory qualities of a therapeutic RNA *via* the type and frequency of a synthetic modification.

Initially, this section describes the synthetic derivatization of two small molecule TLR agonists (smTLRa) with different attachment sites for posttranscriptional immobilization on RNA *via* CuAAC-click chemistry and their evaluation concerning immunostimulatory activity *via* TLR 7 and 8 in human immune cells (Section 3.2.1). Aside from this, the development of a functional mRNA was a further prerequisite (Section 3.2.2). This included the introduction of the alkyne modified nucleoside 5-ethynyl-uridine as triphosphate (EUTP) during *in vitro* transcription, serving later as a reaction partner for the smTLRa-derivatives in CuAAC-reactions. Finally, the synthesized azides were attached through click-chemistry to a set of modified mRNAs, bearing different contents of alkyne-residues leading to the smTLRa-mRNA constructs. Both, alkyne-mRNA and further posttranscriptional modified constructs were analyzed on the nucleoside level concerning their actual EU-content, unveiling the incorporation rate of the clickable nucleoside and efficiency of click-reactions. Beyond this, a set of azide-bearing structures, which represent inherently non-PAMPs for TLR 7 and 8, was applied in the same manner in order to expand the scope of the following investigations regarding immunostimulation.

The central part of this chapter considers the evaluation of cytokine release by human immune cells under the influence of the created smTLRa-mRNA conjugates and their respective building blocks (3.2.3). To this end, human peripheral blood mononuclear cells were studied, which comprise among other subsets plasmacytoid dendritic cells (pDCs), which are in charge of IFN- α release upon TLR7 activation [90], [147], [232]. In parallel, TNF- α secretion by TLR8-activated monocytes could be evaluated. Besides the described long and coding mRNAs, the study involved also the modification and application of siRNA-conjugates, representing short non-coding RNAs (Section 3.2.4).

Counter to the initial hypothesis of achieving a synergistical boost through combining the two TLR-activating motives, covalent conjugation of single stranded RNA with small molecule agonists elicited a reduction in overall receptor activation. These findings raised the question, if the underlying effect could be distinguished from the known inhibitory and antagonistic motive of 2'-O-methylation in RNA [90], [169]. For this purpose, a copy of the afore mentioned siRNA, bearing one 2'-O-methylated guanosine, was used besides four siRNA-conjugates in a comparative study (Section 3.2.5), where PBMCs were co-incubated with a stimulatory siRNA together with one of the respective siRNA-constructs.

Completing the investigations on both types of formed RNA bioconjugates, which demonstrate elementary principles for the development of therapeutic agents in this field, the influence of RNA modifications towards biologic activity was examined in terms of siRNA knock-down capacity and mRNA translational activity (Section 3.2.6).

This chapter contains research, which was in parts published in Hellmuth *et al.* [231].

3.2.1 Azide-functionalized small molecule TLR-agonists

Out of the types of TLR-activating small molecules (see Section 1.3.1.1) [233], the focus of this study lay on the -quimod-family belonging derivatives resiquimod (R848) and gardiquimod (GQI) sharing a common basic molecular structure (Figure 3.8).

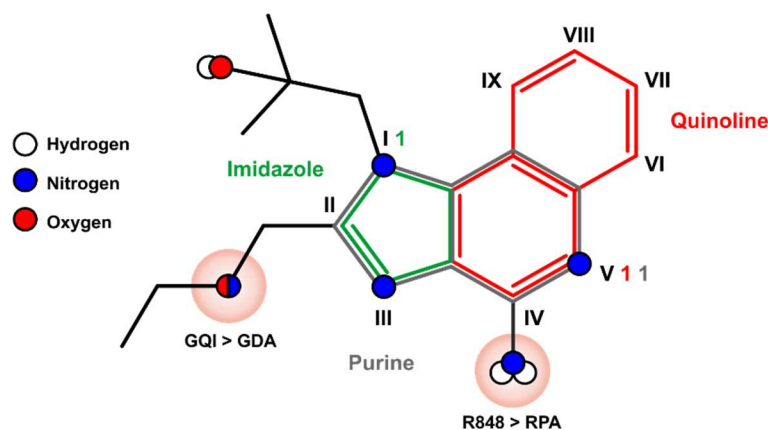


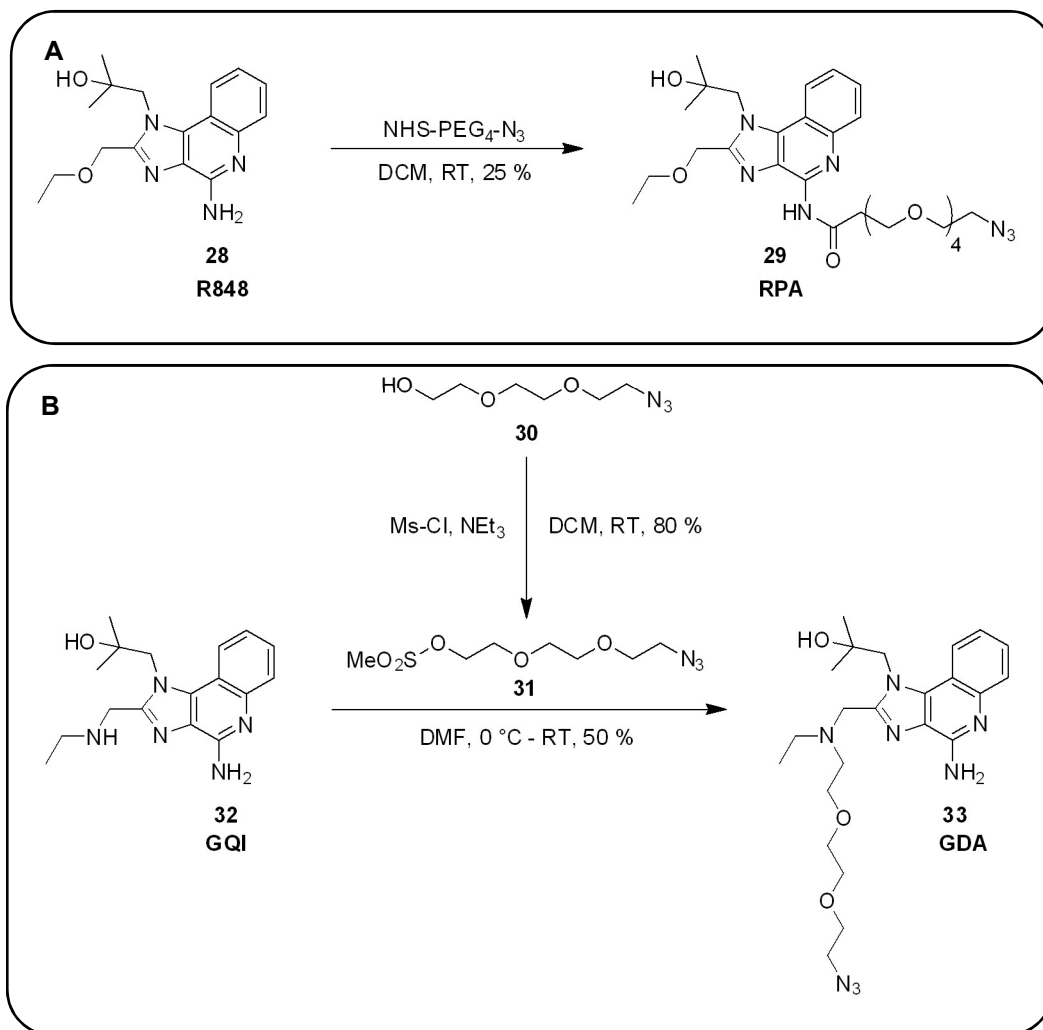
Figure 3.8: Imidazoquinoline based scaffold of the respective small molecules for the nomenclature used in this study. Number ones in green, grey and red tag the individual starting point for atom numbering of the particular heterocyclic rings. The atoms of the overall system are counted in roman numerals. Positions of interest (POI) for the syntheses described in the following section are highlighted within orange circles. (Figure as published in Hellmuth *et al.* [231])

Several previous studies focused on derivatization of known TLR7 small molecule agonists sharing a 1H-imidazo-[4,5-c]-pyridine- or purine-structure [234]–[236], addressing the *N*-9-position (position I in Figure 3.8) of the respective molecule. Regarding R848-derivatives, it was declared as a “tolerant” linker-site upon structure-activity relationship measurements [234], but never the less, they observed losses in activity up to 50 %. In line with recent reports on the small molecule binding site of TLR7 by Zhang *et al.* [153] (see also Figure 3.10), Shukla *et al.* [161] induced with an 3H-regioisomer of gardiquimod inactivation of the molecule right up to TLR7 antagonism by further deamination at the IV-position. Thus, it occurred reasonable for the derivatization attempts to touch the exocyclic secondary amine of GQI and to keep the amine-functionality of R848 at least to a certain extend by conversion to an amide at position IV.

3.2.1.1 Synthesis of azide-bearing smTLRa derivatives

Resiquimod **28** was equipped with an azido-polyethylene-glycol linker by amide-bond formation (see Scheme 3.5 A). Applying standard NHS-ester chemistry [237] between the exocyclic primary amine at position IV (see Figure 3.8) and the activated acid, *N*-hydroxysuccinimide-group, of the linker afforded the product resiquimod-polyethylene-glycol-azide **29** (RPA). Monitoring *via* thin layer chromatography revealed that most of the product was already formed after the addition of the

NHS-PEG₄-N₃. Although the reaction was carried out under inert conditions and run in dry dichloromethane, due to solubility of the starting material and to prevent the NHS-ester from hydrolysis, no further considerable conversion took place, which lead to a yield of 25 % after purification by column chromatography. This might be improved through even more rigorous drying of all reaction partners over a certain time. For the intended purpose, as e.g. reactant in CuAAC-reactions in a μM -range (see section 3.2.2.2), sufficient material with high purity could be achieved.



Scheme 3.5: Synthesis of azide-functionalized small molecule TLR-agonists **(A)** Formation of RPA (Resiquimod-PEG₄-N₃) (**29**) from resiquimod (R848) (**28**) through amide-bond formation with NHS-PEG₄-N₃. **(B)** Synthesis of the linker N₃-EEEt-OMs (**31**) by mesylation of (**30**) and attachment to gardiquimod (**32**) by nucleophilic substitution to form GDA (**33**) (gardiquimod-diethylene-glycol-azide). The synthesis of the second smTLRa-derivative was performed and kindly provided by [REDACTED], analysis and further application were part of the current work. (Procedure as published in Hellmuth *et al.* [231])

To provide gardiquimod **32** with an azido-ethylene glycol linker (see Scheme 3.5) at its aliphatic amine adjacent to position II (see Figure 3.8), the first step comprised the conversion of the hydroxyl

group of 2-[2-(2-azidoethoxy)ethoxy]ethanol **30** (N_3 -EEEt-OH) into a good leaving group. Therefore, a nucleophilic substitution with a methane sulfonyl-moiety was carried out. The resulting linker N_3 -EEEt-OMs **31** was attached to the GQI *via* substitution at the exocyclic secondary amine to give the desired product gardiquimod-diethylene-glycol-azide **33** (GDA) in an adequate yield. A prerequisite for subsequent immunostimulation experiments was the purity of both smTLRa-derivatives, strictly excluding residual starting material, which was confirmed by 1H -NMR, full range and high resolution MS (Figures C.18/19 and C.24/25). The column-purified smTLRa-derivatives were lyophilized and dissolved in endotoxin-free water for further immunostimulatory test series.

3.2.1.2 TLR activity of smTLRa-derivatives depends on conjugation site

It was now of interest, to what extent the attachment of the linker molecules to the small molecule agonists has an impact on immunostimulatory activity. Therefore, cytokine-secretion from incubated PBMCs was examined by sandwich ELISA-based measurements. As resiquimod is known as ligand of TLR7/8 and gardiquimod for TLR7 only, both, IFN- α and TNF- α secretion, through activation of pDCs by TLR7 and macrophages by TLR8, respectively, were evaluated [90], [147], [238]. The related outcomes for the cytokine-secretion of three donors each are given in Figure 3.9.

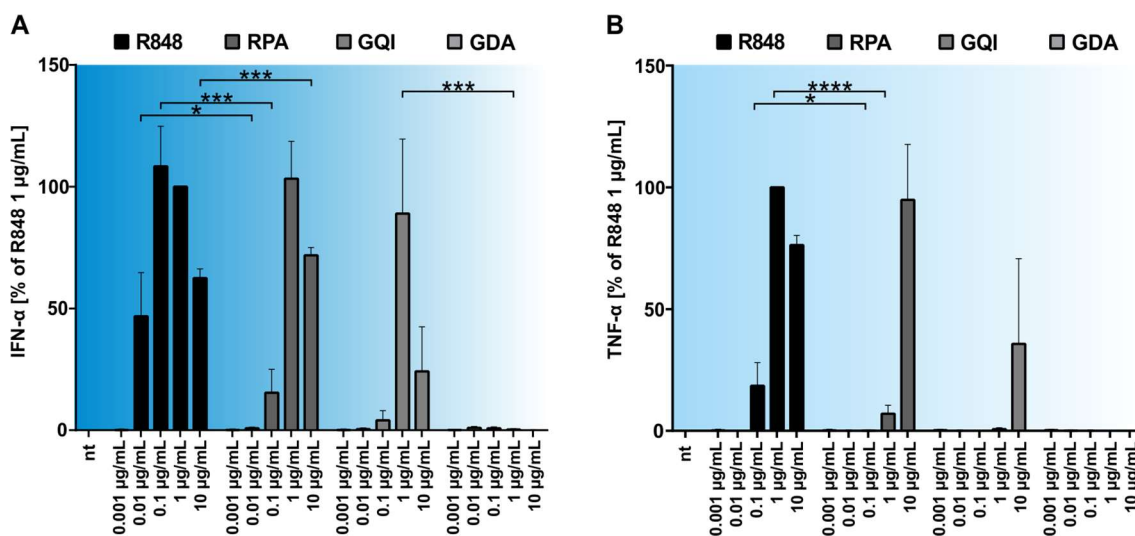


Figure 3.9: Titration of PBMCs with the small molecules (R848, GQI) and their respective azide-derivatives (RPA, GDA): (A) IFN- α and (B) TNF- α production were measured by ELISA. Due to donor variation in the absolute amount of cytokines secreted, data from each individual were normalized to 1.0 μ g/mL R848 (= 100 %) (n = 3; mean + SD; nt: non treated). (Asterisks indicate the respective P values; no declaration = not significant (ns) evaluated by ANOVA and Sidak's multiple comparisons test). PBMC transfections and ELISA based experiments were kindly performed by [REDACTED], prior, experimental setups were developed together. Data-evaluation, statistical analysis and interpretation were part of the current study, which accounts for all following experiments concerning PBMC immunostimulation throughout section 3.2. (Part (A) as published in Hellmuth *et al.* [231])

First, one can clearly distinguish the two types of ligands, as there is a distinct difference in activating the release of the two particular cytokines IFN- α and TNF- α . Both smTLRa exhibited a stronger response to TLR7, whereas the TNF- α secretion by GQI is visibly reduced, showing a reaction only at the highest concentration of 10 $\mu\text{g/mL}$.

The most value has to be attached to the actual influence between the modified derivatives RPA, GDA and their precursor molecules resiquimod, gardiquimod. The coupling of the PEG-linker to the exocyclic primary amine of R848 (**28**), leading to the derivative RPA (**29**), resulted at the lowest concentrations from 0.001 $\mu\text{g/mL}$ up to 0.1 $\mu\text{g/mL}$ in less TLR7 stimulation than **28**. Notably, at a concentration of 1 $\mu\text{g/mL}$ it exhibited a similar outcome and even higher at 10 $\mu\text{g/mL}$ with extremely significance (see also Table 3.3). While the activity of RPA was indeed diminished, the linker-attachment still permitted to obtain a stimulatory activity equal to gardiquimod, which itself is already an improved advancement of imiquimod [158], and showed in fact a very significantly higher effect at 10 $\mu\text{g/mL}$ (Table 3.3). Similar trends between R848, RPA and GQI account for the observation of TNF- α secretion (see Figure 3.9 B) were observed.

Besides, that GQI is not the agent of choice for TLR8-activation, here reflected in the TNF- α release, a distinct outcome showed no remaining activity for the gardiquimod-derivative GDA (**33**) in both cases. Hence, the conjugation of the azido-diethylene-glycol-linker at the C-2-ethyl-amino-methyl-group of the 1*H*-imidazo-[4,5-*c*]-quinolin scaffold of GQI (**32**) (see Figure 3.8) impeded TLR-stimulation of the synthesized derivative **33**. In keeping with this, the previous study of Shukla *et al.* [239] displayed decreased interferon release upon modification at the C2-site.

Table 3.3: Significance evaluation for statistical differences in IFN- α (Figure 3.9 A) and TNF- α secretion (Figure 3.9 B) by PBMCs after incubation with compounds **XX-XX**. Asterisks indicate the respective P values evaluated by ANOVA and Sidak's multiple comparisons test; ns = not significant. (Data for IFN- α as published in Hellmuth *et al.* [231])

IFN- α / (TNF- α)	0.001 $\mu\text{g/mL}$	0.01 $\mu\text{g/mL}$	0.1 $\mu\text{g/mL}$	1 $\mu\text{g/mL}$	10 $\mu\text{g/mL}$
R848 vs. RPA	ns / (ns)	* / (ns)	*** / (*)	ns / (****)	*** / (ns)
GQI vs. GDA	ns / (ns)	ns / (ns)	ns / (ns)	*** / (ns)	ns / (ns)
GQI vs. RPA	ns / (ns)	ns / (ns)	ns / (ns)	ns / (ns)	** / (**)

In accordance with the data for cytokine secretion received from PBMC titrations, comparable results could be achieved from HEK-Blue™ hTLR7 cells [240], a HEK 293 cell line, which expresses the TLR7 gene and an NF κ -B inducible secreted embryonic alkaline phosphatase (SEAP) reporter gene (Figure 6.2). Similar activity could be proven for RPA, R848, GQI and no effect for GDA with increasing concentration.

Considering the stereochemistry of R848 and the crystal structure of the *Mm*TLR7 receptor-dimer [153], see also Figure 3.10, the involved N4 of resiquimod builds two hydrogen bonds (blue dashed lines) between the amino acid residues aspartic acid (Asp) 555 and threonine (Thr) 586 of the A-

chain. As a result, the conjugation with the PEG-linker was supposed to interfere with the TLR binding site only at a single hydrogen bridge, reflected in an appropriate activity of RPA. Thus, one can consider the modulated resiquimod-derivative as a true smTLRa to be compared with its mRNA-conjugate later.

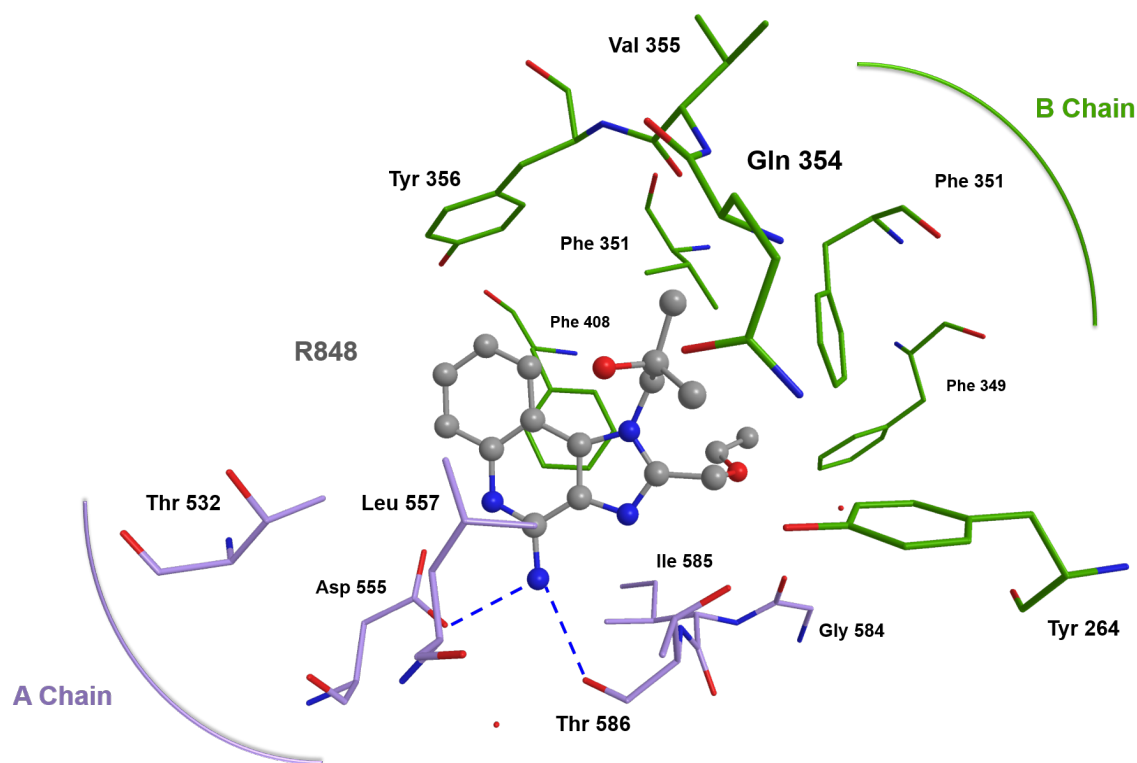


Figure 3.10: Zoom into the 1st site of MmTLR7-dimer crystal structure (PDB ID: 5GMH) [153] with R848 bound in the 1st site (center). Shown are all involved amino acid residues of the A-chain (purple) and the B-chain (green), surrounding the ligand R848 (grey) in a radius of 4 Å, including two water molecules (small red spheres). Figure generated with ChemDraw3D.

Of note, for R848, RPA and GQI (GDA not detectable) an immune response was received, which was not in a linear correlation to the titrated concentration series. The decrease in INF- α release upon increased concentrations could possibly be due to reasons like saturation, cell efflux as for toxic substances or cell death. Indeed, an MTT-based cell viability assay (Figure 6.3) indicated decreased metabolic activity after incubation with 10 $\mu\text{g}/\text{mL}$ resiquimod and only slightly reduction at 1 $\mu\text{g}/\text{mL}$ for R848 and at 10 $\mu\text{g}/\text{mL}$ for RPA, very likely explaining the above findings. Under all other conditions, cells showed normal viability.

The compatibility of the synthesized smTLRa-constructs RPA and GDA in copper-I-catalyzed azide-alkyne cycloaddition reactions for posttranscriptional modification of RNA will be addressed in sections 3.2.2.2 and 3.2.4.

3.2.2 From plasmid to mRNA

Based on the knowledge on therapeutic nucleotides, small molecules and the recent findings concerning TLR7 and 8, this work aimed at the synthesis of a trifunctional mRNA, comprising two types of TLR agonists and a possible vaccine, the latter contained in the mRNA sequence itself. Within this context, two mRNAs were investigated, one comprised the sequence of the melanoma specific antigen MelanA/MART1 [241], [242] and a second bicistronic one included, *via* an IRES-resembling and self-cleaving T2A-segment [243], an additional eGFP-sequence (see Table 5.4). Despite that, the following studies were conducted on a model eGFP only encoding mRNA, which could encompass the entire spectrum of questions, allowing further comfortable investigations on functionality in protein biosynthesis.

3.2.2.1 Synthesis and purification

Beforehand, circular plasmid-DNA (pDNA) was transformed and propagated in a competent DH5 α *E. coli* strain. In order to avoid bacterial contaminations such as lipopolysaccharides (LPS) in downstream experiments, especially those involving immunostimulation [244], pDNA was isolated by an endotoxin-free plasmid kit (see section 5.3.2). Consequently, to exclude such contaminations in general, endotoxin- and RNase/DNase-free water was exclusively utilized for all experiments in section 3.2. The pDNA comprised a poly-dT sequence of 64 dTs, allowing *in situ* synthesis of a 3'-poly-A-tail, one prerequisite for protein expression. Thus, for linearization of the pDNA, it was indispensable to apply a type II restriction enzyme, BcuI in this case, with a cleavage site directly after the poly-dT sequence (see also section 3.2.6), resulting in a freely accessible poly-A-tail for the ribosomal complex [245] (Figure 3.11).

All mRNAs were manufactured by *in vitro* transcription (IVT) with the dsDNA-dependent T7-RNA polymerase. Standard syntheses of unmodified mRNA from 10 μ g linearized pDNA-template using unmodified NTPs of C, U, G and A in a 5 mM end-concentration, afforded 400 to 500 μ g mRNA. Artificial and naturally-occurring modified NTPs [168], [246], [247] were already applied in enzymatic RNA synthesis before and especially C5-modified uridine ribonucleotides are known to be well accepted by the T7 RNA polymerase in IVTs [246]. In conjunction, an IVT protocol from Karikó *et al.* [168] for the incorporation of such naturally occurring modified nucleosides was adapted in order to introduce the alkyne-bearing 5-ethynyl-uridine triphosphate (EUTP). In this case, the UTP end-concentration was substituted with respective amounts (1 %, 2.5 %, 5 %, 10 % and 50 %) of EUTP, which was easily accepted by the T7-RNA polymerase and did not have any reducing impact on IVT yield. The EUTP was our NTP of choice, as it was indeed already mentioned in 2008 by Jao and Salic [248], whose publication focused on the biosynthetic incorporation of the nucleobase 5-ethynyl-uridine *via* the salvage pathway during the S-phase of the cell cycle. Its DNA-derivative 5-ethynyl-deoxyuridine (EdU) is established in immunohistochemical staining of DNA [249]. Although, Jao and Salic [248] envisaged the application of EUTP in RNA modification as a promising outlook, no previous investigations were made on the direct introduction of the alkyne-

bearing EUTP in enzymatic *in vitro* synthesis of a functional mRNA. In 2015, Sawant *et al.* [39] published the synthesis of azide-bearing UTPs and their application in mRNA-transcription, but did not pursue any further investigations regarding immunostimulation or protein expression.

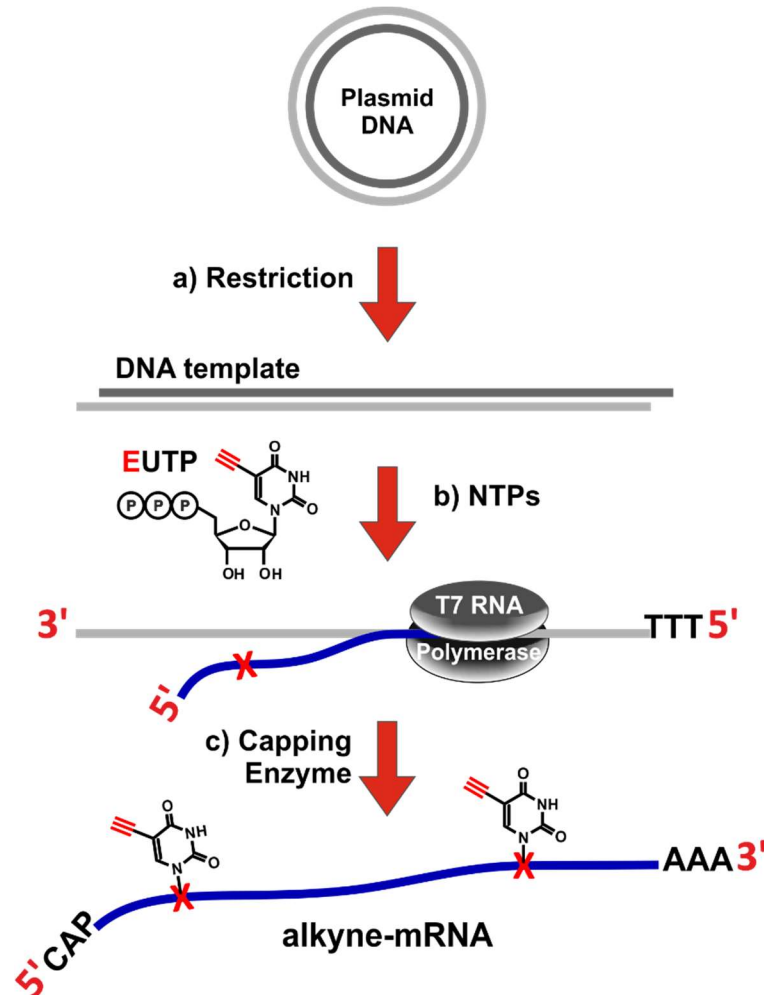


Figure 3.11: Schematic workflow of mRNA synthesis starting from plasmid DNA. (a) pDNA was restricted with restriction enzyme *SpeI* after endotoxin-free isolation from *E. coli*. (b) Linearized DNA served as template for *in vitro* transcription with T7 RNA polymerase. (c) Posttranscriptional 5'-capping was carried out with *vaccinia* capping enzyme in combination with mRNA CAP 2'-O-methyltransferase to afford a Cap1 structure.

As indicated in Figure 3.11 c), after digestion of the DNA-template, the 5'-end of the purified IVT-construct was subsequently provided with a 7-methylguanosine-ppp-Gm cap structure (Cap1) (Figure 3.12 A), serving as exonuclease protection and further prerequisite for the protein translation initiation complex [245], [250]. As co-transcriptional capping with so-called cap-analogs may yield a certain amount of uncapped mRNA with a free 5'-triphosphate [251], [252], known as an activator of the intracellular RNA sensor RIG-I [136], posttranscriptional capping was conducted. This process of combined enzymatic reactions of the *vaccinia* capping enzyme, leading to the Cap0

structure, and the mRNA Cap 2'-O-methyltransferase, finalizing with Cap1 [253], [254], was evaluated through a tritium incorporation assay for optimization of the methyl group-transfer with the co-factor ^3H -S-adenosyl-L-methionine (SAM) (Figure 3.12 B). The manufacturer proposes two procedures: a two-steps method by adding the 2'-O-methyltransferase to an unpurified reaction mixture of the *vaccinia* system after 60 minutes or a one-step variation by a collaborative implementation of both reactions, again for 60 minutes. Figure 3.12 C opposes the plotted capping reactions monitored over 120 minutes. Comparing the Cap1_1step (olive green) at 60 min to the Cap1_1.2 (blue) at 120 min, one can already tell the advantage of the one-step method, reaching a resembling capping efficiency in less time. To be on the safe side, all further capping reactions of the one-step variation were also conducted for 2 h.

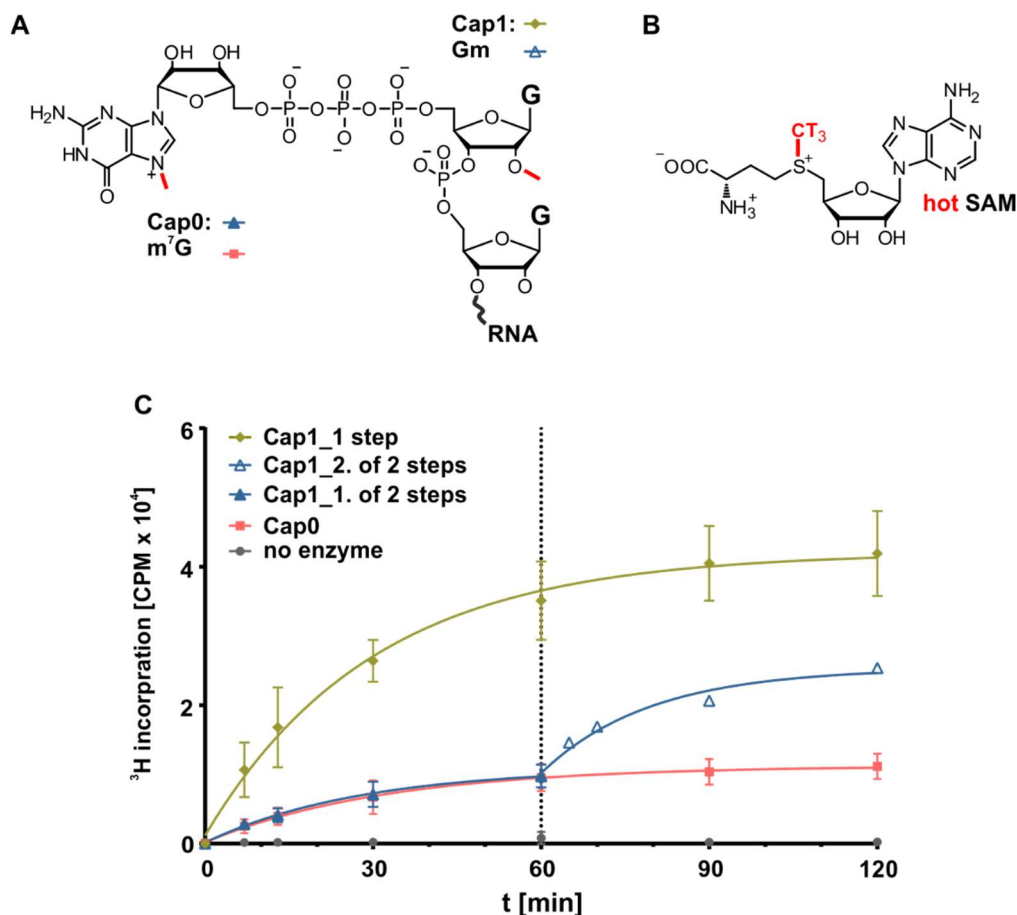


Figure 3.12: Investigation of capping reaction through tritium incorporation assay: **(A)** Structures of Cap0 (m⁷G(5')pppG) and Cap1 (m⁷G(5')pppGm) with respective (tritiated) methyl groups in red. **(B)** Structure of S-(5'-adenosyl)-L-methionine-(methyl-³H) (hot SAM) used as methyl donor in tritium incorporation assay. **(C)** Methylation/Capping reactions of eGFP-mRNA monitored over 120 minutes: Cap0 formation by the *vaccinia* capping enzyme only (orange), Cap1 in two steps by the addition of the mRNA Cap 2'-O-methyltransferase at 60 minutes (1. blue filled triangle, 2. blue framed triangle (one experiment only)) and Cap1 in one step by both enzymes at a time (olive-green). A control reaction was carried out without enzymes. (n = 1-3; mean + SD). (Modified figure as published in Hellmuth *et al.* [231])

Thorough mRNA-purification was a prerequisite, since PRRs such as the cytosolic NOD-like receptors (nucleotide-binding oligomerization domain-like receptors / NLRs) or RIG-I interact with nucleoside triphosphates [136], [255], [256]. Hence, the IVT products, which were at the beginning purified with combinations of conventional methods like phenol-chloroform extraction for protein removal, ethanol precipitation or size exclusion chromatography (SEC) on Sephadex® G25 columns to get rid of small impurities such as excess NTPs, were analyzed by SEC-LC on a Superdex™ 200 SEC column (Figure 6.4). Evident from the results, exhibiting an elution peak for the RNA at 17.0 minutes and a prominent peak for excess NTPs at 39.8 minutes, the implemented purification methods were not sufficient in removal of the large excess of free nucleotides. In addressing this problem, the purification method was changed to the MEGAclean™ transcription clean-up kit (MCK) from Invitrogen. It presented a silica column based spin-column chromatography method, promising a fast procedure with high yields of enzyme-, DNA fragment-, shorter RNA- and NTP-free products. This purification method was evaluated through comparison of results from two methods of concentration determination. In particular, the UV-absorption-based quantitation by NanoDrop (PeqLab) measurements at 260 nm and settings for ssRNA [257] was contrasted to the fluorescence-based method by RNA-specific Qubit™ (Thermo Fisher Scientific) measurements (Figure 3.13). The latter resorts to a fluorescence-reagent (Qubit® RNA HS Assay Kit) based on the dye RiboGreen [258], which binds selectively RNA over dsDNA and tolerates impurities such as proteins or excess NTPs.

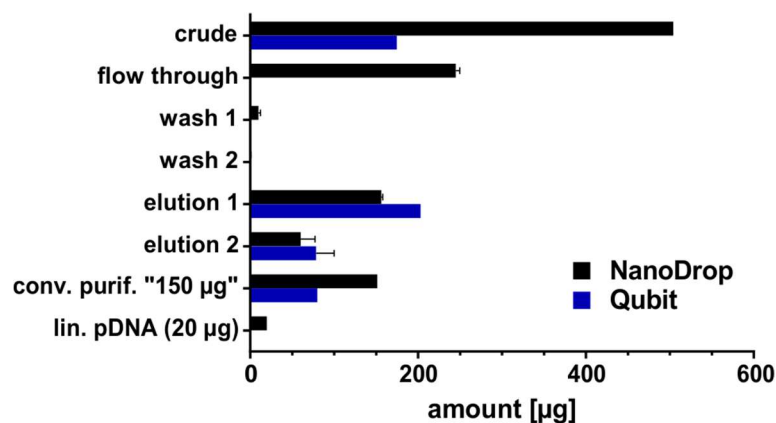


Figure 3.13: Evaluation of IVT-eGFP-mRNA purification via the MEGAclean™ transcription clean-up kit by NanoDrop- and Qubit® measurements. Based on an IVT of eGFP-mRNA from 5 µg pDNA-template, the total amounts of RNA were calculated from NanoDrop (black bars) and Qubit (blue bars) in the respective solutions: crude IVT-mixture (100 µL), flow through (1st step of the MCK), wash 1 & 2 (2nd & 3rd step), elution 1 & 2 in endotoxin-free water (4th & 5th step), "150 µg" (estimated by NanoDrop) from a former conventionally purified IVT and linear pDNA for control of the RNA specificity by the Qubit® RNA HS Assay Kit (Thermo Fisher Scientific).

Figure 3.13 displays the specificity of the Qubit® RNA assay, demonstrated for instance by the NanoDrop-detected false positive results of the “RNA”-content in the flow through- and wash 1-fraction of the MCK, containing the excess NTPs, and the purified linear pDNA control-sample. In relation to this and the SEC experiment described before (Figure 6.4), the conventional purified sample gives an mRNA-value by NanoDrop 87.5 % higher than the one by Qubit. Further on, the Qubit-readout of the crude IVT seems to be influenced by the contents of the mixture. Here, it exhibits a false negative value for the overall RNA-content, but still a better estimation than, the immense false positive one by NanoDrop. The result of the latter coincides with the sum of NTPs plus DNA-digestion products in the flow-through and wash fractions and the actual mRNA in elution 1 & 2. In considering the outcomes of purified RNA in elution 1 & 2, with an average difference of 23 % between NanoDrop and Qubit, one can finally claim the MCK- transcription clean-up assay as a well-suited and superior purification method for the demands of the following study.

3.2.2.2 Click-modification and analysis

As already announced, the CuAAC-click reaction, which was introduced in Section 1.1.2.1, takes also an essential part for the scientific implementations of the current investigations. Drawing on a set of eGFP-mRNAs provided with terminal alkyne-moieties and azide-functionalized small molecule derivatives (Figure 3.14 A), optimized CuAAC-click reaction conditions [228] were applied according to the achievements described in section 3.1.3.3, with the adaptation of using the respective azides in 20 times molar equivalents of alkyne. The verification of smTLRa-mRNA-integrity after click reaction by PAGE is illustrated in Figure 3.17 C, revealing no significant degradation.

To evaluate the actual incorporation of clickable nucleoside *via* IVT and the efficiency from succeeding CuAAC-reactions, both, alkyne-containing *in vitro* transcripts and products from click-reactions, were analyzed on the nucleoside-level regarding their existing/remaining EU-content. Therefore, the RNA-oligonucleotides were digested stepwise through incubation with nuclease P1, snake venom phosphodiesterase and alkaline phosphatase to nucleosides and subjected to quantitative HPLC analysis [259]. Owing to the sequence of the unmodified eGFP-mRNA, containing 119 uridines (Section 5.1.4), and the findings from Karikó *et al.* [168], it was expected to receive 1-2 (1 %) and respectively 12 (10 %) of them to be substituted by 5-ethynyl-uridine (dark-green bars in Figure 3.14) during IVT. This assumption could be confirmed by the quantification results shown in Figure 3.14 B (light-green bars of EU-mRNA), where efficiency and yield of the implemented click-reactions were also displayed through the determination of residual EU (light green and blue bars). Results from CuAAC-reactions are reflected for both ligands in 82 % successfully modified 1 %-EU-mRNA, corresponding to 1-2 smTLRa-molecules per molecule mRNA, and 70 % of the 10 %-EU-mRNA, equaling 8-9 conjugated smTLRa-molecules per molecule mRNA.

A conceivable explanation for the decreasing efficiency from 1 % to 10 % might give the incorporation of EUTP during IVT already, which follows a statistical distribution throughout the

RNA molecule, very likely ending up in easier accessible regions first, until it comes to areas with enhanced secondary structure and furthermore, enhanced sterical hindrance. One could get more insight into this problem in future experiments through combinations of sequential mRNA synthesis and the power of deep sequencing methods [260]. The process covered here and depicted in Figure 3.14 accounts also for the experiments described in section 3.2.3.2 and Figure 3.17 B.

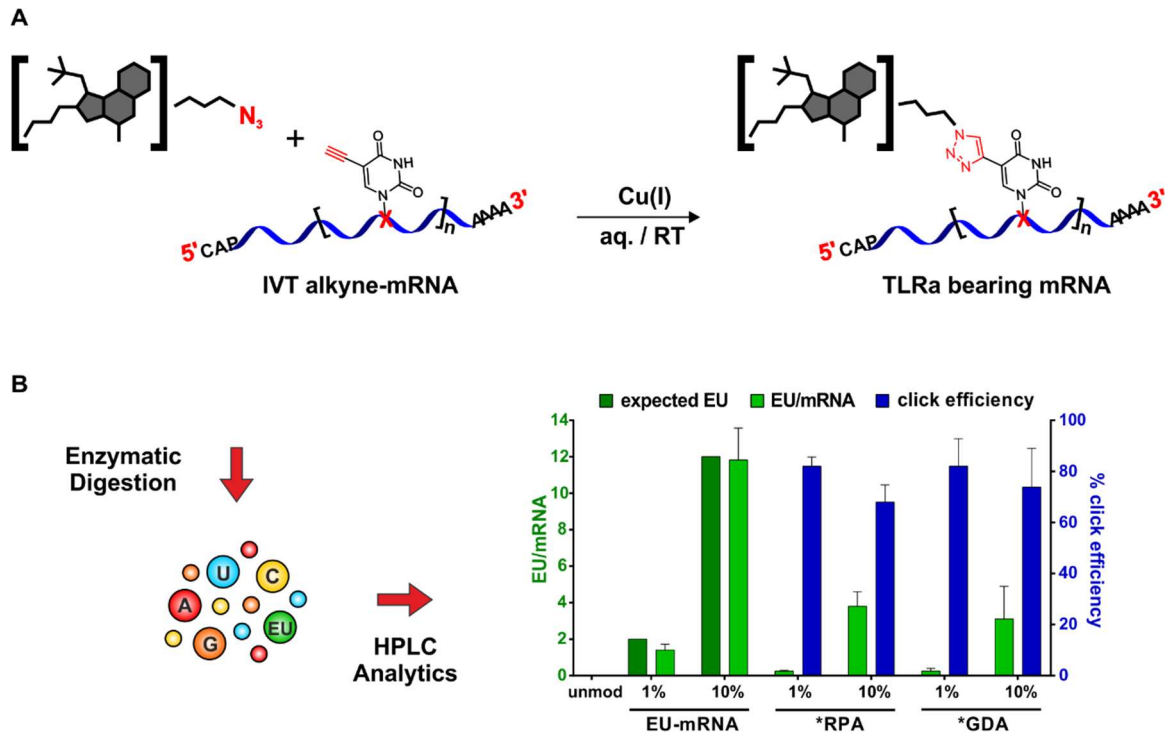


Figure 3.14: Synthesis of small molecule-TLRa bearing eGFP-mRNA by click-chemistry. **(A)** Symbolic synthesis scheme of Cu(I)-catalyzed azide-alkyne-cycloaddition between azide-functionalized smTLR-agonists and *in vitro* transcribed (n)alkyne-modified eGFP-mRNA. **(B)** Digestion of the RNA to nucleosides was followed by HPLC-quantification of EU content (light green) in IVT- and smTLRa-eGFP-mRNA including click efficiency (blue) ($n = 5$; mean + SD). (Modified figure published in Hellmuth *et al.* [231])

3.2.3 mRNA, small molecules and endosomal TLRs in human immune cells: collaboration & opposition

As already pointed out in the introduction (Section 1.3), steering of the innate immune system, particularly *via* the modulation of TLR activation, gained an important role for therapeutic approaches towards bacterial and viral infections, autoimmune diseases, and cancer biology [107]–[109]. These consider among others, diverse RNAi approaches [92], [175], [261] or mRNAs for tumor vaccines [174]. Strategies, which follow the intention of limited immunostimulatory activity through inhibition of TLR response, *e.g.* for mRNA protein replacement methods [174], [247], [262],

as well as numerous siRNA systems [87], [88], [176], profit from immunomodulatory approaches. In addition, the induction of a boost in immune stimulation *via* nucleic acid derived adjuvants to intensify the potency of certain vaccines [109], [177], [178] represents modulations towards the opposite effect. In this regard, it was of essential interest to tailor such stimulatory properties by combining the TLR7 and 8 activation by smTLRAs and mRNA in a bidentate ligand, under investigation of the kind and density of the synthetic modifications. Influenced by the work of the Weber group [151] and supported by the Shimizu group on TLR7 and 8 [152]–[154], [156], a possible solution to reach both binding sites of the receptors as illustrated for monkey TLR7 in Figure 3.15, bearing a guanosine in the 1st and poly-U in the 2nd binding region. Average distances between the two lay in the range of 30 Å, which suggested to be very likely bridged by the, to resiquimod and gardiquimod, respectively, PEG-chain linked mRNA molecules.

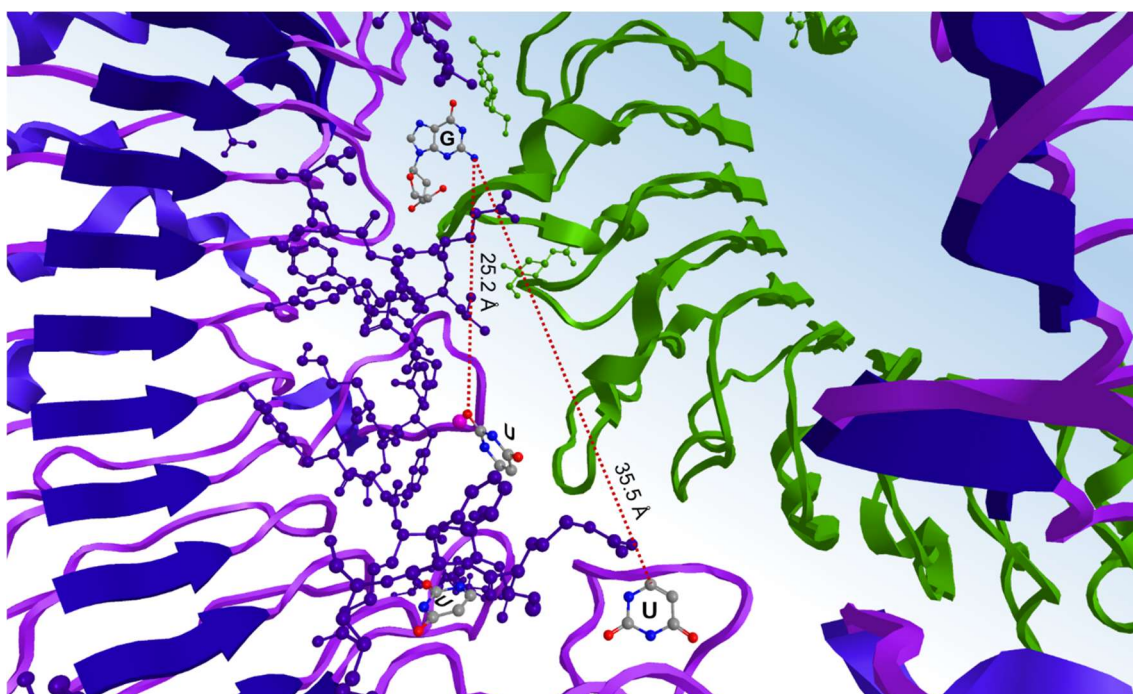


Figure 3.15: Zoom into the A-chain (purple) of the MmTLR7-dimer crystal structure (PDB ID: 5GMF) [153] with distinct binding sites of guanosine (G) in the 1st site and poly-U (only three nucleobases depicted as U) in the 2nd site. Dotted red lines indicate the distances between involved ligand residues (grey) occupying the two binding sites. The B-chain (green) is visible in the background. Figure generated with ChemDraw3D.

In the recent two years, various groups strived to model the innate immune system through different approaches in covalently conjugating TLR ligands, reaching moderate to quite good success in immune response. To name but a few, a trimeric construct of TLR4, 7 and 9 ligands, combined *via* a central core of a triazine-based molecule, was evaluated in stimulating NFκB, IL-12 and other cytokines from bone-marrow derived DCs (BMDCs) [263]. For the purpose of stability, transport and ligand concentration in vaccine adjuvants, TLR7 and 8 small molecule agonists have been

attached to polymeric carriers. As *e.g.*, a adenine derivative by Goff *et al.* [264] comprised at the N9 of the purine ring (I in Figure 3.8) a conjugated phospholipid. Alike that, a further TLR7 ligand-derivative was conjugated to polysaccharides [265]. Another attempt involved the linkage of block copolymers to position I of an imiquimod derivative, forming nanogels in the end [266]. In addition, a similar kind of nanosized particles was composed by the self-assembly of N1-derivatives of resiquimod (R848) and alkane or PEG chains [267]. Shukla *et al.* conceptualized also a series of imidazoquinoline-dimers [268], linked *via* varying positions. Dimers through the C4 (IV), C8 (VIII) and N4 (IV) positions, were revealed to behave as TLR7 agonists, whereas a C2-dimer occurred as antagonist of TLR7 and 8. Further encouraged by these findings and the consideration of Figure 3.15, the investigations of the actual objects of interest were pursued.

3.2.3.1 Effect of smTLRa, mRNA, and covalent conjugates on human DCs

With the aim of investigating the influence of the covalent conjugation between the two ligand patterns, a comparative study between various PBMC incubations with RNA and small molecules was conducted (Figure 3.16 and Figure 6.5). All RNAs were delivered through complexation with the cationic transfection agent DOTAP (N-[1-(2, 3-dioleoyloxy)propyl]-N, N, N-trimethylammonium-methylsulfate), which itself did not evoke any stimulating effect [170]. To map a potential cooperative stimulation, two cases were considered in contrast to a control-series of untreated eGFP-mRNA (grey bars) and individual smTLRas (light blue bars) (see also Figure 3.9 A). Namely, the first case was the co-incubation of small molecules (dark blue bars), each at a fixed concentration (0.1 µg/mL, equivalent to the middle one of the respective light blue bars) titrated with unmodified eGFP-mRNA, and the second one comprising a 1 and 10 % covalently click-modified mRNA (yellow and orange bars) of both types.

As the co-incubation reveals, smTLRa based IFN- α secretion can be increased by the addition of mRNA. It resulted for GQI and GDA in an enhanced signal approximately alike the IFN- α secretion by native eGFP-mRNA and for the resiquimod substances even in an additive boosted effect. In contrast to that, IFN- α levels decreased significantly as soon as one of the two ligands was covalently attached to the oligomer. The effect was milder for 1-2 smTLRa functions per molecule mRNA and even dropped for the higher degrees of modification to at least 50 % of stimulation. Thus, the anticipated cooperativity could not be evidenced, although it is set out in Figure 3.15, that the distance of 21.4 Å between the C-5 of a uridine, initially EU, and the amide-N of a coupled RPA lies plausible in the range of the two distinct binding sites for SMs and ssRNA, moreover if one consider a certain length and flexibility of the mRNA. Having in mind the two postulated signaling modes of TLR7, especially with a poly-U sequence in the second site [151], [153], and the immunosuppressive impact of uridine-modifications [168], [172], one could formulate the thought experiment that the “RNA-mechanism” is disturbed to a certain extend through the bound molecules and evokes an opposing effect, than expected. RPA, when bound, might to a definite degree compensate the silencing effect of the covalent conjunction through its own ability to activate as shown before (Figure 3.9 A and light blue bars in Figure 3.16).

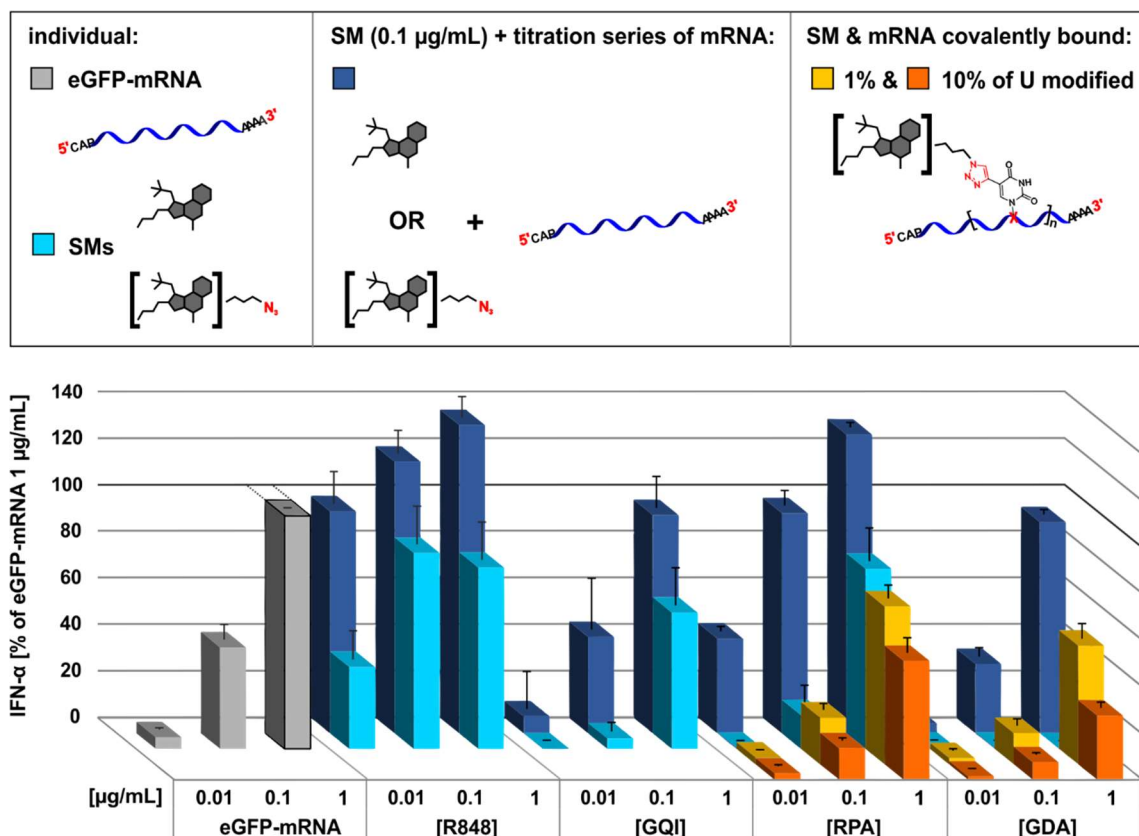


Figure 3.16: Comparative study of the effect of smTLRa, mRNA, and covalent conjugates of both on IFN- α secretion in human PBMCs. Titration of PBMCs: In the second row with eGFP-mRNA (grey bars), small molecules and their respective azide-derivatives (light blue bars). In the back (dark blue bars), 0.1 $\mu\text{g/mL}$ of SMs were titrated individually with eGFP-mRNA. The two front rows represent 1% (yellow bars) and 10% (orange bars) alkyne-eGFP-mRNA clicked with RPA and GDA respectively. IFN- α release was measured by ELISA. To account for donor variation in the absolute amount of IFN- α secreted, data from each individual were normalized to 1.0 $\mu\text{g/mL}$ eGFP-mRNA (= 100%) ($n = 3$; mean + SD). As a consequence of illustration, respective P values can be found in detail in the appendix (see Figure 6.5). (Figure as published in [231])

3.2.3.2 Scope expansion towards bioconjugates with non TLR binding moieties

To widen the ambit of the afore studied effects, besides the smTLRa-mRNA bioconjugates tested so far, the application was expanded to structures, which are inherently non-PAMPs for TLRs and feature increasing molecular weights. Figure 3.17 A shows two azide-equipped hydrophilic sugar molecules mono- **34** and tri-mannose **35**, obtained from our cooperation partners of the Opatz lab and known as ligands for two homologous C-type lectins found on the surface of dendritic cells, DC-SIGN and langerin [269]–[271]. Furthermore two fluorescent dyes with extended delocalized π -system and attenuated lipophilicity by sulfonyl-moieties were applied, namely the blue cyanine dye Sulfo-Cy5-azide [230] and a photostable red/pink perylene-dye PDI-azide from our cooperation partners of the Peneva lab [272], [273].

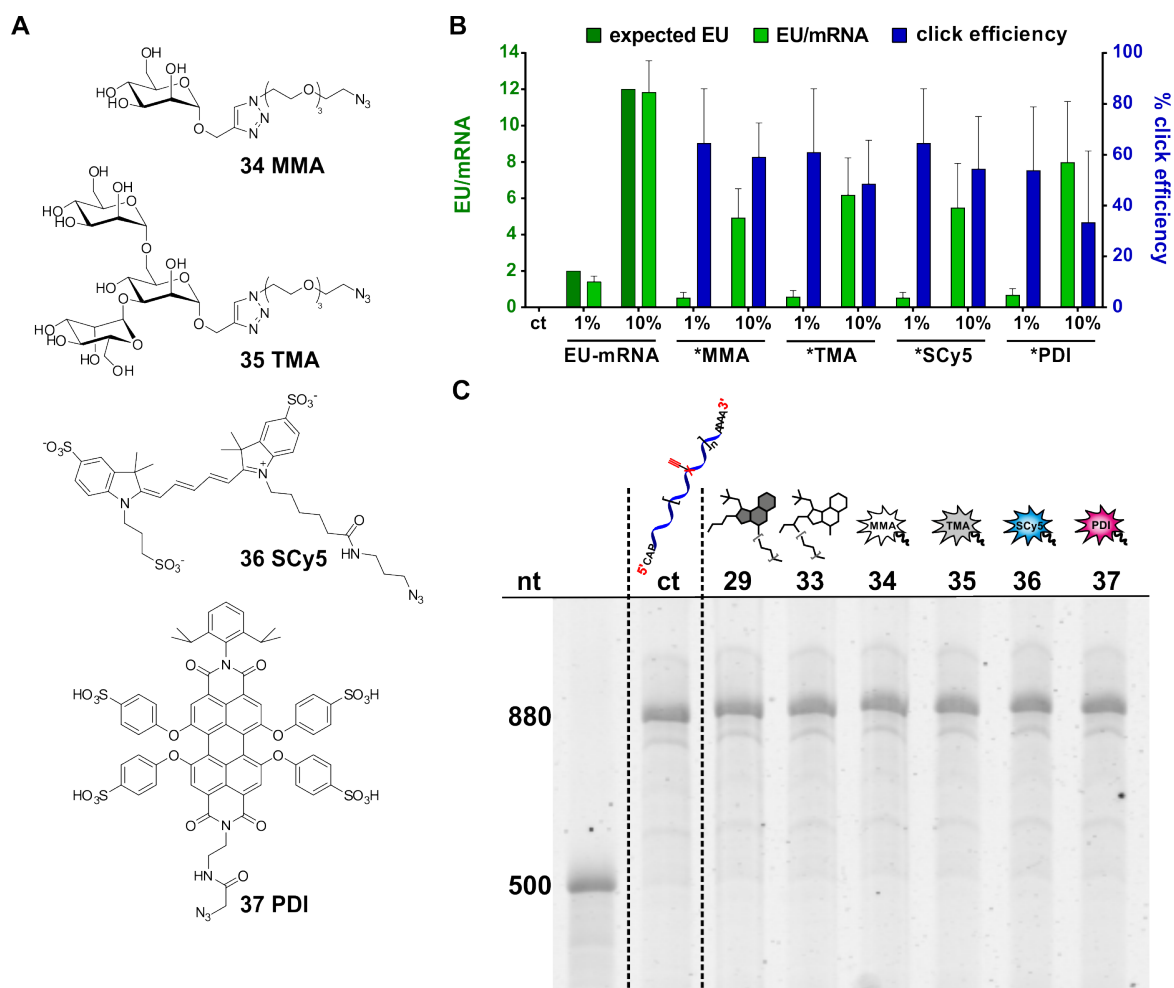


Figure 3.17: Selected azide-bearing molecules for study extension: **(A)** Chemical structure of sugar moieties mono- and tri-mannose (**34**, **35**), fluorescent dyes Sulfo-Cy5 (**36**) and perylene-derivative PDI (**37**). **(B)** HPLC-quantification of existing/remaining EU content in IVT- and clicked-eGFP-mRNA (light green bars) including click efficiency (blue bars) ($n = 2-5$; mean + SD) (ct = unmodified control eGFP-mRNA). **(C)** mRNA integrity after click-reaction: Exemplary degradation control of 10 %-alkyne bearing eGFP-mRNA on a 6 % polyacrylamide gel. The gel was post-stained with Stains-all (Sigma-Aldrich), which was excited at 633 nm and emission signals were recorded at 670 nm on a Typhoon 9400 (GE Healthcare). First lane shows a random RNA (*in vitro* transcript) of 500 nucleotides (nt) for size comparison; ct (control) *in vitro* transcribed and untreated 10 %-alkyne-mRNA; mRNA clicked with the symbolized azide-derivatives **29**) RPA, **33**) GDA, **34**) MMA, **35**) TMA, **36**) SCy5 and **37**) PDI. Clicked products show the same band shift as the untreated control, which confirms no impairment on RNA-stability after CuAAC reaction. (Modified fig. published in Hellmuth *et al.* [231])

Synthesis and analysis of the mRNA conjugates with molecules **34** to **37** was performed as described above (see section 3.2.2.2). A similar trend as in Figure 3.14 B could be observed regarding the 1 and 10 % modified constructs, which exhibit again a decline in yield for the click-outcome in correlation to the available alkyne-residues (Figure 3.17 B). Conversions of 1 and 10 % EU-containing mRNA by click-reaction yielded from 60-50 %, corresponding to 1 or 6, respectively,

successful modifications per molecule RNA. The verification of smTLRa-mRNA-integrity and constructs with molecules **34** to **37** after click reaction by PAGE is illustrated in Figure 3.17 C, revealing no significant degradation.

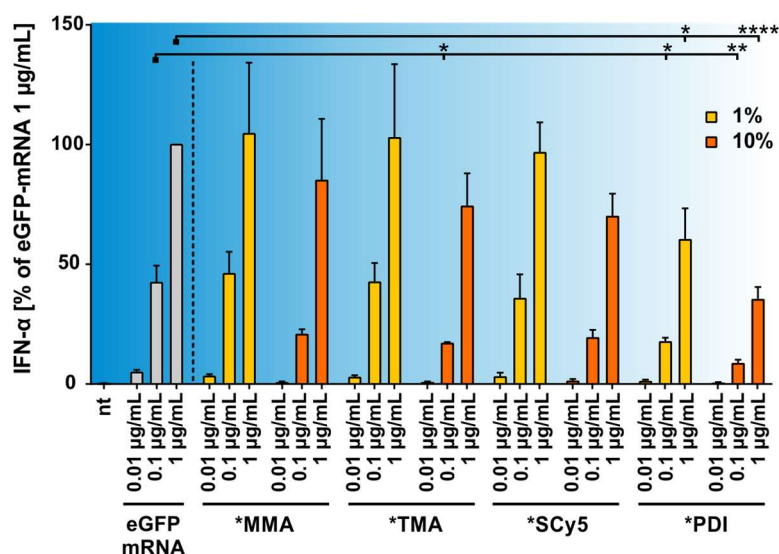


Figure 3.18: Effects of selected azide-bearing molecules of different molecular weight: Titration of PBMCs with eGFP-mRNA in comparison to 1 % (yellow bars) and 10 % (orange bars) alkyne-eGFP-mRNA clicked with molecules **34** to **37** (nt: non treated). IFN- α production was measured by ELISA. To account for donor variation in the absolute amount of IFN- α secreted, data from each individual were normalized to 1.0 $\mu\text{g/mL}$ eGFP-mRNA (= 100 %) ($n = 3$; mean + SD). (Asterisks above bars indicate the respective P values; no declaration = not significant (ns) evaluated by ANOVA and Dunnett's multiple comparisons test). (Data as published in Hellmuth *et al.* [231])

As lined out in Figure 3.18, the PBMC stimulation with the relevant mRNA-constructs showed again an attenuated immune response as opposed to unmodified eGFP-mRNA (grey), albeit to varying degrees. Nevertheless, it evokes the impression that, the smaller the ligand in size, the lesser the influence. This lead also to the most pronounced effect registered for the PDI dye, possessing the largest molecular weight, which showed also a significant response for the 1 % modified mRNA (yellow). Finally, together with the conclusion from Figure 3.16, one unequivocal message can be stated: the higher the degree of modification from 1 to 10 %, the lower the IFN- α level. For completion, the particular azides **34-37** were subjected to the immune cells as well, but did not elicit any detectable IFN- α secretion (not shown).

3.2.4 Transfer to siRNA

The results above revealed, that a covalent binding of small molecules to mRNA, whether TLR-agonists or not, mitigates the competence of RNA to induce IFN- α secretion by TLR7-activation.

They suggested additionally a contribution of the size and number of attached moieties per RNA molecule to the extent of inhibition. Accordingly, as the stimulation seemed to be dependent on the ratio of modification sites per RNA length-unit, it was expected that a single reaction site within a short siRNA exhibits in fact a more distinct outcome.

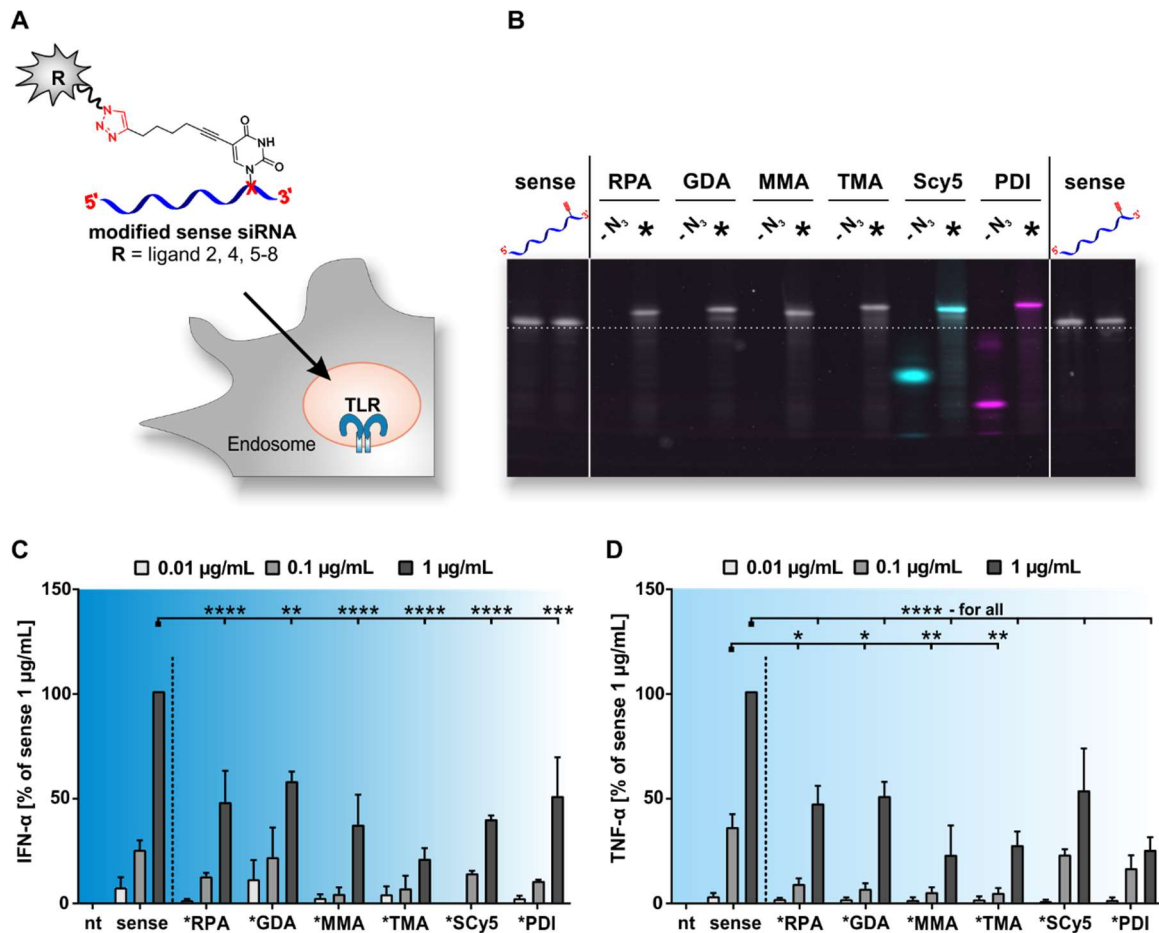


Figure 3.19: Application on mono-alkyne-functionalized sense eGFP-siRNA for diversification of the present study. **(A)** Sense siRNA-constructs for PBMC stimulation bearing the respective moieties (R) after click-functionalization. **(B)** A superimposition of three scan-modes: Denaturing polyacrylamide gel electrophoresis for comparison of the click efficiency of the single stranded, alkyne modified oligonucleotide MH662 (sense), free azides (-N₃) and purified clicked (★) oligonucleotides, showing band shift after click reaction and additional fluorescent signals for SCy5 (blue) and PDI (purple). For visualization before staining, excitation of dye-carrying constructs was done at 532 nm (PDI) and 633 nm (SCy5). Stains-all (grey/633 nm) was used as loading control to visualize non-fluorescent bands. Emission signals were recorded at 610BP30 nm and 670 nm. **(C)** and **(D)** show titration of PBMCs with sense-siRNA, clicked with molecules **29** and **33-37** (nt: non treated). IFN- α **(C)** and TNF- α **(D)** production were measured by ELISA. To account for donor variation in the absolute amount of cytokines secreted, data from each individual were normalized to 1.0 $\mu\text{g/mL}$ unmodified sense strand siRNA (MH662) (= 100 %) (n = 3; mean + SD). Asterisks above bars indicate the respective P values; no declaration = not significant (ns) evaluated by ANOVA and Sidak' s multiple comparisons test). (Part **(A)**-**(C)**) as published in Hellmuth *et al.* [231]

CuAAC reactions, to synthesize the siRNA-conjugates illustrated in Figure 3.19 A of a previously published TLR7 stimulating sequence [88], were again conducted as described before in section 3.1.3.3. In addition, the successful clicked siRNA-constructs, visible *via* band-shifts on PAGE in Figure 3.19 B, could be purified from unreacted material. Consequently, data from associated ELISA readouts could be referred to the 22 nucleotide long sense siRNA strands, each involving exactly a single modification at the 3'-end. The resulting types of cytokine release are reflected in Figure 3.19 C and D, provoked through the activation of both receptors in an analogue manner for TLR7 and 8, respectively. The alkyne-bearing control sense strand (MH662) gives the most pronounced amplitude in IFN- α and TNF- α secretion at a concentration of 1 μ g/mL. In contrast, all siRNA conjugates show at least a very significant decrease to 55 % in TLR activation, with the strongest outcome up to a 6-fold reduction to 20 % for the sugar-conjugates.

3.2.5 The effect of bioconjugates on TLR7-mediated immunostimulation is distinct from inhibition by ribose methylation

One known example of RNA-modification-triggered inhibition of immunostimulation, was effected through 2'-O-ribose methylation of guanosine at position 18 of a tRNA. It was even discovered to generate an actual antagonistic RNA when simultaneously present together with a stimulating RNA [90], [169] and is in many cases already relevant if occurring only once in a sequence [87], [274]. As contrasted with the initial hypothesis of gaining a cooperative boost through covalent combination of two PAMPs, the above findings relativized the impact to an overall decrease of receptor activation, which provoked the question, if this behavior followed an identical mode as known from 2'-O-methylated guanosine (Gm) carrying RNA [169]. For this purpose, a corresponding sequence of the afore mentioned siRNA, bearing a single Gm motive at position 8, was used besides siRNA-conjugates of RPA, GDA, TMA and PDI in a co-delivery assay. To this end, PBMCs were incubated with the stimulatory alkyne-siRNA (MH662) at a constant concentration of 1 μ g/mL and in parallel with increasing concentration of the particular conjugates or the methylated structure, respectively.

Matching with the published insights referred afore, Figure 3.20 shows a remarkable suppression of the stimulatory sense siRNA by the addition of the Gm-modified variant. Instead, stimulatory RNA together with the clicked conjugates entailed an additive increasing effect in IFN- α secretion and therefore do not block a further recognition of such ligands. A similar outcome would be expected for a contrasting juxtaposition of CuAAC-modified mRNA and an accordingly methylated mRNA, which occurs already naturally in many ways to distinguish self from non-self RNA structures [275].

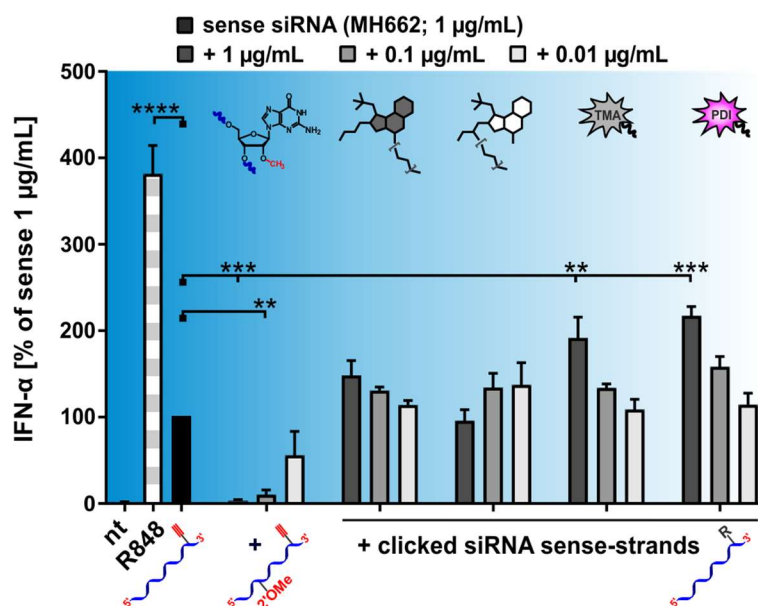


Figure 3.20: A new distinct type of inhibition of TLR7 mediated immunostimulation: Steric shielding acts different from immunosuppressive ribose-methylation. PBMCs were incubated with 1.0 µg/mL sense alkyne-siRNA (MH662) and simultaneously with a titration series of MH662 bearing either a Gm-motive (2'-OMe) at position 8, or MH662 clicked to azides of RPA (**29**), GDA (**33**), TMA (**35**) or PDI (**37**) (nt: non treated). IFN-α production was measured by ELISA. To account for donor variation in the absolute amount of IFN-α secreted, data from each individual were normalized to 1.0 µg/mL unmodified siRNA MH662 (= 100 %) (n = 3; mean + SD). (Asterisks above bars indicate the respective P values; no declaration = not significant (ns) evaluated by ANOVA and Dunnett's multiple comparisons test). (Fig. published in Hellmuth *et al.* [231])

3.2.6 Influence of RNA-modification on biologic activity

Not forgetting a possible therapeutic application of both investigated RNA-types of click-modified conjugates, the acquisition of the remaining biologic activity was included in the following paragraph. Consequences of natural and artificial modifications on structural siRNA features were already discussed in Section 3.1, this one here glances at the impact on knock-down capacity, in other words the RNAi efficiency, of corresponding siRNA-conjugates of the current study. In order to evaluate IC₅₀-values, hybridized double strands of the control MH662, the TMA- and PDI-conjugate with the complementary antisense strand (MH533) were subjected to HeLa MAZ cells, allowing the knock-down control of a destabilized eGFP [276] (Figure 3.21). The cells were incubated with a concentration series of siRNA double strands and fluorescence emission of eGFP was analyzed by FACS 24 hours later. In accordance with formerly published work of the Helm-lab [36], conjugation of the various azides to the 3'-end of the sense strand did not significantly increase the IC₅₀-values. In fact, the *PDI derivative (pink in Figure 3.21) displayed even a ~3-fold improved IC₅₀-value in contrast to the *TMA-construct. One could assume various reasons, as a possible enhanced membrane penetration from the endosome into the cytosol or an influence on siRNA structure and

stability could facilitate the building of the RISC-complex during RNAi [73], [193]. Nevertheless, this issue would require more detailed follow up investigations.

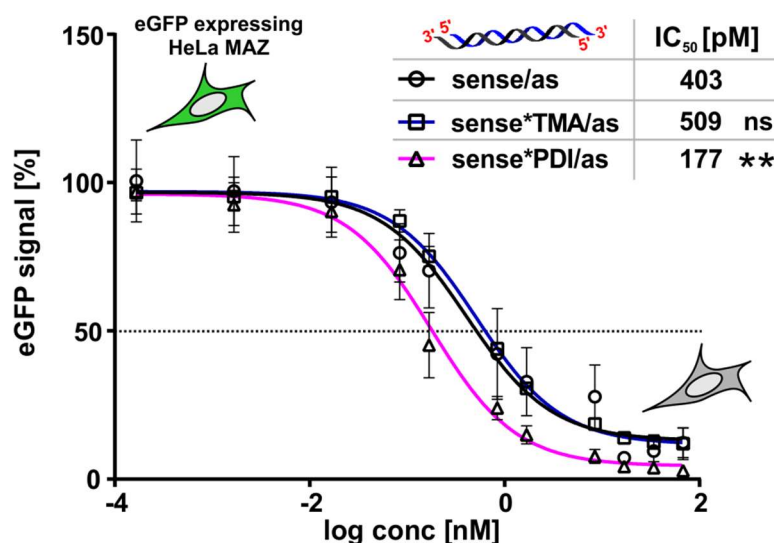


Figure 3.21: Modification does not interfere with, even enhance knock-down capacity. eGFP-knock-down experiments with unlabeled control- (sense), TMA (35)- and PDI (37)- siRNA double strands with antisense-strand (MH533 (as)) in HeLa MAZ (stably expressing eGFP) show similar behavior for the TMA-construct as the unmodified control and a significantly lower IC₅₀ for the PDI-construct. IC₅₀ values were determined through a non-linear fit after logarithmic data-transformation (n = 3; mean + SD). (Asterisks next to IC₅₀ values indicate the respective P values evaluated by ANOVA and Dunnett's multiple comparisons test; not significant (ns)). Knock-down experiments were kindly performed by [REDACTED], data-evaluation, statistical analysis and interpretation was part of the current study. (Data as published in Hellmuth *et al.* [231])

Translation efficiencies resulting from mRNAs owing natural nucleoside modifications seem to benefit through higher and stable expression rates [173]. Although some publications state improved protein expression from “chemically” modified mRNA, they applied in fact exclusively natural occurring nucleoside modifications [75], [247]. Sawant *et al.* [39] introduced actual synthetically modified NTPs during IVT followed by post-transcriptional labeling, so did Holstein *et al.* [227] modify the 5'-cap structure, but both did not comment on mRNA functionality in translation. Finally, as part of the current work, it was explored in which ways the implemented synthetic variations influence expression of the model-protein eGFP. Therefore, immature monocyte derived DCs, were transfected through electroporation with differentially treated mRNA samples. eGFP fluorescence intensity was measured 24 hours later by flow cytometry. The introduction of an alkyne-moiety from 1 to 10 % *via* IVT, did not have any negative impact on protein expression (Figure 6.6), only a to 50 % modified alkyne-mRNA showed strongly reduced fluorescence. However, eGFP expression was diminished through click-mediated attachment of azides 29, 33-37 to the eGFP-mRNA, exemplary by 1 %-SCy5-clicked mRNA in the middle and lower histograms of Figure 3.22 B, which shows in addition the dye signal. Possible influences resulting from click-

reaction conditions were evaluated through testing of samples from azide-excluding mock-reactions, confirming no correlation from there (Figure 3.22 B upper histograms).

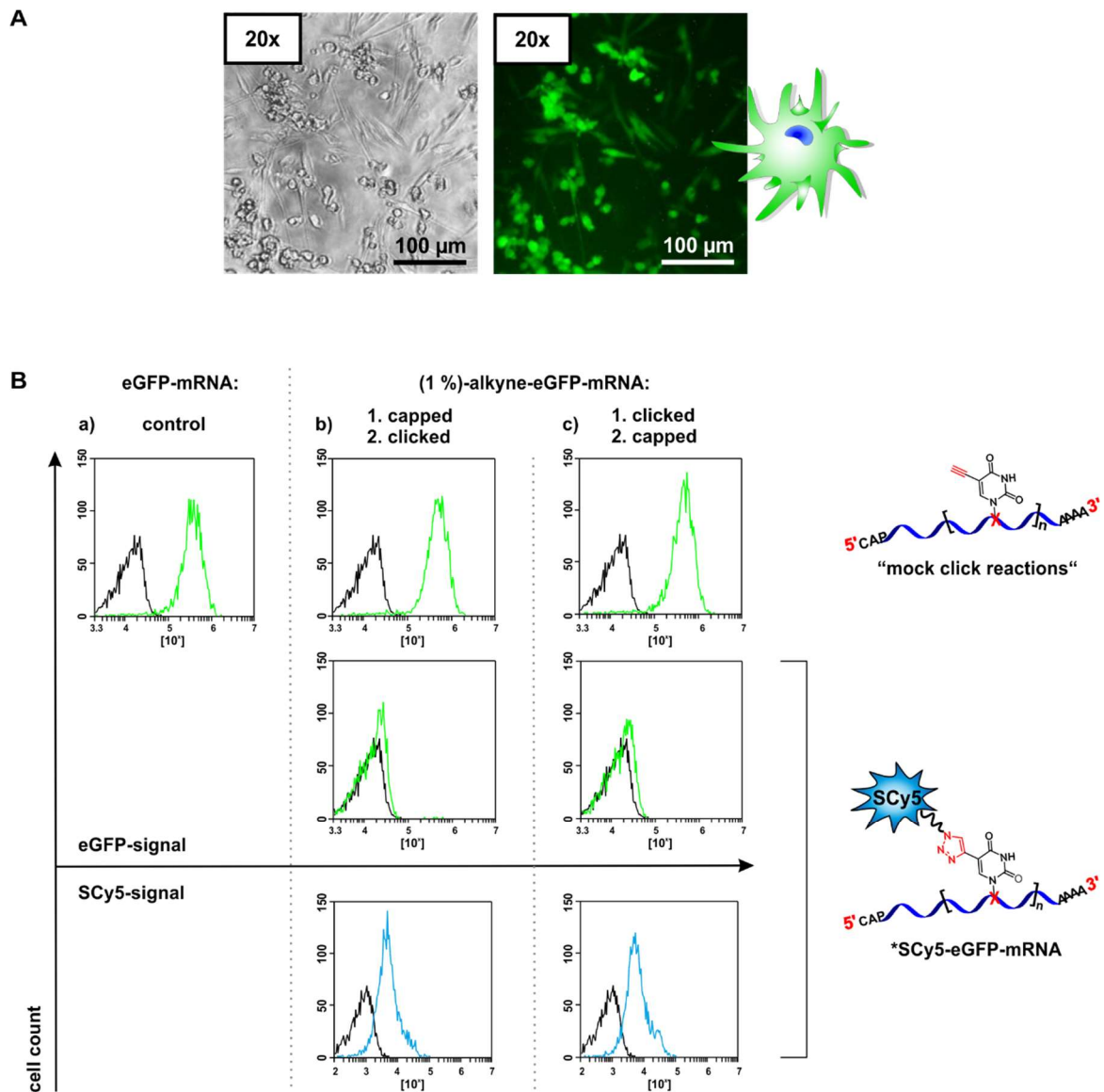


Figure 3.22: Protein expression in DC is inhibited by large mRNA modifications. Electroporation of immature DC: **(A)** Microscopy images of eGFP expressing DC 24 h after electroporation with unmodified eGFP-mRNA. **(B) a)** Treatment of iDCs with capped unmodified eGFP-mRNA (green) and PBS (black) as control. Next, a (1 %)-alkyne-eGFP-mRNA was applied in two different ways: **b)** capping reaction first, followed by click reaction and **c) vice versa**. Mode b) and c) were both conducted in a “mock“ version, missing the azide-reaction partner (upper histograms) and with Sulfo-Cy5-azide as click-reaction partner (lower histograms including SCy5 signal in blue). Microporation experiments and data-evaluation were kindly performed by [REDACTED], data-interpretation was part of the current study. (Figure published in Hellmuth *et al.* [231])

One can conclude, that even a single lateral conjugation anywhere throughout an mRNA is not tolerated by the translational machinery. However, it might be worth to look sequentially at the modification of single mRNA-segments to identify possible permissive regions. This would not be feasible through a full IVT, but by the IVT synthesis of fragments, which can be ligated afterwards. Just for a little outlook, one could compile a library of differentially modified and unmodified mRNA-segments for diverse combinations to study such coherences.

4 Conclusion and Outlook

Conversion of deoxyuridine to a “clickable” deoxycytidine

A synthesis route, comprising six reaction steps, towards the conversion of deoxyuridine into the phosphoramidite of an *N4* modified deoxycytidine (dC), bearing an exocyclic propargyl-moiety, was followed. Based on a model sequence of an anti-eGFP sense siRNA strand, the resulting DNA-building block was applied in solid phase oligodeoxyribonucleotide (ODN) synthesis of seven individually designed strands, each exhibiting the modified base at a varying position from the 3'-end over internal introductions to the 5'-end. For the purpose to carry out a comparative study, the same procedure was in parallel conducted, by Dr. Olwen Domingo, towards a C5-methylated and *N4*-propargylated dC derivative and respective DNA sense strands.

To determine the orientation of the *N4*-propargyl moiety of both cytidines on the nucleoside level, the free nucleosides were obtained from their phosphoramidite precursors and were subjected to 2D NMR experiments concerning rotating-frame nuclear Overhauser effect spectroscopy (ROESY-NMR) investigations. *Via* these experiments, it could be revealed, that the *N4*-propargyl moiety of dC, which has the possibility to adopt either an *s-cis*- or *-trans* conformation, exhibits a certain limited rotation around the C4-*N4* bond, which led to the occurrence of 10 % of the *s-trans* conformation.

The effect of the afore discovered rotation barriers of the alkyne functionalized exocyclic *N4* at dC and 5mdC within a double helix was investigated, in cooperation with Dr. Olwen Domingo, *via* the thermodynamic stability of the different duplexes by accessing UV-melting profiles. It was anticipated, that, within a double strand, the unmethylated derivative adopts its *s-trans*-conformation, which is impeded for 5mdC by the bulky methyl group, driven by the evolving free energy from hybridization processes, in order to permit base-pairing at the Watson-Crick edge. The melting data lead to the conclusion that the mono-substituted *N4*-propargyl cytidines integrate well into a helix, which implies rotating the substituent to the “CH”-edge to allow base pairing [193]. In contrast, the C5-methyl group of 5mdC blocked this mechanism leading to a disrupted W-C base pairing and destabilized double helices, most pronounced for internal sequence modifications, which was reflected in the melting profiles and extended experiments towards helix formation with DNA strands featuring abasic sites opposite selected modified positions. The provided insights of this study should be taken into account for DNA and RNA duplex design and labeling, particularly in the case of siRNA, where the antisense strand profits *e.g.* from a less stable 5'-end in order to be selected for incorporation into the RNA interference-induced silencing complex (RISC) [277].

Further participation of the modified ODNs in CuAAC reactions with fluorescent dyes, exhibited successful labeling for both, dC and 5mdC, even at less accessible internal sequence positions. Such functionalization could serve as a handy tool to investigate subcellular distributions and the fate of transfected oligonucleotides and biological effects of triazole linkages.

Steric shielding of RNA from recognition by TLR7 & 8

Two small molecule TLR agonists (smTLRa), namely resiquimod (R848) and gardiquimod (GQI), were synthetically derivatized for posttranscriptional immobilization on RNA *via* CuAAC-click chemistry and evaluated concerning their immunostimulatory activity *via* TLR 7 and 8 in human immune cells. The resulted interferon levels for the single smTLRas and derivatives (RPA and GDA) revealed a moderate to comparable activity of RPA with R848, but a completely blocked TLR activation of the gardiquimod derivative GDA.

Aside from this, a functional eGFP-mRNA was developed, including the introduction of the alkyne modified nucleoside 5-ethynyl-uridine as triphosphate (EUTP) during *in vitro* transcription. From those two reaction partners, azide-bearing smTLRa and alkyne-bearing mRNA, covalent smTLRa-mRNA constructs, bearing varying contents of modification, were afforded through the application of CuAAC-click reaction. Incorporation rates of the clickable nucleoside and efficiencies of click-reactions could be unveiled through HPLC-quantification, revealing excellent applicability of EUTP during T7-RNA-polymerase mediated *in vitro* transcription and click-successes of 80 % for the smTLRa derivatives. This modification scheme by CuAAC chemistry on mRNA was explored, to the best knowledge, for the first time concerning immunostimulation and protein expression. Hence, the main element of this study considered the evaluation of cytokine release by human immune cells under the influence of the created smTLRa-mRNA conjugates and their respective building blocks. Besides the described long and coding mRNAs, investigations involved also the modification and application of siRNA-conjugates, representing short non-coding RNAs, and a scope expansion towards azide-bearing structures, which represented inherently non-PAMPs for TLR 7 and 8.

In conjunction with findings from past studies, which showed that ODNs/ORNs and purine-like TLR agonistic SMs can counterinfluence each other [232], [278], [279], it was monitored that there is no negative action between RNA and smTLRa, as long as there is no covalent connection. Combined administration of mRNA and (unconjugated) resiquimod could even increase the interferon response, that was already saturated with respect to resiquimod, indicating additional capacity for activation not accessible by R848 alone. While the pursued hypothesis of a cooperative effect of the smTLRa-mRNA conjugates could not be achieved, it led to the observation, that modification of RNA results in efficient decrease of TLR7/8 relevant immunostimulation. However, this was somewhat surprising, due to the fact, that covalent antigen-TLR7/8 conjugates were shown to exhibit enhanced immunity [162]. Thus, the underlying effect of the presented conjugates had to be investigated and could be distinguished from the known inhibitory and antagonistic motive of 2'-O-methylated guanosine in RNA [90], [169].

For completion, the influence of RNA modifications towards biologic activity was examined in terms of siRNA knock-down capacity and mRNA translational activity. To that effect, siRNA conjugates, whose potentially undesired immunostimulation was partially shielded by bulky conjugates, continued promising in its function. The addition of a large dye-molecule (PDI) even improved RNAi efficiency, while detailed follow-up studies would be required to determine the extent of this effect. In contrast, EU-bearing mRNAs kept their translational functionality upon 10 % modification content, but was completely ablated by further “clicked” moieties on 5-position of uridines, even by a single modification. Thus, a single lateral conjugation anywhere throughout an mRNA seemed not able to be tolerated by the translational machinery. However, it might be worth to look deeper into the sequential modification of single mRNA-segments to identify possible permissive regions. This could possibly be realized by the IVT synthesis of ligation-fragments in combination with deep sequencing methods. As an outlook, one could compile a library of differentially modified and unmodified mRNA-segments for diverse combinations to study such coherences.

Although, the working hypothesis of generating immunological and biological active bidentate smTLRa-mRNA constructs could not be realized, such modulation of TLR activation is of high interest in the design and development of therapeutic RNA. To be annotated, siRNA-conjugates bearing trimeric sugar moieties, similar to the tri-mannose-conjugate of the current study, are in pre-clinical trials [280], and their immunogenic potential is likely to be affected in a similar way.

5 Experimental Section

5.1 Materials

5.1.1 Instruments

Analytical balances:

- Sartorius Sartorius (Goettingen, Germany)
- Mettler Toledo PM460 Mettler Toledo (Gießen, Germany)
- Mettler Toledo Excellence Plus Mettler Toledo (Gießen, Germany)

BIOER ThermoCell

BIOER (Hangzhou, China)

Centrifuges:

- 1 - 15 PK Sigma Sigma (Osterode am Harz, Germany)
- Eppendorf Centrifuge 5810 Eppendorf (Hamburg, Germany)
- Avanti J25 Beckmann Coulter (Krefeld, Germany)
- Sprout mini-centrifuge Biozym (Hessisch Oldendorf, Germany)
- SpeedVac Concentrator Plus Eppendorf (Hamburg, Germany)

DNA/RNA synthesizer,

(Applied Biosystems Expedite TM 8909)

Genecust (Dudelange, Luxembourg)

Fluorimeter (JASCO FP-6500)

Jasco (Groß-Umstadt, Germany)

Gel electrophoresis:

- LSG-400-20 NA vertical chamber C.B.S. Scientific (San Diego, USA)
- Consort EV232 power supply Consort (Turnhout, Belgium)
- Model 250/2.5 power supply BioRad (München, Germany)
- PerfectBlue Gelsystem PeqLab (Erlangen, Germany)

HPLC:

- Agilent HP 1100 (DAD, FLD) Agilent (Böblingen, Germany)
- Agilent HP 1200 (DAD) Agilent (Böblingen, Germany)
- C18 RP column (LiChroCART 250-10) Merck (Darmstadt, Germany)
- Superdex™ 200 column GE Healthcare (Buckinghamshire, UK)

– Synergy fusion RP (4 µm particle size, 80 Å pore size, 250 mm length, 2 mm inner diameter)	Phenomenex (Aschaffenburg, Germany)
IR Spectrometer (Nicolet AVATAR 330FT-IR)	Thermo Electron Corporation (USA)
Lyophilizer (Alpha 2-4 LD plus)	Christ (Osterode am Harz, Germany)
Mass spectrometry:	
– ESI; Micromass LCT	Waters (Eschborn, Germany)
– HR-ESI; Q-ToF-Ultima 3	Waters (Eschborn, Germany)
– FD; Finnigan MAT95	Thermo Electron Corporation (USA)
– MALDI; BIFLEX III	Bruker (Leipzig, Germany)
– Triple Quadrupole (Agilent 6560)	Agilent (Böblingen, Germany)
NanoDrop ND-2000	PeqLab (Erlangen, Germany)
NMR spectrometry:	
– NMR tubes	Deutero GmbH (Kastellaun, Germany)
– Avance III HD 300	Bruker (Leipzig, Germany)
– Avance III HD 400	Bruker (Leipzig, Germany)
– Varian Unity-300	Varian (California, USA)
Melting point:	
– KSP1D melting point meter	Krüss Optronic (Hamburg, Germany)
– Capillary tubes	Marienfeld (Lauda-Königshofen, Germany)
pH-meter (FiveEasy™ FE20)	Mettler Toledo (Gießen, Germany)
Pipette boy (Integra)	VWR (Darmstadt, Germany)
Qubit™ 2.0 fluorometer	Thermo Fisher Scientific
Rotary evaporator (VV 60)	Heidolph (Schwabach, Germany)
Shaker (DOS-10L)	neoLab (Heidelberg, Germany)
Spectrophotometer (JASCO V-6500)	Jasco (Groß-Umstadt, Germany)
Thermoshaker Plus	Eppendorf (Hamburg, Germany)
Typhoon 9600 variable mode imager	GE Healthcare (Buckinghamshire, UK)
Ultrapure water purification system MilliQ	Millipore (Schwalbach, Germany)
UV-Lamp 254/365 nm	Herolab (Wiesloch, Germany)
Variable micropipettes (Discovery Comfort) (2, 10, 20, 100, 200 and 1000 µL)	Abimed (Langenfeld, Germany)
Vortex Mixer (7-2020)	neoLab (Heidelberg, Germany)
Wallac 1409 liquid scintillation counter	PerkinElmer (Waltham, USA)

5.1.2 Chemicals & Consumables

Antibiotics:

- Ampicillin Roth (Karlsruhe, Germany)
- Kanamycin Fluka (Buchs, Germany)

Chemicals (general):

Chemical reagents and solvents were obtained from various commercial suppliers: Acros Organics (Belgium), Carl Roth (Karlsruhe, Germany), Sigma Aldrich (Steinheim, Germany), VWR (Darmstadt, Germany).

- Gardiquimod Enzo Life Sciences (Lörrach, Germany)
- Deuterated solvents Deutero GmbH (Kastellaun, Germany)
- Resiquimod InvivoGen (San Diego, California USA)

Dyes:

- AlexaFluor 594 azide Invitrogen (Karlsruhe, Germany)
- Atto 488 azide Atto-Tec (Siegen, Germany)
- Atto 590 azide Atto-Tec (Siegen, Germany)
- 3-(Dansylamino)phenyl boronic acid Sigma Aldrich (Steinheim, Germany)
- Sulfo Cy5 azide Jena Bioscience (Jena, Germany)

Kits:

- GenElute™ HP Endotoxin-Free Plasmid Maxiprep Kit Sigma Aldrich (Steinheim, Germany)
- MEGAclean™ Transcription Clean-up Kit Invitrogen (Karlsruhe, Germany)
- Qubit® RNA HS Assay Kit Thermo Fisher Scientific

Plastic-ware:

- Disposable serological pipettes (5, 10, 25 mL) Sarstedt (Nümbrecht, Germany)
- Disposable plastic macro cuvettes Sarstedt (Nümbrecht, Germany)
- Eppendorf tubes (1.5, 2.0 mL) Roth (Karlsruhe, Germany)
- Falcon® tubes (15, 50 mL) CellStar (Frickenhausen, Germany)
- MicroSpin Sephadex® G-25 columns GE Healthcare (Munich, Germany)
- NAP columns (5/10/25), Sephadex® G-25 GE Healthcare (Munich, Germany)
- Needles (Sterican®) Braun (Melsungen, Germany)
- Parafilm® VWR (Darmstadt, Germany)
- Petri dishes Sarstedt (Nümbrecht, Germany)
- Pipette tips (10, 20, 100, 200, 1000 µL) Greiner Bio-One (Frickenhausen, Germany)
(with filter, sterile RNase/DNase free)
- Scintillation counting vials Roth (Karlsruhe, Germany)

- Spin filters Nanosep® Roth (Karlsruhe, Germany)
- Syringes (1, 2, 5, 10, 20 mL) Braun (Melsungen, Germany)
- Whatman filter paper Roth (Karlsruhe, Germany)
- ZipTip Millipore (Schwalbach, Germany)

SPOS reagents:

Sigma, Proligo (Hamburg, Germany)

- Activator 42 (5-[3,5-Bis(trifluoromethyl)phenyl]-1*H*-tetrazole (0,1 M in CH₃CN))
- Caps A (acetic anhydride in THF (11 % v/v))
- Caps B (*N*-Methylimidazole in THF (16 % v/v))
- DCA Deblock (dichloroacetic acid in DCM (3 % v/v))
- TCA Deblock (trichloroacetic acid in DCM (3 % v/v))
- Wash acetonitrile, extra dry)

5.1.3 Buffers & Media

All buffers and media were prepared either by using MilliQ-water or, if required for cell culture, with RNase/DNase- and endotoxin-free water (Zymo Research). Buffers and media were prepared as described by the manufacturers, otherwise, compositions are depicted below.

E. coli culturing and plasmid preparation

- **LB broth** (Lennox) Sigma Aldrich (Steinheim, Germany)
- **LB broth with agar** (Lennox) Sigma Aldrich (Steinheim, Germany)
- **PBS 10x:**
1.4 M NaCl, 27 mM KCl, 15 mM KH₂PO₄, 80.6 mM Na₂HPO₄ in H₂O (pH 6.8).

RNA in vitro synthesis

- **Straßbourg buffer:**
40 mM Tris-HCl (pH 8.1), 1 mM spermidine, 5 mM DTT, 0.01 % Triton X-100
- **SAM dilution buffer:**
5 mM H₂SO₄ in 10 % aq. EtOH

Gel electrophoresis

- **PAGE - denaturing mixture** (compounds for denaturing PAGE from Carl Roth®)

Table 5.1: Denaturing TBE-PAGE gels for separation of single stranded nucleic acids in 100 mL.

	6 %	10 %	20 %
Gel concentrate (25 %) [mL]	24.0	40.0	80.0
Gel diluent [mL]	66.0	50.0	10.0
10x TBE [mL]	10.0	10.0	10.0

+ 400 μ L APS (10 % m/v ammonium persulfate in MilliQ) (Roth, Karlsruhe/Germany) and 50 μ L TEMED (Roth, Karlsruhe/Germany).

- **PAGE - non-denaturing (native) mixture** (compounds for PAGE from Carl Roth®)

Table 5.2: Native TBE-PAGE gels for separation of double stranded nucleic acids in 100 mL.

	10 %	15 %	20 %
40 % acrylamide mix (19:1) [mL]	25.0	37.5	50.0
10x TBE [mL]	10.0	10.0	10.0
MilliQ water [mL]	65.0	52.5	40.0

+ 800 μ L APS (10 %) and 60 μ L TEMED.

- **PAGE loading buffer, non-denaturing (native), colorless:**
1x TBE (from 10x) and 60 % v/v glycerol.
- **PAGE loading buffer, denaturing, colorless:**
1x TBE (from 10x) and 90 % v/v formamide in water.
- **PAGE loading buffer, denaturing, blue:**
1x TBE (from 10x), 90 % v/v formamide, 0.1 % xylene cyanol, and 0.1 % bromphenol blue in water.

Staining solutions

- **GelRed™** (agarose, PAGE):
GelRed™ (Biotium, Hayward/USA) was diluted 1:3 with 1x TBE. Immersion of gel for 20 minutes.
- **Ninhydrin** (TLC):
0.1 mg ninhydrin, 0.5 mL acetic acid in 100 mL acetone. Immersion of TLC followed by careful heating.
- **Seebach** (TLC):
Phosphor-molybdic acid (2.50 g), $\text{Ce}(\text{SO}_4)_2$ (1.00 g) and concentrated H_2SO_4 (6 mL in 94 mL water). Immersion of TLC followed by careful heating.
- **StainsAll-staining** (PAGE):
10 % v/v StainsAll (Sigma Aldrich) in formamide (0.1 % m/v), 25 % v/v isopropanol and 65 % v/v 1x TBE. Immersion of gel for 20 minutes.
- **StainsAll-destain** (PAGE):
25 % v/v isopropanol and 75 % v/v 1x TBE. Immersion of gel overnight.
- **SYBR®Gold** (agarose, PAGE):
10.000x dilution of SYBR®gold nucleic acid gel stain (Invitrogen) in 1x TBE. Immersion of gels after electrophoresis for 20 minutes.

HPLC analysis

- **Nuclease P1 buffer 10x:**
0.2 M ammonium acetate (pH 5.0) and 0.2 mM ZnCl₂
- **TEAA buffer** (2 M stock solution):
2 mol triethylamine, 2 mol acetic acid in 1 L H₂O.

5.1.4 Enzymes & Oligonucleotides**Enzymes**

- | | |
|---|---|
| - Bcul (SpeI) restriction enzyme | Thermo Fisher Scientific |
| - DNaseI, RNase free | Thermo Fisher Scientific |
| - FastAP thermosensitive alkaline phosphatase | Fermentas (St. Leon-Roth, Germany) |
| - mRNA Cap 2'-O-methyltransferase | New England Biolabs (NEB)
(Frankfurt am Main, Germany) |
| - Nuclease P1 | Sigma Aldrich (Munich, Germany) |
| - Snake venom phosphodiesterase | Worthington (Lakewood, USA) |
| - Vaccinia Capping System | NEB (Frankfurt am Main, Germany) |

RNA oligonucleotides**Table 5.3:** Sequence information for applied commercial RNA oligonucleotides.

Name	Category	Sequence (5'-3')	Supplier
<i>CpDCII2</i> (ODN2.2)	eGFP-sense, DNA	G X AAGCTGACCCTGAAGTTCAT x = N ⁴ -propargyl-2'-deoxycytidine	in house SPOS s. Section 5.3.1
<i>CpDCII6</i> (ODN6.2)	eGFP-sense, DNA	GCAAG X TGACCCTGAAGTTCAT x = N ⁴ -propargyl-2'-deoxycytidine	- -
<i>CpDCII10</i> (ODN10.2)	eGFP-sense, DNA	GCAAGCTGA X CCTGAAGTTCAT x = N ⁴ -propargyl-2'-deoxycytidine	- -
<i>CpDCII11</i> (ODN11.2)	eGFP-sense, DNA	GCAAGCTGAC X CTGAAGTTCAT x = N ⁴ -propargyl-2'-deoxycytidine	- -
<i>CpDCII12</i> (ODN12.2)	eGFP-sense, DNA	GCAAGCTGACC X TGAAGTTCAT x = N ⁴ -propargyl-2'-deoxycytidine	- -
<i>CpDCII20</i> (ODN20.2)	eGFP-sense, DNA	GCAAGCTGACCCTGAAGTT X AT x = N ⁴ -propargyl-2'-deoxycytidine	- -
<i>CpDCII21</i> (ODN21.2)	eGFP-sense, DNA	GCAAGCTGACCCTGAAGTTC X T x = N ⁴ -propargyl-2'-deoxycytidine	- -
MH533	eGFP-antisense, RNA	gaacuucagggucagcuugccg	IBA (Göttingen, Germany)

MH534	eGFP-sense, RNA	gcaagcugaccuccugaaguuc <u>au</u>	IBA
MH661	eGFP-sense, DNA	GCAAGCTGACCCTGAAGTTCAT	IBA
MH662	eGFP-sense, RNA	gcaagcugaccuccugaaguuc <u>X</u> x = C8-alkyne-dtCE phosphoramidite (Glen Research, Virginia, USA)	IBA
MH662- Gm8	eGFP-sense, RNA	gcaagcu <u>Gm</u> accuccugaaguuc <u>au</u>	IBA
MH663 (COMP0)	eGFP-antisense, DNA	GAACTTCAGGGTCAGCTTGCCG	IBA
MH677 (COMP10)	eGFP-antisense, DNA	GAACTTCAG <u>X</u> GTCAGCTTGCCG x = abasic site	IBA
MH674 (COMP11)	eGFP-antisense, DNA	GAACTTCAGG <u>X</u> TCAGCTTGCCG x = abasic site	IBA

pDNA vectors

Table 5.4: Plasmid DNA applied for transformations.

Name	AB resistance gene		Supplier
pUC19 (control)	ampicillin		NEB
pGEM4Z64A-eGFP [242]	ampicillin	Bcul	Gift from AG Jonuleit
pGEM4Z64A-MelanA [242]	ampicillin	Bcul	Gift from AG Jonuleit
pJ201:142870-MelanA-GFP	kanamycin	Bcul	DNA2.0/Atum (Newark, USA)

5.1.5 Software

ApE - plasmid editor v1.17	Wayne Davis
ChemBioDraw Ultra 12.0	CambridgeSoft/PerkinElmer (USA)
CorelDRAW® X7	Corel Corporation (Ottawa, Canada)
GraphPad Prism 7.0 - statistical analysis	GraphPad Software (San Diego, USA)
ImageJ2	LOCI (Madison, USA)
Mendeley Desktop 1.17.6	Mendeley Ltd. (London, UK)
MestReNova v7.1.1-9649	Mestrelab Research (Spain)
OMNIC™ IR spectra software	Thermo Fisher Scientific
QtiPlot 0.9.8.9	Ion Vasilief

5.2 Organic syntheses

General procedures

Chemical reagents and solvents were obtained from various commercial suppliers. All reagents were reagent grade and used without further purification, unless otherwise noted. The eluents for column chromatography were distilled prior to use. All reactions involving air or moisture sensitive reagents or intermediates were performed under an inert atmosphere of argon in glassware that was oven dried using standard Schlenk techniques. Reaction temperatures referred to the temperature of the particular cooling/heating bath.

Thin-layer chromatography (TLC): Pre-coated silica gel plates, Polygram[®] Sil G/UV₂₅₄ (40 x 80 mm) from Macherey-Nagel (Düren, Germany). Compound spots were visualized with UV-light at $\lambda = 254$ nm and/or by immersion in Seebach's reagent. Dimethoxytrityl containing compounds were stained orange and subsequent heating to ~ 90 °C resulted in the formation of blue stains for nearly all compounds. Alternatively, the TLC plates were developed in an iodine-chamber or immersed in a solution of *m*-methoxyphenol (0.1 mL) in ethanol (95 mL) and sulfuric acid (2 mL) followed by heating.

Column chromatography: Silica gel 60 (230-400 mesh) was purchased from Sigma-Aldrich (Taufkirchen, Germany; product manufactured by Fluka, Buchs, Switzerland) and Merck KGaA (Darmstadt, Germany), respectively.

NMR-spectroscopy: NMR spectra were recorded on an *Avance III HD 300* (300 MHz ¹H-NMR, 75 MHz ¹³C-NMR; Bruker) and an *Avance II 400* (400 MHz ¹H-NMR, 101 MHz ¹³C-NMR; Bruker) using 5 mm probe heads at a temperature of 23 °C. The ¹H and ¹³C chemical shifts (δ) were referenced to the residual solvent signal as internal standard (CDCl₃: $\delta = 7.26$ ppm and 77.16 ppm, DMSO-*d*₆: $\delta = 2.50$ ppm and 39.50 ppm, CD₃OD: $\delta = 3.31, 4.78$ ppm and 49.00 ppm for ¹H and ¹³C NMR, respectively) [281]. Coupling constants (*J*) are reported in Hz (splitting abbreviations: s, singlet; d, doublet; t, triplet; q, quartet; m, multiplet; br, broad; and combinations thereof).

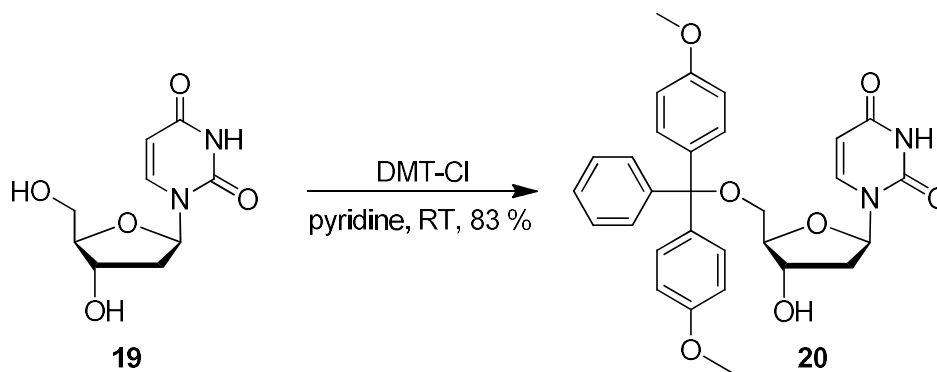
IR spectroscopy: IR spectra were recorded with a Nicolet Avatar 330 FT-IR spectrometer (Thermo Electron Corporation, USA).

Mass spectrometry: Mass spectra were obtained from various instruments depending on the required technology: ESI spectra: Micromass LCT spectrometer; High-resolution masses (ESI) were recorded on a *Q-ToF-Ultima 3* instrument (Waters) with LockSpray[®] interface and a suitable external calibrant. Further ESI measurements were received from a Finnigan MAT TSQ 700 and FD results from a Finnigan MAT95 at the Institute of Organic Chemistry, University of Mainz. MALDI-TOF (positive mode) mass spectra were recorded on a Bruker BIFLEX III (IPMB, University of Heidelberg) spectrometer with matrix 3-hydroxypicolinic acid, (NH₄)₂-citrate.

5.2.1 Synthesis of 3'-O-CEP-5'-O-DMT-N⁴-propargyl-2'-deoxycytidine 25b

The following data are also published in Domingo and Hellmuth *et al.* [193].

5.2.1.1 5'-O-Dimethoxytrityl-2'-deoxyuridine 20



Triethylamine (0.24 mL, 1.72 mmol, 0.78 eq.) was added to a stirred solution of 2'-deoxyuridine **19** (0.50 g, 2.20 mmol) in dry pyridine (2.50 mL) under argon atmosphere, followed by dropwise addition of DMT-Cl (1.12 g, 3.30 mmol, 1.50 eq.), dissolved in a minimal amount of dry pyridine. The reaction mixture was stirred at ambient temperature until all starting material has been converted to the tritylated product **20**, which was monitored *via* TLC. The reaction was quenched with methanol (2 mL) and the resulting mixture was concentrated *in vacuo*. Purification of the residue *via* column chromatography (silica gel) with DCM/MeOH (20:1, containing 1 % triethylamine) yielded a colorless solid **20** (0.96 g, 1.82 mmol, 83 %).

m.p.: $T_m = 98\text{ }^\circ\text{C}$.

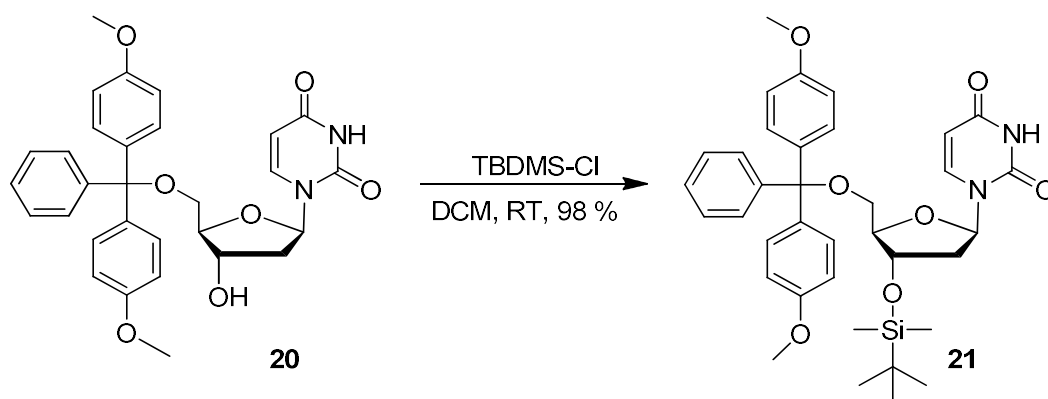
TLC: silica gel, DCM/MeOH (15:1); $R_f = 0.35$.

¹H-NMR (300 MHz, DMSO-*d*₆): δ [ppm] = 11.33 (1H, s, NH), 7.64 (1H, d, H-6, $^2J = 8.1$ Hz), 7.37 (2H, H_{A,A'}), 7.31 (2H, H_{B,B'}), phenyl (AA'BB'X, $^3J = 7.6$ Hz, H_X overlapped by H_{A,A'} aryl), 7.24 (4H, H_{A,A'}), 6.89 (4H, H_{B,B'}), DMT moiety: aryl (AA'BB', $^3J = 8.6$ Hz), 6.14 (ABXY, 1H, m, H-1'x); 5.37 (1H, d, H-5, $^3J = 8.1$ Hz), 5.35 (1H, d, 3'-OH, $^3J = 4.5$ Hz, partially overlapped by H-5), 4.28 (ABXY, 1H, m, H-3'y), 3.87 (ABX, 1H, m, H-4'x), 3.74 (6H, s, OCH₃), 3.20 (ABX, 2H, m, H-5'_{A,B}, $^2J_{AB} = 10.4$ Hz), 2.18 (ABXY, 2H, m, H-2'_{A,B}).

¹³C-NMR (101 MHz, DMSO-*d*₆): δ [ppm] = 163.03 (C-4), 158.10 (aryl), 150.32 (C-2), 144.71 (aryl), 140.44 (C-6), *ipso*-C (phenyl): 135.43, 135.22; 129.75 (O-C, aryl), phenyl (CH): 127.88, 127.69, 126.75; 113.22 (*m*-C, aryl), 101.55 (C-5), 85.77 (quat. C, DMT, aliphatic carbon), 85.36 (C-4'), 84.14 (C-1'), 69.95 (C-3'), 63.44 (C-5'), 55.03 (OCH₃), 39.70 (C-2', hidden under the solvent).

FT-IR: $\tilde{\nu}$ [cm⁻¹] = 3056, 2970, 2929, 2831, 1679, 1605, 1511, 1458, 1376, 1245, 1176, 1090, 1029, 824.

FD-MS: m/z calculated for [C₃₀H₃₀N₂O₇]: 530.2; found: 530.3.

5.2.1.2 3'-O-*tert*-Butyldimethylsilyl-5'-O-dimethoxytrityl-2'-deoxyuridine **21**

Imidazole (0.34 g, 5.0 mmol, 4.4 eq.) was added to a stirred solution of **20** (0.60 g, 1.13 mmol) in dry DCM (6 mL) and under inert atmosphere. TBDMS-Cl (0.38 g, 2.49 mmol, 2.2 eq.) was dissolved in a minimal amount of dry DCM and added dropwise to the reaction mixture. It was stirred at ambient temperature until TLC indicated complete consumption of the starting material (12 hours). Methanol (1 mL) was added and the solution was poured into ethyl acetate (30 mL). The organic layer was extracted with aqueous NaHCO₃ (5 %, 2 x 30 mL), and washed twice with water (20 mL) and brine (1 x 30 mL). Drying of the organic layer with anhydrous MgSO₄ and evaporation of the solvent afforded a colorless solid **21** (0.71 g, 1.10 mmol, 98 %).

m.p.: $T_m = 87\text{--}89\text{ }^\circ\text{C}$.

TLC: silica gel, *n*-Hexane/EtOAc (3:1); $R_f = 0.14$.

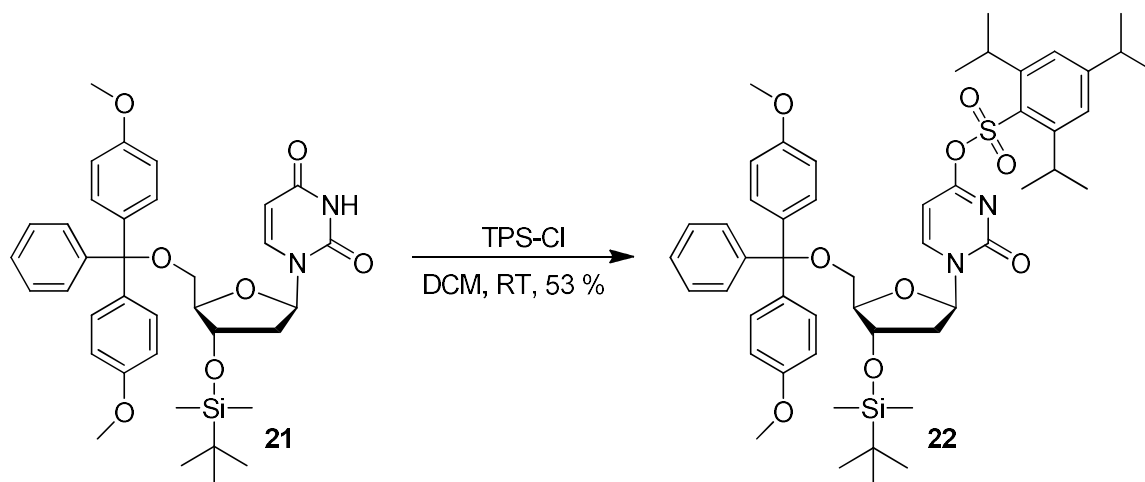
¹H NMR (300 MHz, DMSO-*d*₆): δ [ppm] = 11.37 (1H, s, NH), 7.75 (1H, d, H-6, $^3J = 8.1$ Hz), 7.37 (2H, H_{A,A'}), 7.31 (2H, H_{B,B'}), phenyl (AA'BB'X, $^3J = 7.6$ Hz, H_X overlapped by H_{A,A'} aryl), 7.26 (4H, H_{A,A'}), 6.88 (4H, H_{B,B'}), DMT moiety: aryl (AA'BB', $^3J = 8.4$ Hz), 6.15 (ABXY, 1H, m, H-1'X), 5.43 (1H, d, H-5, $^3J = 8.1$ Hz), 4.43 (ABXY, 1H, m, H-3'Y), 3.81 (ABX, 1H, m, H-4'X), 3.73 (6H, s, OCH₃), 3.25 (ABX, 2H, m, H-5'_{A,B}, $^2J_{AB} = 10.3$ Hz), 2.23 (ABXY, 2H, m, H-2'_{A,B}), 0.78 (9H, s, SiC[CH₃]₃), 0.00 (3H, s, Si[CH₃]), -0.05 (3H, s, Si[CH₃]).

¹³C-NMR (101 MHz, DMSO-*d*₆): δ [ppm] = 163.07 (C-4), 158.17 (aryl), 150.30 (C-2), 144.60 (aryl), 140.58 (C-6), *ipso*-C (phenyl): 135.29, 135.17; 129.73 (*o*-C, aryl), phenyl (CH): 127.83, 127.71, 126.77; 113.17 (*m*-C, aryl), 101.64 (C-5), 85.93 (quat. C, DMT, aliphatic carbon), 84.99 (C-4'), 84.07 (C-1'), 70.95 (C-3'), 62.63 (C-5'), 55.00 (OCH₃), 39.55 (C-2', hidden under the solvent), 25.55 (SiC[CH₃]₃), 17.55 (quat. C, SiC[CH₃]₃), -4.84 (Si[CH₃]), -5.21 (Si[CH₃]).

FT-IR: $\tilde{\nu}$ [cm⁻¹] = 3060, 2945, 2925, 2855, 1687, 1605, 1507, 1462, 1388, 1249, 1172, 1102, 1033, 824.

FD-MS: m/z calculated for [C₃₆H₄₄N₂O₇Si]: 644.3; found: 644.3.

5.2.1.3 3'-O-tert-Butyldimethylsilyl-5'-O-dimethoxytrityl-O⁴-triisopropylbenzenesulfonyl-2'-deoxyuridine **22**



A mixture of DMAP (0.03 g, 0.28 mmol, 0.09 eq.) and triethylamine (2.16 mL, 15.50 mmol, 5.00 eq.) in a minimal amount of DCM was added to a stirred solution of **21** (2.00 g, 3.10 mmol) in dry DCM (2 mL). Subsequently, a solution of TPS-Cl (1.13 g, 3.72 mmol, 1.20 eq.) in a minimal amount of dry DCM was added dropwise to the reaction mixture, which was stirred at ambient temperature overnight. After concentration *in vacuo*, triethylammonium chloride was precipitated with petroleum ether and the precipitate removed by filtration. The filtrate was again concentrated *in vacuo* and purified *via* column chromatography (silica gel) using a gradient system of cHexane/EtOAc (15:1 → 9:1, containing 1 % triethylamine), yielding a colorless solid **22** (1.49 g, 1.64 mmol, 53 %).

m.p.: $T_m = 84\text{--}87\text{ }^\circ\text{C}$.

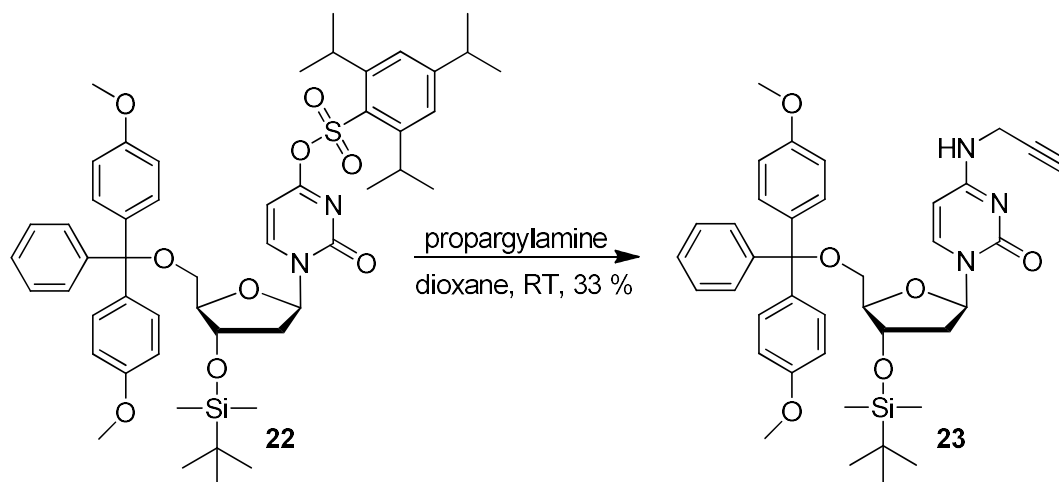
TLC: silica gel, cHexane/EtOAc (3:1); $R_f = 0.70$.

¹H NMR (400 MHz, DMSO-*d*₆): δ [ppm] = 7.72 (1H, d, H-6, $^3J = 8.0$ Hz), 7.15 – 7.40 (7H, m, phenyl DMT and H-3 TPS), 6.89 (4H, H_{B,B'}), 7.24 (4H, H_{A,A'}), DMT and TPS moieties: aryl DMT (AA'BB', $^3J = 8.5$ Hz), -0.06 (3H, s, Si[CH₃]), 6.12 (ABXY, 1H, m, H-1'x), 5.42 (1H, d, H-5, $^3J = 8.0$ Hz), 4.55 (2H, sept, $^3J = 6.8$ Hz, *o*-CH[CH₃]₂), 4.41 (ABXY, 1H, m, H-3'y), 3.79 (ABX, 1H, m, H-4'x, partially overlapped by OCH₃), 3.73 (6H, s, OCH₃), 3.21 (ABX, 2H, m, H-5'A,B, $^3J = 10.7$ Hz), 2.80 (1H, sept, $^3J = 6.8$ Hz, *p*-CH[CH₃]₂), 2.22 (ABXY, 2H, m, H-2'A,B), 1.16 (6H, d, $^3J = 6.8$ Hz, *p*-CH[CH₃]₂), 1.11 (12H, d, $^3J = 6.8$ Hz, *o*-CH[CH₃]₂), 0.77 (9H, s, SiC[CH₃]₃), -0.01 (3H, s, Si[CH₃]).

¹³C-NMR (101 MHz, DMSO-*d*₆): δ [ppm] = 163.04 (C-4), 157.78 (aryl), 150.42 (C-2), 148.33, 147.24, 146.77 (aryl), 141.71, 140.21 (C-6), 135.16 (*ipso*-C, phenyl), 128.89 (*o*-C, aryl), phenyl (CH): 127.62, 127.39, 126.41; 121.35 (CH, TPS), 112.74 (*m*-C, aryl), 99.50 (C-5), 85.89 (quat. C, DMT, aliphatic carbon), 83.74 (C-4'), 79.88 (C-1'), 69.18 (C-3'), 60.85 (C-5'), 54.98 (OCH₃), 39.83 (C-2', hidden under the solvent), 33.26 (*p*-CH[CH₃]₂), 28.02 (*o*-CH[CH₃]₂), 25.68 (SiC[CH₃]₃), 24.80 (*p*-CH[CH₃]₂), 23.83 (*o*-CH[CH₃]₂), 17.57 (quat. C, SiC[CH₃]₃), -4.82 (Si[CH₃]), -5.17 (Si[CH₃]).

FT-IR: $\tilde{\nu}$ [cm⁻¹] = 2953, 2925, 2851, 1683, 1621, 1605, 1635, 1503, 1458, 1384, 1274, 1172, 1102, 1029, 1000, 829.

MS (MALDI-TOF): m/z calculated for [C₅₁H₆₆N₂O₉SSi + K]⁺: 949.39; found: 949.47.

5.2.1.4 3'-O-*tert*-Butyldimethylsilyl-5'-O-dimethoxytrityl-*N*⁴-propargyl-2'-deoxycytidine **23**

Propargylamine (0.21 mL, 3.30 mmol, 10.0 eq.) was added dropwise to a stirred solution of **22** (0.30 g, 0.33 mmol) in dry dioxane (5 mL) and stirred at ambient temperature overnight. After removal of the solvent and excess propargylamine *in vacuo*, purification of the residue *via* column chromatography (aluminium oxide, basic) using a gradient system of *n*Hexane/EtOAc (1:2 → 1:3) → EtOAc/MeOH (5:1 → 1:2) yielded a brown solid **23** (0.07 g, 0.11 mmol, 33 %).

m.p.: $T_m = 81\text{--}83\text{ }^\circ\text{C}$.

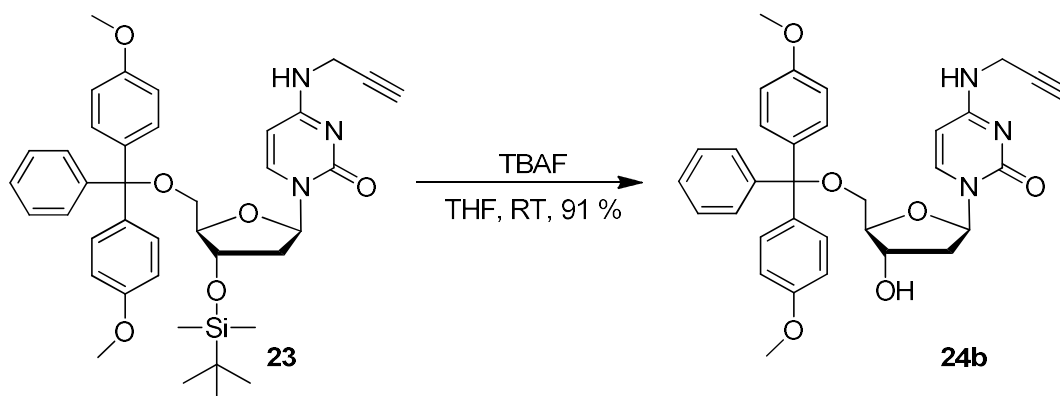
TLC: silica gel, DCM/MeOH (15:1); $R_f = 0.54$.

¹H NMR (300 MHz, DMSO-*d*₆): δ [ppm] = 8.09 (ABXY, 1H, m, NH_x), 7.78 (1H, d, H-6, $^3J = 7.4$ Hz), 7.37 (2H, H_{A,A'}), 7.32 (2H, H_{B,B'}), phenyl (AA'BB'X, $^3J = 7.8$ Hz, H_x overlapped by H_{A,A'} aryl), 7.25 (4H, H_{A,A'}), -0.07 (3H, s, Si[CH₃]), 6.89 (4H, H_{B,B'}), DMT moiety: aryl (AA'BB', $^3J = 8.4$ Hz), 6.13 (ABXY, 1H, m, H-1'X), 5.64 (1H, d, H-5, $^3J = 7.4$ Hz), 4.39 (ABXY, 1H, m, H-3'Y), 4.07 (ABXY, 2H, m, H-8_{A,B}), 3.80 (ABX, 1H, m, H-4'X), 3.74 (6H, s, OCH₃), 3.18 (ABXY, 1H, m, H-10_Y, partially overlapped by H-5'_{A,B}), 3.23 (ABX, 2H, m, H-5'_{A,B}, partially overlapped by both H-10 and H₂O), 2.15 (ABXY, 2H, m, H-2'_{A,B}), 0.77 (9H, s, SiC[CH₃]₃), -0.01 (3H, s, Si[CH₃]).

¹³C-NMR (101 MHz, DMSO-*d*₆): δ [ppm] = 162.86 (C-4), 158.14 (aryl), 149.30 (C-2), 144.49 (aryl), 140.15 (C-6), *ipso*-C (phenyl): 135.24, 135.20; 129.72 (*o*-C, aryl), phenyl (CH): 127.86, 127.69, 126.80; 113.20 (*m*-C, aryl), 99.50 (C-5), 85.88 (quat. C, DMT, aliphatic carbon), 84.88 (C-4'), 84.61 (C-1'), 80.80 (C-9), 73.43 (C-10), 70.82 (C-3'), 62.39 (C-5'), 55.05 (OCH₃), 38.60 (C-2'), 29.03 (C-8), 25.59 (SiC[CH₃]₃), 17.59 (quat. C, SiC[CH₃]₃), -4.80 (Si[CH₃]), -5.18 (Si[CH₃]).

FT-IR: $\tilde{\nu}$ [cm⁻¹] = 3284, 2950, 2925, 2851, 1635, 1604, 1578, 1507, 1459, 1443, 1295, 1248, 1174, 1103, 1029, 828.

MS (MALDI-TOF): m/z calculated for [C₃₉H₄₇N₃O₆Si + K]⁺: 720.29; found: 720.32.

5.2.1.5 5'-O-Dimethoxytrityl-N⁴-propargyl-2'-deoxycytidine **24b**

Under argon atmosphere, TBAF (0.34 mL of a 1 M solution in THF, 0.34 mmol, 1.6 eq.) was added to a stirred solution of **23** (0.14 g, 0.21 mmol) in anhydrous THF (5 mL). Stirring at ambient temperature was continued until TLC analysis indicated complete loss of the butyldimethylsilyl-group (1 hour). The mixture was quenched with (20 mL) and was washed with saturated aqueous NaHCO₃ (3 x 10 mL). The organic layer was dried with anhydrous Na₂SO₄ and concentrated *in vacuo*. Purification of the residue *via* flash column chromatography (aluminium oxide, basic), using the gradient system cHexane/EtOAc (1:2 → 1:3) → EtOAc/MeOH (5:1 → 1:2) afforded a brown solid **24b** (0.11 g, 0.19 mmol, 91 %).

m.p.: T_m = 123–125 °C.

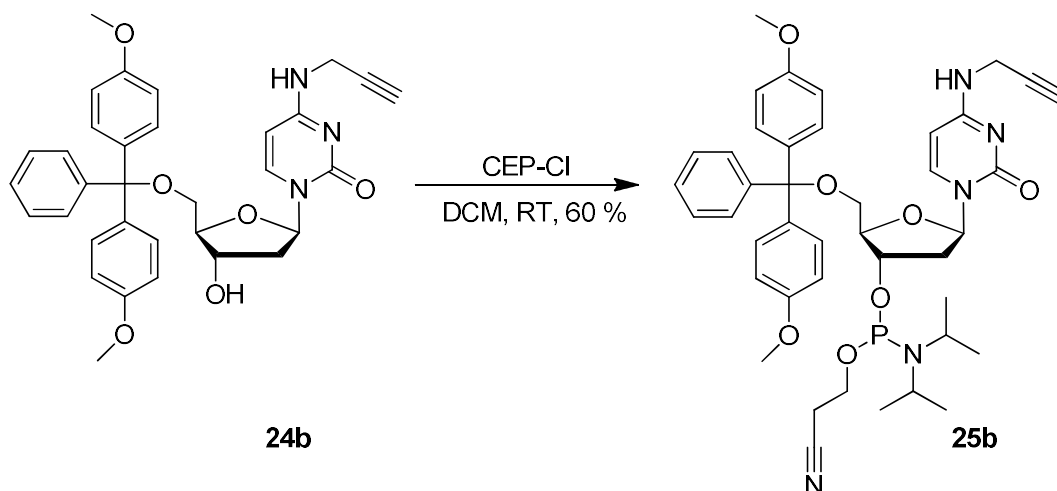
TLC: silica gel, DCM/MeOH (15:1); R_f = 0.24.

¹H NMR (300 MHz, DMSO-*d*₆): δ [ppm] = 8.15 (ABXY, 1H, m, NH_x), 7.67 (1H, d, H-6, ³J = 7.4 Hz), 7.38 (2H, H_{A,A'}), 7.31 (2H, H_{B,B'}), phenyl (AA'BB'X, ³J = 7.9 Hz, H_x overlapped by H_{A,A'} aryl), 7.22 (4H, H_{A,A'}), 6.89 (4H, H_{B,B'}), DMT moiety: aryl (AA'BB', ³J = 8.4 Hz), 6.16 (ABXY, 1H, m, H-1'x), 5.62 (1H, d, H-5, ³J = 7.4 Hz), 5.39 (1H, m, 3'-OH), 4.25 (ABXY, 1H, m, H-3'y), 4.06 (ABXY, 2H, m, H-8_{A,B}), 3.87 (ABX, 1H, m, H-4'x), 3.74 (6H, s, OCH₃), 3.20 (ABX, 2H, m, H-5'_{A,B}, partially overlapped by H-10), 3.17 (ABXY, 1H, m, H-10_y, partially overlapped by H-5'_{A,B}), 2.11 (ABXY, 2H, m, H-2'_{A,B}).

¹³C-NMR (101 MHz, DMSO-*d*₆): δ [ppm] = 162.86 (C-4), 158.11 (aryl), 154.71 (C-2), 144.72 (aryl), 140.09 (C-6), *ipso*-C (phenyl): 135.43, 135.31, 129.74 (*o*-C, aryl), phenyl (CH): 127.90, 127.71, 126.78; 113.24 (*m*-C, aryl), 99.53 (C-5), 85.76 (quat. C, DMT, aliphatic carbon), 85.21 (C-4'), 84.74 (C-1'), 80.86 (C-10), 73.42 (C-9), 69.90 (C-3'), 63.33 (C-5'), 55.07 (OCH₃), 39.64 (C-2', hidden under the solvent), 29.04 (C-8).

FT-IR: $\tilde{\nu}$ [cm⁻¹] = 3276, 2925, 2835, 1638, 1572, 1458, 1442, 1298, 1245, 1168, 1082, 1029, 824.

MS (MALDI-TOF): m/z calculated for [C₃₃H₃₃N₃O₆]: 567.2; found: 567.3.

5.2.1.6 Phosphoramidite synthesis **25b**

Following a consecutive azeotropic evaporation of **24b** (0.15 g, 0.26 mmol) with pyridine, toluene and DCM, the pre-phosphoramidite was dissolved in anhydrous DCM (5 mL) and placed under inert atmosphere. *Hünig's base* (0.23 mL, 1.32 mmol, 5.0 eq.) was added to the stirred solution, followed by the dropwise addition of CEP-Cl (0.09 mL, 0.39 mmol, 1.5 eq.) and stirred for 3 hours at room temperature. The crude mixture was extracted with aqueous NaHCO₃ (5 %, 10 mL) and the DCM (3 x 15 mL). The organic layer was dried with anhydrous MgSO₄ and concentrated *in vacuo*. Purification of the brown foam *via* column chromatography (aluminium oxide, basic) with DCM/MeOH (70:1) afforded a pale brown oil **25b** (0.12 g, 0.16 mmol, 60 %), bearing a mixture of two diastereomers (dr = 85:15, ¹H NMR).

TLC: silica gel, DCM/MeOH (15:1); R_f = 0.45, 0.49.

¹H NMR (400 MHz, DMSO-*d*₆) (only the resonances of the major diastereomer are indicated): δ [ppm] = 8.10 (ABXY, 1H, m, NH_x), 7.70 (1H, d, H-6, ³J = 7.3 Hz), 7.37 (2H, H_{A,A'}), 7.30 (2H, H_{B,B'}), phenyl (AA'BB'X, ³J = 7.7 Hz, H_x overlapped by H_{A,A'} aryl), 7.24 (4H, H_{A,A'}), 6.88 (4H, H_{B,B'}), DMT moiety: aryl (AA'BB', ³J = 8.4 Hz), 6.18 (ABXY, 2H, m, H-1'x), 5.63 (2H, d, H-5, ³J = 7.3 Hz), 4.49 (ABXY, 1H, m, H-3'y), 4.07 (ABXY, 2H, m, H-8_{A,B}), 3.99 (ABX, 1H, m, H-4'x), 3.73 (6H, s, OCH₃), 3.43 – 3.79 (4H, m, CH₂PO and CH[CH₃]₂, partially hidden under OCH₃), 3.25 (ABX, 2H, m, H-5'_{A,B}), 3.18 (ABXY, 1H, m, H-10_γ), 2.76 (2H, t, CH₂CN, ³J = 5.8 Hz), 2.29 (ABXY, 2H, m, H-2'_{A,B}), 1.10 (12H, d, CH[CH₃]₂, ³J = 6.6 Hz).

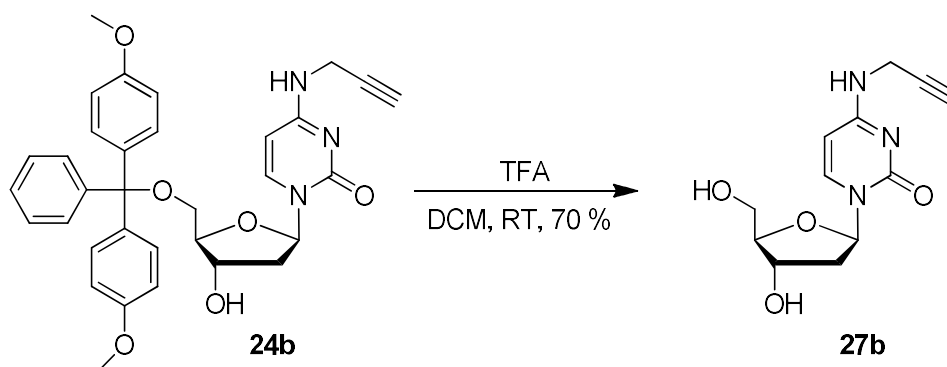
¹³C-NMR (101 MHz, DMSO-*d*₆) (only the resonances of the major diastereomer are indicated): δ [ppm] = 162.85 (aryl), 158.14 (C-4), 154.60 (C-2), 144.59 (aryl), 140.28 (C-6), 129.71 (o-C, aryl), *ipso*-C (phenyl): 135.28, 135.17, phenyl (CH): 127.87, 127.66, 126.79, 118.97 (quat. C, C≡N), 113.21 (*m*-C, aryl), 95.28 (C-3'), 94.42 (C-5), 85.84 (C-4'), 84.86 (C-1'), 84.85 (quat. C, DMT, aliphatic carbon), 80.77 (C-9), 73.48 (C-10), 62.93 (C-5'), 58.37 (CH₂-OP), 55.05 (OCH₃), 42.57 (CH[CH₃]₂), 39.67 (C-2', partially overlapped by solvent), 29.06 (C-8), 24.29 (CH[CH₃]₂), 24.19 (CH[CH₃]₂), 19.80 (CH₂-C≡N).

$^{31}\text{P-NMR}$ (162 MHz, $\text{DMSO-}d_6$): δ [ppm] = 148.789 (major diastereomer), 148.379 (minor diastereomer).

FT-IR: $\tilde{\nu}$ [cm^{-1}] = 3280, 3084, 3031, 2962, 2921, 2863, 2353, 2332, 2246, 1638, 1572, 1503, 1459, 1437, 1300, 1250, 1170, 1117, 1068, 1026, 973, 824.

HR-MS (ESI): m/z calculated for $[\text{C}_{42}\text{H}_{51}\text{N}_5\text{O}_7\text{P} + \text{H}]^+$: 768.3526; found: 768.3522.

5.2.1.7 Synthesis of N^4 -propargyl-2'-deoxycytidine **27b**



The deprotection of **24b** (0.10 g, 0.18 mmol) was carried out in DCM (5 mL) with TFA (20 μL , 0.26 mmol, 1.5 eq.). The mixture was stirred at ambient temperature until TLC analysis showed complete loss of the DMT-group. Distillation of the solvent and excess TFA, followed by purification of the residue *via* column chromatography with DCM/MeOH (15:1) gave a beige-colored solid **27b** (0.03 g, 0.12 mmol, 70 %).

m.p.: $T_m = 170\text{--}175\text{ }^\circ\text{C}$.

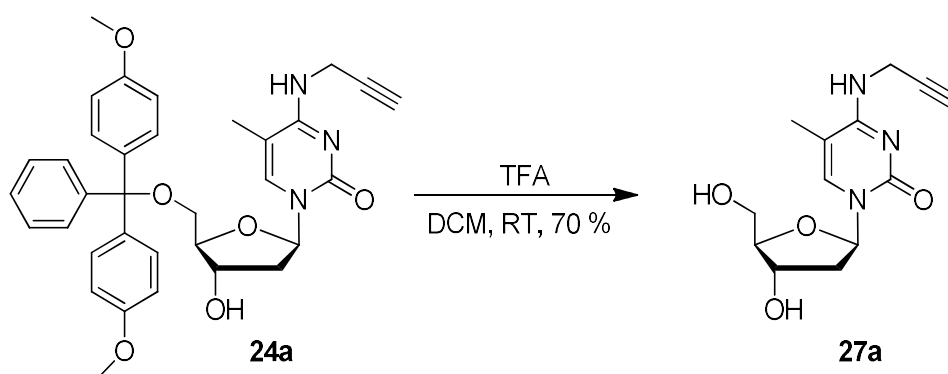
TLC: silica gel, DCM/MeOH (5:1); $R_f = 0.27$.

$^1\text{H NMR}$ (300 MHz, $\text{DMSO-}d_6$): δ [ppm] = 8.09 (ABXY, 1H, m, NH_x), 7.81 (1H, d, H-6, $^3J = 7.5$ Hz), 6.14 (ABXY, 1H, m, H-1' $_x$), 5.78 (1H, d, H-5, $^3J = 7.5$ Hz), 5.20 (1H, d, 3'-OH, $^3J = 3.9$ Hz), 4.99 (1H, m, 5'-OH), 4.19 (ABXY, 1H, m, H-3' $_y$), 4.05 (ABXY, 2H, m, H-8 $_{A,B}$), 3.76 (ABX, 1H, m, H-4' $_x$), 3.54 (ABX, 2H, m, H-5' $_{A,B}$), 3.16 (ABXY, 1H, m, H-10 $_y$), 2.02 (ABXY, 2H, m, H-2' $_{A,B}$, $^2J_{AB} = 13.1$ Hz).

$^{13}\text{C-NMR}$ (75 MHz, $\text{DMSO-}d_6$): δ [ppm] = 162.90 (C-4), 154.87 (C-2), 140.48 (C-6), 94.67 (C-5), 87.26 (C-4'), 84.95 (C-1'), 80.89 (C-9), 73.39 (C-10), 70.36 (C-3'), 61.32 (C-5'), 40.39 (C-2', partially overlapped by solvent), 29.05 (C-8).

FT-IR: $\tilde{\nu}$ [cm^{-1}] = 3375, 2975, 2931, 2874, 2357, 2325, 1808, 1672, 1563, 1521, 1448, 1376, 1308, 1182, 1130, 1049, 945, 845.

HR-MS (ESI): m/z calculated for $[\text{C}_{12}\text{H}_{15}\text{N}_3\text{O}_4 + \text{Na}]^+$: 288.0960; found: 288.0971.

5.2.1.8 Synthesis of 5-methyl-*N*⁴-propargyl-2'-deoxycytidine **24a**

The deprotection of **24a** (0.24 g, 0.41 mmol) was carried out in DCM (5 mL) with TFA (63 μ L, 0.83 mmol, 2.0 eq.). The mixture was stirred at ambient temperature until TLC analysis showed complete loss of the DMT-group. Distillation of the solvent and excess TFA, followed by purification of the residue *via* silica gel column chromatography with DCM/MeOH (15:1) gave a colorless solid **27a** (0.08 g, 0.29 mmol, 70 %).

m.p.: $T_m = 180$ °C with decomposition.

TLC: silica gel, DCM/MeOH (6:1); $R_f = 0.32$.

¹H NMR (300 MHz, DMSO-*d*₆): δ [ppm] = 7.66 (1H, m, H-6), 7.60 (ABXY, 1H, m, NH_X), 6.16 (ABXY, 1H, m, H-1'_X), 5.22 (1H, d, 3'-OH, ³*J* = 4.2 Hz), 5.04 (1H, t, 5'-OH, ³*J* = 5.2 Hz), 4.20 (ABXY, 1H, m, H-3'_Y), 4.08 (ABXY, 2H, m, H-8_{A,B}), 3.75 (ABX, 1H, m, H-4'_X), 3.56 (ABX, 2H, m, H-5'_{A,B}), 3.09 (ABXY, 1H, m, H-10_Y), 2.01 (ABXY, 2H, m, H-2'_{A,B}, ²*J*_{AB} = 13.2 Hz), 1.84 (3H, m, 5-CH₃).

¹³C-NMR (75 MHz, DMSO-*d*₆): δ [ppm] = 162.33 (C-4), 154.81 (C-2), 149.38 (C-6), 101.55 (C-5), 87.50 (C-4'), 84.63 (C-1'), 81.53 (C-9), 72.67 (C-10), 70.19 (C-3'), 61.23 (C-5'), 40.39 (C-2'), 29.43 (C-8), 13.08 (5-CH₃).

FT-IR: $\tilde{\nu}$ [cm⁻¹] = 3280, 2929, 2275, 1711, 1679, 1609, 1556, 1503, 1442, 1335, 1200, 1180, 1049, 1080, 1049, 1021, 1000, 972, 824, 792, 763, 714.

HR-MS (ESI): *m/z* calculated for [C₁₃H₁₇N₃O₄ + Na]⁺: 302.1116; found: 302.1127.

5.2.1.9 ROESY-NMR spectroscopy

As published in Domingo *et al.* [193], the NMR samples were prepared by dissolving the nucleosides in 9/1 H₂O/D₂O. For CpDCII **25b** NMR data were acquired on a Bruker Avance II+ instrument operating at 14.1 T. ¹H NMR spectra were acquired using a double-pulsed field gradient spin-echo (DPFGSE) pulse sequence [200]. NOESY spectra were acquired at 273 K, 278 K, 283 K and 288 K with mixing times of 10, 25, 50, 75, 125, 200, 400, 750 and 1000 ms. The size of the data matrices for each spectrum was 2048*256 complex data points, the number of scans was 8 and the interscan delay was 1.5 s, yielding a total measuring time of approximately 6 hours at each temperature.

Determination of exchange kinetics

Spectral processing and peak integration were performed using NMRPipe and the NMRDraw software package [202]. All subsequent steps were performed using in-house written software written in Matlab (The MathWorks, www.mathworks.com) according to an earlier published protocol [203]. Errors in the extracted rate constants were determined by Monte Carlo analysis, where peak intensities were randomly modulated according to the signal to noise levels in the 2D correlation maps.

Arrhenius Analysis

The temperature dependence of the rate constants for CpDCII **25b** obtained from the exchange data was obtained by linear regression of ln(k_{AB}) or ln(k_{BA}) vs. 1/T, respectively, yielding the activation barriers for the *s-cis* to *s-trans* isomerization step.

5.2.2 Synthesis procedures azide-modified TLR ligands

The following data are also published in Hellmuth *et al.* [231].

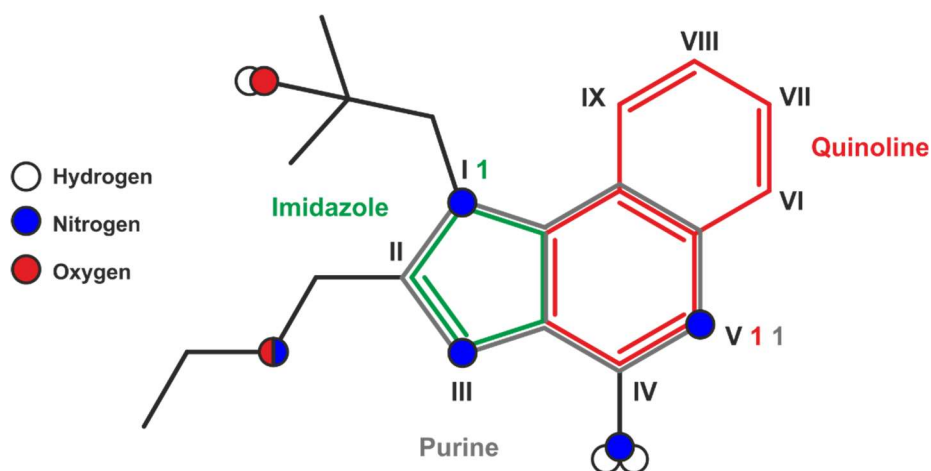
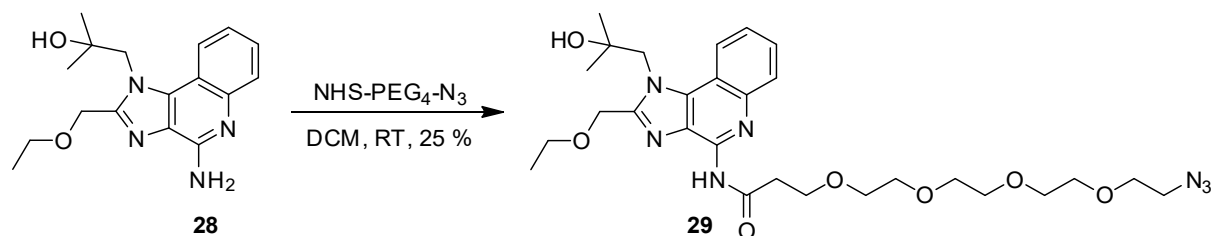


Figure 5.1: Numbering of small molecule scaffolds for nomenclature. See also Section 3.2.1.

5.2.2.1 Synthesis of 1-azido-N-(2-(ethoxymethyl)-1-(2-hydroxy-2-methylpropyl)-1H-imidazo[4,5-c]quinolin-4-yl)-3,6,9,12-tetraoxapentadecan-15-amide (Resiquimod-PEG₄-N₃ / RPA) **29**



Resiquimod **28** (22 mg, 70 μmol , 1 eq.) was dissolved in 4.0 mL dry dichloromethane. After the addition of 2,5-dioxopyrrolidin-1-yl-1-azido-3,6,9,12-tetraoxapentadecan-15-oate (NHS-PEG₄-N₃) (32 mg, 84 μmol , 1.2 eq.), the reaction mixture was stirred under argon until no further conversion could be observed, monitored *via* TLC (CHCl₃/EtOH, 9:1). The reaction mixture was extracted three times with water (2.0 mL) in order to get rid of excess starting material **28**, organic phases were combined and concentrated *in vacuo* to dryness on a rotary evaporator. For further purification, a column chromatography (silica) with a solvent-gradient 100-88 % CHCl₃ and 0-12 % EtOH was performed. Fractions containing product were combined and concentrated *in vacuo*, yielding the title compound **29** (9.05 mg, 15.4 μmol , 25 %) as highly viscous colorless oil.

TLC: silica gel, CHCl₃/EtOH (9:0.5); R_f = 0.33.

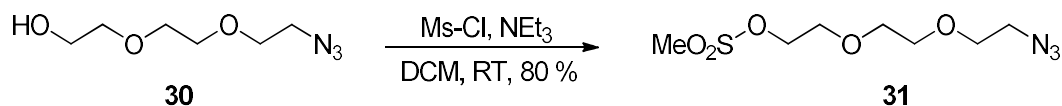
¹H-NMR (300 MHz, DMSO-*d*₆): δ [ppm] = 8.42 (d, ³*J* = 8.2 Hz, 1H, H-Ar), 8.02 (d, ³*J* = 8.2 Hz, 1H, H-Ar), 7.70 (t, ³*J* = 15.2 Hz, ³*J* = 7.5 Hz, 1H, H-Ar), 7.62 (t, ³*J* = 15.1 Hz, ³*J* = 7.5 Hz, 1H, H-Ar), 4.99 (s, 2H, CH₂-O), 4.81 (s, 2H, imidazo-CH₂), 4.40 (q, ³*J* = 7.2 Hz, 1H, NH), 3.97 (t, ³*J* = 11.8 Hz, ³*J* = 5.9 Hz, 2H, O=C-CH₂), 3.76 (s, 4H, 2 x CH₂), 3.27-3.21 (m, 14H, 7 x CH₂), 3.35 (t, ³*J* = 10.1 Hz, ³*J* = 5.0 Hz, 2H, CH₂-N₃), 3.20 (br s, 1H, -OH), 1.39-1.36 (br s, 6H, 2 x CH₃), 1.25-1.21 (m, 3H, CH₂-CH₃).

¹³C-NMR (75 MHz, DMSO-*d*₆): δ [ppm] = 172.5, 143.8, 116.2, 77.3, 71.6, 70.8, 70.77, 70.75, 70.7, 70.5, 70.1, 67.0, 66.6, 65.5, 56.7, 50.7, 38.2, 28.1, 25.5, 15.1.

FT-IR: $\tilde{\nu}$ [cm⁻¹] = 2971, 2920, 2868, 2100 (s) (v, N₃), 1710 (s) (v, C=O), 1581 (m) (v, amide), 1528 (s), 1471 (m), 1371 (s), 1208 (s), 1093 (br, s), 757 (s).

HR-MS (ESI): *m/z* calculated for [C₂₈H₄₁N₇O₇ + Na]⁺: 610.2965; found: 610.2945.

5.2.2.2 Synthesis of 2-(2-(2-azidoethoxy)ethoxy)ethyl methanesulfonate **31**



2-[2-(2-Azidoethoxy)ethoxy]ethanol **30** (200 mg, 1.14 mmol, 1.0 eq.) was dissolved in molecular sieve-dried dichloromethane (2.0 mL). The mixture was stirred and cooled to 0 °C after which methanesulfonyl chloride (157 mg, 1.37 mmol, 1.5 eq.) was added as a solution in dry DCM. The catalyst trimethylamine (231 mg, 2.28 mmol, 2.0 eq.) was then added in drops after which the reaction mixture was allowed to warm to room temperature. Stirring for 1 h led to complete conversion, monitored on TLC-plate (DCM/MeOH, 9:1) *via* iodine-staining. After removing the solvent *in vacuo*, the crude mixture was purified *via* column chromatography by using DCM and 10 % MeOH as eluent, giving the title compound **31** (230 mg, 0.91 mmol, 80 %) as a yellowish oil.

TLC: silica gel, DCM/MeOH (9:1); *R_f* = 0.28.

¹H-NMR (300 MHz, DMSO-*d*₆): δ [ppm] = 4.30 (t, ³*J* = 8.8 Hz, ³*J* = 4.4 Hz, 2H, CH₂), 3.68 (t, ³*J* = 8.8 Hz, ³*J* = 4.4 Hz, 2H, CH₂), 3.62-3.58 (m, 6H, 3 x CH₂), 3.39 (t, ³*J* = 9.8 Hz, ³*J* = 4.9 Hz, 2H, CH₂), 3.17 (s, 3H, CH₃).

¹³C-NMR (75 MHz, DMSO-*d*₆): δ [ppm] = 69.75 (CH₂), 69.64 (CH₂), 69.60 (CH₂), 69.24 (CH₂), 68.32 (CH₂), 49.97 (C-N₃), 36.78 (CH₃).

5.2.2.3 Synthesis of 1-(4-amino-2-(((2-(2-(2-azidoethoxy)ethoxy)ethyl)(ethyl)amino)methyl)-1H-imidazo[4,5-c]quinolin-1-yl)-2-methylpropan-2-ol (Gardiquimod-DEG-N3 / GDA) 33



Gardiquimod **32** (37.6 mg, 0.12 mmol, 1 eq.) and compound **31** (50.0 mg, 0.19 mmol, 1.6 eq.) were dissolved in dry *N,N'*-dimethylformamide (10.0 mL), giving a clear solution. The reaction mixture was stirred overnight at room temperature. Monitoring by TLC (DCM/MeOH, 7:3) showed an estimated conversion of 60 %. After removing the solvent *in vacuo*, the crude mixture was purified *via* column chromatography by using a gradient system of DCM and 10-30 % MeOH as eluent, giving the title compound **33** (28 mg, 0.06 mmol, 50 %) as a white powder.

m.p.: $T_M > 300$ C

TLC: silica gel, DCM/MeOH (7:3); $R_f = 0.33$.

$^1\text{H-NMR}$ (300 MHz, MeOD): δ [ppm] = 8.24 (d, $^3J = 8.2$ Hz, 1H, H-Ar), 7.66 (d, $^3J = 8.3$ Hz, 1H, H-Ar), 7.47 (t, $^3J = 15.3$ Hz, $^3J = 7.6$ Hz, 1H, H-Ar), 7.32 (t, $^3J = 15.2$ Hz, $^3J = 7.6$ Hz, 1H, H-Ar), 4.90 (s, 2H, $\text{CH}_2\text{-N}$), 3.57 (t, $^3J = 10.6$ Hz, $^3J = 5.3$ Hz, 2H, CH_2), 3.52-3.49 (m, 6H, 3 x CH_2), 3.27-3.21 (m, 6H, 2 x CH_2 , -NH_2), 2.76 (t, $^3J = 10.9$ Hz, $^3J = 5.4$ Hz, 2H, CH_2), 2.71-2.64 (m, 3H, $\text{CH}_2\text{-CH}_3$, -OH), 1.24 (br s, 6H, 2 x CH_3), 1.08 (t, $^3J = 14.1$ Hz, $^3J = 7.1$ Hz, 3H, $\text{CH}_2\text{-CH}_3$).

$^{13}\text{C-NMR}$ (75 MHz, MeOD): δ [ppm] = 154.1, 152.6, 144.2, 136.9, 128.8, 126.6, 125.8, 123.4, 122.5, 116.4, 72.2, 71.4, 71.3, 71.0, 70.2, 56.7, 53.6, 52.9, 52.8, 51.7, 46.7, 39.4, 11.4.

HR-MS (ESI): m/z calculated for $[\text{C}_{23}\text{H}_{34}\text{N}_8\text{O}_3 + \text{H}]^+$: 471.2832; found: 471.2832.

5.3 Molecular biology techniques

Working with DNA and RNA

All DNA and RNA samples were handled in DNase/RNase- and endotoxin-free water (Zymo Research). Concentrations of DNA and RNA samples were determined using a NanoDrop™ spectrophotometer (Thermo Fisher Scientific). Additional confirmation of RNA concentration was carried out with a Qubit™ fluorometer (Thermo Fisher Scientific), excluding false positive results.

5.3.1 Solid phase oligonucleotide synthesis & work up

An Expedite 8909 DNA/RNA synthesizer (ABI/PerSeptiveBiosystems) was operated on a 1 μmol-scale for all controlled pore glass(CPG)-based oligonucleotide syntheses. All phosphoramidites were applied in a concentration of 100 mM, except for guanosine phosphoramidites, which were diluted to 50 mM as a consequence of limited solubility. Therefore, the protocol was modified to doubled injection volume and doubled coupling time. In addition, RNA syntheses required higher amount of pulses and longer reaction times for certain steps, as it was for DNA.

Table 5.5: Program settings for DNA (RNA) SPOS on Expedite 8909 DNA/RNA synthesizer.

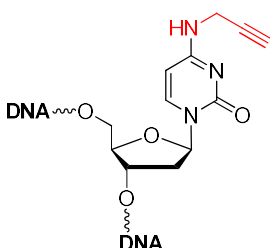
STEP	FUNCTION	MODE	AMOUNT		TIME		DESCRIPTION
			DNA	RNA	DNA	RNA	
DEBLOCKING	144/*Index Fract. Coll.	N/A	1	1	0	0	Event out ON
	0/*Default	WAIT	0	0	1.5	1.5	Wait
	141/*Trityl Mon. On/Off	N/A	1	1	1	1	START data collection
	16/*Dbk	PULSE	10	10	0	0	Dbk to column
	16/*Dbk	PULSE	50	50	49	60	Deblock
	38/*Diverted Wsh A	PULSE	40	40	0	0	Flush system with Wsh A
	141/*Trityl Mon. On/Off	N/A	0	0	1	1	STOP data collection
	38/*Diverted Wsh A	PULSE	40	40	0	0	Flush system with Wsh A
144/*Index Fract. Coll.	N/A	2	2	0	0	Event out OFF	
COUPLING	1/*Wsh	PULSE	5	5	0	0	Flush system with Wsh
	2/*Act	PULSE	5	5	0	0	Flush system with Act
	#/*Base + Act	PULSE	5	6	0	0	Monomer + Act to column
	#/*Base + Act	PULSE	2	9	16	402	Couple monomer
	2/*Act	PULSE	3	0	24	0	Couple monomer
	1/*Wsh	PULSE	7	8	56	357	Couple monomer
	1/*Wsh	PULSE	8	7	0	0	Flush system with Wsh
	(Repeat for guanosine)						

CAPPING I	12/*Wsh A	PULSE	20	20	0	0	Flush system with Wsh A
	13/*Caps	PULSE	8	7	0	0	Caps to column
	13/*Caps	PULSE	0	6	0	15	Cap
	12/*Wsh A	PULSE	6	6	15	15	Cap
	12/*Wsh A	PULSE	14	14	0	0	Flush system with Wsh A
OXIDIZING	15/*Ox	PULSE	15	20	0	0	Ox to column
	12/*Wsh A	PULSE	15	15	0	0	Flush system with Wsh A
CAPPING II	13/*Caps	PULSE	7	7	0	0	Caps to column
	12/*Wsh A	PULSE	30	30	0	0	End of cycle wash

5.3.1.1 Synthesis of CpDCII bearing DNA sense oligonucleotides

Table 5.6 shows the sequence of the DNA sense oligonucleotide. The bases in red were singularly substituted with the modified nucleoside **25b**.

Table 5.6: Sequences of the synthesized unmodified (ODN0) and the seven modified DNA oligonucleotides: Asterisks (*) indicate the positions of incorporated CpDCII (black) as part of this work. (Table as published in Domingo et al. [193])

ODN0	
5' -GCAAGCTGACCCTGAAGTTCAT-3'	
5' -G*AAGCTGACCCTGAAGTTCAT-3'	ODN2.2
5' -GCAAG*TGACCCTGAAGTTCAT-3'	ODN6.2
5' -GCAAGCTGA*CCTGAAGTTCAT-3'	ODN10.2
5' -GCAAGCTGAC*CTGAAGTTCAT-3'	ODN11.2
5' -GCAAGCTGACC*TGAAGTTCAT-3'	ODN12.2
5' -GCAAGCTGACCCTGAAGTT*AT-3'	ODN20.2
5' -GCAAGCTGACCCTGAAGTTC*T-3'	ODN21.2

The DMT-off mode was applied for all DNA oligonucleotides, following the protocol as in Table 5.5. Cleavage from solid support CPG-columns and deprotection was accomplished by incubation in a mixture of concentrated ammonia and ethanol (3:1) for 2 hours at ambient temperature. The columns were then rinsed with ethanol/water/acetonitrile (3:1:1), which was combined with the first mixture. The resulting fraction was dried overnight in a SpeedVac concentrator. After redissolving the pellet in MilliQ water, desalting was carried out on a NAP-10 column. A last purification step was done by PAGE separation and gel-extraction. Therefore, the desalted oligonucleotides were loaded and run on a 20 % denaturing PAGE gel, followed by visualization by UV-shadowing. The respective bands were excised and gel-pieces were incubated overnight in 0.5 M NH₄OAc (pH 5.0). Afterwards, the gel residues were filtered off and the oligonucleotides were received by lithium perchlorate precipitation (see Section 5.3.8.4).

5.3.1.2 MALDI-TOF analysis of synthesized oligonucleotides

Before measurement, all oligonucleotides were desalted *via* ZipTip pipette tips and eluted with acetonitrile/water (1:1) in a minimal concentration of 1 μM, as detected by NanoDrop measurement. Mass determination was performed on a Bruker BIFLEX III, situated at the Institute of Pharmacy and Molecular Biotechnology, Heidelberg University, and operated by Heiko Rudy. A matrix of 3-hydroxypicolinic acid was used and the samples were applied by a sandwich method with ammonium citrate, which masked possible residual salts. All measurements were conducted in the positive mode.

5.3.2 pDNA amplification, preparation and linearization

Transformation into competent DH5α *E.coli* strain (Invitrogen) with pDNA (for vectors see Section 5.1.4, pUC was used as control) was carried out according to the manufacturer's instructions and selected *via* the respective resistance gene on LB-agar plates, whilst one plate with an additional antibiotic and one without any were used as growth control. pDNA was isolated from *E.coli* overnight culture (OD₆₀₀ ~ 1.5) following the Spin Format Protocol Modification of a GenElute™ high performance endotoxin-free plasmid maxiprep kit (Sigma Aldrich). Plasmid linearization was carried out with the individual restriction enzyme as described by the manufacturer and finally purified *via* phenol/chloroform extraction and following ethanol-precipitation.

5.3.3 mRNA synthesis & purification

mRNAs were transcribed *in vitro* from 5.0 μg linearized pDNA-template using in house expressed and purified T7 RNA polymerase at 37 °C for 4 hours in a total volume of 100 μL. Nucleoside triphosphates were applied in a 5 mM final concentration, whereas alkyne-modified 5-ethynyluridine-5'-triphosphate (EUTP) (Jena Bioscience, Germany) was used in indicated percentages of 5 mM and UTP in the remaining amount. Additionally, the reaction contained 1x

Straßbourg buffer, DTT (5 mM), MgCl₂ (30 mM) and BSA (2.5 µg/mL). *In vitro* transcriptions were stopped by DNaseI treatment as described by the manufacturer (Thermo Fisher Scientific). Subsequent capping-reactions were carried out using the combination of *Vaccinia* Capping System and mRNA Cap 2'-O-methyltransferase (NEB) following the one-step reaction protocol prolonged to 2 h. All *in vitro* transcripts and capped mRNA-constructs were purified using the MEGAclean™ Kit (Invitrogen) silica spin column system. Instead of the supplied elution buffer, which contained EDTA and could thus interfere with subsequent enzyme-reactions, endotoxin-free water from Zymo was used for eluting the mRNA products.

5.3.4 Click functionalization of RNA through CuAAC

All copper-catalyzed click reactions were performed in aqueous solutions containing up to 5 % (v/v) dimethyl sulfoxide. The solutions were buffered to pH 8 with NaH₂PO₄ (100 mM) and contained 50 µg (5 µM) mRNA or 1 nmol sense-siRNA (MH662; sequence see Section 5.1.4; IBA, Goettingen/Germany) respectively, 120-200 µM azido functionalized ligand, 250 µM CuSO₄ · 5H₂O, 1.25 mM *tris*-[4-(3-hydroxypropyl)-(1,2,3)triazolyl-1-methyl]amine (TPTA) and 2.5 mM sodium ascorbate. The reaction mixtures were argon flushed and agitated under light protection at 25 °C for 2 h. Reactions were stopped through addition of equivalent volumes of a 1 mM EDTA-solution and purified through ethanol-precipitation.

5.3.5 Hybridization of siRNA double strands

The hybridization experiments of siRNA single strands were carried out in 1x phosphate buffered saline (pH 5.3). Due to concentration variations, the best hybridization ratios were determined by PAGE analysis of a series of different ratios. The two complementary strands were mixed in the respective best ratio, 1:1 most of the time, to result in a final duplex concentration of 5 µM. The strands were first incubated at 90 °C for 3 minutes and duplex formation was allowed at 37 °C, alternatively at 30 °C for less stable constructs, over 1 hour. The prepared duplex siRNA was analyzed by native PAGE (see Section 5.3.7.2) and stored at -20 °C.

5.3.6 Temperature-dependent UV melting curves

As published in Domingo *et al.* [193], the duplexes were diluted to a final concentration of 0.5 µM in degassed, RNase-free buffer, containing 10 mM NaH₂PO₄ (pH 8) and NaCl (45 mM), to a final volume of 800 µL. Melting curves were recorded at 260 nm, a pathlength of 10 mm and with a heating rate of 0.4 °C/min, a slit of 2 nm and a response of 0.2 s. All measurements were carried out at least three times in the temperature ranges between 20 °C and 85 °C.

To determine the effect of the modification on different helix conformations, the same hybridization and UV-melting experiments were repeated with duplexes formed with complementary RNA strands, also obtained from IBA (Goettingen, Germany). For the oligonucleotides that contain the

modifications at positions 10 and 11 from the 5'-end (*ODN10.1*, *ODN11.1*, *ODN10.2* and *ODN11.2* in Table 5.6) hybridizations were carried out with DNA strands that contain an abasic site directly opposite the modification. As control, the same duplexes were formed with the unmodified DNA strand (*ODN0*).

5.3.7 Electrophoretic mobility shift assays (EMSA) by means of agarose- & polyacrylamide gel electrophoresis

5.3.7.1 Agarose gel electrophoresis

DNA or mRNA samples (10 ng – 1 µg) were dissolved in gel loading buffer containing 20 % glycerol and loaded onto a 1 % agarose gel, pre-stained with SYBR®Gold nucleic acid gel stain (Invitrogen™). Therefore, the agarose was melted in 9/10 x the volume needed for gel-casting and the heat-labile SYBR® Gold was dissolved in the other tenth. Both solutions were combined and poured into the casting frame. After loading the samples, electrophoresis was carried out in 1x TBE buffer at 120 Volts for 90 minutes. If not pre-stained, gels were stained afterwards with either SYBR® Gold or GelRed™. Nucleic acid bands were visualized on a Typhoon 9400 (GE Healthcare) using the respective settings depicted in Table 5.7.

5.3.7.2 PAGE

Both, denaturing and native gels were casted in 20 cm x 20 cm x 1.5 mm frames. In the case of oligonucleotide purification of the *CpDCII*-series, 30 cm long gels were prepared. To monitor the migration of samples, blue PAGE loading buffers with bromophenol blue and xylene cyanol were applied at either side.

- denaturing

mRNA samples (1 µg) were dissolved in gel loading buffer containing 20 % glycerol and loaded onto 6 % denaturing polyacrylamide gels, which were prepared as described in Section 5.1.3. Electrophoresis was carried out in 1x TBE buffer at 12 Watts for 4 hours. Gels were post-stained for 20 min with Stains-all (Sigma Aldrich) and destained overnight in 75 % isopropanol. Nucleic acid bands were visualized on a Typhoon 9400 (GE Healthcare) using the respective settings depicted in Table 5.7.

Single-stranded siRNA samples were analyzed by denaturing PAGE as well. 25 pmol of oligonucleotides were loaded onto a denaturing polyacrylamide gel (percentages as indicated) containing 1x TBE. PAGE was performed in 1x TBE buffer (12 Watts / 4 h), gels were then post-stained with one of the mentioned stains (see Section 5.1.3). Detection was carried out on a Typhoon 9400 (GE Healthcare), before and after staining, using the respective settings depicted in Table 5.7.

- native

In the case of double-stranded siRNA, samples were analyzed by native PAGE in order to prevent strand separation. 25 pmol of double strands and 50 pmol of underlying single strands were loaded onto a native polyacrylamide gel (percentages as indicated) containing 1x TBE. PAGE was performed in 1x TBE buffer (12-8 Watts / 4-6 h), gels were then post-stained with one of the mentioned stains (see Section 5.1.3). Detection was carried out on a Typhoon 9400 (GE Healthcare), before and after staining, using the respective settings depicted in Table 5.7.

5.3.7.3 Visualization on Typhoon imager

Gels bearing fluorescently modified RNA samples were scanned before and after staining, which could be visualized in image-overlays generated with the software ImageJ. All other gels, containing no fluorescent samples, were stained with a respective medium and scanned afterwards.

Table 5.7: Settings for gel scans based on spectroscopic properties of staining dyes and dye-labels.

	Type	Laser excitation [nm]	Emission filter [nm]
GelRed	staining	532	610 BP 30
StainsAll	staining	633	670 BP 30
SybrGold	staining	488 / 532	526 SP
Atto 488	dye label	488	520 BP 40
Atto 590	dye label	532	670 BP 30
Atto 647N azide	dye label	633	670 BP 30
Sulfo Cy5	dye label	633	670 BP 30
PDI	dye label	532	610 BP 30

BP: band pass filter; SP: short pass filter

5.3.8 Purification & concentration methods for oligonucleotides**5.3.8.1 Phenol-chloroform extraction**

By means of this method, restricted pDNA could be separated from proteins and prepared suitable for further enzymatic reactions. In a first step, TE-buffered phenol (pH 7.5-8.0, Carl Roth) was added in an equal volume to the oligonucleotide sample in a 15 mL falcon® tube, vortexed and centrifuged for 2 minutes for phase separation. The aqueous phase was transferred into a new tube and the procedure was repeated with a 1:1 mixture of phenol/chloroform. After a third extraction with pure chloroform, a last extraction with diethyl ether was conducted in order to remove residual phenol traces. Therefore, the absorption of the aqueous phase was controlled at 270 nm. If necessary, individual extraction steps were repeated.

5.3.8.2 Elution of gel-purified RNA

After separating the desired RNA samples by PAGE, gels were placed on a fluorescent TLC plate and examined under UV-light (254 nm). The respective UV-absorbing oligonucleotides could be detected as dark bands and excised from the gel. Before the gel-samples could be incubated with 0.5 M NH₄OAc (pH 5.0) overnight, they had to be cut and crushed into small pieces. Nanosep spin filters with a 0.45 µm membrane were used to separate the elution buffer from the gel residues by centrifugation for 1 minute at 750 rpm. Oligonucleotides were received by lithium perchlorate precipitation (see 5.3.8.4) and stored at -20 °C.

5.3.8.3 Ethanol precipitation

An oligonucleotide solution was mixed with 0.1x volumes of an NH₄OAc-solution (5 M, pH 5.2) and 2-2.5x volumes of ethanol (-80 °C) were added. The solution was stored at -20 °C over night and followed by centrifugation at -4 °C for one hour and 15.000 x g. After removal of the supernatant, the pellet was washed with 75 % ethanol (-20 °C) and centrifuged again for 30 minutes. The supernatant was removed again and the air-dried pellet redissolved in water. This method was preferably applied for longer oligonucleotides as mRNA.

5.3.8.4 Lithium perchlorate precipitation

A 2 % solution of lithium perchlorate in acetone was added ten times of the volume of oligonucleotide solution. After centrifugation of 30 minutes at 14000 rpm, the supernatant was removed and the pellet washed with acetone by a second centrifugation for 10 minutes at 14000 rpm. The supernatant was removed again and the air-dried pellet redissolved in water. This method was preferably applied for short oligonucleotides as siRNA.

5.3.8.5 Lyophilization

This method of freeze-drying by sublimation was used in order to gently remove traces of water, dry chemicals or concentrate oligonucleotide samples. Samples were frozen at - 80 °C or in liquid nitrogen in an appropriate container and attached in a round bottom flask or a wide-neck filter bottle (Christ, Osterode am Harz, Germany) to the instrument.

5.3.9 Liquid chromatography (LC) methods

5.3.9.1 Size exclusion chromatography (SEC)

mRNA stock solutions (0.1 and 0.25 $\mu\text{g}/\mu\text{L}$) were loaded with a maximal volume of 20 μL per run onto a Superdex™ 200 SEC column, which was attached to an Agilent 1100 HPLC series. Prior to sample loading, the column was equilibrated with 100 % 1x PBS pH 7.4 at constant flow rate of 0.5 mL/min (\sim 11 bar) and the same was used for the sample analysis of a 50 minutes run.

5.3.9.2 Analysis of EU-containing mRNA

As published in Hellmuth *et al.* [231].

Sample preparation

Prior to HPLC analysis, 20 pmol of each mRNA sample were digested to the nucleosides level according to the following protocol [259]. Samples were incubated in presence of 1/10 volume of 10x nuclease P1 buffer (0.2 M NH_4OAc pH 5.0, ZnCl_2 0.2 mM), 0.3 U nuclease P1 (Sigma Aldrich, Munich, Germany) and 0.1 U snake venom phosphodiesterase (Worthington, Lakewood, USA) at 37 °C for 2 h. Next, 1/10 volume of 10x fast alkaline phosphatase buffer (Fermentas, St. Leon-Roth, Germany) and 1 U fast alkaline phosphatase (Fermentas, St. Leon-Roth, Germany) were added, and samples were incubated for additional 60 min at 37 °C. For the calibration series of EU, commercially available EU-triphosphate was digested analogously.

HPLC method

The digested mRNA samples were analyzed on an Agilent 1260 HPLC series equipped with a diode array detector (DAD). A Synergi Fusion-RP column (4 μm particle size, 80 Å pore size, 250 mm length, 2 mm inner diameter) from Phenomenex (Aschaffenburg, Germany) was used at 35 °C column temperature for the chromatographic separation of the nucleosides. The solvents applied were a 5 mM ammonium acetate buffer adjusted to pH 5.3 using acetic acid (solvent A) and pure acetonitrile (solvent B). The elution was performed at a flow rate of 0.35 mL/min using a linear gradient from 0 % to 8 % solvent B at 10 min, 40 % solvent B at 20 min and 0 % solvent B at 23 min. For additional 7 min, the column was rinsed with 100 % solvent A to restore the initial conditions. The detection of EU and the four canonical nucleosides was performed by measuring the column effluent photometrically at 254 nm using the DAD. For analysis of the recorded UV-chromatograms and extracting the respective peak areas of EU and guanosine (G), the Agilent MassHunter Qualitative Analysis software was used. The exact retention times of EU and the main nucleosides were determined using commercially available standard substances.

Quantification of EU in mRNA by HPLC analysis

For quantification of EU in the mRNA samples, external calibration series were run for both EU (calibration range 2 to 120 pmol) and the guanosine (calibration range 50 to 3500 pmol) using commercially available reference substances. The detected peak areas for each calibration solution were plotted against the injected amount of EU or the guanosine, and the slope of the linear fit of the resulting curves were used for calculation of the EU and guanosine amounts in each sample. The amount of G was divided by the number of its sites per mRNA molecule, yielding the injected amount of mRNA molecules. The result was then used to calculate the amount of EU residues per mRNA (mol EU per mol mRNA).

5.3.10 Stimulation of PBMCs

As published in Hellmuth *et al.* [231], human PBMCs were isolated from heparinized blood of healthy donors upon informed consent and approval by the local ethics committee by standard Ficoll-Hypaque density gradient centrifugation (Ficoll 1.078 g/mL) [88] PBMCs were resuspended in complete medium prepared of RPMI 1640 (Biochrom, Berlin, Germany) supplemented 10 % with heat-inactivated (1 h, 56°C) FCS (Gibco/Thermo Fisher Scientific, Schwerte, Germany). For stimulation, mRNA was encapsulated with DOTAP (N-[1-(2, 3-dioleoyloxy)propyl]-N, N, N-trimethylammonium-methylsulfate) (Carl Roth, GmbH Karlsruhe, Germany) at a ratio of 3 μ L DOTAP per 1 μ g of RNA in Opti-MEM Reduced Serum medium (Life Technologies) and incubation for 10 min at room temperature. As a control, cells were incubated with the individual clickable small molecule-, dye-, and mannose-derivatives only at indicated concentrations. Additionally, cells were co-stimulated with unmodified mRNA in the presence or absence of small molecules and their respective clickable derivatives. All stimulations were performed in duplicates per individual donor at a density of 4×10^5 cells/well PBMCs in a 96-well flat bottom plate. Cells were incubated in a humidified 5 % CO₂ atmosphere at 37 °C for 16-20 h. Cell-free supernatants were analyzed by sandwich ELISA for secretion of TNF- α (OptEIA Kit, BD Biosciences, Heidelberg, Germany) and IFN- α (Affymetrix eBioscience, Frankfurt, Germany). Each experiment was repeated minimum three times. Cytokine secretion of individual donors was normalized to a stimulation with 1 μ g/mL eGFP-mRNA or R848 respectively, which served as internal calibrator.

Statistical analysis

Data were analyzed using GraphPad Prism 7.0 (GraphPad Software Inc.). Significant differences were assessed by two-way ANOVA followed by multiple comparisons tests. In all figures, the P values are indicated by ns (not significant; $P > 0.05$), * (significant; $P \leq 0.05$), ** (very significant; $P \leq 0.01$), *** (extremely significant; $P \leq 0.001$), **** (extremely significant; $P < 0.0001$).

5.3.11 Generation and transfection of human dendritic cells

Myeloid DC were generated from buffy coats of healthy volunteers as described previously [282], [283]. In brief, PBMC were isolated by Ficoll density gradient centrifugation and monocytes were isolated by plastic adherence and cultured in X-VIVO-15 (Lonza) supplemented with 1 % heat-inactivated autologous plasma, 800 IU/mL GM-CSF (Leukine, Berlex) and 100 IU/mL IL-4 (CellGenix). Fresh media with GM-CSF (1600 U/mL) and IL-4 (100 IU/mL) was given at day 2 and day 4. Immature DC were harvested at day 6 and subsequently used for further electroporation experiments. All electroporation experiments with human DC were performed with Neon Transfection System (Thermo Fisher Scientific). According to the manufacturer's instruction, 0.5×10^6 DC were electroporated with various amounts of mRNA in a total volume of 100 μ L of electroporation buffer. To achieve high transfection efficiencies, the following program was used: Pulse voltage: 1500 V; Pulse width: 30 ms; Pulse number: 1. Afterwards, DC were cultured in pre-warmed X-VIVO-15 supplemented with 1 % heat-inactivated autologous plasma, 800 IU/mL GM-CSF and 100 IU/mL IL-4 for 24 hours at 37 °C, 5 % CO₂. RNA translation was analyzed by flow cytometry (BD Accuri™ C6 Cytometer).

5.3.12 Knock down in HeLa MAZ

As published in Hellmuth *et al.* [231].

Cells

HeLa MAZ cells [276] contain the episomal vector pMARS-mODC-AZ, which encodes for a destabilized eGFP. Cells were a kind gift from Dr. Andriy Khobta from the group of Prof. B. Epe (Institute of Pharmacy and Biochemistry, Mainz)

Hybridization

siRNA single strands (antisense MH533 and sense MH662; sequences see SI p. 24) were obtained from IBA (Goettingen, Germany). The hybridization experiments were carried out in 1x phosphate buffered saline (pH 7.4), with the two complementary strands in a 1:1 ratio, to result in a final duplex concentration of 5 μ M. The strands were first incubated at 70 °C for 3 minutes and duplex formation was allowed at 37 °C over 1 hour. The prepared duplex siRNA was stored at -20 °C.

Knock down experiments

Prior to transfection, 5×10^4 cells were seeded in 24 well plate in 1 mL DMEM (Thermo Fisher Scientific) with 10 % fetal bovine serum (FBS, Sigma-Aldrich). After one day, medium was replaced by 500 μ L of 10 % FCS DMEM and cells were transfected with siRNA. Briefly, to prepare siRNA/lipid transfection mixture, 40 pmol from a starting 5 μ M siRNA duplex were diluted in Opti-MEM® (Thermo Fisher Scientific) in twofold dilution series and mixed with transfection agent Lipofectamine™ (Thermo Fisher Scientific) according to the manufacturer's instruction. In the transfection time, 100 μ L of siRNA were added in dropwise to the wells. Transfection experiment

was realized in duplicate and each experiment was repeated 3 times. Cells were incubated 24 hours, later then medium was replaced by 185 μL of 10 % FCS medium and 65 μL of 2 M MG115 (proteasome inhibitor, Sigma Aldrich). This was followed by another 6 hours incubation. For FACS analysis, cells were washed with 500 μL DPBS, trypsinized with 200 μL Trypsin/EDTA, re-suspended in 400 μL DPBS and the eGFP signal measured by flow cytometry instrument (LSR-FortessaSORP, BD Biosciences) with excitation at 488 nm and a 530BP30 nm emission filter. Data was used for IC50 curves. The calculated eGFP signal corresponds to the product of the percentage of eGFP positive cells and their median fluorescence intensity, normalized to the value of positive controls (untreated with siRNA duplex). For acquisition and analysis, the FACSDiva Software (BD Biosciences) was used.

5.3.13 Tritium incorporation assay of 5'-mRNA capping reaction

Capping reactions for Cap0, Cap1 in stepwise- and one-step-format were pursued as described by the manufacturer with the *Vaccinia* Capping System and mRNA Cap 2'-O-methyltransferase (both from New England Biolabs, UK). The standard reaction volume was 70 μL for the methylation of 35 μg mRNA. As radioactive methyl-donor, 3 μL of [^3H]-S-adenosyl methionine (^3H -SAM, 1 $\mu\text{Ci}/\mu\text{L}$, 80 Ci/ mmol, 12.5 μM , Hartmann Analytics, Germany) were used together with the SAM supplied with the enzymes. All reactions were monitored over 120 minutes, whereas for the stepwise Cap1-procedure, the 2'-O-methyltransferase was added after 60 min.

Samples (8 μL) were spotted onto 1.5 x 1.0 cm Whatman filters (Roth) at indicated time points and precipitated in 5 % ice-cold trichloroacetic acid (TCA), followed by two washes at room temperature for 20 min and 10 min, respectively in 5 % TCA. The filters were swirled in ethanol, dried overnight and transferred into scintillation vials including 3 mL of Ultima Gold MV liquid scintillation cocktail (PerkinElmer, Waltham, USA). Incorporated tritium was measured with a Wallac 1409 liquid scintillation counter (PerkinElmer, Waltham, USA) (20 sec/sample), which took 60 seconds per vial. The SAM-stock solution (1 μL) was taken as a standard for specific activity.

6 Appendix

6.1 Ad 3.1

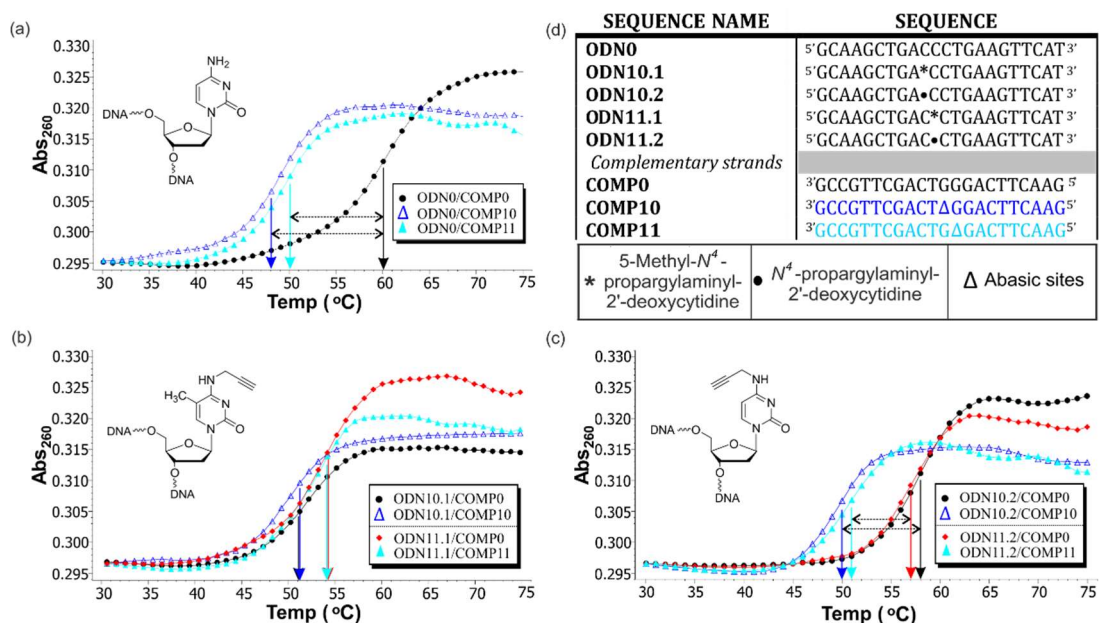


Figure 6.1: Temperature dependent UV-absorption melting curves, showing the differences in T_m between duplexes with and without abasic sites for DNA strands containing (a) no modifications, (b) the 5-methyl-*N*^d-propargyl-2'-deoxycytidine derivative and (c) the *N*^d-propargyl-2'-deoxycytidine derivative as modification at two varying positions. The sequences of the different DNA strands, as well as the position of the modifications are indicated (d). (Figure adopted from Domingo et al. [193])

6.2 Ad 3.2

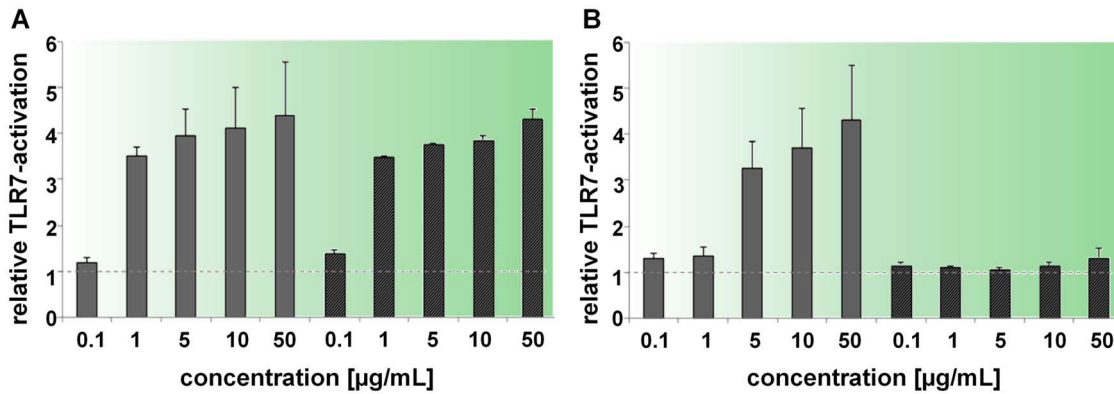


Figure 6.2: Titration of HEK-blue-hTLR7 with the commercial small molecules (R848, GQI) and their respective azide-derivatives (RPA, GDA): experiments were kindly performed by [REDACTED], data-interpretation was part of the current study.

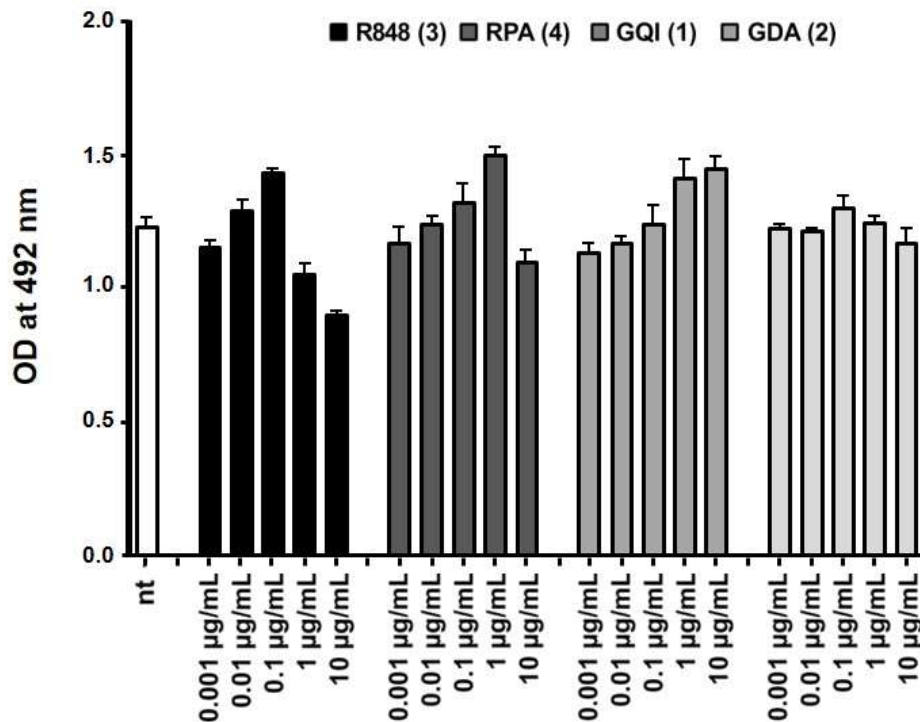


Figure 6.3: Cytotoxicity assay of commercial small molecules and azide-derivatives in PBMC (nt = not treated). Increasing concentrations of small molecules exhibit to some extent even a positive effect on cell viability compared to untreated PBMCs. Only for R848 the two highest and for RPA the highest concentration of 10 µg/mL show a minimal impact. (Figure as published in Hellmuth *et al.* [231])

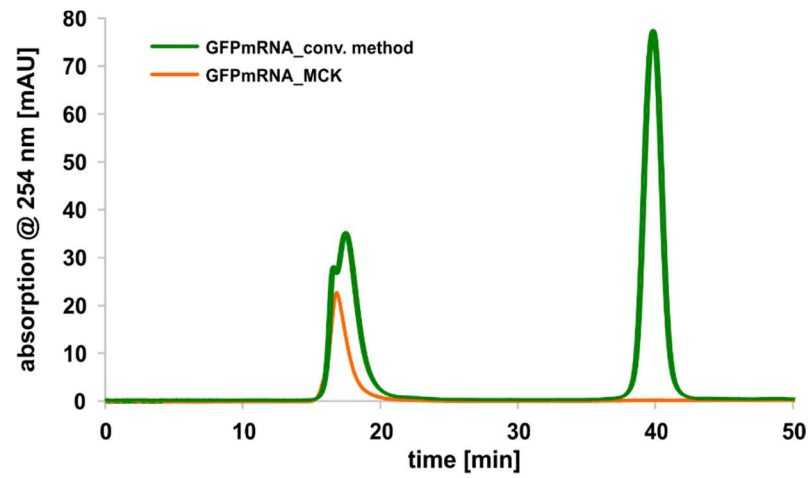


Figure 6.4: Size exclusion chromatography (Superdex 200 10/300 GL) of mRNA in 1x PBS. Purification via conventional methods of phenol-chloroform extraction for protein removal and ethanol precipitation (green), Purification via MegaClear Kit (orange).

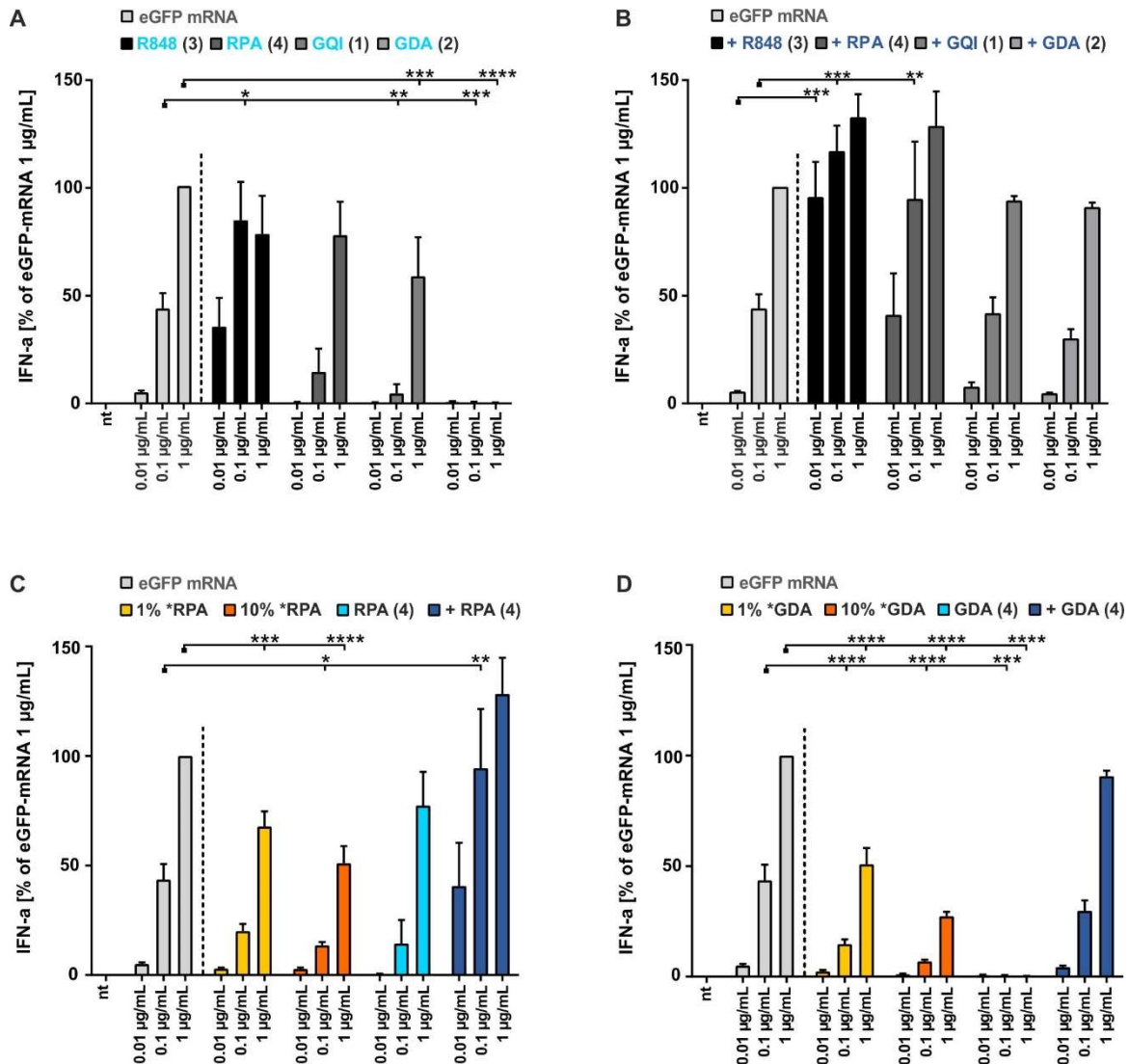


Figure 6.5: PBMC stimulation (A) with eGFP-mRNA, commercial small molecules and their respective azide-derivatives **(B)** Fixed concentration of 0.1 µg/mL of SMs titrated individually with the indicated amounts of eGFP-mRNA. **(C)** Comparing results related to RPA. **(D)** Comparing results related to GDA. IFN-α production was measured by ELISA. Due to donor variation in the absolute amount of IFN-α secreted, data from each individual were normalized to 1.0 µg/mL eGFP-mRNA (= 100 %) (n = 3; mean + SD). (Asterisks above bars indicate the respective P values evaluated by ANOVA and Dunnett's multiple comparisons test; no declaration = not significant (ns)). (Figure as published in *Hellmuth et al.* [231])

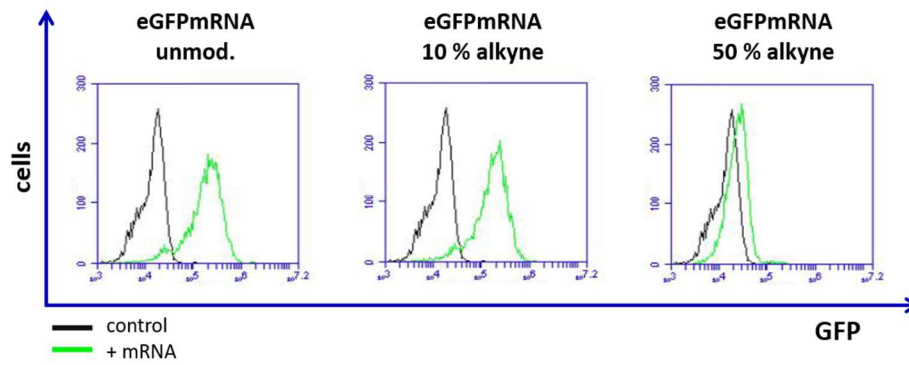


Figure 6.6: Protein expression in DC is inhibited by high amounts of alkyne modifications. FACS analysis of the introduction of an alkyne-moiety via IVT: Modifications of 1 to 10 %, did not have any negative impact on protein expression, only a to 50 % modified alkyne-mRNA showed strongly reduced fluorescence.

6.3 Spectra

6.3.1 Spectra of 3'-O-CEP-5'-O-DMT-N⁴-propargyl-2'-deoxycytidine (25b)

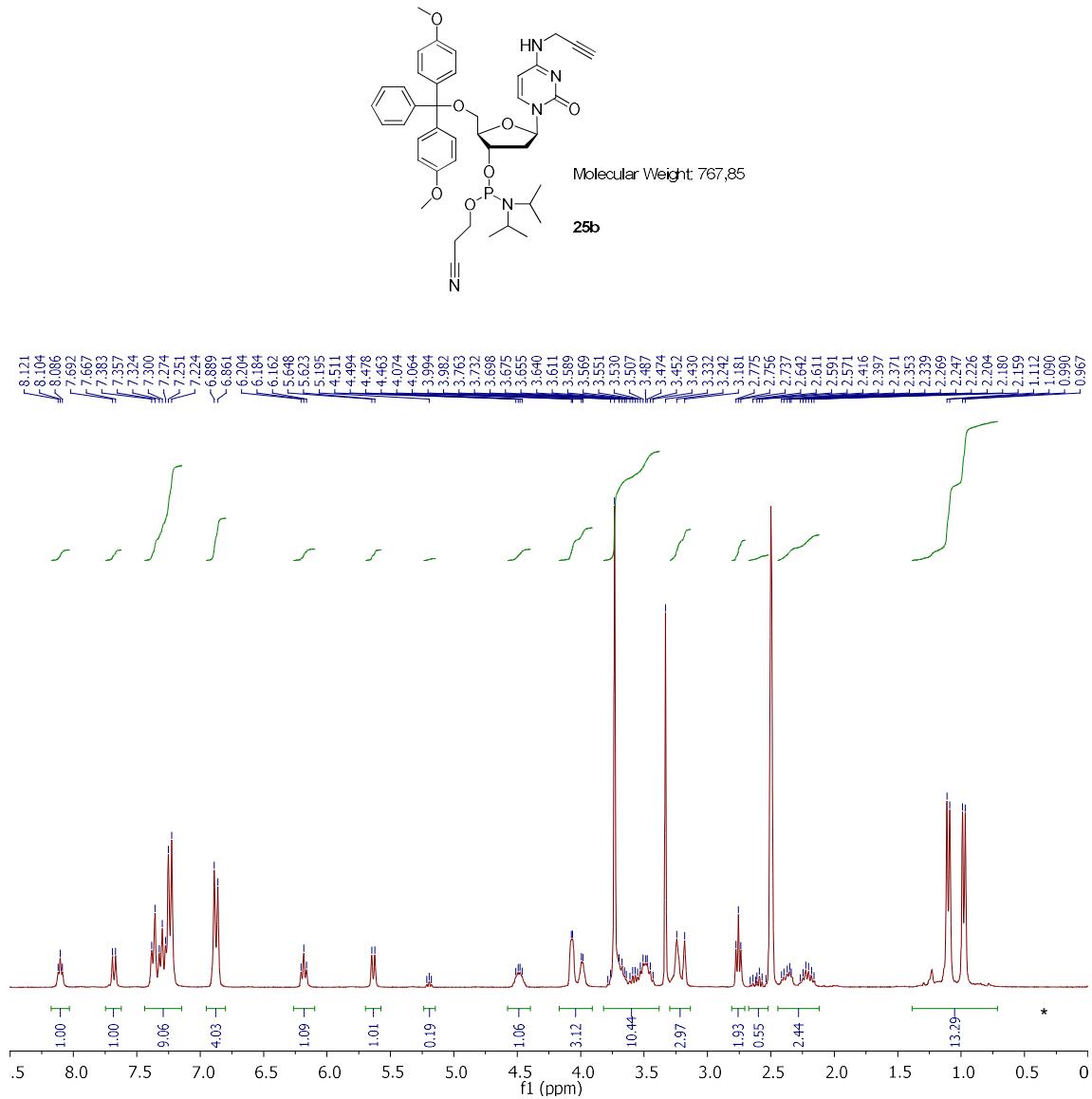


Figure 6.7: ¹H-NMR (400 MHz, DMSO-*d*₆) of 3'-O-CEP-5'-O-DMT-N⁴-propargyl-2'-deoxycytidine (**25b**).

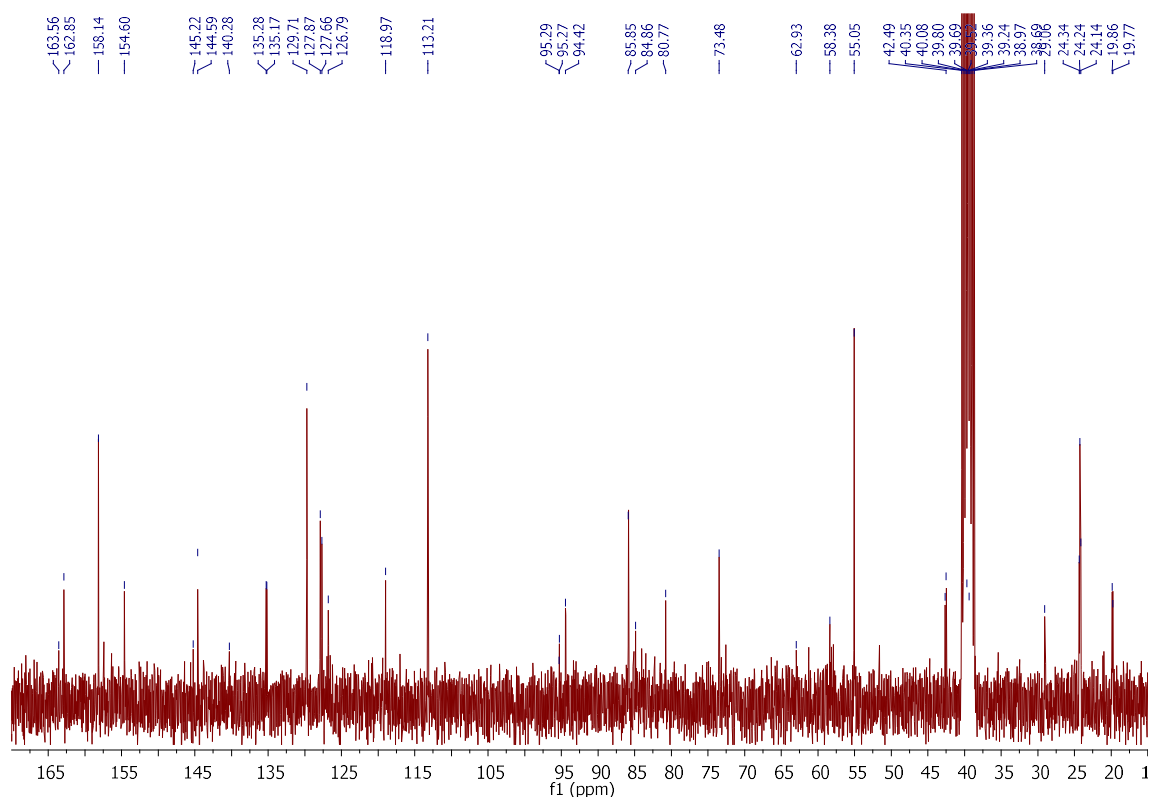


Figure 6.8: ^{13}C -NMR (100 MHz, $\text{DMSO-}d_6$) of 3'-O-CEP-5'-O-DMT- N^4 -propargyl-2'-deoxycytidine (**25b**).

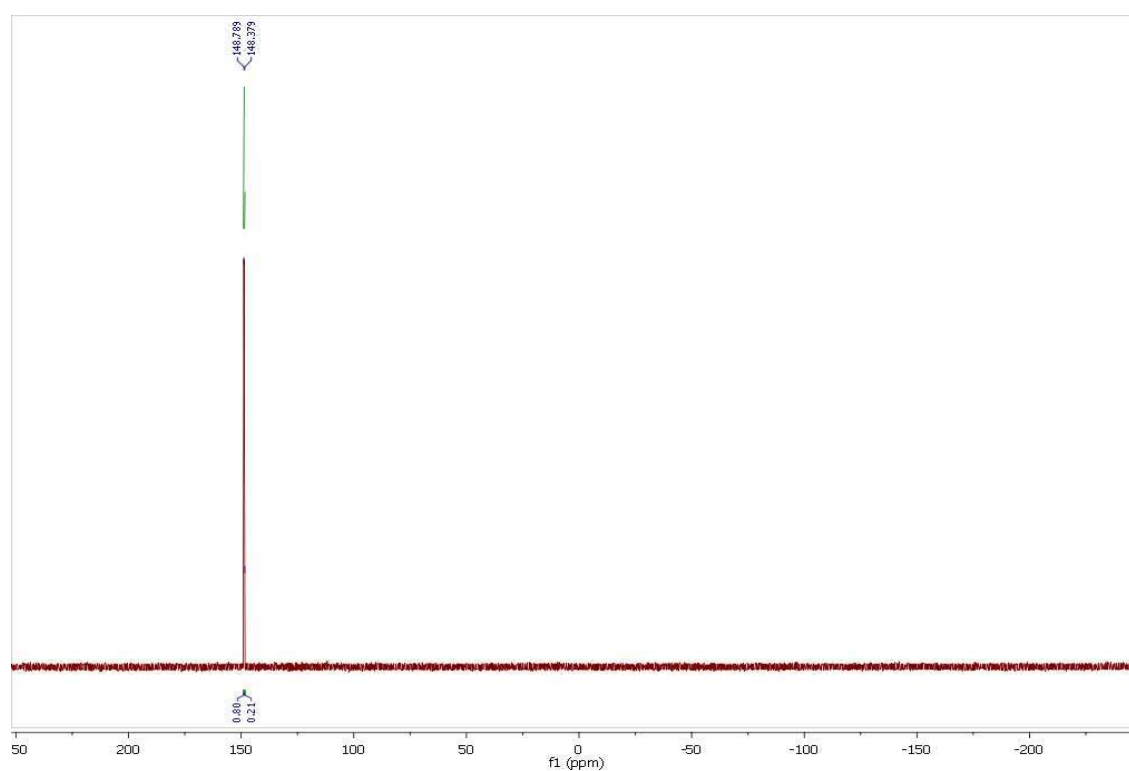


Figure 6.9: ^{31}P -NMR (162 MHz, $\text{DMSO-}d_6$) of 3'-O-CEP-5'-O-DMT- N^4 -propargyl-2'-deoxycytidine (**25b**).

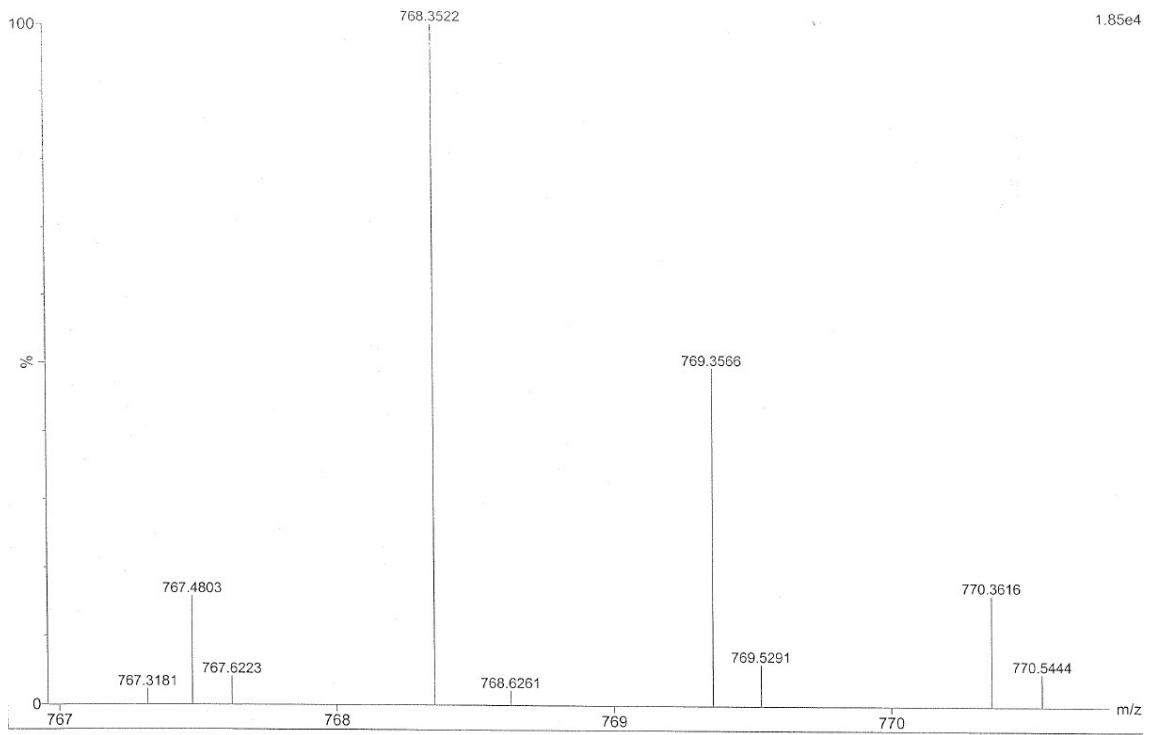
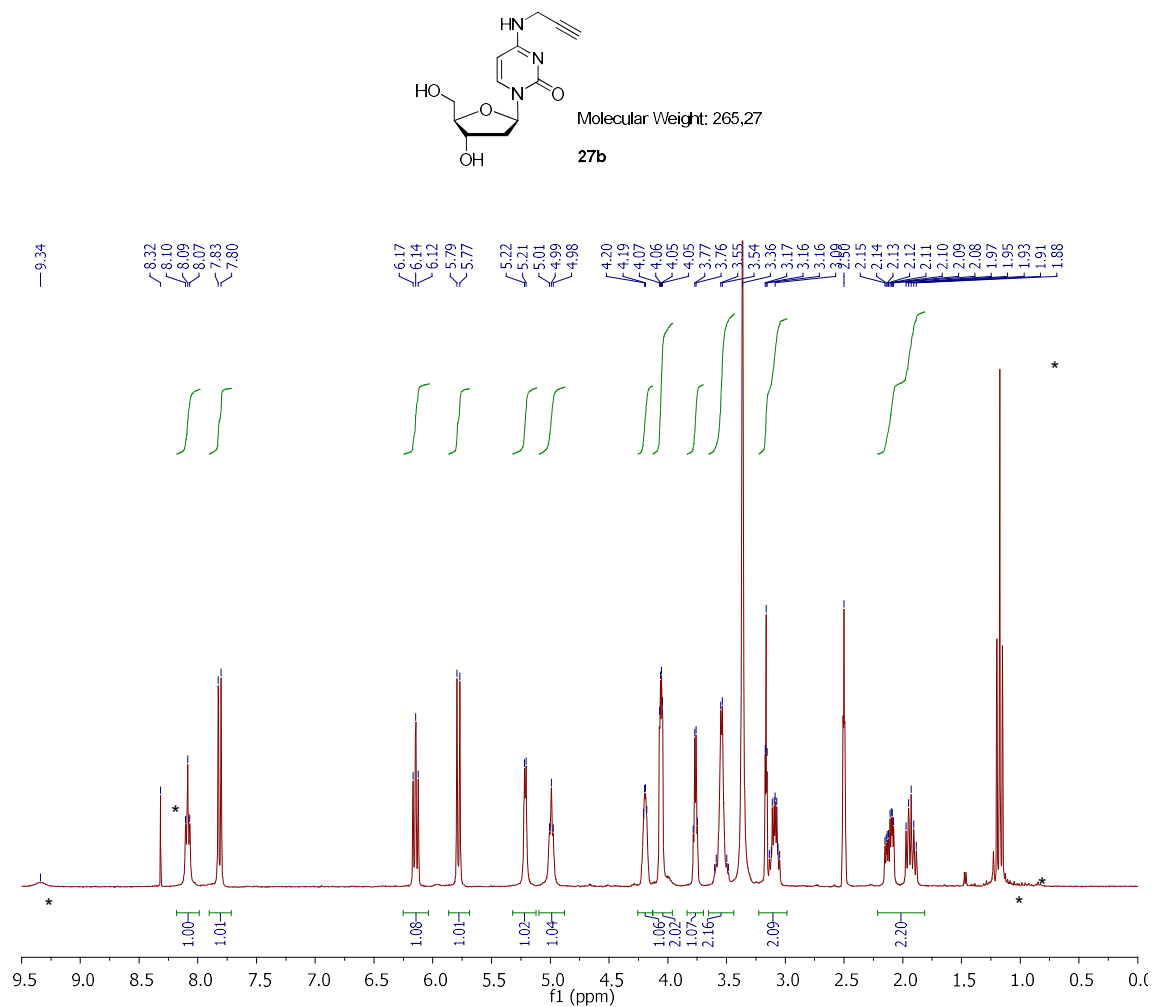


Figure 6.10: HR-MS (ESI) of 3'-O-CEP-5'-O-DMT-*N*⁴-propargyl-2'-deoxycytidine (**25b**).

6.3.2 Spectra of *N*⁴-propargyl-2'-deoxycytidine (**27b**)

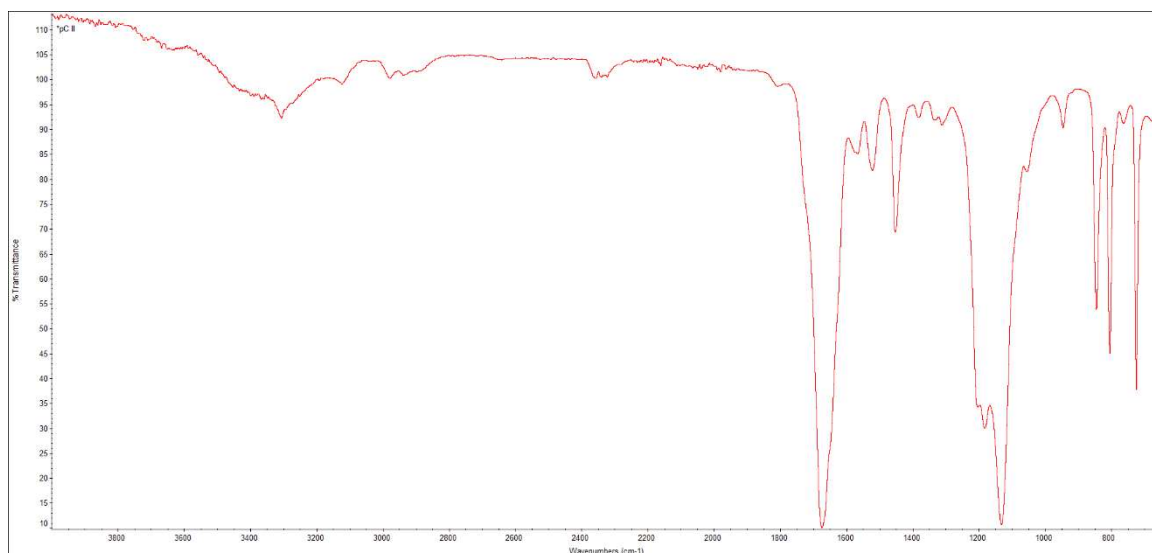


Figure 6.12: FT-IR of N^4 -propargyl-2'-deoxycytidine (**27b**).

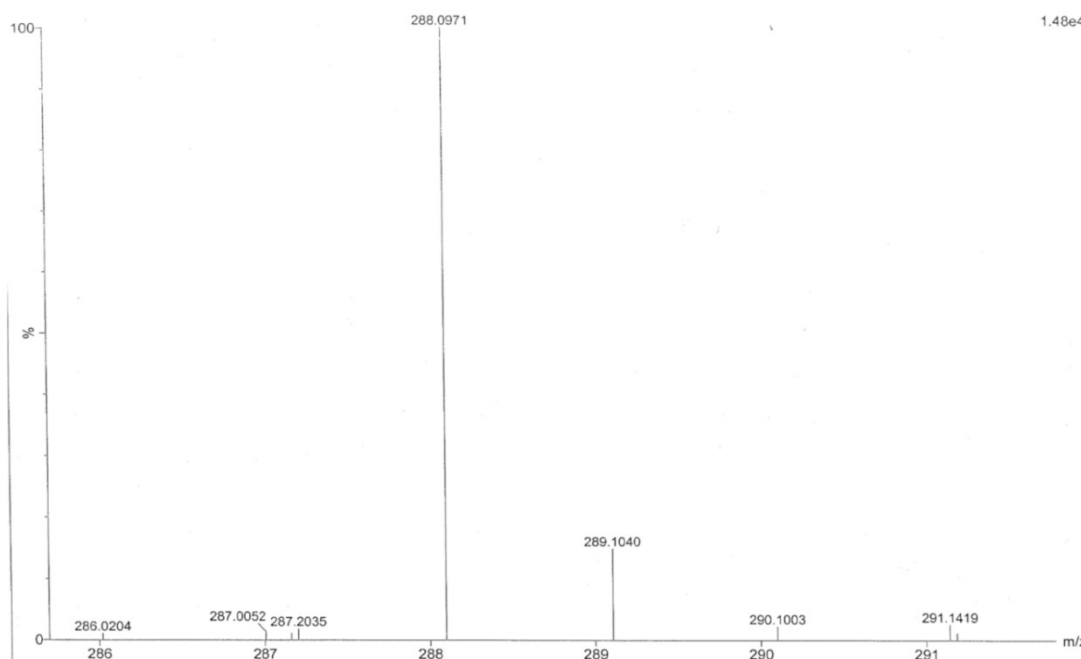


Figure 6.13: HR-MS (ESI) of N^4 -propargyl-2'-deoxycytidine (**27b**).

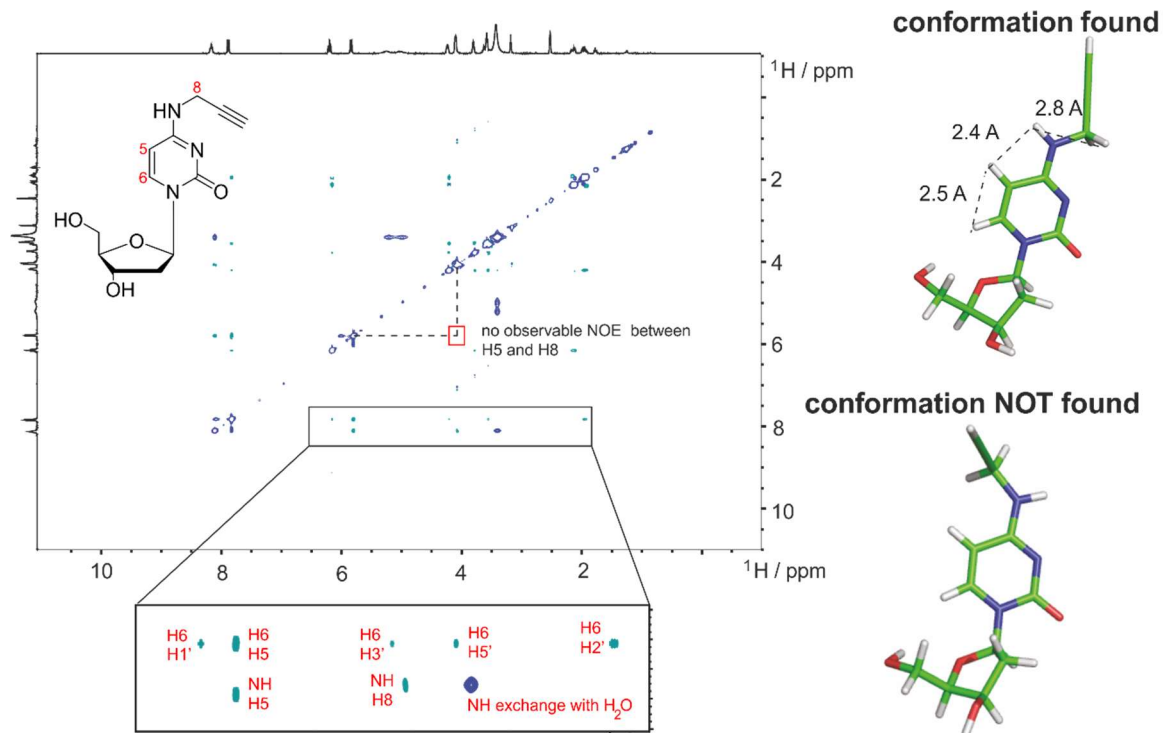


Figure 6.14: ROESY NMR experiments (300 MHz, $D_2O/H_2O = 1:9$) of *N*⁴-propargyl-2'-deoxycytidine (27b).

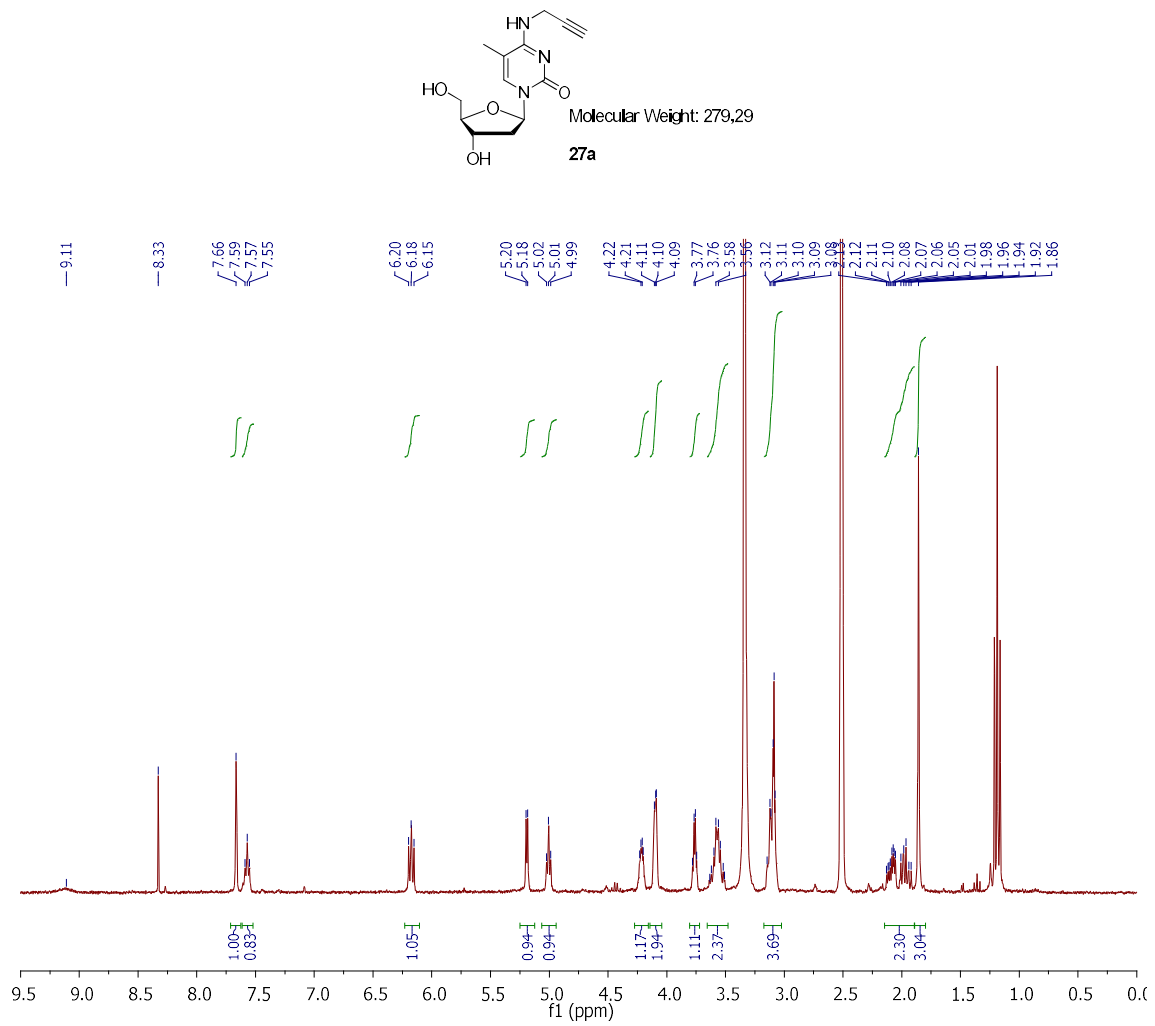
6.3.3 Spectra of 5-methyl-*N*⁴-propargyl-2'-deoxycytidine (27a)

Figure 6.15: ¹H-NMR (300 MHz, DMSO-d₆) of 5-methyl-*N*⁴-propargyl-2'-deoxycytidine (**27a**).

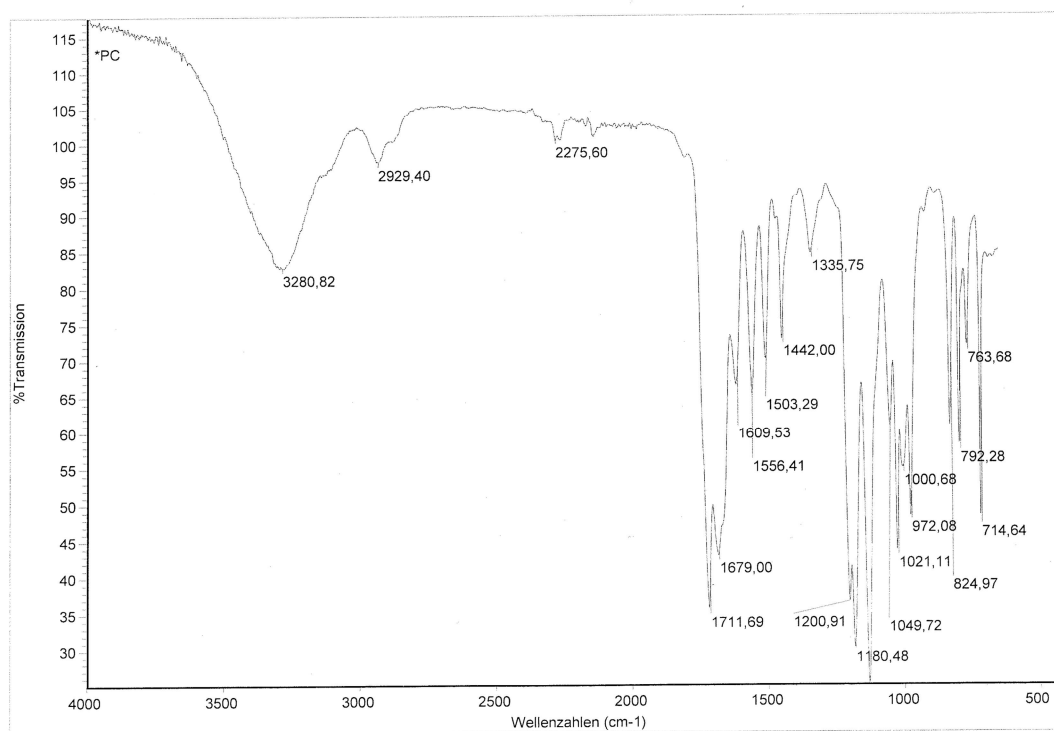


Figure 6.16: FT-IR of 5-methyl-*N*⁴-propargyl-2'-deoxycytidine (27a).

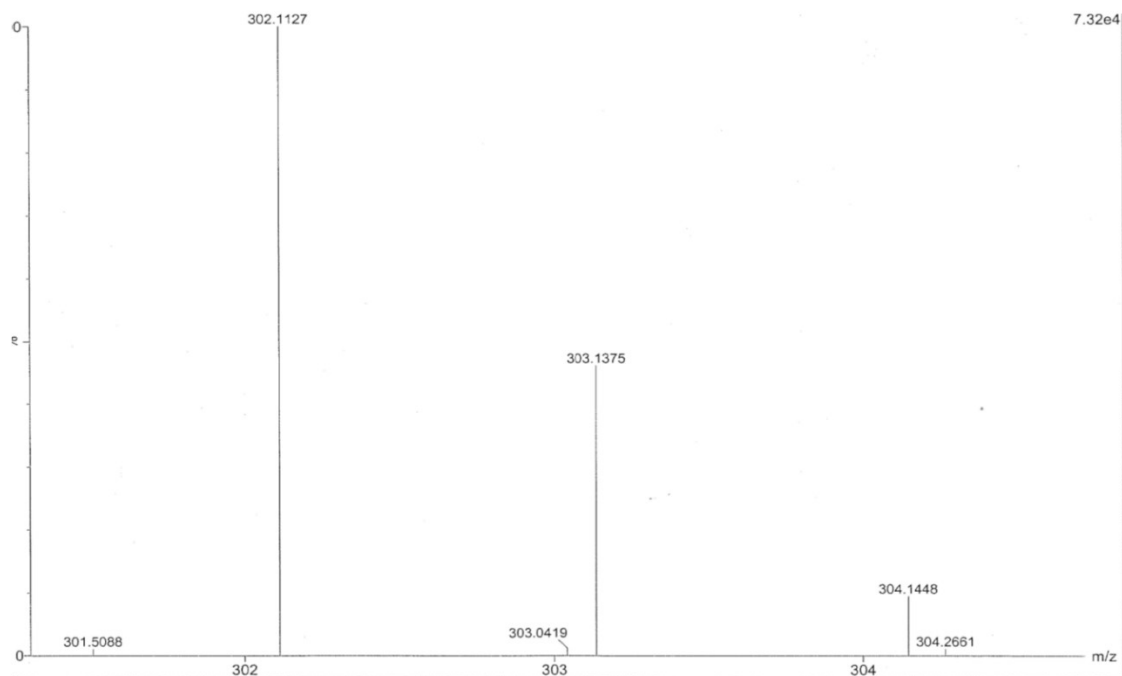


Figure 6.17: HR-MS (ESI) of 5-methyl-*N*⁴-propargyl-2'-deoxycytidine (27a).

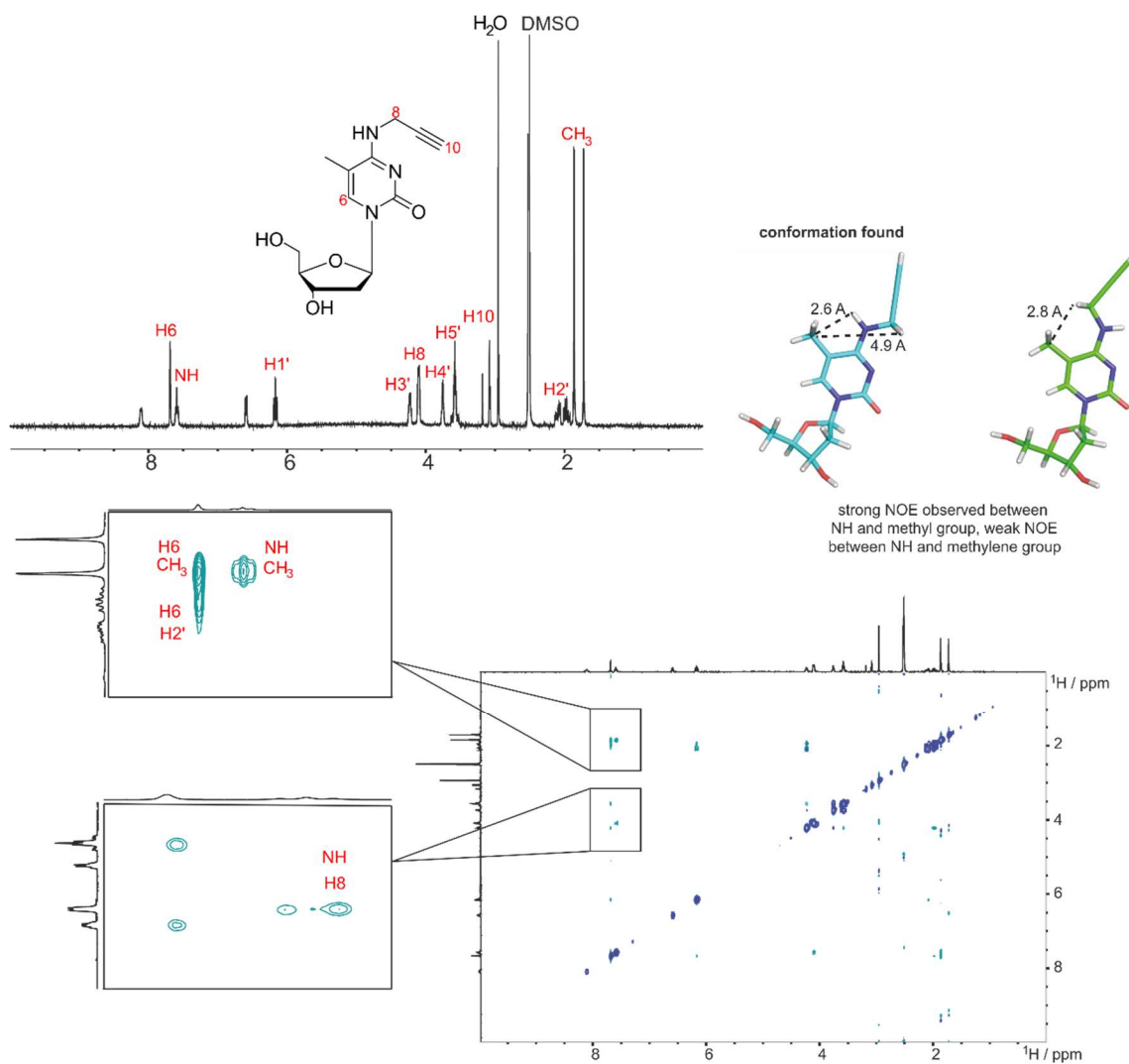


Figure 6.18: ROESY NMR experiments (300 MHz, $D_2O/H_2O = 1:9$) of 5-methyl-*N*⁴-propargyl-2'-deoxycytidine (27b).

6.3.4 ROESY kinetic studies

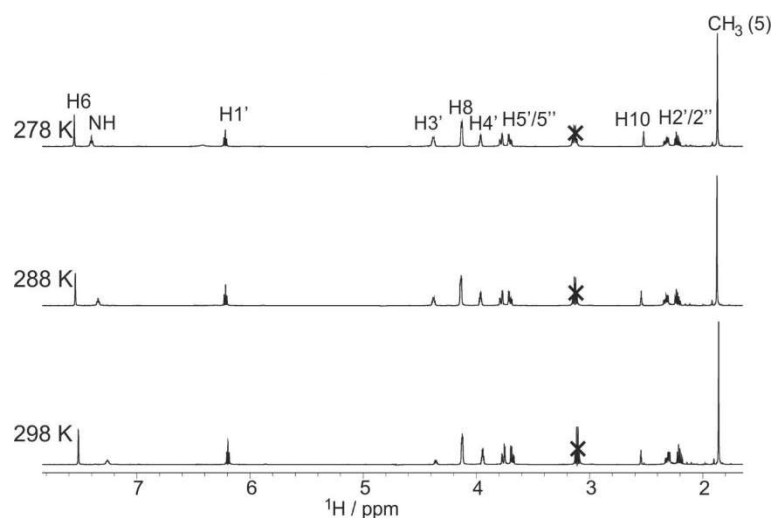


Figure 6.19: Temperature dependent ^1H NMR experiments (300 MHz, $\text{D}_2\text{O}/\text{H}_2\text{O} = 1:9$) of 5-methyl- N^4 -propargyl-2'-deoxy-cytidine (**27a**) for comparison with the corresponding experiment of N^4 -propargyl-2'-deoxycytidine (**27b**, see Figure 3.2 C). (Figure as published in Domingo *et al.* [193])

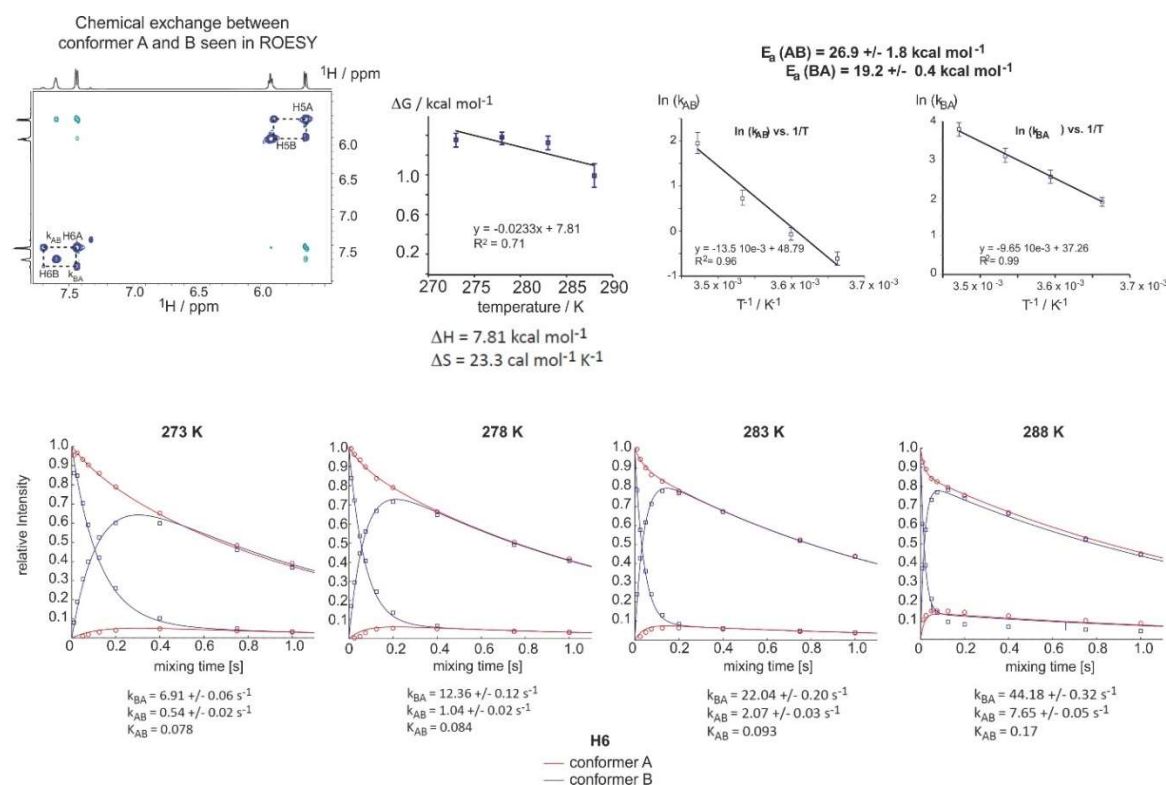


Figure 6.20: Temperature dependent ROESY NMR experiments (300 MHz, $\text{D}_2\text{O}/\text{H}_2\text{O} = 1:9$) and Arrhenius analysis of N^4 -propargyl-2'-deoxycytidine (**27b**). Details are described in the Materials and Methods section. (Figure as published in Domingo *et al.* [193])

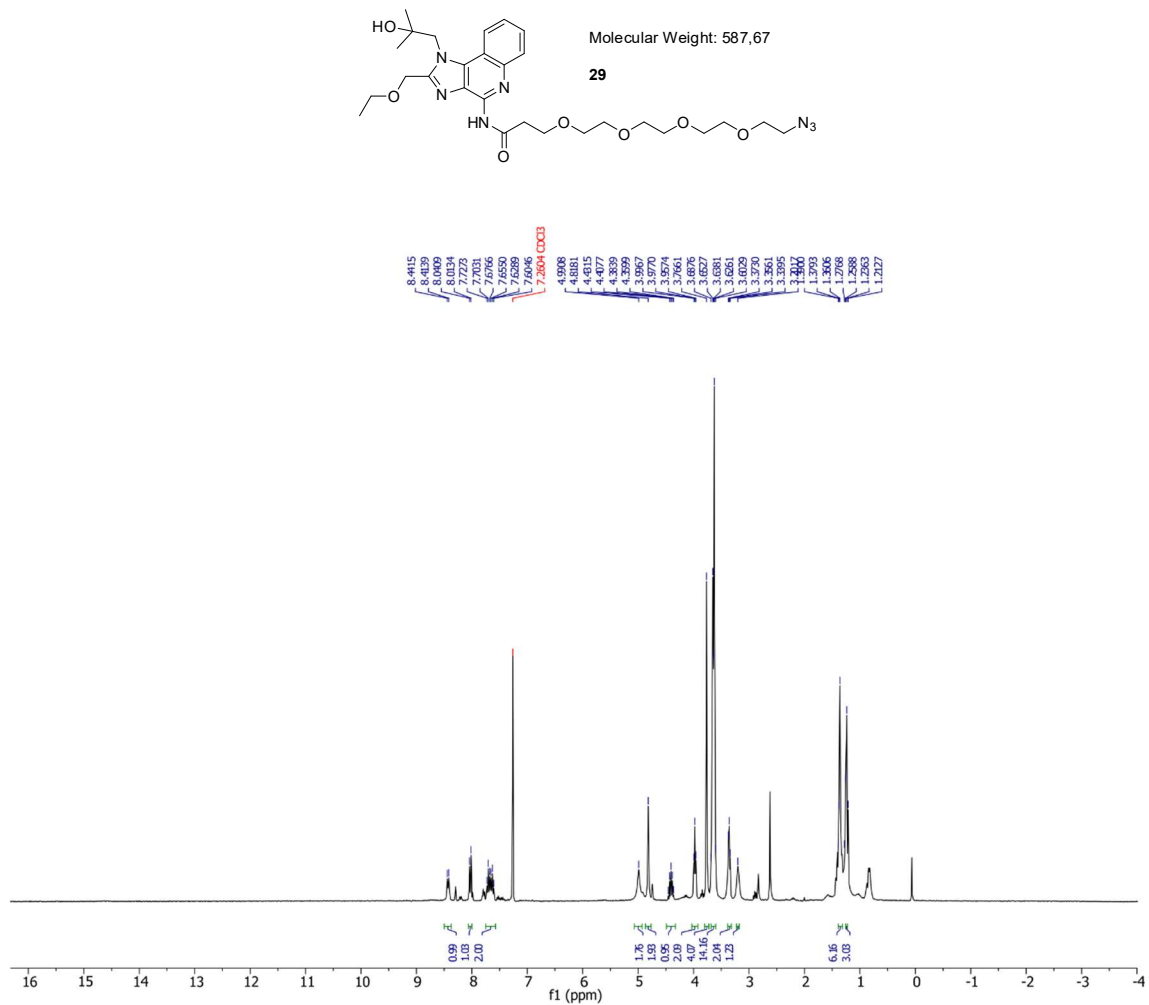
6.3.5 Spectra of Resiquimod-PEG₄-N₃ / RPA 29

Figure 6.21: ¹H-NMR (300 MHz, CDCl₃) of RPA (29).

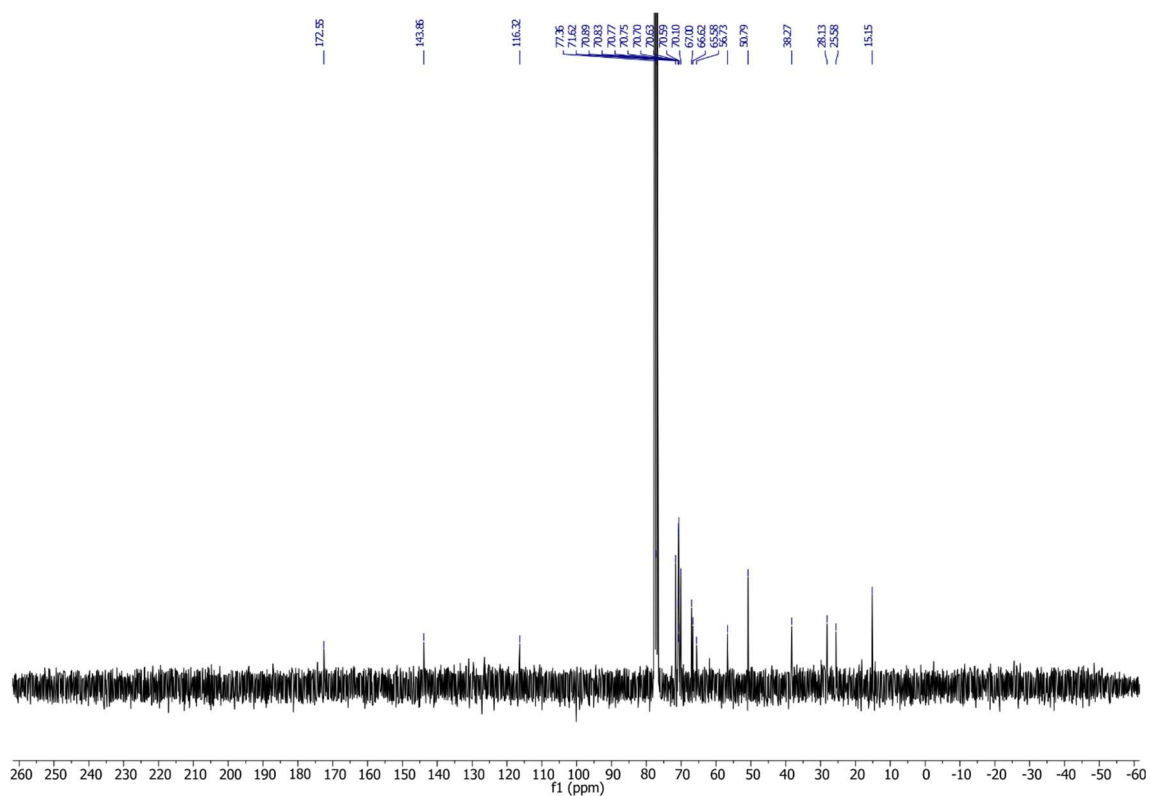


Figure 6.22: $^{13}\text{C-NMR}$ (75 MHz, CDCl_3) of RPA (29).

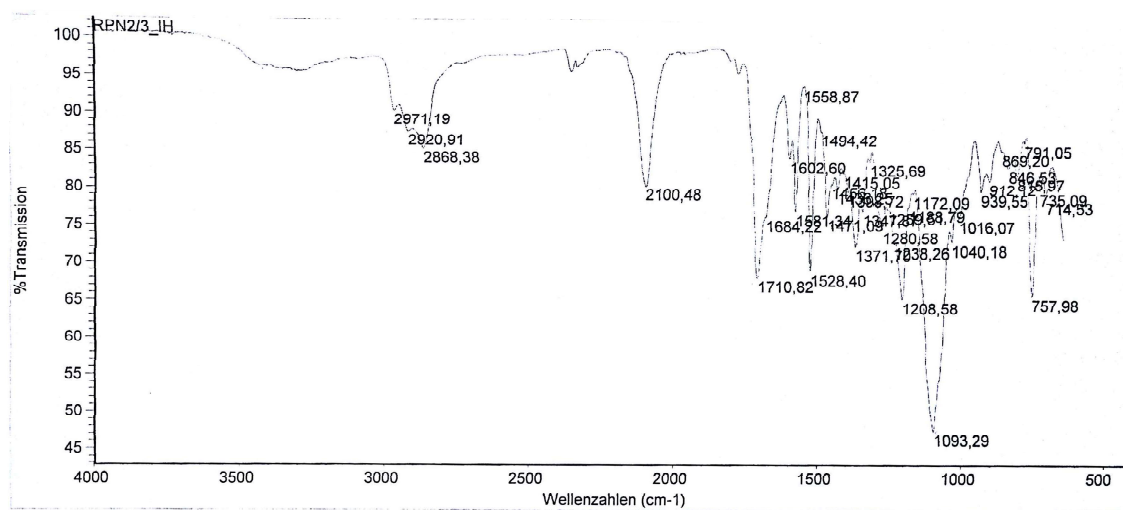


Figure 6.23: FT-IR of RPA (29).

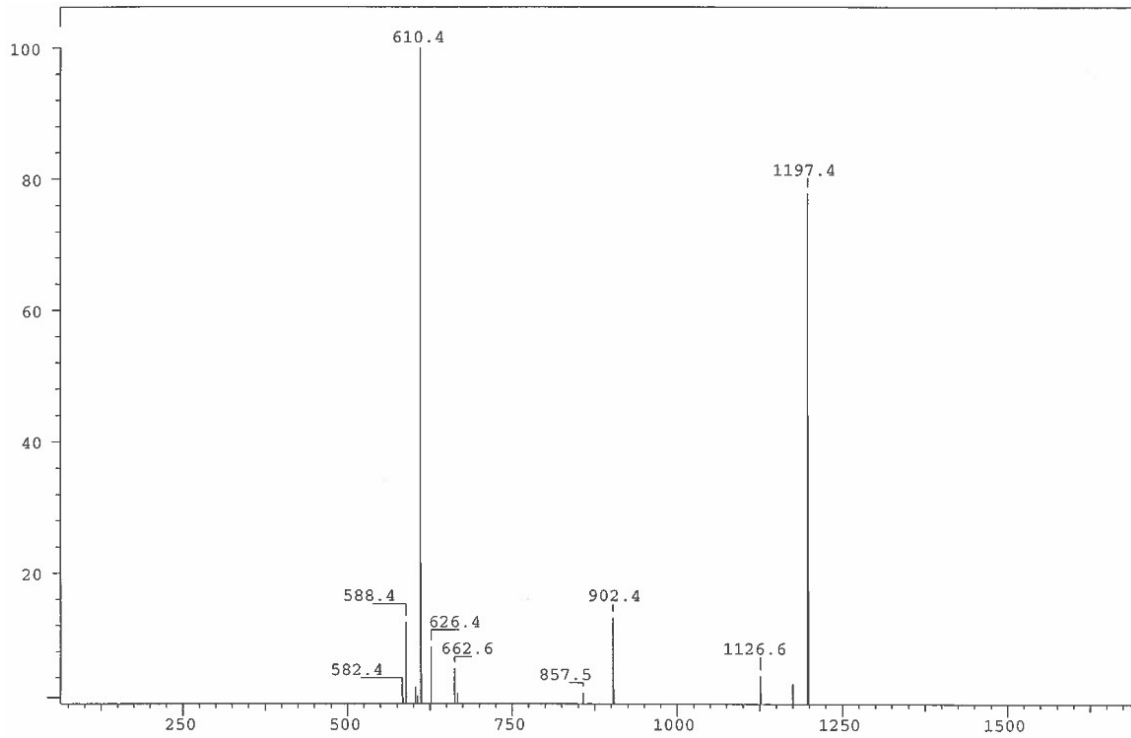


Figure 6.24: Full range MS (FD) of RPA (29).

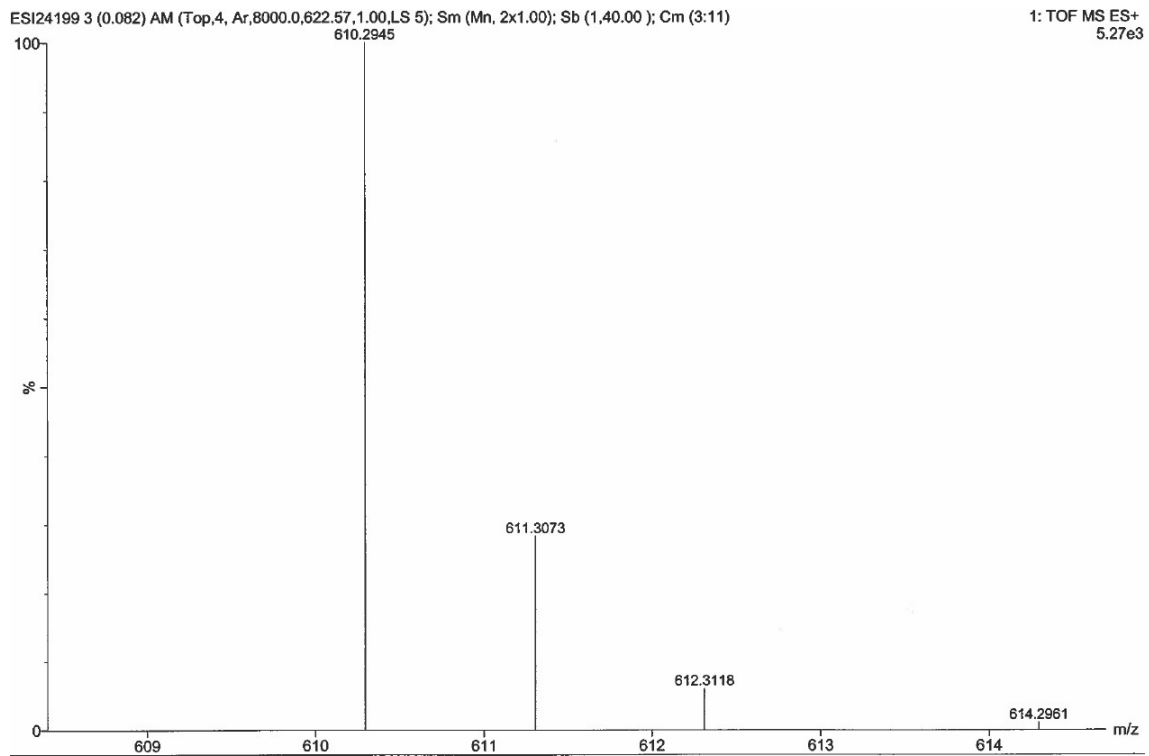
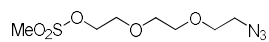


Figure 6.25: HR-MS (ESI) of RPA (29).

6.3.6 Spectra of 2-(2-(2-azidoethoxy)ethoxy)ethyl methanesulfonate (N₃-EEEt-OMs) **31**



Molecular Weight: 253,28

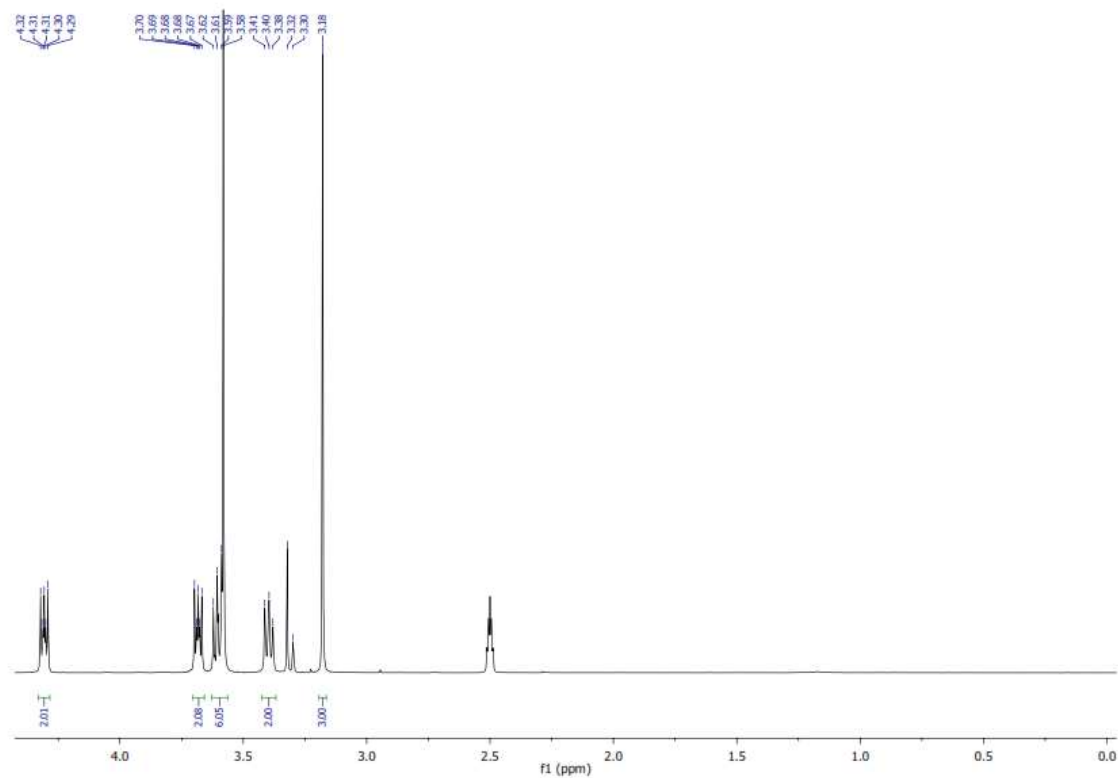
31

Figure 6.26: ¹H-NMR (300 MHz, CDCl₃) of N₃-EEEt-OMs (**31**).

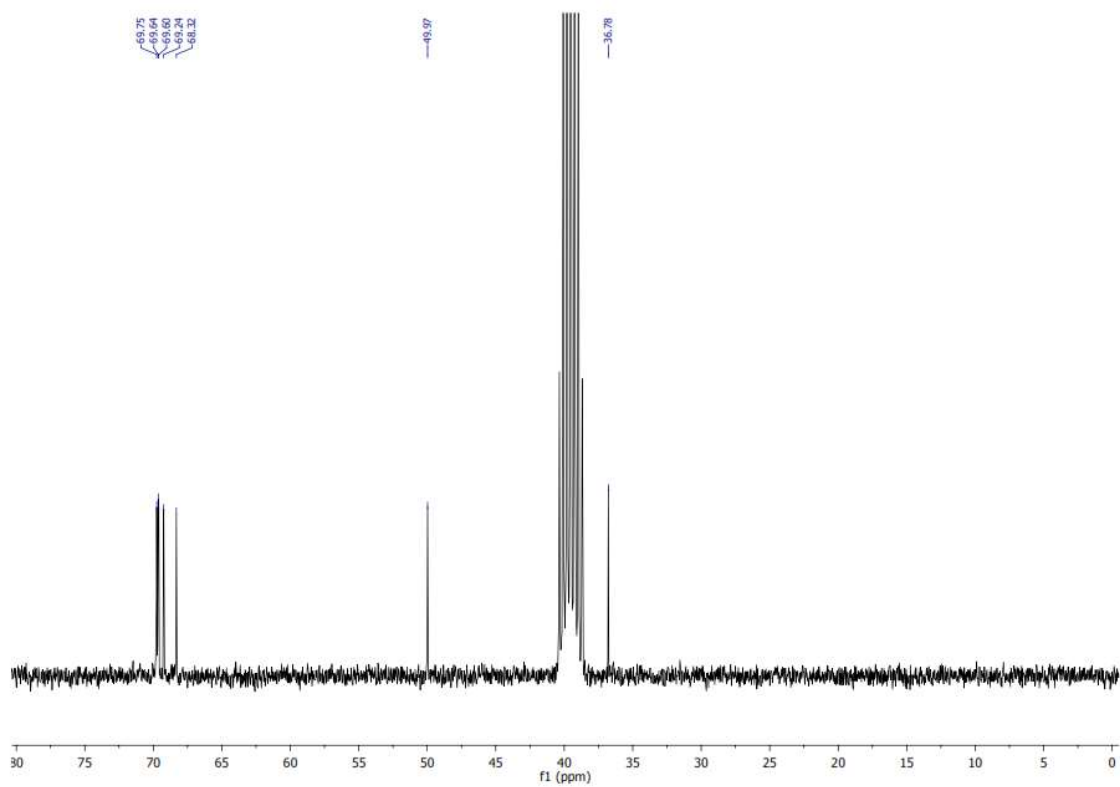
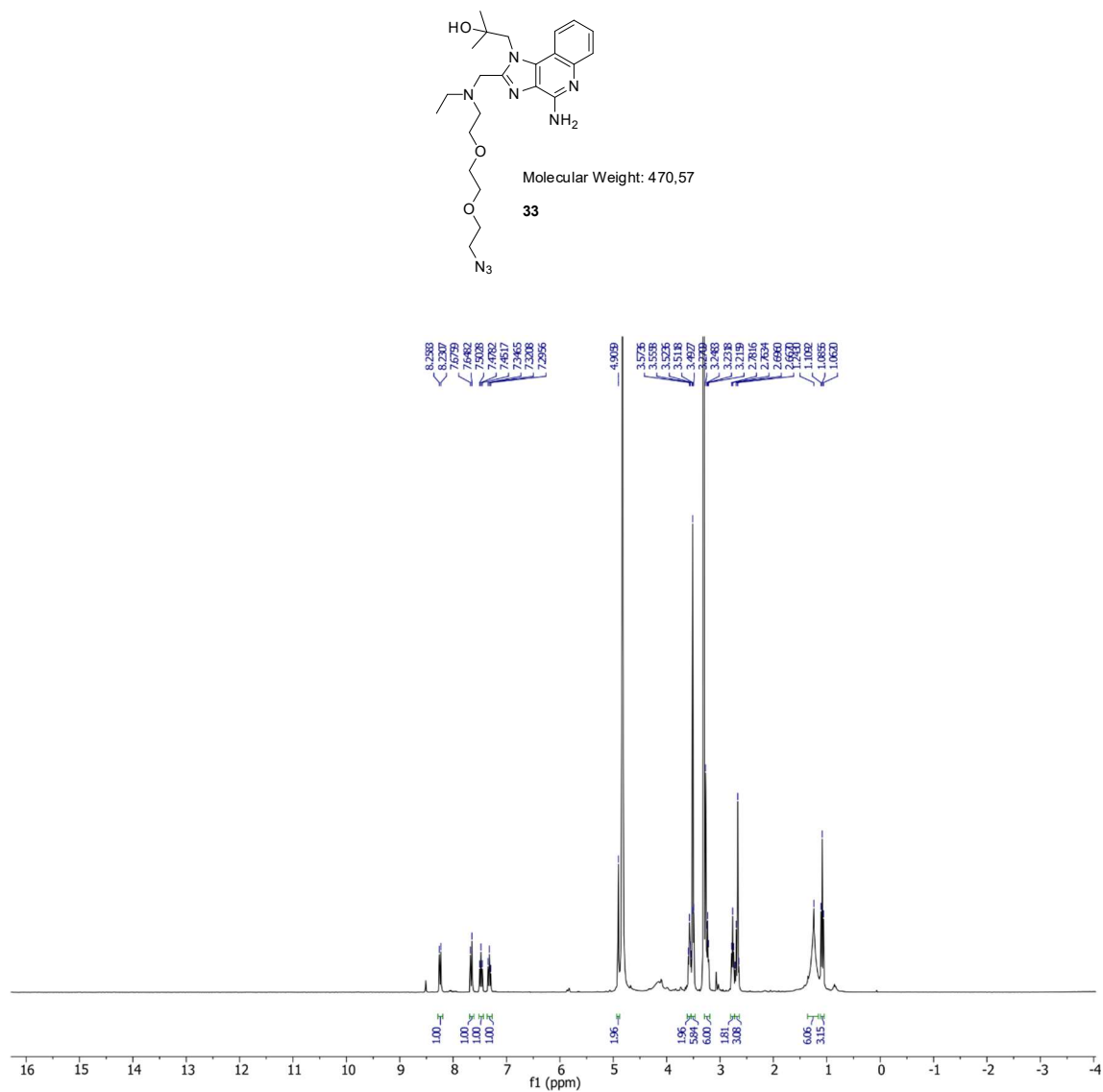


Figure 6.27: ^{13}C -NMR (75 MHz, CDCl_3) of $\text{N}_3\text{-EEEt-OMs}$ (31).

6.3.7 Spectra of Gardiquimod-DEG-N3 / GDA 33

Figure 6.28: $^1\text{H-NMR}$ (300 MHz, MeOD), GDA (**33**).

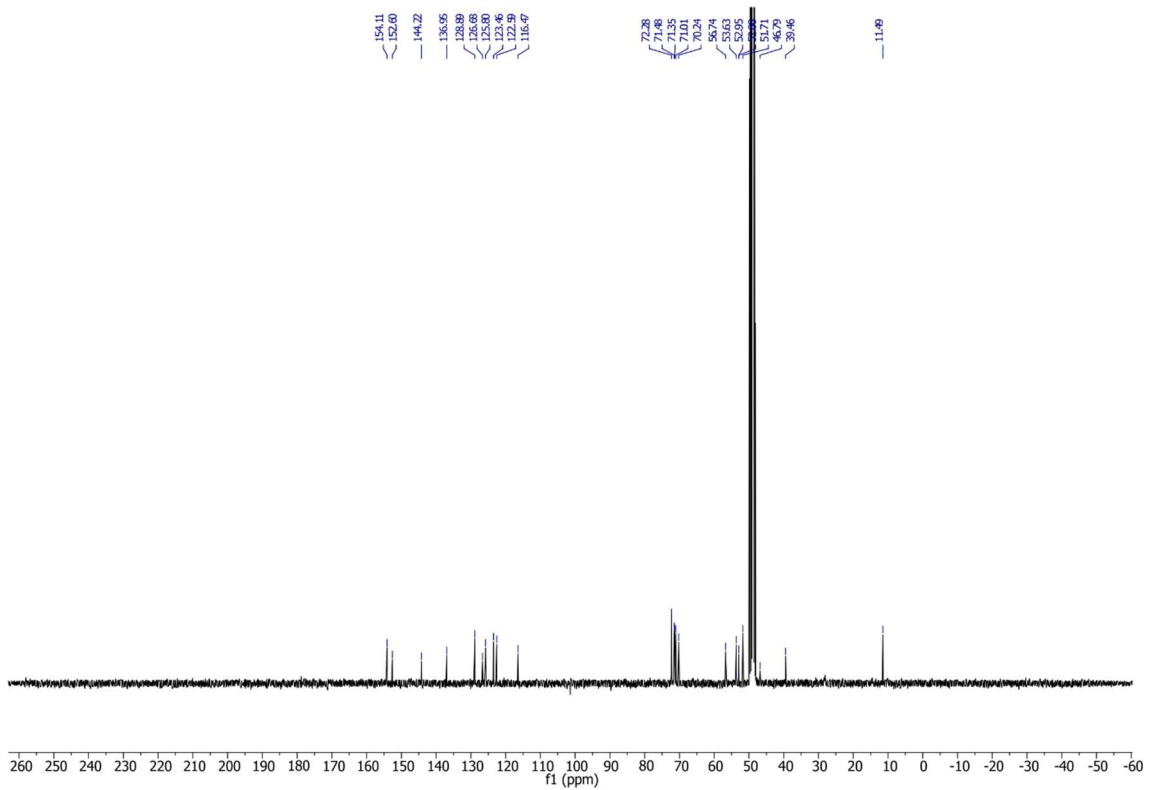


Figure 6.29: $^{13}\text{C-NMR}$ (75 MHz, MeOD), GDA (**33**).

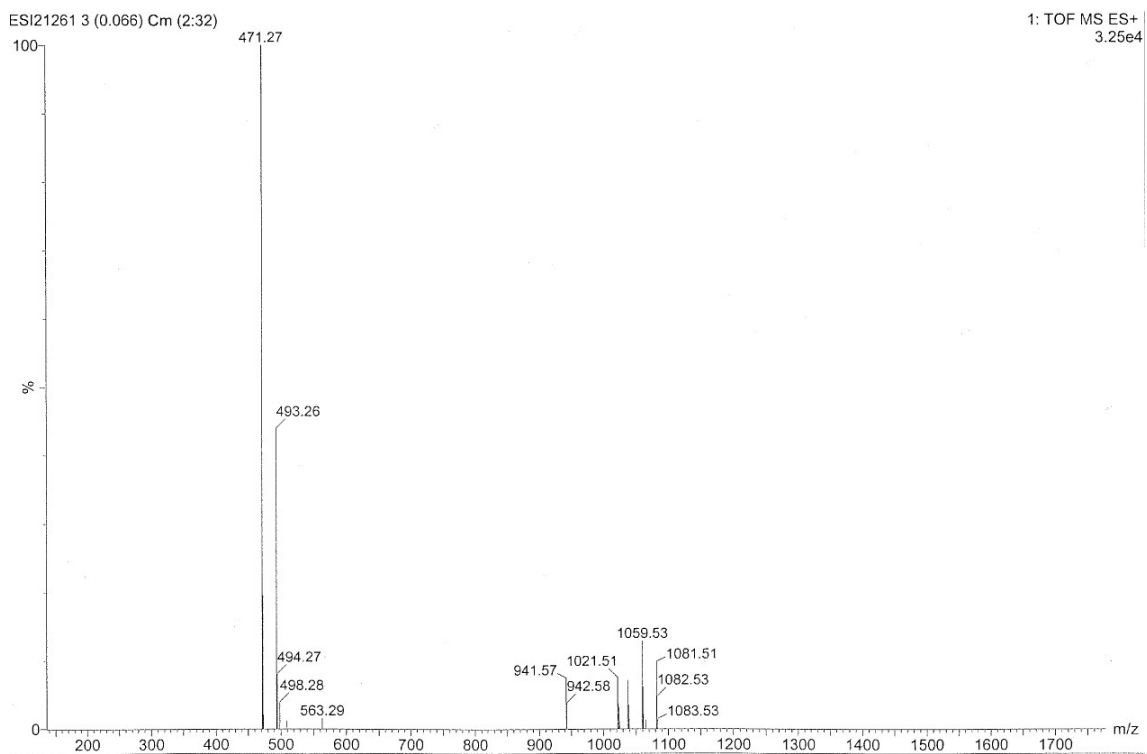


Figure 6.30: Full range MS (ESI) GDA (**33**).

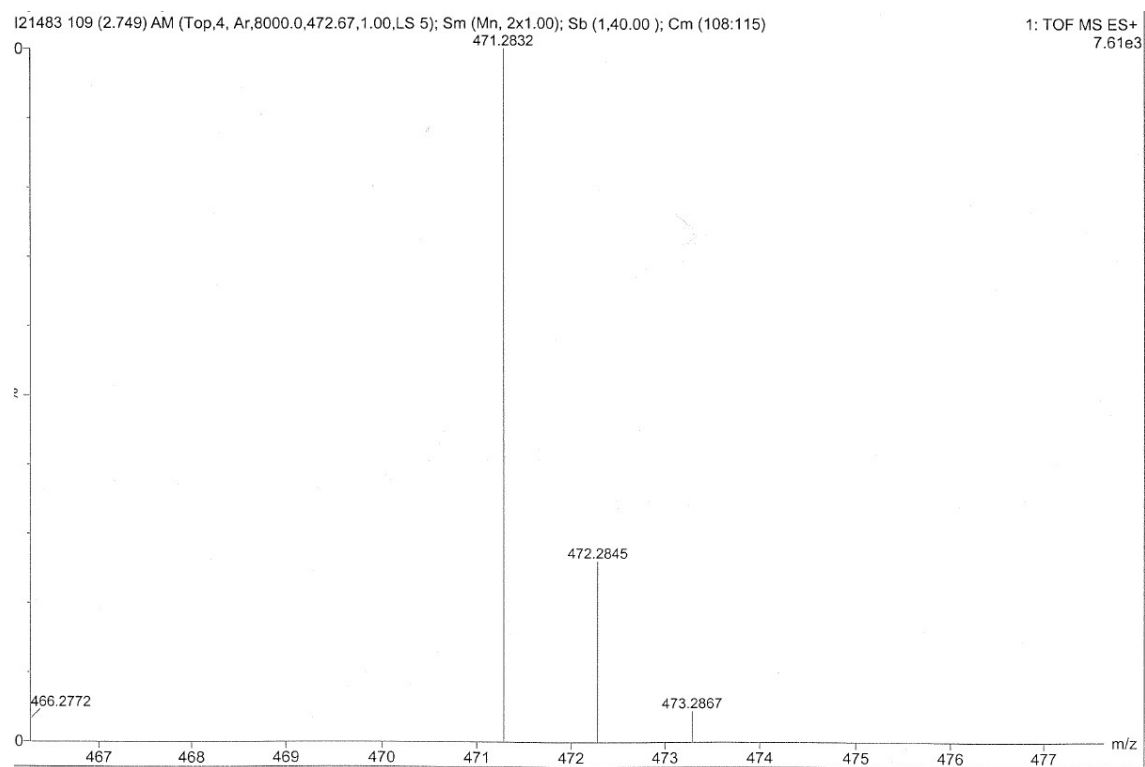


Figure 6.31: HR-MS (ESI) GDA (**33**).

Bibliography

- [1] G. M. Bonora, G. Biancotto, M. Maffini, and C. L. Scremin, "Large scale, liquid phase synthesis of oligonucleotides by the phosphoramidite approach," *Nucleic Acids Res.*, vol. 21, no. 5, pp. 1213–1217, 1993.
- [2] C. Chaix, D. Molko, and R. Téoule, "The use of labile base protecting groups in oligoribonucleotide synthesis," *Tetrahedron Lett.*, vol. 30, no. 1, pp. 71–74, 1989.
- [3] C. Bleasdale, S. B. Ellwood, and B. T. Golding, "4,4'-Dimethoxytrityl and 4-Monomethoxytrityl Tetrafluoroborate: Convenient Reagents for the Protection of Primary Alcohols Including Sugars," *J. Chem. Soc. Perkin Trans. 1*, vol. 1, pp. 803–805, 1990.
- [4] M. K. Lakshman and B. Zajc, "A Rapid, High-Yield Method for 5'-Hydroxyl Protection in Very Reactive and Amino Group Modified Nucleosides Using Dimethoxytrityl Tetrafluoroborate," *Nucleosides, Nucleotides and Nucleic Acids*, vol. 15, no. 5, pp. 1029–1039, 1996.
- [5] R. L. Letsinger and W. B. Lunsford, "Synthesis of thymidine oligonucleotides by phosphite triester intermediates," *J. Am. Chem. Soc.*, vol. 98, no. 12, pp. 3655–3661, Jun. 1976.
- [6] M. D. Matteucci and M. H. Caruthers, "Synthesis of deoxyoligonucleotides on a polymer support," *J. Am. Chem. Soc.*, vol. 103, no. 11, pp. 3185–3191, Aug. 1981.
- [7] R. T. Pon, M. J. Damha, and K. K. Ogilvie, "Modification of guanine bases by nucleoside phosphoramidite reagents during the solid phase synthesis of oligonucleotides," *Nucleic Acids Res.*, vol. 13, no. 18, pp. 6447–6465, 1985.
- [8] S. L. Beaucage and R. P. Iyer, "Advances in the Synthesis of Oligonucleotides by the Phosphoramidite Approach," *Tetrahedron*, vol. 48, no. 12, pp. 2223–2311, Mar. 1992.
- [9] S. L. Beaucage and R. P. Iyer, "The Functionalization of Oligonucleotides Via Phosphoramidite Derivatives," *Tetrahedron*, vol. 49, no. 10, pp. 1925–1963, Mar. 1993.
- [10] R. K. Gaur and K. C. Gupta, "A spectrophotometric method for the estimation of amino groups on polymer supports," *Anal. Biochem.*, vol. 180, no. 2, pp. 253–258, 1989.
- [11] S. Berner, K. Mühlegger, and H. Seliger, "Studies on the role of tetrazole in the activation of phosphoramidites," *Nucleic Acids Res.*, vol. 17, no. 3, pp. 853–864, 1989.
- [12] C. Vargeese, J. Carter, J. Yegge, S. Krivjansky, A. Settle, E. Kropp, K. Peterson, and W. Pieken, "Efficient activation of nucleoside phosphoramidites with 4,5-dicyanoimidazole during oligonucleotide synthesis," *Nucleic Acids Res.*, vol. 26, no. 4, pp. 1046–1050, 1998.
- [13] L. J. McBride and N. H. Caruthers, "An Investigation of Several Deoxynucleoside Phosphoramidites Useful for Synthesizing Deoxyoligonucleotides," *Tetrahedron Lett.*, vol.

- 24, no. 3, pp. 245–248, 1983.
- [14] I. K. Farrance, J. S. Eadie, and R. Ivarie, "Improved chemistry for oligodeoxyribonucleotide synthesis substantially improves restriction enzyme cleavage of a synthetic 35mer," *Nucleic Acids Res.*, vol. 17, no. 3, pp. 1231–1245, 1989.
- [15] J. Biernat, A. Wolter, and H. Köster, "Purification orientated synthesis of oligodeoxynucleotides in solution," *Tetrahedron Lett.*, vol. 24, no. 8, pp. 751–754, 1983.
- [16] S. A. Surzhikov, E. N. Timofeev, B. K. Chernov, J. B. Golova, and A. D. Mirzabekov, "Advanced method for oligonucleotide deprotection.," *Nucleic Acids Res.*, vol. 28, no. 8, p. E29, 2000.
- [17] M. P. Reddy, N. B. Hanna, and F. Farooqui, "Fast cleavage and deprotection of oligonucleotides," *Tetrahedron Lett.*, vol. 35, no. 25, pp. 4311–4314, 1994.
- [18] N. Usman, K. K. Ogilvie, M. Y. Jiang, and R. J. Cedergren, "The automated chemical synthesis of long oligoribonucleotides using 2'-O-silylated ribonucleoside 3'-O-phosphoramidites on a controlled-pore glass support: synthesis of a 43-nucleotide sequence similar to the 3'-half molecule of an Escherichia coli formylm," *J. Am. Chem. Soc.*, vol. 109, no. 25, pp. 7845–7854, 1987.
- [19] S. Welz, R. and Müller, "5- (Benzylmercapto) -1 H -tetrazole as activator for 2'-O-TBDMS phosphoramidite building blocks in RNA synthesis," *Tetrahedron*, vol. 43, pp. 795–797, 2002.
- [20] X. Wu and S. Pitsch, "Synthesis and pairing properties of oligoribonucleotide analogues containing a metal-binding site attached to β -D-allofuranosyl cytosine," *Nucleic Acids Res.*, vol. 26, no. 19, pp. 4315–4323, 1998.
- [21] C. Höbartner, C. Kreutz, E. Flecker, E. Ottenschläger, W. Pils, K. Grubmayr, and R. Micura, "The Synthesis of 2'- O -[(Triisopropylsilyl)oxy] methyl (TOM) Phosphoramidites of Methylated Ribonucleosides (m 1 G , m 2 G , m 2 2 G , m 1 I , m 3 U , m 4 C , m 6 A , m 6 2 A) for Use in Automated RNA Solid-Phase Synthesis," *Monatshefte für Chemie / Chem. Mon.*, vol. 134, no. 6, pp. 851–873, May 2003.
- [22] S. A. Scaringe, F. E. Wincott, and M. H. Caruthers, "Novel RNA Synthesis Method Using 5' - O -Silyl-2' - O -orthoester Protecting Groups," *J. Am. Chem. Soc.*, vol. 120, no. 13, pp. 11820–11821, 1998.
- [23] J. Temsamani, M. Kubert, and S. Agrawal, "Sequence identity of the n-1 product of a synthetic oligonucleotide," *Nucleic Acids Res.*, vol. 23, no. 11, pp. 1841–1844, 1995.
- [24] K. H. Hecker and R. L. Rill, "Error Analysis of Chemically Synthesized Polynucleotides," *Biotechniques*, vol. 24, no. Feb, pp. 256–260, 1998.
- [25] M. A. Jensen, M. S. Akhras, M. Fukushima, N. Pourmand, and R. W. Davis, "Direct oligonucleotide synthesis onto super-paramagnetic beads," *J. Biotechnol.*, vol. 167, no. 4, pp. 448–453, Sep. 2013.
- [26] J. Cieślak, C. Ausín, A. Grajkowski, and S. L. Beaucage, "The 2-Cyano-2,2-dimethylethanamine- N -oxymethyl Group for the 2'-Hydroxyl Protection of Ribonucleosides in the Solid-Phase Synthesis of RNA Sequences," *Chem. - A Eur. J.*, vol. 19, no. 14, pp. 4623–4632, Apr. 2013.

- [27] M. P. Reddy, N. B. Hanna, and F. Farooqui, "Ultrafast Cleavage and Deprotection of Oligonucleotides Synthesis and Use of CAc Derivatives," *Nucleosides and Nucleotides*, vol. 16, no. 7–9, pp. 1589–1598, 1997.
- [28] R. T. Wu, T., Ogilvie, K. and Pon, "Prevention of chain cleavage in the chemical synthesis of 2'-silylated oligoribonucleotides," *Nucleic Acids Res.*, vol. 17, no. 9, pp. 3501–3517, 1989.
- [29] N. D. Sinha, J. Biernat, and H. Köster, "beta-Cyanoethyl N,N-dialkylamino/N-morpholinomono-chloro phosphoramidites, new phosphitylating agents facilitating ease of deprotection and work-up of synthesized oligonucleotides," *Tetrahedron Lett.*, vol. 24, no. 52, pp. 5843–5846, 1983.
- [30] F. Wincott, A. DiRenzo, C. Shaffer, S. Grimm, D. Tracz, C. Workman, D. Sweedler, C. Gonzalez, S. Scaringe, and N. Usman, "Synthesis, deprotection, analysis and purification of RNA and ribosomes," *Nucleic Acids Res.*, vol. 23, no. 14, pp. 2677–2684, 1995.
- [31] C. Xie, M. A. Staszak, J. T. Quatroche, C. D. Sturgill, V. V. Khau, and M. J. Martinelli, "Nucleosidic phosphoramidite synthesis via phosphitylation: Activator selection and process development," *Org. Process Res. Dev.*, vol. 9, no. 6, pp. 730–737, 2005.
- [32] G. D. McFarland and P. N. Borer, "Separation of oligo-RNA by reverse-phase HPLC," *Nucleic Acids Res.*, vol. 7, no. 4, pp. 1067–1080, 1979.
- [33] M. Gilar, "Analysis and Purification of Synthetic Oligonucleotides by Reversed-Phase High-Performance Liquid Chromatography with Photodiode Array and Mass Spectrometry Detection," *Anal. Biochem.*, vol. 298, no. 2, pp. 196–206, Nov. 2001.
- [34] H. J. Fritz, R. Belagaje, E. L. Brown, R. H. Fritz, R. a Jones, R. G. Lees, and H. G. Khorana, "High-pressure liquid chromatography in polynucleotide synthesis.," *Biochemistry*, vol. 17, no. 7, pp. 1257–67, 1978.
- [35] R. Narukulla, "Post-synthetic and site-specific modification of endocyclic nitrogen atoms of purines in DNA and its potential for biological and structural studies," *Nucleic Acids Res.*, vol. 33, no. 6, pp. 1767–1778, Mar. 2005.
- [36] S. Seidu-Larry, B. Krieg, M. Hirsch, M. Helm, and O. Domingo, "A modified guanosine phosphoramidite for click functionalization of RNA on the sugar edge," *Chem. Commun.*, vol. 48, no. 89, pp. 11014–11016, 2012.
- [37] J. D. Trzupcek and T. L. Sheppard, "Photochemical generation of ribose abasic sites in RNA oligonucleotides," *Org. Lett.*, vol. 7, no. 8, pp. 1493–1496, 2005.
- [38] A. S. Wahba, F. Azizi, G. F. Deleavey, C. Brown, F. Robert, M. Carrier, A. Kalota, A. M. Gewirtz, J. Pelletier, R. H. E. Hudson, and M. J. Damha, "Phenylpyrrolocytosine as an unobtrusive base modification for monitoring activity and cellular trafficking of siRNA," *ACS Chem. Biol.*, vol. 6, no. 9, pp. 912–919, 2011.
- [39] A. A. Sawant, A. A. Tanpure, P. P. Mukherjee, S. Athavale, A. Kelkar, S. Galande, and S. G. Srivatsan, "A versatile toolbox for posttranscriptional chemical labeling and imaging of RNA," *Nucleic Acids Res.*, vol. 44, no. 2, p. gkv903, 2015.
- [40] A. M. MacMillan and G. L. Verdine, "Engineering tethered DNA molecules by the convertible nucleoside approach," *Tetrahedron*, vol. 47, no. 14–15, pp. 2603–2616, 1991.

- [41] C. R. Allerson, S. L. Chen, and G. L. Verdine, "A Chemical Method for Site-Specific Modification of RNA: The Convertible Nucleoside Approach," *J. Am. Chem. Soc.*, vol. 119, no. 32, pp. 7423–7433, Aug. 1997.
- [42] H. C. Kolb, M. G. Finn, and K. B. Sharpless, "Click Chemistry: Diverse Chemical Function from a Few Good Reactions," *Angew. Chemie - Int. Ed.*, vol. 40, no. 11, pp. 2004–2021, 2001.
- [43] J. C. Jewett and C. R. Bertozzi, "Cu-free click cycloaddition reactions in chemical biology," *Chem. Soc. Rev.*, vol. 39, no. 4, p. 1272, 2010.
- [44] A.-C. Knall and C. Slugovc, "Inverse electron demand Diels–Alder (IEDDA)-initiated conjugation: a (high) potential click chemistry scheme," *Chem. Soc. Rev.*, vol. 42, no. 12, p. 5131, 2013.
- [45] J. Schoch, M. Staudt, A. Samanta, M. Wiessler, and A. Jäschke, "Site-specific one-pot dual labeling of DNA by orthogonal cycloaddition chemistry," *Bioconjug. Chem.*, vol. 23, no. 7, pp. 1382–1386, 2012.
- [46] D. Schulz and A. Rentmeister, "Current Approaches for RNA Labeling in Vitro and in Cells Based on Click Reactions," *ChemBioChem*, vol. 15, no. 16, pp. 2342–2347, Nov. 2014.
- [47] E. Saxon and C. R. Bertozzi, "Cell Surface Engineering by a Modified Staudinger Reaction," *Science (80-.)*, vol. 287, no. 5460, pp. 2007–2010, 2000.
- [48] V. V. Rostovtsev, L. G. Green, V. V. Fokin, and K. B. Sharpless, "A Stepwise Huisgen Cycloaddition Process: Copper(I)-Catalyzed Regioselective 'Ligation' of Azides and Terminal Alkynes," *Angew. Chemie Int. Ed.*, vol. 41, no. 14, pp. 2596–2599, Jul. 2002.
- [49] F. Himo, T. Lovell, R. Hilgraf, V. V. Rostovtsev, L. Noodleman, K. B. Sharpless, and V. V. Fokin, "Copper(I)-catalyzed synthesis of azoles. DFT study predicts unprecedented reactivity and intermediates," *J. Am. Chem. Soc.*, vol. 127, no. 1, pp. 210–216, 2005.
- [50] V. O. Rodionov, V. V. Fokin, and M. G. Finn, "Mechanism of the ligand-free CuI-catalyzed azide-alkyne cycloaddition reaction," *Angew. Chemie - Int. Ed.*, vol. 44, no. 15, pp. 2210–2215, Apr. 2005.
- [51] V. D. Bock, H. Hiemstra, and J. H. van Maarseveen, "CuI-Catalyzed Alkyne-Azide 'Click' Cycloadditions from a Mechanistic and Synthetic Perspective," *European J. Org. Chem.*, vol. 2006, no. 1, pp. 51–68, Jan. 2006.
- [52] J. Gierlich, G. A. Burley, P. M. E. Gramlich, D. M. Hammond, and T. Carell, "Click Chemistry as a Reliable Method for the High-Density Postsynthetic Functionalization of Alkyne-Modified DNA," *Org. Lett.*, vol. 8, no. 17, pp. 3639–3642, Aug. 2006.
- [53] P. M. E. Gramlich, S. Warncke, J. Gierlich, and T. Carell, "Click-click-click: Single to triple modification of DNA," *Angew. Chemie - Int. Ed.*, vol. 47, no. 18, pp. 3442–3444, 2008.
- [54] A. H. El-Sagheer and T. Brown, "Click chemistry with DNA," *Chem. Soc. Rev.*, vol. 39, no. 4, p. 1388, 2010.
- [55] E. Paredes and S. R. Das, "Click Chemistry for Rapid Labeling and Ligation of RNA," *ChemBioChem*, vol. 12, no. 1, pp. 125–131, Jan. 2011.
- [56] A. H. El-Sagheer and T. Brown, "Click Nucleic Acid Ligation: Applications in Biology and

- Nanotechnology," *Acc. Chem. Res.*, vol. 45, no. 8, pp. 1258–1267, Aug. 2012.
- [57] S. H. Weisbrod and A. Marx, "Novel strategies for the site-specific covalent labelling of nucleic acids," *Chem. Commun.*, no. 44, p. 5675, 2008.
- [58] K. Burgess and D. Cook, "Syntheses of nucleoside triphosphates," *Chem. Rev.*, vol. 100, no. 6, pp. 2047–2059, 2000.
- [59] M. Hollenstein, "Nucleoside Triphosphates — Building Blocks for the Modification of Nucleic Acids," *Molecules*, vol. 17, no. 12, pp. 13569–13591, Nov. 2012.
- [60] Q. Sun, J. P. Edathil, R. Wu, E. D. Smidansky, C. E. Cameron, and B. R. Peterson, "One-Pot Synthesis of Nucleoside 5'-Triphosphates from Nucleoside 5'-H -Phosphonates," *Org. Lett.*, vol. 10, no. 9, pp. 1703–1706, May 2008.
- [61] M. Hocek, "Synthesis of Base-Modified 2'-Deoxyribonucleoside Triphosphates and Their Use in Enzymatic Synthesis of Modified DNA for Applications in Bioanalysis and Chemical Biology," *J. Org. Chem.*, vol. 79, no. 21, pp. 9914–9921, Nov. 2014.
- [62] J. Schoch and A. Jäschke, "Synthesis and enzymatic incorporation of norbornene-modified nucleoside triphosphates for Diels–Alder bioconjugation," *RSC Adv.*, vol. 3, no. 13, p. 4181, 2013.
- [63] A. Efstratiadis, J. N. Vournakis, H. Donis-keller, G. Chaconas, D. K. Dougall, and F. C. Kafatos, "End labeling of enzymatically decapped mRNA," *Nucleic Acids Res.*, vol. 4, no. 12, pp. 4165–4174, 1977.
- [64] Y. Motorin, J. Burhenne, R. Teimer, K. Koynov, S. Willnow, E. Weinhold, and M. Helm, "Expanding the chemical scope of RNA:methyltransferases to site-specific alkylation of RNA for click labeling," *Nucleic Acids Res.*, vol. 39, no. 5, pp. 1943–1952, 2011.
- [65] D. Schulz, J. M. Holstein, and A. Rentmeister, "A chemo-enzymatic approach for site-specific modification of the RNA cap," *Angew. Chemie - Int. Ed.*, 2013.
- [66] A. Samanta, A. Krause, and A. Jäschke, "A modified dinucleotide for site-specific RNA-labelling by transcription priming and click chemistry," *Chem. Commun.*, vol. 50, no. 11, pp. 1313–1316, 2014.
- [67] M.-L. Winz, A. Samanta, D. Benzinger, and A. Jäschke, "Site-specific terminal and internal labeling of RNA by poly(A) polymerase tailing and copper-catalyzed or copper-free strain-promoted click chemistry," *Nucleic Acids Res.*, vol. 40, no. 10, pp. e78–e78, May 2012.
- [68] M. A. Machnicka, K. Milanowska, O. Osman Oglou, E. Purta, M. Kurkowska, A. Olchowik, W. Januszewski, S. Kalinowski, S. Dunin-Horkawicz, K. M. Rother, M. Helm, J. M. Bujnicki, and H. Grosjean, "MODOMICS: a database of RNA modification pathways--2013 update," *Nucleic Acids Res.*, vol. 41, no. D1, pp. D262–D267, Jan. 2013.
- [69] F. Crick, "Central dogma of molecular biology," *Nature*, vol. 227, pp. 561–563, 1970.
- [70] T. P. Hoernes, N. Clementi, K. Faserl, H. Glasner, K. Breuker, H. Lindner, A. Hüttenhofer, and M. D. Erlacher, "Nucleotide modifications within bacterial messenger RNAs regulate their translation and are able to rewire the genetic code," *Nucleic Acids Res.*, vol. 44, no. 2, pp. 852–862, Jan. 2016.
- [71] M. Helm and Y. Motorin, "Detecting RNA modifications in the epitranscriptome: predict and

- validate," *Nat. Rev. Genet.*, 2017.
- [72] X. Tang, J. Zhang, J. Sun, Y. Wang, J. Wu, and L. Zhang, "Caged nucleotides/nucleosides and their photochemical biology," *Org. Biomol. Chem.*, vol. 11, no. 45, pp. 7814–7824, 2013.
- [73] Y.-L. Chiu and T. M. Rana, "siRNA function in RNAi: A chemical modification analysis," *RNA*, vol. 9, no. 9, pp. 1034–1048, Sep. 2003.
- [74] O. Andries, S. Mc Cafferty, S. C. De Smedt, R. Weiss, N. N. Sanders, and T. Kitada, "N1-methylpseudouridine-incorporated mRNA outperforms pseudouridine-incorporated mRNA by providing enhanced protein expression and reduced immunogenicity in mammalian cell lines and mice," *J. Control. Release*, 2015.
- [75] B. Li, X. Luo, and Y. Dong, "Effects of Chemically Modified Messenger RNA on Protein Expression," *Bioconjug. Chem.*, vol. 27, no. 3, pp. 849–853, 2016.
- [76] M. Terrazas and E. T. Kool, "RNA major groove modifications improve siRNA stability and biological activity," *Nucleic Acids Res.*, vol. 37, no. 2, pp. 346–353, 2009.
- [77] H. Xiong and F. Seela, "Stepwise 'Click' Chemistry for the Template Independent Construction of a Broad Variety of Cross-Linked Oligonucleotides: Influence of Linker Length, Position, and Linking Number on DNA Duplex Stability," *J. Org. Chem.*, vol. 76, no. 14, pp. 5584–5597, Jul. 2011.
- [78] A. Rodrigues-Correia, M. B. Koeppel, F. Schäfer, K. B. Joshi, T. Mack, and A. Heckel, "Comparison of the duplex-destabilizing effects of nucleobase-caged oligonucleotides," *Anal. Bioanal. Chem.*, vol. 399, no. 1, pp. 441–447, 2011.
- [79] M. Helm, "Post-transcriptional nucleotide modification and alternative folding of RNA," *Nucleic Acids Res.*, vol. 34, no. 2, pp. 721–733, Jan. 2006.
- [80] I. Hirao, Y. Harada, M. Kimoto, T. Mitsui, T. Fujiwara, and S. Yokoyama, "A Two-Unnatural-Base-Pair System toward the Expansion of the Genetic Code," *J. Am. Chem. Soc.*, vol. 126, no. 41, pp. 13298–13305, Oct. 2004.
- [81] D. H. Turner, "Thermodynamics of base pairing," *Curr. Opin. Struct. Biol.*, vol. 6, no. 3, pp. 299–304, Jun. 1996.
- [82] S. M. Freier and K.-H. Altmann, "The ups and downs of nucleic acid duplex stability: structure-stability studies on chemically-modified DNA:RNA duplexes," *Nucleic Acids Res.*, vol. 25, no. 22, pp. 4429–4443, 1997.
- [83] N. B. Leontis and E. Westhof, "Conserved geometrical base-pairing patterns in RNA," *Q. Rev. Biophys.*, vol. 31, no. 4, pp. 399–455, 1998.
- [84] D. De Paula, M. V. L. B. Bentley, R. I. Mahato, D. De Paula, M. V. L. B. Bentley, R. I. Mahato, D. De Paula, M. V. L. B. Bentley, and R. I. Mahato, "Hydrophobization and bioconjugation for enhanced siRNA delivery and targeting," *Rna*, vol. 13, no. 4, pp. 431–456, 2007.
- [85] L. L. Cummins, S. R. Owens, L. M. Risen, E. A. Lesnik, S. M. Freier, D. Mc Gee, C. J. Cook, and P. D. Cook, "Characterization of fully 2'-modified oligoribonucleotide hetero- and homoduplex hybridization and nuclease sensitivity," *Nucleic Acids Res.*, vol. 23, no. 11, pp. 2019–2024, 1995.
- [86] M. Majlessi, N. C. Nelson, and M. M. Becker, "Advantages of 2'-O-methyl oligoribonucleotide

- probes for detecting RNA targets," *Nucleic Acids Res.*, vol. 26, no. 9, pp. 2224–2229, 1998.
- [87] A. D. Judge, G. Bola, A. C. H. Lee, and I. MacLachlan, "Design of noninflammatory synthetic siRNA mediating potent gene silencing in vivo," *Mol. Ther.*, vol. 13, no. 3, pp. 494–505, 2006.
- [88] F. Eberle, K. Giessler, C. Deck, K. Heeg, M. Peter, C. Richert, and A. H. Dalpke, "Modifications in small interfering RNA that separate immunostimulation from RNA interference.," *J. Immunol.*, vol. 180, no. 5, pp. 3229–37, 2008.
- [89] R. Broering, C. I. Real, M. J. John, K. Jahn-Hofmann, L. M. Ickenstein, K. Kleinehr, A. Paul, K. Gibbert, U. Dittmer, G. Gerken, and J. F. Schlaak, "Chemical modifications on siRNAs avoid toll-like receptor-mediated activation of the hepatic immune system in vivo and in vitro," *Int. Immunol.*, vol. 26, no. 1, pp. 35–46, 2014.
- [90] S. Gehrig, M.-E. Eberle, F. Botschen, K. Rimbach, F. Eberle, T. Eigenbrod, S. Kaiser, W. M. Holmes, V. a. Erdmann, M. Sprinzl, G. Bec, G. Keith, a. H. Dalpke, and M. Helm, "Identification of modifications in microbial, native tRNA that suppress immunostimulatory activity," *J. Exp. Med.*, vol. 209, no. 2, pp. 225–233, 2012.
- [91] S. Jöckel, G. Nees, R. Sommer, Y. Zhao, D. Cherkasov, H. Hori, G. Ehm, M. Schnare, M. Nain, A. Kaufmann, and S. Bauer, "The 2'-O-methylation status of a single guanosine controls transfer RNA-mediated Toll-like receptor 7 activation or inhibition.," *J. Exp. Med.*, vol. 209, no. 2, pp. 235–41, 2012.
- [92] M. Manoharan, A. Akinc, R. K. Pandey, J. Qin, P. Hadwiger, M. John, K. Mills, K. Charisse, M. A. Maier, L. Nechev, E. M. Greene, P. S. Pallan, E. Rozners, K. G. Rajeev, and M. Egli, "Unique gene-silencing and structural properties of 2'-fluoro-modified siRNAs," *Angew. Chemie - Int. Ed.*, vol. 50, no. 10, pp. 2284–2288, 2011.
- [93] Y. Lee, J. H. Urban, L. Xu, B. A. Sullenger, and J. Lee, "2'Fluoro Modification Differentially Modulates the Ability of RNAs to Activate Pattern Recognition Receptors," *Nucleic Acid Ther.*, vol. 0, no. 0, p. nat.2015.0575, 2016.
- [94] K. Bondensgaard, M. Petersen, S. K. Singh, V. K. Rajwanshi, R. Kumar, J. Wengel, and J. P. Jacobsen, "Structural Studies of LNA:RNA Duplexes by NMR: Conformations and Implications for RNase H Activity," *Chem. - A Eur. J.*, vol. 6, no. Scheme 1, pp. 2687–2695, 2000.
- [95] A. R. Kore, M. Shanmugasundaram, I. Charles, A. V. Vlassov, and T. J. Barta, "Locked nucleic acid (LNA)-Modified dinucleotide mRNA cap analogue: Synthesis, enzymatic incorporation, and utilization," *J. Am. Chem. Soc.*, vol. 131, no. 18, pp. 6364–6365, 2009.
- [96] K. Tomaya, M. Takahashi, N. Minakawa, and A. Matsuda, "Convenient RNA synthesis using a phosphoramidite possessing a biotinylated photocleavable group," *Org. Lett.*, vol. 12, no. 17, pp. 3836–3839, 2010.
- [97] S. Verma and F. Eckstein, "MODIFIED OLIGONUCLEOTIDES: Synthesis and Strategy for Users," *Annu. Rev. Biochem.*, vol. 67, no. 1, pp. 99–134, Jun. 1998.
- [98] A. Wilk, A. Grajkowski, L. R. Phillips, and S. L. Beaucage, "Deoxyribonucleoside cyclic N-acylphosphoramidites as a new class of monomers for the stereocontrolled synthesis of oligothymidyl- and oligodeoxycytidyl- phosphorothioates," *J. Am. Chem. Soc.*, vol. 122,

- no. 10, pp. 2149–2156, 2000.
- [99] A. N. Kuhn, M. Diken, S. Kreiter, A. Selmi, J. Kowalska, J. Jemielity, E. Darzynkiewicz, C. Huber, O. Türeci, and U. Sahin, “Phosphorothioate cap analogs increase stability and translational efficiency of RNA vaccines in immature dendritic cells and induce superior immune responses in vivo.,” *Gene Ther.*, vol. 17, no. 8, pp. 961–71, 2010.
- [100] J. Hayashi, T. Hamada, I. Sasaki, O. Nakagawa, S. I. Wada, and H. Urata, “Synthesis of novel cationic spermine-conjugated phosphotriester oligonucleotide for improvement of cell membrane permeability,” *Bioorganic Med. Chem. Lett.*, vol. 25, no. 17, pp. 3610–3615, 2015.
- [101] A. P. Sanzone, A. H. El-Sagheer, T. Brown, and A. Tavassoli, “Assessing the biocompatibility of click-linked DNA in *Escherichia coli*,” *Nucleic Acids Res.*, vol. 40, no. 20, pp. 10567–10575, 2012.
- [102] C. N. Birts, A. P. Sanzone, A. H. El-Sagheer, J. P. Blaydes, T. Brown, and A. Tavassoli, “Transcription of Click-Linked DNA in Human Cells,” *Angew. Chemie Int. Ed.*, vol. 53, no. 9, pp. 2362–2365, Feb. 2014.
- [103] Y.-L. Chiu and T. M. Rana, “RNAi in human cells: basic structural and functional features of small interfering RNA.,” *Mol. Cell*, vol. 10, no. 3, pp. 549–561, 2002.
- [104] T. P. Prakash, C. R. Allerson, P. Dande, T. A. Vickers, N. Sioufi, R. Jarres, B. F. Baker, E. E. Swayze, R. H. Griffey, and B. Bhat, “Positional effect of chemical modifications on short interference RNA activity in mammalian cells,” *J. Med. Chem.*, vol. 48, no. 13, pp. 4247–4253, 2005.
- [105] S. A. Ingale, P. Leonard, Q. N. Tran, and F. Seela, “Duplex DNA and DNA–RNA Hybrids with Parallel Strand Orientation: 2'-Deoxy-2'-fluoroisocytidine, 2'-Deoxy-2'-fluoroisoguanosine, and Canonical Nucleosides with 2'-Fluoro Substituents Cause Unexpected Changes on the Double Helix Stability,” *J. Org. Chem.*, vol. 80, no. 6, pp. 3124–3138, Mar. 2015.
- [106] E. Brencicova and S. S. Diebold, “Nucleic acids and endosomal pattern recognition: how to tell friend from foe?,” *Front. Cell. Infect. Microbiol.*, vol. 3, no. July, pp. 1–14, 2013.
- [107] A. H. Dalpke and M. Helm, “RNA mediated Toll-like receptor stimulation in health and disease,” *RNA Biol.*, vol. 9, no. 6, pp. 828–842, Jun. 2012.
- [108] W. Barchet, V. Wimmenauer, M. Schlee, and G. Hartmann, “Assessing the therapeutic potential of immunostimulatory nucleic acids,” *Curr. Opin. Immunol.*, vol. 20, no. 4, pp. 389–395, 2008.
- [109] T. Junt and W. Barchet, “Translating nucleic acid-sensing pathways into therapies,” *Nat Rev Immunol*, vol. 15, no. 9, pp. 529–544, 2015.
- [110] S. Akira, S. Uematsu, and O. Takeuchi, “Pathogen Recognition and Innate Immunity,” *Cell*, vol. 124, no. 4, pp. 783–801, 2006.
- [111] M. P. Belvin and K. V Anderson, “A conserved signaling pathway: the *Drosophila* toll-dorsal pathway.,” *Annu. Rev. Cell Dev. Biol.*, vol. 12, pp. 393–416, 1996.
- [112] J. C. Roach, G. Glusman, L. Rowen, A. Kaur, M. K. Purcell, K. D. Smith, L. E. Hood, and A. Aderem, “The evolution of vertebrate Toll-like receptors.,” *Proc. Natl. Acad. Sci. U. S. A.*,

- vol. 102, no. 27, pp. 9577–9582, 2005.
- [113] T. Kawai and S. Akira, “The role of pattern-recognition receptors in innate immunity: update on Toll-like receptors,” *Nat. Immunol.*, vol. 11, no. 5, pp. 373–384, May 2010.
- [114] O. Takeuchi, S. Sato, T. Horiuchi, K. Hoshino, K. Takeda, Z. Dong, R. L. Modlin, and S. Akira, “Cutting edge: role of Toll-like receptor 1 in mediating immune response to microbial lipoproteins.,” *J. Immunol.*, vol. 169, no. 1, pp. 10–14, 2002.
- [115] M. O’Neill, J. McPartlin, K. Arthure, S. Riedel, and N. McMillan, “Comparison of the TLDA with the Nanodrop and the reference Qubit system,” *J. Phys. Conf. Ser.*, vol. 307, p. 12047, Aug. 2011.
- [116] J. W. Huleatt, V. Nakaar, P. Desai, Y. Huang, D. Hewitt, A. Jacobs, J. Tang, W. McDonald, L. Song, R. K. Evans, S. Umlauf, L. Tussey, and T. J. Powell, “Potent immunogenicity and efficacy of a universal influenza vaccine candidate comprising a recombinant fusion protein linking influenza M2e to the TLR5 ligand flagellin,” *Vaccine*, vol. 26, no. 2, pp. 201–214, 2008.
- [117] R. T. Gazzinelli, R. Mendonca-Neto, J. Lilue, J. Howard, and A. Sher, “Innate resistance against *Toxoplasma gondii*: An evolutionary tale of mice, cats, and men,” *Cell Host Microbe*, vol. 15, no. 2, pp. 132–138, 2014.
- [118] L. A. J. O’Neill, D. Golenbock, and A. G. Bowie, “The history of Toll-like receptors - redefining innate immunity.,” *Nat. Rev. Immunol.*, vol. 13, no. 6, pp. 453–60, 2013.
- [119] M. E. Peter, A. V. Kubarenko, A. N. R. Weber, and A. H. Dalpke, “Identification of an N-terminal recognition site in TLR9 that contributes to CpG-DNA-mediated receptor activation.,” *J. Immunol.*, vol. 182, no. 12, pp. 7690–7697, 2009.
- [120] O. De Bouteiller, E. Merck, U. A. Hasan, S. Hubac, B. Benguigui, G. Trinchieri, E. E. M. Bates, and C. Caux, “Recognition of double-stranded RNA by human toll-like receptor 3 and downstream receptor signaling requires multimerization and an acidic pH,” *J. Biol. Chem.*, vol. 280, no. 46, pp. 38133–38145, 2005.
- [121] L. Alexopoulou, A. Czopik Holt, R. Medzhitov, and R. A. Flavell, “Recognition of double-stranded RNA and activation of NF-kappa B by Toll-like receptor 3,” *Nature*, vol. 413, no. 6857, pp. 732–738, 2001.
- [122] L. Liu, I. Botos, Y. Wang, J. N. Leonard, J. Shiloach, D. M. Segal, and D. R. Davies, “Structural Basis of Toll-Like Receptor 3 Signaling with Double-Stranded RNA,” *Science (80-.)*, vol. 320, no. 5874, pp. 379–381, Apr. 2008.
- [123] J. Choe, M. S. Kelker, and I. a. Wilson, “Crystal structure of human toll-like receptor 3,” *Science*, vol. 22, no. 309(5734), pp. 581–5, 2005.
- [124] N. Pirher, K. Ivicak, J. Pohar, M. Bencina, and R. Jerala, “A second binding site for double-stranded RNA in TLR3 and consequences for interferon activation.,” *Nat. Struct. Mol. Biol.*, vol. 15, no. 7, pp. 761–763, 2008.
- [125] X.-D. Li, Z. J. Chen, N. Balenga, N. Ban, P. Nissen, J. Hansen, P. Moore, T. Steitz, M. Brinkmann, E. Spooner, K. Hoebe, B. Beutler, H. Ploegh, Y. Kim, T. Cech, X. Li, Y. Chiu, A. Ismail, C. Behrendt, M. Wight-Carter, L. Hooper, K. McCusker, D. Fujimori, P. Nissen, J.

- Hansen, N. Ban, P. Moore, T. Steitz, M. Oldenburg, A. Krüger, R. Ferstl, A. Kaufmann, G. Nees, A. Sigmund, R. Pifer, A. Benson, C. Sturge, F. Yarovinsky, J. Roach, G. Glusman, L. Rowen, A. Kaur, M. Purcell, K. Smith, S. Schattgen, K. Fitzgerald, K. Tabet, K. Hoebe, E. Janssen, X. Du, P. Georgel, K. Crozat, O. Takeuchi, S. Akira, F. Yarovinsky, D. Zhang, J. Andersen, G. Bannenberg, C. Serhan, M. Hayden, M. Yoneyama, and T. Fujita, "Sequence specific detection of bacterial 23S ribosomal RNA by TLR13," *Elife*, vol. 1, p. 456, 2012.
- [126] M. Oldenburg, A. Krüger, R. Ferstl, A. Kaufmann, G. Nees, A. Sigmund, B. Bathke, H. Lauterbach, M. Suter, S. Dreher, U. Koedel, S. Akira, T. Kawai, J. Buer, H. Wagner, S. Bauer, H. Hochrein, and C. J. Kirschning, "TLR13 recognizes bacterial 23S rRNA devoid of erythromycin resistance-forming modification.," *Science (80-.)*, vol. 337, no. 6098, pp. 1111–1115, 2012.
- [127] A. Hidmark, A. von Saint Paul, and A. H. Dalpke, "Cutting edge: TLR13 is a receptor for bacterial RNA.," *J. Immunol.*, vol. 189, pp. 2717–21, 2012.
- [128] W. Song, J. Wang, Z. Han, Y. Zhang, H. Zhang, W. Wang, J. Chang, B. Xia, S. Fan, D. Zhang, J. Wang, H.-W. Wang, and J. Chai, "Structural basis for specific recognition of single-stranded RNA by Toll-like receptor 13.," *Nat. Struct. Mol. Biol.*, vol. 22, no. 10, pp. 782–787, 2015.
- [129] H. Hemmi, T. Kaisho, O. Takeuchi, S. Sato, H. Sanjo, K. Hoshino, T. Horiuchi, H. Tomizawa, K. Takeda, and S. Akira, "Small anti-viral compounds activate immune cells via the TLR7 MyD88-dependent signaling pathway.," *Nat. Immunol.*, vol. 3, no. 2, pp. 196–200, Feb. 2002.
- [130] M. Jurk, F. Heil, J. Vollmer, C. Schetter, A. M. Krieg, H. Wagner, G. Lipford, and S. Bauer, "Human TLR7 or TLR8 independently confer responsiveness to the antiviral compound R-848.," *Nat. Immunol.*, vol. 3, no. 6, p. 499, 2002.
- [131] F. Heil, H. Hemmi, H. Hochrein, F. Ampenberger, C. Kirschning, S. Akira, G. Lipford, H. Wagner, and S. Bauer, "Species-Specific Recognition of Single-Stranded RNA via Toll-like Receptor 7 and 8," *Science*, vol. 303, no. 5663, pp. 1526–1529, 2004.
- [132] S. S. Diebold, T. Kaisho, H. Hemmi, S. Akira, and C. R. e Sousa, "Innate Antiviral Responses by Means of TLR7-Mediated Recognition of Single-Stranded RNA TL - 303," *Science (80-.)*, vol. 303, no. 5663, pp. 1529–1531, 2004.
- [133] J. M. Lund, L. Alexopoulou, a Sato, M. Karow, N. C. Adams, N. W. Gale, a Iwasaki, and R. a Flavell, "Recognition of single-stranded RNA viruses by Toll-like receptor 7," *Proc Natl Acad Sci U S A*, vol. 101, no. 15, pp. 5598–5603, 2004.
- [134] K. B. Gorden, K. S. Gorski, S. J. Gibson, R. M. Kedl, W. C. Kieper, X. Qiu, M. a Tomai, S. S. Alkan, and J. P. Vasilakos, "Synthetic TLR agonists reveal functional differences between human TLR7 and TLR8.," *J. Immunol.*, vol. 174, no. 3, pp. 1259–1268, 2005.
- [135] O. Takeuchi and S. Akira, "Pattern Recognition Receptors and Inflammation," *Cell*, vol. 140, no. 6, pp. 805–820, 2010.
- [136] V. Hornung, J. Ellegast, S. Kim, K. Brzozka, A. Jung, H. Kato, H. Poeck, S. Akira, K.-K. Conzelmann, M. Schlee, S. Endres, and G. Hartmann, "5'-Triphosphate RNA Is the Ligand for RIG-I," *Science (80-.)*, vol. 314, no. 5801, pp. 994–997, Nov. 2006.

- [137] C. Schuberth-Wagner, J. Ludwig, A. K. Bruder, A. M. Herzner, T. Zillinger, M. Goldeck, T. Schmidt, J. L. Schmid-Burgk, R. Kerber, S. Wolter, J. P. Stümpel, A. Roth, E. Bartok, C. Drosten, C. Coch, V. Hornung, W. Barchet, B. M. Kümmerer, G. Hartmann, and M. Schlee, "A Conserved Histidine in the RNA Sensor RIG-I Controls Immune Tolerance to N1-2'O-Methylated Self RNA," *Immunity*, vol. 43, no. 1, pp. 41–52, 2015.
- [138] M. Yoneyama, M. Kikuchi, T. Natsukawa, N. Shinobu, T. Imaizumi, M. Miyagishi, K. Taira, S. Akira, and T. Fujita, "The RNA helicase RIG-I has an essential function in double-stranded RNA-induced innate antiviral responses.," *Nat. Immunol.*, vol. 5, no. 7, pp. 730–737, 2004.
- [139] H. Kato, O. Takeuchi, S. Sato, M. Yoneyama, M. Yamamoto, K. Matsui, S. Uematsu, A. Jung, T. Kawai, K. J. Ishii, O. Yamaguchi, K. Otsu, T. Tsujimura, C.-S. Koh, C. Reis e Sousa, Y. Matsuura, T. Fujita, and S. Akira, "Differential roles of MDA5 and RIG-I helicases in the recognition of RNA viruses.," *Nature*, vol. 441, no. 7089, pp. 101–105, 2006.
- [140] T. Fernandes-Alnemri, J.-W. Yu, P. Datta, J. Wu, and E. S. Alnemri, "AIM2 activates the inflammasome and cell death in response to cytoplasmic DNA.," *Nature*, vol. 458, no. 7237, pp. 509–513, 2009.
- [141] V. Hornung, A. Ablasser, M. Charrel-Dennis, F. Bauernfeind, G. Horvath, D. R. Caffrey, E. Latz, and K. A. Fitzgerald, "AIM2 recognizes cytosolic dsDNA and forms a caspase-1-activating inflammasome with ASC," *Nature*, vol. 458, no. 7237, pp. 514–518, 2009.
- [142] T. L. Roberts, A. Idris, J. A. Dunn, G. M. Kelly, C. M. Burnton, S. Hodgson, L. L. Hardy, V. Garceau, M. J. Sweet, I. L. Ross, D. A. Hume, and K. J. Stacey, "HIN-200 Proteins Regulate Caspase Activation in Response to Foreign Cytoplasmic DNA," *Science (80-.)*, vol. 323, no. February, pp. 1057–1060, 2009.
- [143] T. Burckstummer, C. Baumann, S. Bluml, E. Dixit, G. Durnberger, H. Jahn, M. Planavsky, M. Bilban, J. Colinge, K. L. Bennett, and G. Superti-Furga, "An orthogonal proteomic-genomic screen identifies AIM2 as a cytoplasmic DNA sensor for the inflammasome.," *Nat. Immunol.*, vol. 10, no. 3, pp. 266–272, 2009.
- [144] L. Sun, J. Wu, F. Du, X. Chen, and Z. J. Chen, "Cyclic GMP-AMP Synthase Is a Cytosolic DNA Sensor That Activates the Type I Interferon Pathway," *Science (80-.)*, vol. 339, no. February, pp. 786–791, 2013.
- [145] A. Ablasser, M. Goldeck, T. Cavlar, T. Deimling, G. Witte, I. Rohl, K.-P. Hopfner, J. Ludwig, and V. Hornung, "cGAS produces a 2'-5'-linked cyclic dinucleotide second messenger that activates STING.," *Nature*, vol. 498, no. 7454, pp. 380–384, 2013.
- [146] N. Vabret and J. M. Blander, "Sensing microbial RNA in the cytosol," *Front. Immunol.*, vol. 4, no. DEC, pp. 1–9, 2013.
- [147] V. Hornung, S. Rothenfusser, S. Britsch, A. Krug, B. Jahrsdörfer, T. Giese, S. Endres, G. Hartmann, B. Jahrsdorfer, T. Giese, S. Endres, and G. Hartmann, "Quantitative expression of toll-like receptor 1-10 mRNA in cellular subsets of human peripheral blood mononuclear cells and sensitivity to CpG oligodeoxynucleotides.," *J. Immunol.*, vol. 168, no. 9, pp. 4531–4537, May 2002.
- [148] T. Eigenbrod and A. H. Dalpke, "Bacterial RNA: An Underestimated Stimulus for Innate

- Immune Responses," *J. Immunol.*, vol. 195, no. 2, pp. 411–418, 2015.
- [149] R. J. Gibbard, P. J. Morley, and N. J. Gay, "Conserved features in the extracellular domain of human toll-like receptor 8 are essential for pH-dependent signaling," *J. Biol. Chem.*, vol. 281, no. 37, pp. 27503–27511, 2006.
- [150] T. Wei, J. Gong, F. Jamitzky, W. M. Heckl, R. W. Stark, and S. C. Rössle, "Homology modeling of human Toll-like receptors TLR7, 8, and 9 ligand-binding domains," *Protein Sci.*, vol. 18, no. 8, pp. 1684–1691, 2009.
- [151] E. Colak, A. Leslie, K. Zausmer, E. Khatamzas, A. V. Kubarenko, T. Pichulik, S. N. Klimosch, A. Mayer, O. Siggs, A. Hector, R. Fischer, B. Klessner, A. Rautanen, M. Frank, A. V. S. Hill, B. Manoury, B. Beutler, D. Hartl, A. Simmons, and A. N. R. Weber, "RNA and imidazoquinolines are sensed by distinct TLR7/8 ectodomain sites resulting in functionally disparate signaling events.," *J. Immunol.*, vol. 192, no. 12, pp. 5963–73, Jun. 2014.
- [152] H. Tanji, U. Ohto, T. Shibata, K. Miyake, and T. Shimizu, "Structural Reorganization of the Toll-Like Receptor 8 Dimer Induced by Agonistic Ligands," *Science (80-.)*, vol. 339, no. 6126, pp. 1426–1429, Mar. 2013.
- [153] Z. Zhang, U. Ohto, T. Shibata, E. Krayukhina, M. Taoka, Y. Yamauchi, H. Tanji, T. Isobe, S. Uchiyama, K. Miyake, and T. Shimizu, "Structural Analysis Reveals that Toll-like Receptor 7 Is a Dual Receptor for Guanosine and Single-Stranded RNA," *Immunity*, vol. 45, no. 4, pp. 737–748, Oct. 2016.
- [154] H. Tanji, U. Ohto, T. Shibata, M. Taoka, Y. Yamauchi, T. Isobe, K. Miyake, and T. Shimizu, "Toll-like receptor 8 senses degradation products of single-stranded RNA," *Nat. Struct. Mol. Biol.*, vol. 22, no. 2, pp. 109–115, 2015.
- [155] K. Maeda and S. Akira, "TLR7 Structure: Cut in Z-Loop," *Immunity*, vol. 45, no. 4, pp. 705–707, Oct. 2016.
- [156] T. Shibata, U. Ohto, S. Nomura, K. Kibata, Y. Motoi, Y. Zhang, Y. Murakami, R. Fukui, T. Ishimoto, S. Sano, T. Ito, T. Shimizu, and K. Miyake, "Guanosine and its modified derivatives are endogenous ligands for TLR7," *Int. Immunol.*, vol. 28, no. 5, pp. 211–222, May 2015.
- [157] M. A. Stanley, "Imiquimod and the imidazoquinolones: mechanism of action and therapeutic potential," *Clin. Exp. Dermatol.*, vol. 27, no. 7, pp. 571–577, Oct. 2002.
- [158] F. Ma, J. Zhang, J. Zhang, and C. Zhang, "The TLR7 agonists imiquimod and gardiquimod improve DC-based immunotherapy for melanoma in mice.," *Cell. Mol. Immunol.*, vol. 7, no. 5, pp. 381–388, 2010.
- [159] J. Lee, T.-H. Chuang, V. Redecke, L. She, P. M. Pitha, D. A. Carson, E. Raz, and H. B. Cottam, "Molecular basis for the immunostimulatory activity of guanine nucleoside analogs: activation of Toll-like receptor 7.," *Proc. Natl. Acad. Sci. U. S. A.*, vol. 100, no. 11, pp. 6646–51, 2003.
- [160] F. Heil, P. Ahmad-Nejad, H. Hemmi, H. Hochrein, F. Ampenberger, T. Gellert, H. Dietrich, G. Lipford, K. Takeda, S. Akira, H. Wagner, and S. Bauer, "The Toll-like receptor 7 (TLR7)-specific stimulus loxoribine uncovers a strong relationship within the TLR7, 8 and 9 subfamily," *Eur. J. Immunol.*, vol. 33, no. 11, pp. 2987–2997, 2003.

- [161] N. M. Shukla, M. R. Kimbrell, S. S. Malladi, and S. A. David, "Regioisomerism-dependent TLR7 agonism and antagonism in an imidazoquinoline," *Bioorg. Med. Chem. Lett.*, vol. 19, no. 8, pp. 2211–2214, Apr. 2009.
- [162] J. P. Vasilakos and M. a Tomai, "The use of Toll-like receptor 7/8 agonists as vaccine adjuvants," *Expert Rev. Vaccines*, vol. 12, no. 7, pp. 809–819, 2013.
- [163] K. Karikó, H. Ni, J. Capodici, M. Lamphier, and D. Weissman, "mRNA Is an Endogenous Ligand for Toll-like Receptor 3," *J. Biol. Chem.*, vol. 279, no. 13, pp. 12542–12550, 2004.
- [164] M. Zamanian-Daryoush, J. T. Marques, M. P. Gantier, M. A. Behlke, M. John, P. Rayman, J. Finke, and B. R. G. Williams, "Determinants of Cytokine Induction by Small Interfering RNA in Human Peripheral Blood Mononuclear Cells," *J. Interf. CYTOKINE Res.*, vol. 28, pp. 221–233, 2008.
- [165] M. Sioud, "Single-stranded small interfering RNA are more immunostimulatory than their double-stranded counterparts: A central role for 2'-hydroxyl uridines in immune responses," *Eur. J. Immunol.*, vol. 36, no. 5, pp. 1222–1230, 2006.
- [166] M. P. Gantier, S. Tong, M. A. Behlke, A. T. Irving, M. Lappas, U. W. Nilsson, E. Latz, N. A. J. McMillan, and B. R. G. Williams, "Rational design of immunostimulatory siRNAs," *Mol. Ther.*, vol. 18, no. 4, pp. 785–95, 2010.
- [167] A. L. Jackson and P. S. Linsley, "Recognizing and avoiding siRNA off-target effects for target identification and therapeutic application," *Nat. Rev. Drug Discov.*, vol. 9, no. 1, pp. 57–67, 2010.
- [168] K. Karikó, M. Buckstein, H. Ni, and D. Weissman, "Suppression of RNA recognition by Toll-like receptors: The impact of nucleoside modification and the evolutionary origin of RNA," *Immunity*, vol. 23, no. 2, pp. 165–175, 2005.
- [169] S. Kaiser, K. Rimbach, T. Eigenbrod, A. H. Dalpke, and M. Helm, "A modified dinucleotide motif specifies tRNA recognition by TLR7," *RNA*, vol. 20, pp. 1351–1355, 2014.
- [170] K. Rimbach, S. Kaiser, M. Helm, A. H. Dalpke, and T. Eigenbrod, "2'-O-Methylation within Bacterial RNA Acts as Suppressor of TLR7/TLR8 Activation in Human Innate Immune Cells," *J. Innate Immun.*, vol. 7, pp. 482–493, 2015.
- [171] M. Robbins, A. Judge, L. Liang, K. McClintock, E. Yaworski, and I. MacLachlan, "2'-O-methyl-modified RNAs Act as TLR7 Antagonists," *Mol. Ther.*, vol. 15, no. 9, pp. 1663–1669, Sep. 2007.
- [172] K. Karikó and D. Weissman, "Naturally occurring nucleoside modifications suppress the immunostimulatory activity of RNA: Implication for therapeutic RNA development," *Curr. Opin. Drug Discov. Devel.*, vol. 10, no. 5, pp. 523–532, Sep. 2007.
- [173] K. Karikó, H. Muramatsu, F. a Welsh, J. Ludwig, H. Kato, S. Akira, and D. Weissman, "Incorporation of Pseudouridine Into mRNA Yields Superior Nonimmunogenic Vector With Increased Translational Capacity and Biological Stability," *Mol. Ther.*, vol. 16, no. 11, pp. 1833–1840, 2008.
- [174] U. Sahin, K. Kariko, and O. Tureci, "mRNA-based therapeutics - developing a new class of drugs," *Nat. Rev. Drug Discov.*, vol. 13, no. 10, pp. 759–780, 2014.

- [175] K. Sridharan and N. J. Gogtay, "Therapeutic Nucleic Acids: Current clinical status.," *Br. J. Clin. Pharmacol.*, vol. 82, no. 3, pp. 1–14, Sep. 2016.
- [176] A. D. Judge, V. Sood, J. R. Shaw, D. Fang, K. McClintock, and I. MacLachlan, "Sequence-dependent stimulation of the mammalian innate immune response by synthetic siRNA," *Nat Biotechnol.*, vol. 23, no. 4, pp. 457–462, 2005.
- [177] C. J. Desmet and K. J. Ishii, "Nucleic acid sensing at the interface between innate and adaptive immunity in vaccination," *Nat. Rev. Immunol.*, vol. 12, no. 7, pp. 479–491, 2012.
- [178] F. Bagnoli, M. R. Fontana, E. Soldaini, R. P. N. Mishra, L. Fiaschi, E. Cartocci, V. Nardi-Dei, P. Ruggiero, S. Nosari, M. G. De Falco, G. Lofano, S. Marchi, B. Galletti, P. Mariotti, M. Bacconi, A. Torre, S. Maccari, M. Scarselli, C. D. Rinaudo, N. Inoshima, S. Savino, E. Mori, S. Rossi-Paccani, B. Baudner, M. Pallaoro, E. Swennen, R. Petracca, C. Brettoni, S. Liberatori, N. Norais, E. Monaci, J. B. Wardenburg, O. Schneewind, D. T. O'Hagan, N. M. Valiante, G. Bensi, S. Bertholet, E. De Gregorio, R. Rappuoli, and G. Grandi, "Vaccine composition formulated with a novel TLR7-dependent adjuvant induces high and broad protection against *Staphylococcus aureus*," *Proc. Natl. Acad. Sci.*, vol. 112, no. 12, pp. 3680–3685, 2015.
- [179] N. Pardi, M. J. Hogan, R. S. Pelc, H. Muramatsu, H. Andersen, C. R. DeMaso, K. A. Dowd, L. L. Sutherland, R. M. Scarce, R. Parks, W. Wagner, A. Granados, J. Greenhouse, M. Walker, E. Willis, J.-S. Yu, C. E. McGee, G. D. Sempowski, B. L. Mui, Y. K. Tam, Y.-J. Huang, D. Vanlandingham, V. M. Holmes, H. Balachandran, S. Sahu, M. Lifton, S. Higgs, S. E. Hensley, T. D. Madden, M. J. Hope, K. Karikó, S. Santra, B. S. Graham, M. G. Lewis, T. C. Pierson, B. F. Haynes, and D. Weissman, "Zika virus protection by a single low-dose nucleoside-modified mRNA vaccination," *Nature*, Feb. 2017.
- [180] L. Gold, B. Polisky, and M. Yarus, "Diversity of oligonucleotide functions," *Annu. Rev. Biochem.*, vol. 64, pp. 763–797, 1995.
- [181] J.-S. Choi and A. J. Berdis, "Visualizing nucleic acid metabolism using non-natural nucleosides and nucleotide analogs," *Biochim. Biophys. Acta - Proteins Proteomics*, vol. 1864, no. 1, pp. 165–176, Jan. 2016.
- [182] I. K. Astakhova and J. Wengel, "Interfacing Click Chemistry with Automated Oligonucleotide Synthesis for the Preparation of Fluorescent DNA Probes Containing Internal Xanthene and Cyanine Dyes," *Chem. - A Eur. J.*, vol. 19, no. 3, pp. 1112–1122, Jan. 2013.
- [183] L. Aagaard and J. J. Rossi, "RNAi therapeutics: Principles, prospects and challenges," *Adv. Drug Deliv. Rev.*, vol. 59, no. 2–3, pp. 75–86, 2007.
- [184] C. M. Wei, A. Gershowitz, and B. Moss, "Methylated nucleotides block 5' terminus of HeLa cell messenger RNA," *Cell*, vol. 4, no. 4, pp. 379–386, 1975.
- [185] M. Ehrlich, G. G. Wilson, K. C. Kuo, and C. W. Gehrke, "N4-methylcytosine as a minor base in bacterial DNA," *Journal of Bacteriology*, vol. 169, no. 3, pp. 939–943, 1987.
- [186] V. Valinluck, P. Liu, A. Burdzy, J. Ryu, and L. C. Sowers, "Influence of local duplex stability and N6-methyladenine on uracil recognition by mismatch-specific uracil-DNA glycosylase (Mug)," *Chem. Res. Toxicol.*, vol. 15, no. 12, pp. 1595–1601, 2002.

- [187] A. R. Cervi, A. Guy, G. A. Leonard, R. Téoule, and W. N. Hunter, "The crystal structure of N4-methylcytosine-guanosine basepairs in the synthetic hexanucleotide d(CGCGm4CG)," *Nucleic Acids Res.*, vol. 21, no. 24, pp. 5623–5629, 1993.
- [188] M. Helm, R. Giegé, and C. Florentz, "A Watson-Crick base-pair-disrupting methyl group (m1A9) is sufficient for cloverleaf folding of human mitochondrial tRNA(Lys)," *Biochemistry*, vol. 38, no. 40, pp. 13338–13346, 1999.
- [189] J. P. Rife, C. S. Cheng, P. B. Moore, and S. A. Strobel, "N2-methylguanosine is iso-energetic with guanosine in RNA duplexes and GNRA tetraloops," *Nucleic Acids Res.*, vol. 26, no. 16, pp. 3640–3644, 1998.
- [190] C. Höbartner, H. Mittendorfer, K. Breuker, and R. Micura, "Triggering of RNA secondary structures by a functionalized nucleobase," *Angew. Chemie - Int. Ed.*, vol. 43, no. 30, pp. 3922–3925, 2004.
- [191] P. S. Pallan, C. Kreutz, S. Bosio, R. Micura, and M. Egli, "Effects of N2,N2 - dimethylguanosine on RNA structure and stability: Crystal structure of an RNA duplex with tandem m2 2G:A pairs," *RNA*, vol. 14, no. 10, pp. 2125–2135, Aug. 2008.
- [192] M. Münzel, L. Lercher, M. Müller, and T. Carell, "Chemical discrimination between dC and 5MedC via their hydroxylamine adducts," *Nucleic Acids Res.*, vol. 38, no. 21, pp. e192–e192, Nov. 2010.
- [193] O. Domingo, I. Hellmuth, A. Jäschke, C. Kreutz, and M. Helm, "Intermolecular 'cross-torque': The N⁴-cytosine propargyl residue is rotated to the 'CH'-edge as a result of Watson-Crick interaction," *Nucleic Acids Res.*, vol. 43, no. 11, pp. 5275–5283, 2015.
- [194] A. S. Hansen, A. Thalhammer, A. H. El-Sagheer, T. Brown, and C. J. Schofield, "Improved synthesis of 5-hydroxymethyl-2'-deoxycytidine phosphoramidite using a 2'-deoxyuridine to 2'-deoxycytidine conversion without temporary protecting groups," *Bioorg. Med. Chem. Lett.*, vol. 21, no. 4, pp. 1181–1184, Feb. 2011.
- [195] B. L. Gaffney, L. A. Marky, and R. A. Jones, "The influence of the purine 2-amino group on DNA conformation and stability.," *Tetrahedron*, vol. 40, no. 1, pp. 3–13, 1984.
- [196] G. B. Fox, J.J., Van Praag, D., Wempen, I., Doerr, I.L., Cheong, L., Knoll, J.E., Eidinoff, M.L., Bendich, A. and Brown, "Thiation of Nucleosides. II. Synthesis of 5-Methyl-2'-deoxycytidine and Related Pyrimidine Nucleosides," *J. Am. Chem. Soc.*, vol. 81, pp. 178–187, 1959.
- [197] F. Schäfer, K. B. Joshi, M. A. H. Fichte, T. Mack, J. Wachtveitl, and A. Heckel, "Wavelength-Selective Uncaging of dA and dC Residues," *Org. Lett.*, vol. 13, no. 6, pp. 1450–1453, Mar. 2011.
- [198] Engel and von Hippel, "Effect of methylation on nucleic acid conformations: Studies at the monomer level," *Biochemistry*, vol. 13, no. 20, p. 4143, 1974.
- [199] R. R. Shoup, H. T. Miles, and E. D. Becker, "Restricted rotation about the exocyclic carbon-nitrogen bond in cytosine derivatives," *J. Phys. Chem.*, vol. 76, no. 1, pp. 64–70, 1972.
- [200] T. L. Hwang and A. J. Shaka, "Water Suppression That Works. Excitation Sculpting Using Arbitrary Wave-Forms and Pulsed-Field Gradients," *J. Magn. Reson. Ser. A*, vol. 112, no. 2, pp. 275–279, Feb. 1995.

- [201] G. V. Fazakerley, A. Kraszewski, R. Teüoule, and W. Guschlbauer, "NMR and CD studies on an oligonucleotide containing N4-methylcytosine," *Nucleic Acids Res.*, vol. 15, no. 5, pp. 2191–2201, 1987.
- [202] F. Delaglio, S. Grzesiek, G. Vuister, G. Zhu, J. Pfeifer, and A. Bax, "NMRPipe: A multidimensional spectral processing system based on UNIX pipes," *J. Biomol. NMR*, vol. 6, no. 3, pp. 277–293, Nov. 1995.
- [203] R. Spitzer, K. Kloiber, M. Tollinger, and C. Kreutz, "Kinetics of DNA Refolding from Longitudinal Exchange NMR Spectroscopy," *ChemBioChem*, vol. 12, no. 13, pp. 2007–2010, Sep. 2011.
- [204] A. Bart, M. W. J. van Passel, K. van Amsterdam, and A. van der Ende, "Direct detection of methylation in genomic DNA," *Nucleic Acids Res.*, vol. 33, no. 14, pp. 1–6, Aug. 2005.
- [205] S. Klimasauskas, D. Steponaviciene, Z. Maneliene, M. Petrusyte, V. Butkus, and A. Janulaitis, "M.Smal is an N4-methylcytosine specific DNA-methylase," *Nucleic Acids Res.*, vol. 18, no. 22, pp. 6607–6609, 1990.
- [206] B. Guennewig, M. Stoltz, M. Menzi, A. M. Dogar, and J. Hall, "Properties of N(4)-methylated cytidines in miRNA mimics," *Nucleic Acid Ther.*, vol. 22, no. 2, pp. 109–16, 2012.
- [207] R. Micura, W. Pils, C. Höbartner, K. Grubmayr, M. O. Ebert, and B. Jaun, "Methylation of the nucleobases in RNA oligonucleotides mediates duplex-hairpin conversion," *Nucleic Acids Res.*, vol. 29, no. 19, pp. 3997–4005, 2001.
- [208] M. J. Grasby, J.A., Singh, M., Karn, J. and Gait, "Synthesis and applications of oligonucleotides containing N(4)-methylcytidine," *Nucleosides, Nucleotides and Nucleic Acids*, vol. 14, p. 1129, 1995.
- [209] L. Zhang, C. Wu, R. Carta, and H. Zhao, "Free energy of DNA duplex formation on short oligonucleotide microarrays," *Nucleic Acids Res.*, vol. 35, no. 3, pp. 1–5, 2007.
- [210] X. Gao and R. A. Jones, "Nitrogen-15-Labeled Oligodeoxynucleotides. Characterization by ¹⁵N NMR of d[CGTACG] Containing ¹⁵N6- or ¹⁵N1-Labeled Deoxyadenosine," *J. Am. Chem. Soc.*, vol. 109, pp. 3169–3171, 1987.
- [211] S. L. Beaucage and R. P. Iyer, "The synthesis of modified oligonucleotides by the phosphoramidite approach and their applications," *Tetrahedron*, vol. 49, no. 28, pp. 6123–6194, Jul. 1993.
- [212] K. J. Wu, T. A. Shaler, and C. H. Becker, "Time-of-Flight Mass Spectrometry of Underivatized Single-Stranded DNA Oligomers by Matrix-Assisted Laser Desorption," *Anal. Chem.*, vol. 66, pp. 1637–1645, 1994.
- [213] A. M. B. Giessing and F. Kirpekar, "Mass spectrometry in the biology of RNA and its modifications," *Journal of Proteomics*. 2012.
- [214] A. Rich, "Discovery of the Hybrid Helix and the First DNA-RNA Hybridization," *J. Biol. Chem.*, vol. 281, no. 12, pp. 7693–7696, Mar. 2006.
- [215] V. P. Chuprina, A. A. Lipanov, O. Y. Fedoroff, S.-G. Kim, A. Kintanar, and B. R. Reid, "Sequence effects on local DNA topology," *Biochemistry*, vol. 88, pp. 9087–9091, 1991.
- [216] C. Schildkraut and S. Lifson, "Dependence of the Melting Temperature of DNA on Salt

- Concentration," *Biopolymers*, vol. 3, pp. 195–208, 1965.
- [217] C. F. Anderson and T. M. J. Record, "Salt-Nucleic Acid," *Annu. Rev. Phys. Chem.*, vol. 46, pp. 657–700, 1995.
- [218] R. N. Veedu and J. Wengel, "Locked Nucleic Acids : Promising Nucleic Acid Analogs for Therapeutic Applications," *Chem. Biodivers.*, vol. 7, pp. 536–542, 2010.
- [219] L. E. Xodo, G. Manzini, F. Quadrioglio, G. A. van der Marel, and J. H. van Boom, "Effect of 5-methylcytosine on the stability of triple-stranded DNA--a thermodynamic study.," *Nucleic Acids Res.*, vol. 19, no. 20, pp. 5625–31, 1991.
- [220] S. Xuan, Q. Wu, L. Cui, D. Zhang, and F. Shao, "5-Hydroxymethylcytosine and 5-formylcytosine containing deoxyoligonucleotides: Facile syntheses and melting temperature studies," *Bioorg. Med. Chem. Lett.*, vol. 25, no. 6, pp. 1186–1191, Mar. 2015.
- [221] A. Lescoute, N. B. Leontis, C. Massire, and E. Westhof, "Recurrent structural RNA motifs, Isostericity matrices and sequence alignments," *Nucleic Acids Res.*, vol. 33, no. 8, pp. 2395–2409, 2005.
- [222] E. T. Kool, "Hydrogen Bonding, Base Stacking, and Steric Effects in DNA Replication," *Annu. Rev. Biophys. Biomol. Struct.*, vol. 30, no. 1, pp. 1–22, 2001.
- [223] F. Wojciechowski and C. J. Leumann, "Alternative DNA base-pairs: from efforts to expand the genetic code to potential material applications," *Chem. Soc. Rev.*, vol. 40, no. 12, p. 5669, 2011.
- [224] A. Rodrigues-Correia, X. M. M. Weyel, and A. Heckel, "Four Levels of Wavelength-Selective Uncaging for Oligonucleotides," *Org. Lett.*, vol. 15, no. 21, pp. 5500–5503, Nov. 2013.
- [225] E. Lallana, R. Riguera, and E. Fernandez-Megia, "Reliable and efficient procedures for the conjugation of biomolecules through Huisgen azide-alkyne cycloadditions," *Angewandte Chemie - International Edition*, vol. 50, no. 38, pp. 8794–8804, 2011.
- [226] A. B. Neef and N. W. Luedtke, "An Azide-Modified Nucleoside for Metabolic Labeling of DNA," *ChemBioChem*, vol. 15, no. 6, pp. 789–793, Apr. 2014.
- [227] J. M. Holstein, D. Schulz, and A. Rentmeister, "Bioorthogonal site-specific labeling of the 5'-cap structure in eukaryotic mRNAs," *Chem. Commun.*, vol. 50, no. 34, p. 4478, 2014.
- [228] V. Hong, S. I. Presolski, C. Ma, and M. G. Finn, "Analysis and optimization of copper-catalyzed azide-alkyne cycloaddition for bioconjugation.," *Angew. Chem. Int. Ed. Engl.*, vol. 48, no. 52, pp. 9879–83, Jan. 2009.
- [229] S. I. Presolski, V. P. Hong, and M. G. Finn, "Copper-Catalyzed Azide-Alkyne Click Chemistry for Bioconjugation," in *Current Protocols in Chemical Biology*, Hoboken, NJ, USA: John Wiley & Sons, Inc., 2011.
- [230] E. M. S. Stennett, M. A. Ciuba, and M. Levitus, "Photophysical processes in single molecule organic fluorescent probes," *Chem. Soc. Rev.*, vol. 43, no. 4, pp. 1057–1075, 2014.
- [231] I. Hellmuth, I. Freund, J. Schlöder, S. Seidu-Larry, K. Thüring, K. Slama, J. Langhanki, S. Kaloyanova, T. Eigenbrod, M. Krumb, S. Röhm, K. Peneva, T. Opatz, H. Jonuleit, A. H. Dalpke, and M. Helm, "Bioconjugation of Small Molecules to RNA Impedes Its Recognition by Toll-Like Receptor 7," *Front. Immunol.*, vol. 8, no. March, pp. 1–13, Mar. 2017.

- [232] M. Jurk, A. Kritzler, B. Schulte, S. Tluk, C. Schetter, A. M. Krieg, and J. Vollmer, "Modulating responsiveness of human TLR7 and 8 to small molecule ligands with T-rich phosphorothiate oligodeoxynucleotides," *Eur. J. Immunol.*, vol. 36, no. 7, pp. 1815–1826, 2006.
- [233] S. Lata, G. P. S. Raghava, and G. P. S. Raghava, "PRRDB: a comprehensive database of pattern-recognition receptors and their ligands.," *BMC Genomics*, vol. 9, p. 180, 2008.
- [234] C. Russo, I. Cornella-Taracido, L. Galli-Stampino, R. Jain, E. Harrington, Y. Isome, S. Tavarini, C. Sammicheli, S. Nuti, M. L. Mbow, N. M. Valiante, J. Tallarico, E. De Gregorio, and E. Soldaini, "Small molecule Toll-like receptor 7 agonists localize to the MHC class II loading compartment of human plasmacytoid dendritic cells," *Blood*, vol. 117, no. 21, pp. 5683–5691, 2011.
- [235] P. Jones, D. C. Pryde, T. D. Tran, F. M. Adam, G. Bish, F. Calo, G. Ciaramella, R. Dixon, J. Duckworth, D. N. A. Fox, D. A. Hay, J. Hitchin, N. Horscroft, M. Howard, C. Laxton, T. Parkinson, G. Parsons, K. Proctor, M. C. Smith, N. Smith, and A. Thomas, "Discovery of a highly potent series of TLR7 agonists," *Bioorganic Med. Chem. Lett.*, vol. 21, no. 19, pp. 5939–5943, 2011.
- [236] T. Nakamura, H. Wada, H. Kurebayashi, T. Mcinally, R. Bonnert, and Y. Isobe, "Synthesis and evaluation of 8-oxoadenine derivatives as potent Toll-like receptor 7 agonists with high water solubility.," *Bioorg. Med. Chem. Lett.*, vol. 23, no. 3, pp. 669–72, 2013.
- [237] G. Mattson, E. Conklin, S. Desai, G. Nielander, M. D. Savage, and S. Morgensen, "A practical approach to crosslinking," *Mol. Biol. Rep.*, vol. 17, no. 3, pp. 167–183, 1993.
- [238] F. Eberle, M. Sirin, M. Binder, and A. H. Dalpke, "Bacterial RNA is recognized by different sets of immunoreceptors," *Eur. J. Immunol.*, vol. 39, no. 9, pp. 2537–2547, 2009.
- [239] N. M. Shukla, S. S. Malladi, C. A. Mutz, R. Balakrishna, and S. A. David, "Structure-activity relationships in human toll-like receptor 7-active imidazoquinoline analogues," *J. Med. Chem.*, vol. 53, no. 11, pp. 4450–4465, 2010.
- [240] J. D. Hood, H. J. Warshakoon, M. R. Kimbrell, N. M. Shukla, S. S. Malladi, X. Wang, and S. A. David, "Immunoprofiling toll-like receptor ligands: Comparison of immunostimulatory and proinflammatory profiles in ex vivo human blood models.," *Hum. Vaccin.*, vol. 6, no. February, pp. 322–335, 2010.
- [241] P. Larrieu, V. Renaud, Y. Godet, F. Jotereau, and J.-F. Fonteneau, "A HLA-Cw*0701 restricted Melan-A/MART1 epitope presented by melanoma tumor cells to CD8+ tumor infiltrating lymphocytes," *Cancer Immunol. Immunother.*, vol. 57, no. 5, pp. 745–752, May 2008.
- [242] N. Schaft, J. Dörrie, P. Thumann, V. E. Beck, I. Müller, E. S. Schultz, E. Kämpgen, D. Dieckmann, and G. Schuler, "Generation of an optimized polyvalent monocyte-derived dendritic cell vaccine by transfecting defined RNAs after rather than before maturation.," *J. Immunol.*, vol. 174, no. 5, pp. 3087–3097, 2005.
- [243] J. H. Kim, S. R. Lee, L. H. Li, H. J. Park, J. H. Park, K. Y. Lee, M. K. Kim, B. A. Shin, and S. Y. Choi, "High cleavage efficiency of a 2A peptide derived from porcine teschovirus-1 in human cell lines, zebrafish and mice," *PLoS One*, vol. 6, no. 4, pp. 1–8, 2011.

- [244] S. M. Mäkelä, P. Österlund, and I. Julkunen, "TLR ligands induce synergistic interferon- β and interferon- λ 1 gene expression in human monocyte-derived dendritic cells," *Mol. Immunol.*, vol. 48, no. 4, pp. 505–515, 2011.
- [245] D. R. Gallie, "The cap and poly(A) tail function synergistically to regulate mRNA translational efficiency," *Genes Dev.*, vol. 5, no. 11, pp. 2108–2116, 1991.
- [246] S. G. Srivatsan and Y. Tor, "Fluorescent pyrimidine furanylpurine ribonucleotide synth & enzymatic Incorporation," *J. Am. Chem. Soc.*, vol. 129, no. 7, pp. 2044–2053, 2007.
- [247] M. S. D. Kormann, G. Hasenpusch, M. K. Aneja, G. Nica, A. W. Flemmer, S. Herber-jonat, M. Huppmann, L. E. Mays, M. Illenyi, A. Schams, M. Griese, I. Bittmann, R. Handgretinger, D. Hartl, J. Rosenecker, and C. Rudolph, "Expression of therapeutic proteins after delivery of chemically modified mRNA in mice.," *Nat. Biotechnol.*, vol. 29, no. 2, pp. 154–157, 2011.
- [248] C. Y. Jao and A. Salic, "Exploring RNA transcription and turnover in vivo by using click chemistry.," *Proc. Natl. Acad. Sci. U. S. A.*, vol. 105, no. 41, pp. 15779–84, 2008.
- [249] F. Chehrehasa, A. C. B. Meedeniya, P. Dwyer, G. Abrahamsen, and A. Mackay-Sim, "EdU, a new thymidine analogue for labelling proliferating cells in the nervous system," *J. Neurosci. Methods*, vol. 177, no. 1, pp. 122–130, 2009.
- [250] W. Filipowicz, "Functions of the 5'-terminal m7G cap in eukaryotic mRNA," *FEBS Lett.*, vol. 96, no. 1, pp. 1–11, 1978.
- [251] A. Ramanathan, G. B. Robb, and S. Chan, "mRNA capping: biological functions and applications," *Nucleic Acids Res.*, vol. 44, no. 16, pp. 7511–7526, Sep. 2016.
- [252] E. Grudzien, J. Stepinski, M. Jankowska-Anyszka, R. Stolarski, E. Darzynkiewicz, and R. E. Rhoads, "Novel cap analogs for in vitro synthesis of mRNAs with high translational efficiency," *RNA*, vol. 10, no. 9, pp. 1479–1487, Sep. 2004.
- [253] S. Shuman, "Catalytic activity of vaccinia mRNA capping enzyme subunits coexpressed in *Escherichia coli*," *J. Biol. Chem.*, vol. 265, no. 20, pp. 11960–11966, 1990.
- [254] S. R. Langberg and B. Moss, "Post-transcriptional modifications of mRNA," *J. Biol. Chem.*, vol. 256, no. 19, pp. 10054–10060, 1981.
- [255] H. Wen, E. A. Miao, and J. P.-Y. Ting, "Mechanisms of NOD-like Receptor-Associated Inflammasome Activation," *Immunity*, vol. 39, no. 3, pp. 432–441, Sep. 2013.
- [256] N. Inohara, M. Chamailard, C. McDonald, and G. Nuñez, "NOD-LRR PROTEINS: Role in Host-Microbial Interactions and Inflammatory Disease," *Annu. Rev. Biochem.*, vol. 74, no. 1, pp. 355–383, Jun. 2005.
- [257] P. Desjardins and D. Conklin, "NanoDrop Microvolume Quantitation of Nucleic Acids," *J. Vis. Exp.*, no. 1, Nov. 2010.
- [258] L. J. Jones, S. T. Yue, C.-Y. Cheung, and V. L. Singer, "RNA Quantitation by Fluorescence-Based Solution Assay: RiboGreen Reagent Characterization," *Anal. Biochem.*, vol. 265, pp. 368–374, 1998.
- [259] K. Thüring, K. Schmid, P. Keller, and M. Helm, "Analysis of RNA modifications by liquid chromatography–tandem mass spectrometry," *Methods*, vol. 107, pp. 1–9, Sep. 2016.
- [260] J. Zhou, J. Wan, X. Gao, X. Zhang, S. R. Jaffrey, and S.-B. Qian, "Dynamic m(6)A mRNA

- methylation directs translational control of heat shock response.," *Nature*, vol. 526, no. 7574, pp. 591–594, Oct. 2015.
- [261] K. Gavrillov and W. M. Saltzman, "Therapeutic siRNA: Principles, challenges, and strategies," *Yale Journal of Biology and Medicine*, vol. 85, no. 2, pp. 187–200, 2012.
- [262] S. M. Johler, J. Rejman, S. Guan, and J. Rosenecker, "Nebulisation of IVT mRNA Complexes for Intrapulmonary Administration," *PLoS One*, vol. 10, no. 9, p. e0137504, Sep. 2015.
- [263] J. K. Tom, E. Y. Dotsey, H. Y. Wong, L. Stutts, T. Moore, D. H. Davies, P. L. Felgner, and A. P. Esser-Kahn, "Modulation of Innate Immune Responses via Covalently Linked TLR Agonists," *ACS Cent. Sci.*, vol. 1, no. 8, pp. 439–448, Nov. 2015.
- [264] P. H. Goff, T. Hayashi, L. Martínez-Gil, M. Corr, B. Crain, S. Yao, H. B. Cottam, M. Chan, I. Ramos, D. Eggink, M. Heshmati, F. Krammer, K. Messer, M. Pu, A. Fernandez-Sesma, P. Palese, and D. A. Carson, "Synthetic Toll-Like Receptor 4 (TLR4) and TLR7 Ligands as Influenza Virus Vaccine Adjuvants Induce Rapid, Sustained, and Broadly Protective Responses," *J. Virol.*, vol. 89, no. 6, pp. 3221–3235, 2015.
- [265] H. Shinchi, B. Crain, S. Yao, M. Chan, S. S. Zhang, A. Ahmadiiveli, Y. Suda, T. Hayashi, H. B. Cottam, and D. A. Carson, "Enhancement of the Immunostimulatory Activity of a TLR7 Ligand by Conjugation to Polysaccharides," *Bioconjug. Chem.*, vol. 26, no. 8, pp. 1713–1723, Aug. 2015.
- [266] L. Nuhn, N. Vanparijs, A. De Beuckelaer, L. Lybaert, G. Verstraete, K. Deswarte, S. Lienenklaus, N. M. Shukla, A. C. D. Salyer, B. N. Lambrecht, J. Grooten, S. A. David, S. De Koker, and B. G. De Geest, "pH-degradable imidazoquinoline-ligated nanogels for lymph node-focused immune activation," *Proc. Natl. Acad. Sci.*, vol. 113, no. 29, pp. 8098–8103, Jul. 2016.
- [267] G. M. Lynn, R. Laga, P. A. Darrah, A. S. Ishizuka, A. J. Balaci, A. E. Dulcey, M. Pechar, R. Pola, M. Y. Gerner, A. Yamamoto, C. R. Buechler, K. M. Quinn, M. G. Smelkinson, O. Vanek, R. Cawood, T. Hills, O. Vasalatiy, K. Kastenmüller, J. R. Francica, L. Stutts, J. K. Tom, K. A. Ryu, A. P. Esser-Kahn, T. Etrych, K. D. Fisher, L. W. Seymour, and R. A. Seder, "In vivo characterization of the physicochemical properties of polymer-linked TLR agonists that enhance vaccine immunogenicity," *Nat. Biotechnol.*, vol. 33, no. 11, pp. 1201–1210, Oct. 2015.
- [268] N. M. Shukla, C. A. Mutz, S. S. Malladi, H. J. Warshakoon, R. Balakrishna, and S. A. David, "Toll-Like Receptor (TLR)-7 and -8 Modulatory Activities of Dimeric Imidazoquinolines," *J. Med. Chem.*, vol. 55, no. 3, pp. 1106–1116, Feb. 2012.
- [269] A. Holla and A. Skerra, "Comparative analysis reveals selective recognition of glycans by the dendritic cell receptors DC-SIGN and Langerin.," *Protein Eng. Des. Sel.*, vol. 24, no. 9, pp. 659–69, Sep. 2011.
- [270] Y. Guo, H. Feinberg, E. Conroy, D. A. Mitchell, R. Alvarez, O. Blixt, M. E. Taylor, W. I. Weis, and K. Drickamer, "Structural basis for distinct ligand-binding and targeting properties of the receptors DC-SIGN and DC-SIGNR.," *Nat. Struct. Mol. Biol.*, vol. 11, no. 7, pp. 591–8, 2004.

- [271] H. Feinberg, D. a Mitchell, K. Drickamer, and W. I. Weis, "Structural basis for selective recognition of oligosaccharides by DC-SIGN and DC-SIGNR.," *Science*, vol. 294, no. 5549, pp. 2163–6, 2001.
- [272] K. Peneva, G. Mihov, F. Nolde, S. Rocha, J. I. Hotta, K. Braeckmans, J. Hofkens, H. Uji-i, A. Herrmann, and K. Müllen, "Water-soluble monofunctional perylene and terylene dyes: Powerful labels for single-enzyme tracking," *Angew. Chemie - Int. Ed.*, vol. 47, no. 18, pp. 3372–3375, 2008.
- [273] K. Peneva, K. Gundlach, A. Herrmann, H. Paulsen, and K. Müllen, "Site-specific incorporation of perylene into an N-terminally modified light-harvesting complex II," *Org. Biomol. Chem.*, vol. 8, no. 21, p. 4823, Apr. 2010.
- [274] D. N. Nguyen, S. C.-Y. Chen, J. Lu, M. Goldberg, P. Kim, A. Sprague, T. Novobrantseva, J. Sherman, S. Shulga-Morskaya, A. de Fougerolles, J. Chen, R. Langer, and D. G. Anderson, "Drug delivery-mediated control of RNA immunostimulation.," *Mol. Ther.*, vol. 17, no. 9, pp. 1555–62, 2009.
- [275] J. Liu and G. Jia, "Methylation Modifications in Eukaryotic Messenger RNA," *Journal of Genetics and Genomics*. 2014.
- [276] N. Kitsera, A. Khobta, and B. Epe, "Destabilized green fluorescent protein detects rapid removal of transcription blocks after genotoxic exposure," *Biotechniques*, vol. 43, no. 2, pp. 222–227, 2007.
- [277] D. S. Schwarz, G. Hutvágner, T. Du, Z. Xu, N. Aronin, and P. D. Zamore, "Asymmetry in the assembly of the RNAi enzyme complex," *Cell*, vol. 115, no. 2, pp. 199–208, 2003.
- [278] K. K. B. Gorden, X. Qiu, J. J. L. Battiste, P. P. D. Wightman, J. P. Vasilakos, and S. S. Alkan, "Oligodeoxynucleotides differentially modulate activation of TLR7 and TLR8 by imidazoquinolines.," *J. Immunol.*, vol. 177, no. 11, pp. 8164–70, 2006.
- [279] A. Kuznik, M. Bencina, U. Svajger, M. Jeras, B. Rozman, and R. Jerala, "Mechanism of Endosomal TLR Inhibition by Antimalarial Drugs and Imidazoquinolines," *J. Immunol.*, vol. 186, no. 8, pp. 4794–4804, 2011.
- [280] J. K. Nair, J. L. S. Willoughby, A. Chan, K. Charisse, M. R. Alam, Q. Wang, M. Hoekstra, P. Kandasamy, A. V. Kelin, S. Milstein, N. Taneja, J. O Shea, S. Shaikh, L. Zhang, R. J. Van Der Sluis, M. E. Jung, A. Akinc, R. Hutabarat, S. Kuchimanchi, K. Fitzgerald, T. Zimmermann, T. J. C. Van Berkel, M. A. Maier, K. G. Rajeev, and M. Manoharan, "Multivalent N -acetylgalactosamine-conjugated siRNA localizes in hepatocytes and elicits robust RNAi-mediated gene silencing," *J. Am. Chem. Soc.*, vol. 136, no. 49, pp. 16958–16961, 2014.
- [281] G. R. Fulmer, A. J. M. Miller, N. H. Sherden, H. E. Gottlieb, A. Nudelman, B. M. Stoltz, J. E. Bercaw, and K. I. Goldberg, "NMR chemical shifts of trace impurities: Common laboratory solvents, organics, and gases in deuterated solvents relevant to the organometallic chemist," *Organometallics*, vol. 29, no. 9, pp. 2176–2179, 2010.
- [282] H. Jonuleit, U. Kühn, G. Müller, K. Steinbrink, L. Paragnik, E. Schmitt, J. Knop, and A. H. Enk, "Pro-inflammatory cytokines and prostaglandins induce maturation of potent

- immunostimulatory dendritic cells under fetal calf serum-free conditions," *Eur. J. Immunol.*, vol. 27, no. 12, pp. 3135–3142, 1997.
- [283] M. Hubo, B. Trinschek, F. Kryczanowsky, A. Tuettenberg, K. Steinbrink, and H. Jonuleit, "Costimulatory molecules on immunogenic versus tolerogenic human dendritic cells," *Front. Immunol.*, vol. 4, no. APR, pp. 1–14, 2013.

Publications and Collaborations

I. Hellmuth, I. Freund, J. Schlöder, S. Seidu-Larry, K. Thüring, K. Slama, J. Langhanki, S. Kaloyanova, T. Eigenbrod, M. Krumb, S. Röhm, K. Peneva, T. Opatz, H. Jonuleit, A. H. Dalpke, and M. Helm, “Bioconjugation of Small Molecules to RNA Impedes Its Recognition by Toll-Like Receptor 7,” *Front. Immunol.*, vol. 8, no. March, pp. 1–13, Mar. 2017.

O. Domingo, I. Hellmuth, A. Jäschke, C. Kreutz, and M. Helm, “Intermolecular ‘cross-torque’: The N4-cytosine propargyl residue is rotated to the ‘CH’-edge as a result of Watson-Crick interaction,” *Nucleic Acids Res.*, vol. 43, no. 11, pp. 5275–5283, 2015.

[REDACTED]

Danksagung

CURRICULUM VITAE

